

Copyright

by

Jun Ki Lee

2007

**The Dissertation Committee for Jun Ki Lee Certifies that this is the approved  
version of the following dissertation:**

**Evaluation of External Post-Tensioned Tendons using Vibration  
Signatures**

**Committee:**

---

Sharon L. Wood, Supervisor

---

John E. Breen

---

David W. Fowler

---

James O. Jirsa

---

Harovel G. Wheat

**Evaluation of External Post-Tensioned Tendons using Vibration  
Signatures**

**by**

**Jun Ki Lee, B.S.; M.S.**

**Dissertation**

Presented to the Faculty of the Graduate School of

The University of Texas at Austin

in Partial Fulfillment

of the Requirements

for the Degree of

**Doctor of Philosophy**

**The University of Texas at Austin**

**May 2007**

## **Acknowledgements**

I wish to express my deepest and sincere appreciation to Dr. Sharon L. Wood for her encouragement and support. I am greatly indebted for the wisdom and patience she has shown to me.

My sincere thanks are also to the committee members of this dissertation, Dr. John E. Breen, Dr. David W. Fowler, Dr. James O. Jirsa, and Dr. Harovel G. Wheat for their invaluable suggestions and constructive criticism. It has been my pleasure and proud privilege to have them as my graduate committees.

It's been very pleasure for me to conduct a research project in an excellent environment; the Ferguson Structural Engineering Laboratory. I truly believe that knowledge and experience earned during the Ph.D period will nourish the urge for further research career.

My sincere appreciation goes to the technical support provided by a project engineer, Eric Shell. His contributions on my research work offered the project proceed effectively. I wish to acknowledge the assistance of the administrative and technical staffs of the Ferguson Structural Engineering Laboratory especially Blake Stasney, Mike Bell, Dennis Phillip, Barbara Howard, and Ella Schwartz.



I give my sincerest thanks to Matt Bean. I will not forget his contribution of this dissertation. I also would like to thanks to undergraduate students for their help: Royce Owens and Francisco Romo de Vivar.

# **Evaluation of External Post-Tensioned Tendons using Vibration Signatures**

Publication No. \_\_\_\_\_

Jun Ki Lee, Ph.D.

The University of Texas at Austin, 2007

Supervisor: Sharon L. Wood

Recent findings regarding corrosion of post-tensioned bridges have highlighted the urgent need to develop reliable methods to predict the behavior of the structural system after damage has occurred and inspection techniques to assess the condition of the structure. Corrosion in strands is undesirable in that it often progresses without visual signs of distress, but may cause a brittle failure. To complicate the inspection, access to the strands for visual inspection is usually blocked by the concrete cross section.

To date, significant efforts have been taken to improve the durability of the post-tensioned bridges. However, the behavior of the post-tensioned bridges with corrosion damage is not clearly understood and the currently available inspection techniques tend to provide only limited information about the nature and extent of the damage.

The research project discussed in this dissertation was developed to evaluate the feasibility of using the vibration technique to detect and estimate the extent of damage in an external tendon due to corrosion. To accomplish this goal, damage was induced in five specimens, which were monitored periodically to correlate the measured changes in the

frequency response to the level of damage. The induced damage simulated the degradation of a post-tensioned structure from corrosion. This dissertation describes the experimental program and the numerical scheme used to estimate the condition of the specimens.

Three types of specimens were tested during the experimental phase of the research: individual strands, cables specimens, and external tendons. A series of tension tests of individual strands were conducted to investigate changes in the uniaxial behavior after damage was induced. Simulated damage included uniform corrosion of the strand, mechanical wire cuts, and an initial defect in one wire. Three cable specimens and one tendon specimen were subjected to fatigue loading. The loading was selected to simulate the loss of cross-sectional area in the strands, and also caused grout damage. The frequency response of the specimens was recorded periodically during the fatigue tests and acoustic sensors were used to detect the occurrence of wire breaks. A second tendon specimen was exposed to an acid solution to simulate the hydrogen induced cracking in the strand at three different locations along the length of the specimen. A number of wires fractured during the exposure test and damage was inspected visually. Natural frequencies were also measured periodically.

The residual prestressing force of the specimens was extracted from the measured natural frequencies. The stiff string model was used to determine optimum values of tension and flexural stiffness from the frequency response. The numerical results from this optimization demonstrated the feasibility of using the vibration technique as a nondestructive testing method for external tendons.

## Table of Contents

List of Tables .....	xvi
List of Figures .....	xx
<b>CHAPTER 1 : INTRODUCTION</b>	<b>1</b>
1.1 Durability of Post-Tensioned Bridges .....	1
1.2 Post-Tensioned Bridges with External Tendons.....	3
1.3 Research Objectives and Scope .....	5
<b>CHAPTER 2 : LITERATURE REVIEW</b>	<b>8</b>
2.1 Corrosion of Prestressing Strand .....	8
2.1.1 Uniform Corrosion .....	8
2.1.2 Hydrogen Induced Cracking and Stress Corrosion Cracking .....	10
2.2 Corrosion of Post-Tensioned Tendons .....	11
2.3 Structural Properties of Corroded Strand.....	13
2.3.1 Individual High Strength Wires .....	13
2.3.2 Corroded Strand .....	15
2.3.3 Corroded Strand with Broken Wires.....	17
2.4 Variation of Lateral Stiffness with Fatigue Damage .....	19
2.5 Inspection of External Post-Tensioned Tendons .....	21
2.6 Vibration Technique .....	25
2.6.1 Frequency-Domain Data .....	26
2.6.2 Vibration Technique Applied to External Post-Tensioned Tendons .....	27
<b>CHAPTER 3 : UNIAXIAL TESTS OF INDIVIDUAL STRAND</b>	<b>32</b>
3.1 Test Setup .....	34
3.1.1 Phase 1.....	34
3.1.2 Phase 2.....	36

3.1.3	Phase 3.....	38
3.2	Preparation of Damaged Specimens .....	39
3.2.1	Uniformly Corroded Strands.....	39
3.2.2	Estimated Weight Loss.....	41
3.2.3	Mechanically Damaged Strands.....	43
3.3	Phase 1 Tests.....	45
3.3.1	Elastic Modulus.....	45
3.3.2	Apparent Modulus of Elasticity .....	49
3.4	Phase 2 Tests.....	52
3.4.1	Tensile Strength.....	56
3.4.2	Response of Corroded Strand.....	58
3.4.3	Response of Strand with Cut Wire(s).....	68
3.5	Phase 3 Tests.....	72
3.6	Summary .....	77
<b>CHAPTER 4 : FATIGUE TESTS OF TWO-STRAND STAY CABLES</b>		<b>80</b>
4.1	Background.....	80
4.2	Overview of Testing Program.....	82
4.2.1	Fatigue Tests .....	82
4.2.2	Acoustic Sensors .....	84
4.2.3	Periodic Static Tests .....	85
4.2.4	Instrumentation for Static Tests .....	86
4.2.5	Free-Vibration Tests.....	86
4.2.6	Instrumentation for Free-Vibration Tests.....	86
4.3	Measured Response of Specimens.....	90
4.4	Cable 01 .....	90
4.4.1	Transverse Stiffness .....	92
4.4.2	Distribution of Strains.....	94
4.4.3	Natural Frequencies .....	97

4.4.4	Acoustic Sensor Monitoring .....	97
4.4.5	Autopsy of Cable 01 .....	99
4.5	Cable 02 .....	102
4.5.1	Transverse Stiffness .....	103
4.5.2	Distribution of Strains .....	105
4.5.3	Natural Frequencies.....	108
4.5.4	Acoustic Sensor Monitoring.....	109
4.5.5	Autopsy of Cable 02.....	110
4.6	Cable 03 .....	112
4.6.1	Transverse Stiffness .....	113
4.6.2	Strain Distribution Measurement .....	114
4.6.3	Natural Frequencies.....	120
4.6.4	Acoustic Sensor Monitoring.....	121
4.6.5	Autopsy of Cable 03.....	122
4.7	Summary .....	124
<b>CHAPTER 5 : RESPONSE OF POST-TENSIONED TENDONS</b>		<b>126</b>
5.1	Overview of Tests .....	126
5.2	Construction of Tendon Specimens .....	128
5.2.1	Reaction frame .....	128
5.2.2	Concrete Anchor Blocks .....	128
5.2.3	Assembly of Tendon Specimens .....	129
5.2.4	Prestressing Procedure .....	131
5.2.5	Grouting Procedure .....	133
5.2.6	Intentional Voids in Tendon 02.....	133
5.3	Instrumentation .....	136
5.3.1	Acoustic Sensors .....	136
5.3.2	Accelerometers.....	136
5.4	Tendon 01 .....	139
5.4.1	Transverse Stiffness .....	141

5.4.2	Natural Frequencies.....	144
5.4.3	Damage Detected by Acoustic Sensors.....	148
5.4.4	Autopsy of Tendon 01.....	149
5.5	Tendon 02 .....	152
5.5.1	Corrosion Induced by Exposure to Hydrochloric Acid.....	152
5.5.2	Natural Frequencies.....	156
5.5.3	Screwdriver Penetration Test .....	163
5.5.4	Autopsy of Tendon 02.....	165
5.6	Summary .....	166
<b>CHAPTER 6 : EVALUATION OF INITIAL RESPONSE OF TEST SPECIMENS</b>		<b>168</b>
6.1	Analytical Models.....	168
6.2	Inverse Problems.....	170
6.3	Initial Estimates of Structural Parameters.....	171
6.3.1	Length.....	171
6.3.2	Tension .....	171
6.3.3	Mass per Unit Length.....	171
6.3.4	Flexural Stiffness.....	172
6.4	Optimization of Solutions .....	174
6.5	Response of Cable Specimens .....	176
6.5.1	Initial Calculations .....	176
6.5.2	Optimized Parameters .....	178
6.6	Response of Tendon Specimens .....	183
6.6.1	Initial Calculations .....	183
6.6.2	Optimized Parameters .....	185
6.6.3	Presence of Multiple Peaks in Frequency Response.....	190

6.7	Summary .....	193
<b>CHAPTER 7 : EVALUATION OF DAMAGED SPECIMENS USING VIBRATION SIGNATURES</b>		<b>194</b>
7.1	Measured Response of Specimens .....	194
7.1.1	Cable Specimens .....	195
7.1.2	Tendon Specimens .....	197
7.2	Calculated Sensitivity of Natural Frequencies to Changes in Tension and Flexural Stiffness .....	200
7.3	Estimated Structural Parameters at Conclusion of Fatigue Tests .....	203
7.3.1	Multi-Variable Optimization.....	205
7.3.2	Cable 02.....	207
7.3.3	Cable 03.....	208
7.3.4	Tendon 01.....	210
7.3.5	Summary .....	212
7.4	Variation of Structural Parameters with Increasing Damage .....	212
7.4.1	Cable Specimens .....	213
7.4.2	Tendon Specimens .....	217
7.5	Limitations of Vibration Technique for Evaluating External Post-Tensioned Tendon .....	221
7.6	Summary .....	225
<b>CHAPTER 8 : SUMMARY AND CONCLUSIONS</b>		<b>226</b>
8.1	Summary .....	226
8.2	Conclusions.....	228
8.2.1	Individual Strands .....	228
8.2.2	Cable Specimens .....	229
8.2.3	Tendon Specimens .....	229
8.2.4	Evaluation of Natural Frequency Response .....	231



8.3 Recommendations for Future Research .....	232
<b>APPENDIX A : ASSEMBLY OF ANCHOR BARREL ASSEMBLY AND STEEL PLATE</b>	<b>234</b>
<b>APPENDIX B : STRAIN MEASUREMENTS FROM DEF SPECIMENS</b>	<b>236</b>
<b>APPENDIX C : CONSTRUCTION OF CABLE SPECIMEN</b>	<b>240</b>
C.1 Anchorage System .....	240
C.2 Reaction Frame .....	240
C.3 Assembly of Stay Cable Specimen .....	241
C.4 Stressing Procedure.....	242
C.5 Strain Gage Instrumentation and Pipe Connection.....	243
C.6 Grouting Procedure.....	244
<b>APPENDIX D : HYDRAULIC ACTUATOR SYSTEM AND CONTROLLER</b>	<b>246</b>
D.1 Hydraulic Actuator Configuration for Cable Specimen .....	246
D.2 Hydraulic System for Tendon Specimen .....	247
D.3 Operation of Hydraulic Loading System .....	247
<b>APPENDIX E : PORTABLE DATA ACQUISITION SYSTEM DEVELOPMENT</b>	<b>249</b>
E.1 Data Acquisition System.....	249
E.2 Accelerometer .....	250
E.3 PC based Software .....	252
<b>APPENDIX F : DISTRIBUTION OF STRAINS FOR CABLE SPECIMEN</b>	<b>254</b>
F.1 Cable 01 .....	254
F.2 Cable 02 .....	255
F.3 Cable 03 .....	259
<b>APPENDIX G : NATURAL FREQUENCIES OF CABLE SPECIMENS</b>	<b>264</b>

G.1 Cable 01 .....	264
G.2 Cable 02 .....	267
G.3 Cable 03 .....	272
<b>APPENDIX H : SUMMARIZED TEST SCHEDULE FOR CABLE SPECIMENS</b>	<b>275</b>
H.1 Cable 01 .....	275
H.2 Cable 02 .....	276
H.3 Cable 03 .....	277
<b>APPENDIX I : CONCRETE BLOCK DESIGN</b>	<b>278</b>
<b>APPENDIX J : SUMMARIZED SCHEDULE FOR TENDON 01</b>	<b>280</b>
<b>APPENDIX K : NATURAL FREQUENCIES OF TENDON SPECIMENS</b>	<b>282</b>
K.1 Tendon 01 .....	282
K.2 Tendon 02 .....	290
<b>APPENDIX L : CORROSION PROPAGATION IN TENDON 01</b>	<b>303</b>
<b>APPENDIX M : ACID INDUCED CORROSION ON STRAND WITHOUT PRESTRESSING</b>	<b>308</b>
<b>APPENDIX N : ESTIMATION OF CROSS-SECTIONAL PROPERTIES</b>	<b>311</b>
N.1 Cable Specimen .....	311
N.2 Tendon 01 .....	313
N.3 Tendon 02 .....	315
<b>APPENDIX O : SENSITIVITY OF STRUCTURAL PARAMETERS</b>	<b>317</b>
O.1 Cable 01 .....	317
O.2 Cable 02 .....	318
O.3 Cable 03 .....	320
O.4 Tendon 01 .....	321

O.5 Tendon 02 .....	322
<b>REFERENCES</b>	<b>324</b>
<b>VITA</b>	<b>328</b>

## List of Tables

Table 2.1	Characteristics of Stress Corrosion Cracking and Hydrogen Induced Cracking (Jones 1996) .....	11
Table 2.2	Visual Indicator and Mechanical Properties of Specimen.....	16
Table 3.1	List of Single Strand Specimens.....	33
Table 3.2	Mechanical Properties of Strand Reported on Mill Certificate .....	34
Table 3.3	Chemical Cleaning Procedures in ASTM G1 (2003) .....	42
Table 3.4	Elastic Modulus of Strand.....	47
Table 3.5	Apparent Modulus of Elasticity of Strand .....	50
Table 3.6	Tensile Strength of Specimens Tested in Phase 2 (kip).....	56
Table 3.7	Estimated Weight Loss due to Corrosion .....	59
Table 3.8	Measured Elastic Modulus of COR Specimens.....	62
Table 3.9	Apparent Modulus of Elasticity of Corroded Strand.....	67
Table 3.10	Change in Apparent Modulus after First Wire Fractured.....	68
Table 3.11	Apparent Modulus of Outer Wires for Specimen CUT 2.....	69
Table 3.12	Elastic Modulus for Specimens with Cut Wire(s) .....	72
Table 3.13	Apparent Modulus of DEF Specimens before Wire Fracture.....	77
Table 3.14	Average Test Results .....	78
Table 4.1	Overview of Testing Program for Cable 01.....	91
Table 4.2	Series of Tests for Cable 01 .....	92
Table 4.3	Summary of Variation in Transverse Stiffness for Cable 01 .....	93
Table 4.4	Strain Measurements for Cable 01.....	94
Table 4.5	Locations of Strain Gages for Cable 01.....	95
Table 4.6	Measured Natural Frequencies for Cable 01 (Hz).....	97
Table 4.7	Summary of Wire Breaks Detected by Acoustic Sensors for Cable 01.....	99
Table 4.8	Overview of Testing Program for Cable 02.....	102
Table 4.9	Series of Tests for Cable 02.....	103
Table 4.10	Summary of Variation in Transverse Stiffness for Cable 02.....	104
Table 4.11	Strain Measurements for Cable 02.....	105

Table 4.12	Locations of Strain Gages for Cable 02.....	106
Table 4.13	Measured Natural Frequencies for Cable 02 (Hz).....	108
Table 4.14	Summary of Wire Breaks Detected by Acoustic Sensors for Cable 02.....	109
Table 4.15	Overview of Testing Program for Cable 03.....	112
Table 4.16	Series of Tests for Cable 03.....	113
Table 4.17	Summary of Variation in Transverse Stiffness for Cable 03.....	114
Table 4.18	Strain Measurements for Cable 03.....	115
Table 4.19	Initial Strain Measurements for Cable 03.....	115
Table 4.20	Locations of Strain Gages for Cable 03.....	117
Table 4.21	Measured Natural Frequency for Cable 03 (Hz) .....	121
Table 4.22	Summary of Wire Breaks Detected by Acoustic Sensors for Cable 03.....	122
Table 4.24	Variation of Natural Frequencies (Hz) .....	125
Table 5.1	Test Schedule for Tendon Specimens.....	127
Table 5.2	Periodic Tests - Tendon 01 .....	140
Table 5.3	Fatigue Tests – Tendon 01 .....	141
Table 5.4	Transverse Stiffness of Tendon 01 .....	142
Table 5.5	Measured Natural Frequencies for Tendon 01 .....	147
Table 5.6	Summary of Wire Breaks – Tendon 01 .....	149
Table 5.7	Schedule of Acid Exposure.....	152
Table 5.8	Summary of Test Program – Tendon 02.....	157
Table 5.9	Variation of Natural Frequencies in Tendon 02 before Exposure to Acid..	157
Table 5.10	Variation of Natural Frequencies (Void 1) (Hz).....	158
Table 5.11	Variation of Natural Frequencies (Void 2) (Hz).....	159
Table 5.12	Variation of Natural Frequencies (Void 3) (Hz).....	159
Table 5.13	Wire Breaks in each Void Detected by Visual Inspection.....	161
Table 5.14	Variation of Natural Frequencies with Number of Wire Fractures .....	166
Table 6.1	Weight per Unit Length .....	172
Table 6.2	Transformed Moment of Inertia for the Idealized Cross Sections.....	174
Table 6.3	Flexural Stiffness .....	174
Table 6.4	Ranges of Structural Parameters Considered.....	174

Table 6.5	Natural Frequencies of Cable Specimens Corresponding to Initial Set of Parameters.....	177
Table 6.6	Ranges of Parameters Considered in Evaluation of Cable Specimens.....	178
Table 6.7	Parameters Corresponding to Minimum Total Error for Cable Specimens.	179
Table 6.8	Comparison of Measured Natural and Calculated Frequencies Using Optimized Parameters for Cable Specimens.....	180
Table 6.9	Natural Frequencies for Tendon 01 .....	183
Table 6.10	Natural Frequencies for Tendon 02 .....	184
Table 6.11	Ranges of Parameters Considered in Evaluation of Tendon 01 .....	185
Table 6.12	Ranges of Parameters Considered in Evaluation of Tendon 02 .....	185
Table 6.13	Parameters Corresponding to Minimum Total Error for Tendon Specimens .....	186
Table 6.14	Comparison of Measured Natural and Calculated Frequencies Using Optimized Parameters for Tendon Specimens.....	190
Table 6.15	Frequencies of Multiple Peaks Observed for Tendon Specimens .....	191
Table 7.1	Condition of Test Specimens at Conclusion of Fatigue Tests.....	204
Table 7.2	Calculated Stress in Strand with Broken Wires.....	204
Table 7.3	Parameters used in Three Series of Analyses .....	206
Table 7.4	Summary of Results of Multi-Parameter Optimization for Cable 02.....	207
Table 7.5	Comparison of Natural Frequencies for Cable 02 .....	208
Table 7.6	Summary of Results of Multi-Parameter Optimization for Cable 03.....	209
Table 7.7	Comparison of Natural Frequencies for Cable 03 .....	209
Table 7.8	Summary of Results of Multi-Parameter Optimization for Tendon 01 .....	210
Table 7.9	Comparison of Natural Frequencies for Tendon 01 .....	211
Table 7.10	Optimized Parameters for Cable 01 .....	213
Table 7.11	Optimized Parameters for Cable 02.....	215
Table 7.12	Optimized Parameters for Cable 03.....	216
Table 7.13	Optimized Parameters for Tendon 01 .....	218
Table 7.14	Optimized Parameters for Tendon 02.....	219
Table E.1	Description of Menu and Parameters .....	253

Table H.1 Summarized Test Schedule for Cable 01.....	275
Table H.2 Summarized Test Schedule for Cable 02.....	276
Table H.3 Summarized Test Schedule for Cable03.....	277
Table I.1 Compressive Test Results (ksi).....	279
Table J.1: Summarized Schedule for Tendon 01.....	280
Table N.1 Constants for Computation.....	311
Table N.2 Sectional Dimension of Cable Specimen.....	311
Table N.3 Computation of Mass Quantity of Cable Specimen.....	312
Table N.4 Computation of Moment of Inertia of Cable Specimen.....	312
Table N.5 Sectional Dimension of Tendon 01.....	313
Table N.6 Computation of Mass Quantity of Tendon 01.....	313
Table N.7 Computation of Moment of Inertia of Tendon 01.....	314
Table N.8 Sectional Dimension of Tendon 02.....	315
Table N.9 Computation of Mass Quantity of Tendon 02.....	315
Table N.10 Computation of Moment of Inertia of Tendon 02.....	316

## List of Figures

Figure 1.1	Layout of the Long Beach Bridge (Powell et al 1990).....	4
Figure 1.2	San Antonio Y Project.....	4
Figure 1.3	Corrosion Damage Observed on the Mid-Bay Bridge (Corven Engineering 2001).....	5
Figure 2.1	Schematic Pourbaix Diagram (Jones 1996) .....	9
Figure 2.2	Likely Causes of Corrosion of Post-Tensioned Tendons (Matt 2001).....	12
Figure 2.3	Mechanical Properties of Wire Specimens.....	14
Figure 2.4	Fatigue and Elongation Test after Surface Treatment.....	15
Figure 2.5	Elongation Behavior of Corroded Strand.....	18
Figure 2.6	Strain Distribution of Strand with Two Wire Breaks.....	18
Figure 2.7	Geometry of Cable Specimen 7.....	19
Figure 2.8	Peak Load during Fatigue Test for Specimen 7 (Ridd 2004).....	20
Figure 2.9	Variation of Natural Frequencies in Cable-Stay Specimen.....	21
Figure 2.10	Degradation of Strand due to Corrosion (Corven Engineering 2001; Poston et al 2003) .....	22
Figure 2.11	Visual Grout Void Results from Bore Scope: (a),(b) Partial strand exposure, (c) Complete strand exposure, (d) No strand exposure (DMJM Harris 2003) .....	24
Figure 2.12	Mid-Bay Bridge Inspection Program (Corven Engineering 2001) .....	24
Figure 2.13	Equipment used for NDT of Tendons (Bergamini et al 2003; Scheel et al 2003).....	25
Figure 2.14	Mid-Bay Bridge Span Layout (Corven Engineering 2001) .....	26
Figure 2.15	Preliminary Vibration Test for Cable Specimen .....	28
Figure 2.16	Tensile Stress per Strand Extracted from Measured Frequencies in Tendons on the Mid-Bay Bridge (Corven Engineering 2001) .....	30
Figure 2.17	Variations in Tensile Forces Calculated for Each Segment of Tendon in Span 9 of Mid-Bay Bridge (Corven Engineering 2001).....	30
Figure 3.1	Load Frame for First Series of Strand Tests.....	35
Figure 3.2	Aluminum Block for Strand Grip.....	35



Figure 3.3	Load Frame for Second Series of Strand Tests .....	36
Figure 3.4	Anchor below Middle Cross Head in Second Series of Tests.....	37
Figure 3.5	Linear Potentiometer Used to Measure Relative Displacement between Cross Heads .....	37
Figure 3.6	Test Setup Used in Phase 3 .....	38
Figure 3.7	Uniformly-Corroded Specimens .....	40
Figure 3.8	Specimen Preparation.....	41
Figure 3.9	Procedures Used to Remove Corrosion Products.....	43
Figure 3.10	Simulation of Broken Wires in Phase 2 .....	44
Figure 3.11	Cross Sections Tested in Phases 2 and 3.....	45
Figure 3.12	Instrumentation Used to Measure Elongation and Strain in Phase 1 .....	46
Figure 3.13	Stress-Strain Relationship for UND 1 .....	47
Figure 3.14	Stress-Strain Relationship for UND 2 .....	48
Figure 3.15	Stress-Strain Relationship for UND 3 .....	48
Figure 3.16	Geometry of Strand Specimen.....	49
Figure 3.17	Strain Gages Positioned along Longitudinal Axes of Wires .....	49
Figure 3.18	Apparent Stress-Strain Relationship for UND 1 .....	50
Figure 3.19	Apparent Stress-Strain Relationship for UND 2 .....	51
Figure 3.20	Apparent Stress-Strain Relationship for UND 3 .....	51
Figure 3.21	Representative Load and Displacement Relationship in Test Series 2 .....	52
Figure 3.22	Slip of Strand at Anchors .....	53
Figure 3.23	First Wire Fracture .....	54
Figure 3.24	Instrumentation Used to Measure Elongation of Strand in Phase 2.....	55
Figure 3.25	Strain Gages in Phase 2 .....	55
Figure 3.26	Measured Tensile Strength of Strands.....	56
Figure 3.27	Failure of Strand with Cut Wire(s).....	57
Figure 3.28	Observed Corrosion on Surface of 6-in. Specimens .....	60
Figure 3.29	Surface Conditions for Corroded Specimens .....	61
Figure 3.30	Longitudinal Stress-Strain Relationship for COR Specimens.....	63
Figure 3.31	Strain Gages Attached to Corroded Strand .....	65

Figure 3.32	Representative Apparent Stress-Strain Relationship (COR 4).....	65
Figure 3.33	Apparent Stress-Strain Response of Outer Wires (COR Specimens) .....	66
Figure 3.34	Arrangement of Strain Gages for Specimen CUT 2.....	68
Figure 3.35	Strain Response of Specimen CUT 2.....	69
Figure 3.36	Opening of Gap between Cut Wires.....	71
Figure 3.37	Stress-Strain Relationship .....	72
Figure 3.38	Strain Gages in Phase 3 .....	73
Figure 3.39	Configuration of Specimens Tested in Phase 3.....	74
Figure 3.40	Specimens after Initial Wire Fracture.....	74
Figure 3.41	Measured Strain Response of Specimen DEF 3.....	76
Figure 3.42	Schematic Elongation Behavior of Strand .....	79
Figure 4.1	Test Setup for Cable Specimens.....	80
Figure 4.2	Arrangement of Load Frame, Accelerometers, and Acoustic Sensors.....	83
Figure 4.3	Acoustic Sensors Attached to Cable Specimens .....	84
Figure 4.4	Watch Dog-PS6 (SoundPrint™) Hardware.....	85
Figure 4.5	Location of Impact for Cable Specimens .....	86
Figure 4.6	Normalized Mode Shapes for Cable Specimens .....	87
Figure 4.7	Accelerometer Attached to Cable Specimens .....	88
Figure 4.8	Representative Free-Vibration Response .....	89
Figure 4.9	Positions of Load Frame for Cable 01.....	92
Figure 4.10	Measured Transverse Stiffness of Cable 01 .....	93
Figure 4.11	Locations of Strain Gages for Cable 01 .....	94
Figure 4.12	Strain Distribution for Cable 01 .....	96
Figure 4.13	Locations of Wire Breaks Reported for Cable 01 .....	98
Figure 4.14	Specimen Collapse of Cable 01.....	100
Figure 4.15	Wire Breaks and Typical Section for Cable 01 .....	101
Figure 4.16	Measured Transverse Stiffness of Cable02 .....	104
Figure 4.17	Locations of Strain Gage for Cable 02.....	106
Figure 4.18	Strain Distributions for Cable 02.....	107
Figure 4.19	Location of Wire Break Report for Cable 02.....	109

Figure 4.20	Wire Fractures at North Anchor Head for Cable 02.....	110
Figure 4.21	Grout Condition of Cable 02 .....	111
Figure 4.22	Measured Transverse Stiffness for Cable03.....	114
Figure 4.23	Locations of Strain Gages for Cable 03 .....	116
Figure 4.24	Initial Stain Distributions for Cable 03 .....	118
Figure 4.25	Stain Distribution along the Length of Cable 03.....	119
Figure 4.26	Strain Distributions at North End of Cable 03 .....	120
Figure 4.27	Location of Reported Wire Break for Cable 03 .....	121
Figure 4.28	Wire Fractures for Cable 03 .....	123
Figure 4.29	Crack Propagation for Cable 03 .....	124
Figure 5.1	Reaction Frame.....	128
Figure 5.2	Construction of Concrete Anchor Blocks.....	129
Figure 5.3	Configuration of Tendon Specimens.....	130
Figure 5.4	VSL Mechanical Coupler for HDPE Duct .....	131
Figure 5.5	Initial Prestressing Procedure .....	132
Figure 5.6	Arrangement of Equipment for Final Prestressing.....	132
Figure 5.7	Application of Final Prestressing .....	133
Figure 5.8	Arrangement of Grout Inlet and Vents.....	134
Figure 5.9	Location of Grout Voids in Tendon 02 .....	135
Figure 5.10	Construction of Grout Voids – Tendon 02.....	135
Figure 5.11	Position of Load Frame, Accelerometers, and Acoustic Sensors for Tendon 01.....	137
Figure 5.12	Position of Accelerometers for Tendon 02.....	138
Figure 5.13	Acoustic Sensors used to Monitor Tendon 01.....	138
Figure 5.14	Accelerometer Attached to Tendon 01 .....	138
Figure 5.15	Accelerometer Attached to Tendon 02.....	139
Figure 5.16	Overview of Tendon 01 .....	140
Figure 5.17	Transverse Stiffness of Tendon 01 .....	142
Figure 5.18	Recorded Load-Displacement Response on January 10, 2006 .....	143
Figure 5.19	Recorded Load-Displacement Response on January 11, 2006 .....	144

Figure 5.20	Location for impact for Tendon Specimens .....	145
Figure 5.21	Representative Response of Tendon 01 (NF 4).....	146
Figure 5.22	Location of Wire Breaks Detected by Acoustic Sensors.....	148
Figure 5.23	Demolition of Concrete Anchor Block for Tendon 01.....	150
Figure 5.24	Wire Fractures at Face of Concrete Block .....	150
Figure 5.25	Condition of Grout – Tendon 01 .....	151
Figure 5.26	Overview of Tendon 02.....	153
Figure 5.27	Observed Response of Tendon 02 during Exposure to Acid .....	154
Figure 5.28	Natural Frequency Measurement of Tendon 02.....	158
Figure 5.29	Normalized Root Mean Square (RMS) of Tendon 02.....	160
Figure 5.30	Observed Wire Breaks at Void 1 at Conclusion of Exposure Test .....	162
Figure 5.31	Observed Wire Breaks at Void 2 at Conclusion of Exposure Test .....	162
Figure 5.32	Observed Wire Breaks at Void 3 at Conclusion of Exposure Test .....	163
Figure 5.33	Tested Region and Location of Wire Breaks .....	164
Figure 5.34	Screwdriver Penetration Test .....	164
Figure 5.35	Condition of Strand Observed during Autopsy .....	165
Figure 5.36	Condition of Grout in Vicinity of Void 1 after Autopsy .....	166
Figure 6.1	Schematic Procedure of Forward and Inverse Problem .....	170
Figure 6.2	Portion of Test Specimens used to Determine Weight per Unit Length ....	172
Figure 6.3	Idealized and Observed Locations of Strands within Cross Sections .....	173
Figure 6.4	Modal Errors Corresponding to Initial Set of Parameters for Cable Specimens .....	178
Figure 6.5	Distribution of Modal Errors Corresponding to Minimum Total Error for Cable Specimens.....	180
Figure 6.6	Sensitivity of Total Error to Structural Parameters using Taut String Model (Cable 02).....	181
Figure 6.7	Sensitivity of Total Error to Structural Parameters using Stiff String Model (Cable 02).....	182
Figure 6.8	Modal Errors Corresponding to Initial Set of Parameters for Tendon Specimens .....	184

Figure 6.9	Distribution of Modal Errors Corresponding to Minimum Total Error for Tendon Specimens .....	186
Figure 6.10	Sensitivity of Total Error to Structural Parameters using Taut String Model (Tendon 01).....	187
Figure 6.11	Sensitivity of Total Error to Structural Parameters using Stiff String Model (Tendon 01).....	188
Figure 6.12	Possible Arrangements of Strands in Tendon 01 .....	189
Figure 6.13	Possible Arrangements of Strands in Tendon 02 .....	189
Figure 6.14	Presence of Multiple Peaks in Frequency Response of Tendon Specimens .....	191
Figure 6.15	Time-Domain Response of Tendon 01.....	192
Figure 6.16	Measured Frequency Response of External Tendons in Mid-Bay Bridge (Sagüés et al 2000).....	192
Figure 7.1	Frequency Reduction Ratio for Cable 01 .....	195
Figure 7.2	Frequency Reduction Ratios for Cable 02.....	196
Figure 7.3	Frequency Reduction Ratio for Cable 03 .....	197
Figure 7.4	Frequency Reduction Ratios for Tendon 01.....	198
Figure 7.5	Frequency Reduction Ratios for Tendon 02.....	199
Figure 7.6	Sensitivity of Frequency Reduction Ratios to Changes in Tension and Flexural Stiffness for Cable 02 .....	201
Figure 7.7	Sensitivity of Frequency Reduction Ratios to Changes in Tension and Flexural Stiffness for Tendon 01 .....	202
Figure 7.8	Modal Errors Corresponding to Multi-Variable Optimization for Cable 02 .....	208
Figure 7.9	Modal Errors Corresponding to Multi-Variable Optimization for Cable 03 .....	210
Figure 7.10	Modal Errors Corresponding to Multi-Variable Optimization for Tendon 01 .....	211
Figure 7.11	Variation of T and EI during Fatigue Test for Cable 01 .....	214
Figure 7.12	Variation of T and EI during Fatigue Test for Cable 02 .....	215

Figure 7.13	Variation of T and EI during Fatigue Test for Cable 03 .....	216
Figure 7.14	Variation of T and EI during Fatigue Test for Tendon 01 .....	218
Figure 7.15	Variation of T and EI during Exposure Test for Tendon 02 .....	220
Figure 7.16	Cross Section of External Tendon with Wire Breaks.....	223
Figure 7.17	Idealization of Variation in Structural Capacity with Increasing Damage	224
Figure A.1	Drawing of Anchor Barrel.....	234
Figure A.2	Assembly of Anchor Barrel and Steel Plate .....	235
Figure A.3	Drawing of Steel Plate.....	235
Figure B.1	Redistribution of Strain for Specimen DEF 1.....	236
Figure B.2	Redistribution of Strain for Specimen DEF 2.....	237
Figure B.3	Redistribution of Strain for Specimen DEF 3.....	238
Figure B.4	Redistribution of Strain for Specimen DEF 4.....	239
Figure C.1	Anchor Head and Grout Cap .....	240
Figure C.2	Reaction Frame and Anchorage Assembly.....	241
Figure C.3	Assembly of Cable Specimen .....	242
Figure C.4	Stressing Strand with Hydraulic Ram.....	243
Figure C.5	Strain Gage Installation .....	243
Figure C.6	Completion of Pipe Connection.....	244
Figure C.7	Grouting Procedure.....	245
Figure D.1	Hydraulic Actuator and Control Unit for Cable Specimen .....	246
Figure D.2	Hydraulic Actuator and Control Unit for Tendon 01 .....	247
Figure D.3	Load Input Operation.....	248
Figure E.1	DAQ System .....	249
Figure E.2	Modification of Accelerometer.....	250
Figure E.3	Portable Sensor and Connector .....	251
Figure E.4	Interface of PC based Software.....	252
Figure F.1	Strain Distribution of SM 0.....	254
Figure F.2	Strain Distribution of SM 1 .....	254
Figure F.3	Strain Distribution of SM 0.....	255
Figure F.4	Strain Distribution of SM 1 .....	255

Figure F.5	Strain Distribution of SM 2.....	256
Figure F.6	Strain Distribution of SM 3.....	256
Figure F.7	Strain Distribution of SM 4.....	257
Figure F.8	Strain Distribution of SM 5.....	257
Figure F.9	Strain Distribution of SM 6.....	258
Figure F.10	Strain Distribution of SM 0-0 .....	259
Figure F.11	Strain Distribution of SM 0-1 .....	259
Figure F.12	Strain Distribution of SM 0-2 .....	260
Figure F.13	Strain Distribution of SM 0-3.....	260
Figure F.14	Strain Distribution of SM 0-4 .....	261
Figure F.15	Strain Distribution of SM 0-5 .....	261
Figure F.16	Strain Distribution of SM 0-6 .....	262
Figure F.17	Strain Distribution of SM 1 .....	262
Figure F.18	Strain Distribution of SM 2.....	263
Figure F.19	Strain Distribution of SM 3.....	263
Figure G.1	Normalized Root Mean Square (RMS) of NF 0.....	264
Figure G.2	Normalized Root Mean Square (RMS) of NF 1.....	264
Figure G.3	Normalized Root Mean Square (RMS) of NF 2.....	265
Figure G.4	Normalized Root Mean Square (RMS) of NF 3.....	265
Figure G.5	Normalized Root Mean Square (RMS) of NF 4.....	266
Figure G.6	Normalized Root Mean Square (RMS) of NF 0.....	267
Figure G.7	Normalized Root Mean Square (RMS) of NF 1.....	267
Figure G.8	Normalized Root Mean Square (RMS) of NF 2.....	268
Figure G.9	Normalized Root Mean Square (RMS) of NF 3.....	268
Figure G.10	Normalized Root Mean Square (RMS) of NF 4.....	269
Figure G.11	Normalized Root Mean Square (RMS) of NF 5.....	269
Figure G.12	Normalized Root Mean Square (RMS) of NF 6.....	270
Figure G.13	Normalized Root Mean Square (RMS) of NF 7.....	270
Figure G.14	Normalized Root Mean Square (RMS) of NF 8.....	271
Figure G.15	Normalized Root Mean Square (RMS) of NF 0.....	272

Figure G.16	Normalized Root Mean Square (RMS) of NF 1 .....	272
Figure G.17	Normalized Root Mean Square (RMS) of NF 2.....	273
Figure G.18	Normalized Root Mean Square (RMS) of NF 3.....	273
Figure G.19	Normalized Root Mean Square (RMS) of NF 4.....	274
Figure I.1	Reinforcement Arrangement for Concrete Block .....	279
Figure K.1	Normalized Root Mean Square (RMS) of NF 0.....	282
Figure K.2	Normalized Root Mean Square (RMS) of NF 1.....	283
Figure K.3	Normalized Root Mean Square (RMS) of NF 2.....	283
Figure K.4	Normalized Root Mean Square (RMS) of NF 3.....	284
Figure K.5	Normalized Root Mean Square (RMS) of NF 4.....	284
Figure K.6	Normalized Root Mean Square (RMS) of NF 5.....	285
Figure K.7	Normalized Root Mean Square (RMS) of NF 6.....	285
Figure K.8	Normalized Root Mean Square (RMS) of NF 7.....	286
Figure K.9	Normalized Root Mean Square (RMS) of NF 8.....	286
Figure K.10	Normalized Root Mean Square (RMS) of NF 9.....	287
Figure K.11	Normalized Root Mean Square (RMS) of NF 10.....	287
Figure K.12	Normalized Root Mean Square (RMS) of NF 11.....	288
Figure K.13	Normalized Root Mean Square (RMS) of NF 12.....	288
Figure K.14	Normalized Root Mean Square (RMS) of NF 13.....	289
Figure K.15	Normalized Root Mean Square (RMS) of NF 0-0 .....	290
Figure K.16	Normalized Root Mean Square (RMS) of NF 0-1 .....	290
Figure K.17	Normalized Root Mean Square (RMS) of NF 0-3 .....	291
Figure K.18	Normalized Root Mean Square (RMS) of NF 0-2 .....	291
Figure K.19	Normalized Root Mean Square (RMS) of NF 1.....	292
Figure K.20	Normalized Root Mean Square (RMS) of NF 2.....	292
Figure K.21	Normalized Root Mean Square (RMS) of NF 3.....	293
Figure K.22	Normalized Root Mean Square (RMS) of NF 4.....	293
Figure K.23	Normalized Root Mean Square (RMS) of NF 5.....	294
Figure K.24	Normalized Root Mean Square (RMS) of NF 6.....	294
Figure K.25	Normalized Root Mean Square (RMS) of NF 7.....	295



Figure K.26	Normalized Root Mean Square (RMS) of NF 8.....	295
Figure K.27	Normalized Root Mean Square (RMS) of NF 9.....	296
Figure K.28	Normalized Root Mean Square (RMS) of NF 10.....	296
Figure K.29	Normalized Root Mean Square (RMS) of NF 11.....	297
Figure K.30	Normalized Root Mean Square (RMS) of NF 12.....	297
Figure K.31	Normalized Root Mean Square (RMS) of NF 13.....	298
Figure K.32	Normalized Root Mean Square (RMS) of NF 14.....	298
Figure K.33	Normalized Root Mean Square (RMS) of NF 15.....	299
Figure K.34	Normalized Root Mean Square (RMS) of NF 16.....	299
Figure K.35	Normalized Root Mean Square (RMS) of NF 17.....	300
Figure K.36	Normalized Root Mean Square (RMS) of NF 18.....	300
Figure K.37	Normalized Root Mean Square (RMS) of NF 19.....	301
Figure K.38	Normalized Root Mean Square (RMS) of NF 20.....	301
Figure K.39	Normalized Root Mean Square (RMS) of NF 21.....	302
Figure L.1	Overview of Tendon 01 .....	303
Figure L.2	Anchor Head Status .....	304
Figure L.3	Grouting Condition at Various Locations.....	305
Figure L.4	Corrosion Extent on Anchor Head and Plate.....	306
Figure L.5	Grout Flow of Tendon 02.....	307
Figure L.6	Alternative Grout Cap.....	307
Figure M.1	Acid Immersion Test.....	308
Figure M.2	Preliminary Strand Immersion in Hydrochloric Acid Solution .....	309
Figure M.3	Pitting after 12 days of Immersion.....	310
Figure O.1	Sensitivity of Structural Parameters from Taut String Model.....	317
Figure O.2	Sensitivity of Structural Parameters from Stiff String Model .....	318
Figure O.3	Sensitivity of Structural Parameters from Taut String Model.....	319
Figure O.4	Sensitivity of Structural Parameters from Stiff String Model .....	319
Figure O.5	Sensitivity of Structural Parameters from Taut String Model.....	320
Figure O.6	Sensitivity of Structural Parameters from Stiff String Model .....	321
Figure O.7	Sensitivity of Structural Parameters from Taut String Model.....	321

Figure O.8	Sensitivity of Structural Parameters from Stiff String Model .....	322
Figure O.9	Sensitivity of Structural Parameters from Taut String Model .....	323
Figure O.10	Sensitivity of Structural Parameters from Stiff String Model .....	323

## **Chapter 1: Introduction**

Post-tensioned concrete bridges became popular in Europe in the 1950s, and are widely recognized as economical structures. The use of high-strength steels to apply prestress dramatically increased the length of spans that can be achieved in concrete bridges and compensates for the low tensile strength of concrete. However, recent observations of corrosion damage have raised serious concerns regarding the durability of post-tensioned concrete bridges. Effective inspection of critical tendons is often impossible due to limited access and an incomplete understanding of how corrosion influences the structural characteristics of the tendons.

This dissertation focuses on the use of vibration signatures to detect corrosion damage in external, post-tensioned tendons. The experimental phases of the research may be divided into two parts. In the first, the uniaxial behavior of individual strands with and without damage was investigated. In the second, the frequency response of five grouted tendons was monitored as the extent of damage was increased to evaluate the sensitivity of the natural frequencies to the extent of damage. An optimization scheme was also developed to estimate the change in applied tension and structural parameters from the measured frequency response.

### **1.1 DURABILITY OF POST-TENSIONED BRIDGES**

The concept of prestressed concrete structures was introduced in Europe in the early 20th century, and the number of post-tensioned bridges increased dramatically during the reconstruction boom following World War II. During the early stages of development of post-tensioned construction, the benefits of the effective crack control from the applied prestressing were overestimated. Post-tensioned structures were originally considered to be nearly maintenance-free and potential damage caused by corrosion was not recognized. The early post-tensioned bridges, however, were constructed with inadequate consideration of waterproofing and poor or improper details.

In addition, inappropriate materials, such as quenched or tempered steel and corrosive grouts, were used in construction. Appropriate grouting procedures were also not established. Therefore, the tendons were often exposed to aggressive environments without proper protection against corrosion.

The consequences of corrosion damage were not understood until the post-tensioned bridges had been in service for many years. In spite of the collapse of two pedestrian bridges in the United Kingdom in the 1960s, full attention was not paid to durability of post-tensioned construction until the Ynys-y-Gwas Bridge collapsed suddenly in 1985. The fact that no signs of deterioration were observed before this bridge collapsed under its self-weight only highlighted the seriousness of the situation. The UK Department of Transport issued a moratorium on the construction of internally post-tensioned bridges in 1992 (Woodward 2001), which was partially lifted in 1996. Internal, post-tensioned segmental systems are still banned in the UK (Loudon 2006).

To date, considerable effort has been taken to resolve concerns related to the durability of post-tensioned construction. The Post-Tensioning Institute (PTI) published grouting specifications in 2001 and the American Segmental Bridge Institute (ASBI) initiated a grouting certification program in 2001 (DeHaven 2003; Poston et al 2003). The Florida Department of Transportation inspected several bridges using state-of-the-art nondestructive testing techniques and evaluated the feasibility of each method in 2001 and 2003 (FDOT 2001; FDOT 2003). Florida DOT also published the guidelines for the construction of post-tensioned structures (FDOT 2002).

Two international workshops were sponsored by the *fédération internationale du béton* (fib) and International Association for Bridge and Structural Engineering (IABSE) (2001, 2004) to share experiences regarding the durability of the post-tensioned structures. The American Society of Nondestructive Testing (ASNT) held a conference in 2004 to discuss state-of-the-art inspection techniques for detecting corrosion in post-tensioned bridges.

In spite of these efforts to evaluate the durability of existing post-tensioned bridges, a single, accepted inspection technique has not been established. Current

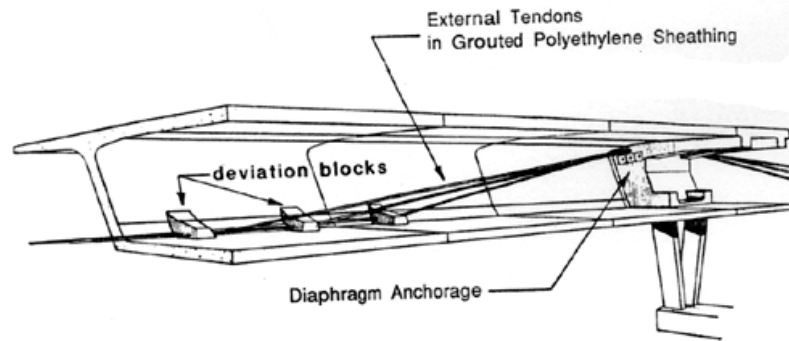
techniques provide only limited information about the extent of damage. Restricted access to the tendons and the variation of material properties and dimensions of the post-tensioned bridges often limit the effectiveness of the inspection techniques.

## **1.2 POST-TENSIONED BRIDGES WITH EXTERNAL TENDONS**

Although the concepts of prestressing bridges using internal and external post-tensioned tendons were developed at the same time, internal tendons were considered to be more durable than external tendons due to the corrosion protection provided by embedding the tendon in concrete. Therefore, external tendons were used primarily to repair and strengthen existing structures until relatively recently (Virlogeux 1990).

The most distinct advantage of bridges with external tendons compared with bridges with internal tendons is that the webs and flanges of the concrete sections are considerably thinner when external tendons are used, resulting in lighter structures. External tendons are commonly used with box sections. The tendons are anchored in diaphragms at the ends of the span and are continuous through deviators, which control the profile of the tendon (Figure 1.1). Each tendon typically comprises numerous prestressing strands, which are enclosed in a high-density polyethylene (HDPE) pipe. The pipe is typically filled with cementitious grout.

External tendons are especially well suited for the construction of segmental bridges. The continuity of the ducts can be easily maintained between spans and the misalignment of ducts at a joint can be prevented. Within the state of Texas, three segmental bridges with external tendons have been constructed in the past 20 years: the San Antonio Y project (Figure 1.2), the Neches River Bridge, and US 183 in Austin.



*Figure 1.1 Layout of the Long Beach Bridge (Powell et al 1990)*



*Figure 1.2 San Antonio Y Project*

External tendons provide two primary advantages over internal tendons with respect to durability: (1) the tendons are easier to inspect because the majority of the length of the tendon is exposed, and (2) if necessary, an external tendon can be replaced without demolition of the bridge. In spite of these advantages, corrosion damage has been reported in several bridges in the US with external tendons (Poston et al 2003).

In Florida, severely corroded tendons were found on the Niles Channel Bridge, the Mid-Bay Bridge, and the Sunshine Skyway Bridge (Figure 1.3). While the extent of the observed damage was not considered to be sufficient to undermine the structural

integrity of the bridges, the durability concerns were considered to be serious enough to initiate a state-wide inspection program (Freyermuth 2001).



*Figure 1.3 Corrosion Damage Observed on the Mid-Bay Bridge (FDOT 2001)*

### **1.3 RESEARCH OBJECTIVES AND SCOPE**

The research program discussed in this dissertation was developed to quantify the changes in the structural response of external post-tensioned tendons as corrosion damage accumulates and to determine if the extent of damage can be extracted from the observed changes in the natural frequencies of the tendon. The natural frequencies are expected to decrease as the extent of corrosion damage increases; but the change in natural frequencies with the level of damage is not understood at present. This method of nondestructive evaluation was selected for study because of the ease of application and the relatively modest cost of required equipment.

In evaluating the extent of corrosion damage, the loss of cross-sectional area of the strand is typically assumed to be directly related to the loss of the prestress force.

However, this simple assumption does not appear to be valid, as tensile stress can be redistributed to adjacent wires after a wire fractures and the fractured wire recovers a portion of the tensile stress due to internal friction among wires. These phenomena influence the overall response of a post-tensioned tendon, but are typically not considered when evaluating a damaged tendon. Background information about the structural characteristics of corroded strand and current nondestructive techniques used to evaluate external tendons is presented in Chapter 2.

The experimental program is discussed in three chapters in this dissertation. In order to investigate the behavior of strands after damage, individual strands were tested in tension in Chapter 3. The elongation behavior of the strands directly influences the level of residual prestressing in the external tendon. Three types of damage were simulated: uniform corrosion on the surface of the strand, strand with cut wire(s), and strand with an initial defect. From the uniaxial tests, material properties such as the elastic modulus, the apparent modulus of elasticity and the tensile strength were determined. Also, the characteristics such as stress recovery and stress redistribution were investigated.

The response of three cable specimens that were subjected to fatigue loads is summarized in Chapter 4. Each cable specimen comprised two 0.6-in. strands stressed to 50% of guaranteed ultimate tensile strength (GUTS). The fatigue loads caused wire fractures and cracks in the grout. The transverse stiffness of the specimens and natural frequencies were recorded periodically during the tests. After the conclusion of the fatigue tests, the specimens were disassembled to determine the extent of damage.

The response of two tendon specimens is discussed in Chapter 5. Tendon 01 comprised twelve 0.6-in. strands stressed to 60% of GUTS and was subjected to fatigue loading to accumulate damage near one end of the specimen. The transverse stiffness and natural frequencies were recorded periodically during the fatigue test. Tendon 02 comprised nine 0.6-in. strands stressed to 80% of GUTS. At three locations along the length of the tendon, the strands were exposed to acid to induce corrosion damage. Natural frequencies were recorded periodically during the exposure test.



Two analytical models are introduced in Chapter 6 to represent the frequency response of the specimens. The optimization scheme was developed to estimate the values of four structural parameters that best matched the measured frequency response of the test specimens before damage was induced. The sensitivity of response to the value of the structural parameters was evaluated.

The same approach was used in Chapter 7 to estimate the variation in frequencies with increasing damage during the tests. The differences between the parameters inferred from the numerical optimization and known conditions of the specimens at various points during the experimental program were assessed to evaluate the applicability of the optimization scheme. The results were used to evaluate the limitations of using the vibration technique to detect damage in external tendons. Conclusions are summarized in Chapter 8.

## **Chapter 2: Literature Review**

Throughout this dissertation, relationships are identified between the structural properties of post-tensioned tendons and the physical condition of the prestressing strand. However, background information about the structural properties of the strand and tendons is needed to interpret the observed trends. Relevant background information is presented in this chapter.

Corrosion of prestressing strand is discussed in Section 2.1, and observed corrosion of external post-tensioned tendons is summarized in Section 2.2. Variations in the structural properties of corroded strand are presented in Section 2.3 and changes in the lateral stiffness and frequency response of a large-scale cable specimen with increasing fatigue damage are discussed in Section 2.4. Techniques currently used to evaluate the condition of external tendons are summarized in Section 2.5 and the fundamental concepts used in the vibration technique are introduced in Section 2.6.

### **2.1 CORROSION OF PRESTRESSING STRAND**

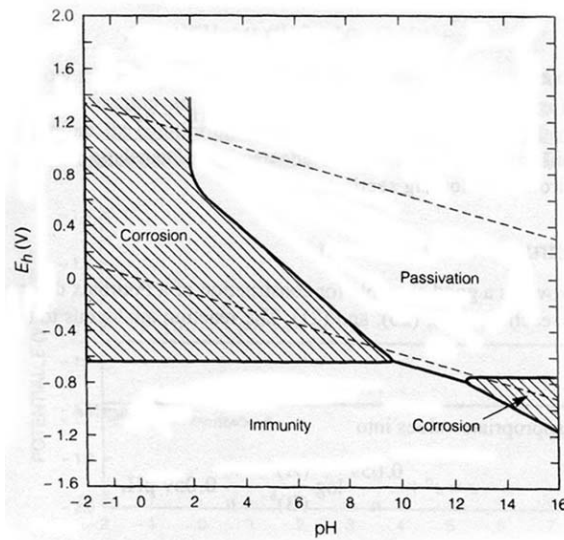
Corrosion is a destructive electrochemical reaction that results in a loss of metal to the surrounding environment. Two forms of corrosion are discussed in this section: uniform corrosion, which may occur in all steel embedded in concrete, and corrosion caused by hydrogen induced cracking and stress corrosion cracking, which is most prevalent in prestressed concrete structures.

#### **2.1.1 Uniform Corrosion**

The uniform corrosion is associated with loss of surface steel. The removed metal chemically reacts with substances in the surrounding environment and forms corrosion products. Because this form of corrosion is an electrochemical reaction requiring the exchange of electrons, equilibrium phases of the electrochemical system are often defined

using a Pourbaix diagram. As shown in Figure 2.1, the stable phases of the electrochemical system are defined in terms of oxidation power (potential) and pH.

In general, the equilibrium phases of a metal may be separated into three regions: immunity, corrosion and passivation. If the system reaches equilibrium within the immunity region, the metal stays intact and no loss of metal ion occurs. However, if the system reaches equilibrium within a corrosion region, electrons are exchanged and corrosion products are generated. If this system reaches equilibrium within a passivation region, the chemical reaction is favored within the given environment, but the corrosion rate is significantly reduced due to the formation of a protective film on the surface of the metal.



**Figure 2.1 Schematic Pourbaix Diagram (Jones 1996)**

For concrete structures, it is generally agreed that the presence of chloride ions initiates the corrosion of steel by compromising the protective passive film. Once the passive layer is breached, the corrosion process is driven by the presence of moisture and oxygen. Within the corrosion phase,  $\text{Fe}^{++}$  or  $\text{Fe}^{+++}$  ions are available by anodic reactions and then these ions form corrosion products such as  $\text{Fe}(\text{OH})_2$  or  $\text{Fe}(\text{OH})_3$ .

Within the passivity phase, iron oxides such as  $\text{Fe}_3\text{O}_4$  and  $\text{Fe}_2\text{O}_3$  are produced which form a protective film (ACI Committee 222 2001). In general, the pH of sound concrete (and grout) is within the range of 13.0 to 13.5. Therefore, the embedded steel is protected from the aggressive environment within the concrete by the protective film. Cracks in the concrete, however, form pathways for chloride ions, water, and oxygen to penetrate the concrete and initiate corrosion.

### **2.1.2 Hydrogen Induced Cracking and Stress Corrosion Cracking**

Hydrogen induced cracking is a highly undesirable form of corrosion, because the corrosion can not be detected visually. Hydrogen induced cracking develops when sufficient hydrogen exists on the surface of the metal that hydrogen atoms dissolve into the metal lattice (the crystal lattice of steel is larger than that of atomic hydrogen). Cracks form along the path of the hydrogen as it penetrates into the steel. For post-tensioned tendons, hydrogen induced cracking may result in sudden failure when the crack extends a sufficient depth that the intact area of the cross section does not have sufficient strength to resist the applied tension.

The corrosion mechanism associated with hydrogen induced cracking of prestressing steel is still under debate. Some researchers link hydrogen induced cracking with stress corrosion cracking (Nürnberg 2001). Stress corrosion cracking occurs when the metal is subjected to a constant tensile stress and is exposed to a corrosive environment. Because the characteristics and appearance of hydrogen induced cracking and stress corrosion cracking are nearly identical, the cause of the damage can often not be determined without a microscopic investigation (Table 2.1). Also, it should be noted that as level of tension in the strand approaches to yielding, the likelihood of corrosion accelerates correspondingly.

Hydrogen induced cracking and stress corrosion cracking rarely occur in reinforced concrete structures because the susceptibility to these forms of corrosion increases with the tensile strength of the metal. Case studies in Germany (fib 2003)

indicated that unqualified prestressing steel was particularly susceptible to this form of corrosion.

***Table 2.1 Characteristics of Stress Corrosion Cracking and Hydrogen Induced Cracking (Jones 1996)***

	<b>Stress Corrosion Cracking</b>	<b>Hydrogen Induced Cracking</b>
Stress	static tensile	static tensile
Corrosion products in the crack	absent (usually)	absent (usually)
Crack surface appearance	cleavage like	cleavage like
Near maximum strength level	susceptible, but hydrogen induced crack often predominates	accelerates

## **2.2 CORROSION OF POST-TENSIONED TENDONS**

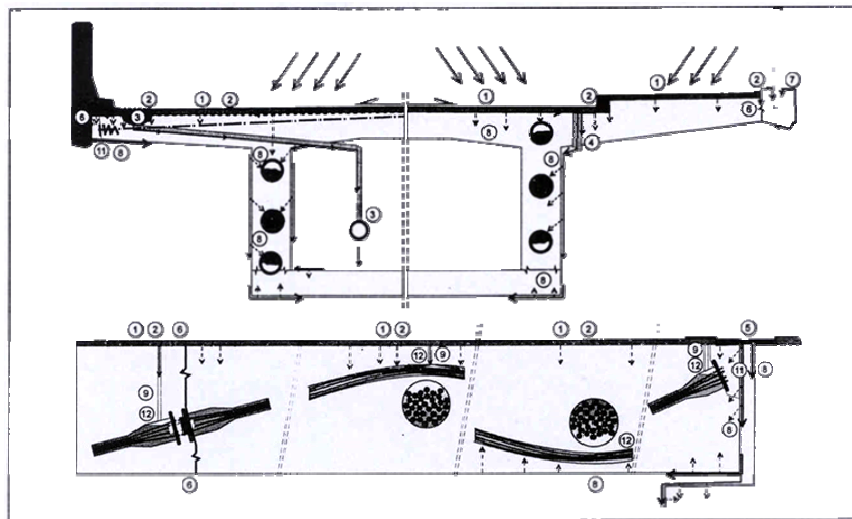
Corrosion of post-tensioned tendons is often critical for the structural integrity of a bridge. The prestressing tendon is a major structural element and supports a considerable fraction of the external load. The strands are manufactured from high strength steel and are typically prestressed to 70 to 80% of GUTS. Therefore, deterioration of the stands represents a considerable reduction in structural capacity. The risk of brittle failure due to hydrogen induced cracking and stress corrosion cracking is also significant.

For most external tendons, corrosion protection is provided by a multi-layer system. The concrete box forms the first barrier against external aggressive agents. The HDPE ducts extend along the entire length of the tendons and are filled with grout. Corrosion of strand is often correlated with the presence of voids in the grout. The grout is intended to protect the strand from corrosion due to the high pH environment. If the grout completely fills the post-tensioning duct, the likelihood of corrosion of the strands is quite low.

However, experience indicates that these protective layers can be compromised in many ways. Likely causes of corrosion in post-tensioned bridges are illustrated in Figure 2.2, where potential paths for aggressive agents to reach to prestressing steels are shown

(Matt 2001). Minor construction details, such as a drainage pipes or electrical inserts, often compromise the corrosion protection system for the prestressing steel.

To date, design alternatives to improve the durability of post-tensioned bridges have been reported, but no unique solution appears to meet the requirements for all cases. Suggestions include replacing the cementitious grout with wax or grease and using less prestressing steel and more conventional reinforcement (Jungwirth 2001). In Japan, transparent ducts have been used to construct external post-tensioned tendons to facilitate inspection (Mutsuyoshi 2001).



<ol style="list-style-type: none"> <li>1. Defective wearing course (e.g. cracks)</li> <li>2. Missing or defective waterproofing membrane incl. edge areas</li> <li>3. Defective drainage intakes and pipes</li> <li>4. Wrongly placed outlets for the drainage of wearing course and waterproofing</li> <li>5. Leaking expansion joint</li> <li>6. Cracked and leaking construction or element joints</li> </ol>	<ol style="list-style-type: none"> <li>7. Inserts (e.g. for electricity)</li> <li>8. Defective concrete cover</li> <li>9. Partly or fully open grouting in and outlets (vents)</li> <li>10. Leaking, damaged metallic ducts mechanically or by corrosion</li> <li>11. Cracked and porous pocket concrete</li> <li>12. Grout voids at tendon high points</li> </ol>
--	--

*Figure 2.2 Likely Causes of Corrosion of Post-Tensioned Tendons (Matt 2001)*

While corrosion of post-tensioned tendons motivated this dissertation, it is important to understand that the major problem of durability of post-tensioned bridges is

not the performance of the tendons during the service life of the bridge, but the difficulty associated with inspection of the tendons. Post-tensioned bridges have been proven to be an economic and durable structural system. However, the integrity of some post-tensioned bridges has been challenged by corrosion damage. Therefore, a combination of adequate protective measures and an effective inspection scheme would ensure the durability of the post-tensioned bridges.

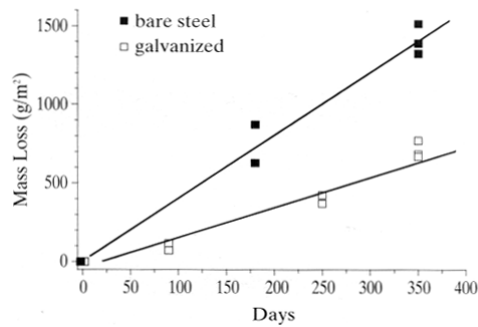
### **2.3 STRUCTURAL PROPERTIES OF CORRODED STRAND**

Three studies that discuss the behavior of corroded prestressing strand are summarized in this section. In spite of the large number of research studies regarding the durability of post-tensioned bridges, few have focused on the influence of corrosion on the structural properties of the strand. As a result, interpretation of damaged external tendons is often based on the simplified assumption that the loss of cross-sectional area due to by corrosion is proportional to the loss of applied prestress force. However, recent studies indicate that considerable capacity can be recovered due to the geometry of the strands and internal friction among the wires.

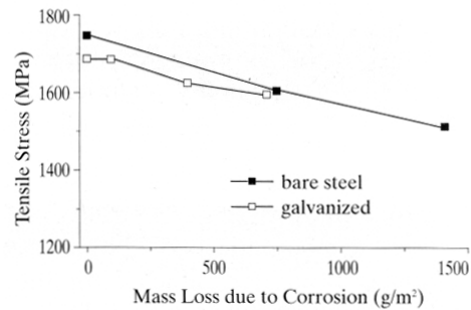
#### **2.3.1 Individual High Strength Wires**

The mechanical properties of high strength wires at different levels of corrosion were reported by Nakamura et al. (2002). In order to stimulate corrosion damage, the 5-mm diameter wires were wrapped in wet gauze at 40 C°. Three different exposure periods were used: 90 days, 250 days and 360 days. After significant corrosion products developed on the surface of the specimens, a series of tests were conducted to investigate the mechanical properties of the wire.

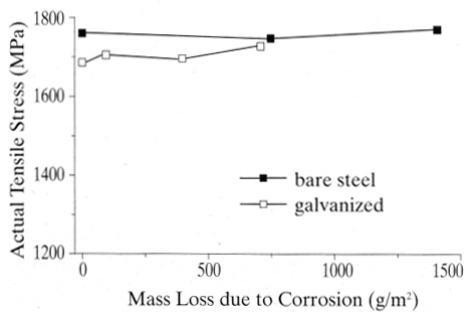
The measured properties of corroded wires are shown in Figure 2.3. The mass loss increased as the exposure period increased (Figure 2.3a). The axial strength (calculated using the nominal cross-sectional area) and the elongation capacity decreased as the corrosion damage increased (Figure 2.3b and Figure 2.3d). However, when the actual cross-sectional area was used to calculate the tensile strength, the loss of area had almost no influence on the response (Figure 2.3c). These trends indicate that the axial tensile strength of the corroded wire is proportional to the actual cross-sectional area of the corroded wire.



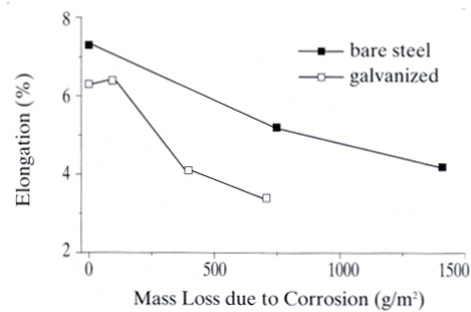
(a) Mass loss of corroded wires



(b) Tensile strength



(c) Actual tensile strength

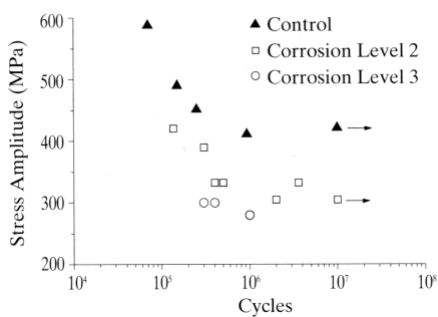


(d) Elongation test

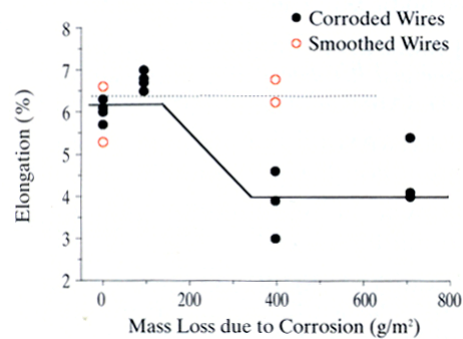
**Figure 2.3 Mechanical Properties of Wire Specimens**



The fatigue capacity of wire decreases as the extent of corrosion damage increases (Figure 2.4a). Undamaged specimens had fatigue lives that were nearly ten times longer than those of the corroded specimens. Another set of elongation test results are displayed in Figure 2.4(b). The surface of corroded wires was severely pitted and covered with corrosion products at the end of the exposure period. In order to study the relationship between the fatigue capacity and surface roughness, the surface irregularities were removed by machining the diameter of the wire from 5 mm to 4 mm. The test results indicated that the smoothed reconditioned wires exhibited nearly the same elongation capacity as the undamaged wires. The result indicates that the elongation capacity is more closely related to the surface roughness than the cross-sectional area.



(a) Fatigue life of corroded wire



(b) Elongation of smoothed wires

**Figure 2.4 Fatigue and Elongation Test after Surface Treatment**

### 2.3.2 Corroded Strand

Sason (2002) studied the mechanical properties of 0.5-in. diameter, seven-wire strand at six levels of corrosion. The study was designed to establish a visual standard for evaluation of lightly corroded strands. Industry design guides (PCI 1985, FIP 1991) allow the use of strands with slight amounts of corrosion, but practical techniques for quantifying the extent of corrosion in the field do not exist. Six specimens with different levels of corrosion were tested. The results with visual indicators are presented in Table

2.2. Surface corrosion was removed by rubbing the surface of the strand with a 3M™ brush.




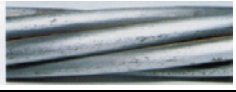








The test results clearly indicate that corrosion damage caused a reduction in the tensile strength and the yield strength, but a clear trend was not observed in the elongation data. It appears that the induced levels of corrosion were too low to generate an appreciable loss in capacity, as all specimens satisfied the strength and elongation requirements in ASTM A 416:

Breaking Strength: 41.3 kip

Load at 1 Percent Extension: 37.2 kip

Ultimate Elongation (24-in. Gauge Length): 3.5 %

**Table 2.2 Visual Indicator and Mechanical Properties of Specimen**

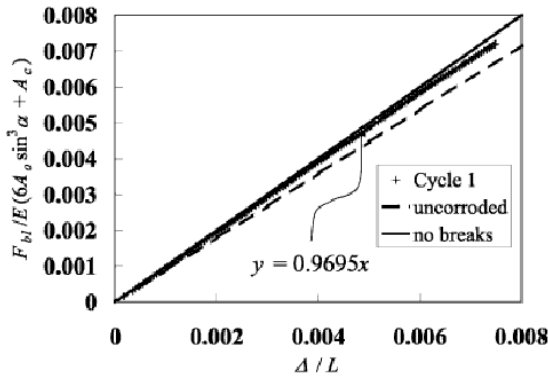
Sample No.	Visual Indicator		Breaking Strength (kip)	Load at 1% Extension (kip)	Ultimate Elongation (%)
	Before Cleaning	After Cleaning			
1			43.8	40.0	5.00
2			43.7	39.8	4.95
3			43.5	39.7	5.73
4			43.3	39.6	5.21
5			42.8	38.9	5.73
6			42.4	38.8	5.21

### 2.3.3 Corroded Strand with Broken Wires

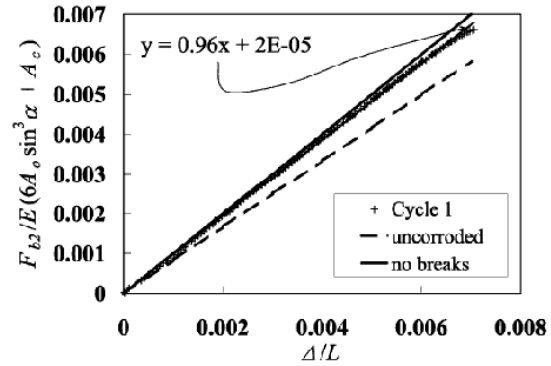
MacDougall et al. (2002) studied the elongation behavior of corroded strands with broken wires. Six specimens were installed in an 18-m (59-ft) long reaction frame and pulled to a maximum elongation of 120 mm (4.7 in.). The diameter of strands was 13 mm (0.5 in.) and the tensile strength of the strand was 1860 MPa (270 ksi). In order to induce corrosion on the surface of the specimens, the wires in the strand were unraveled and exposed to a 5% sodium chloride solution for two weeks. The wires were then reassembled and exposed to an environment of 100% humidity. Two specimens were exposed to the humid environment for 10 days, HC (10), and two specimens for 34 days, HC (34). The other two specimens (LC) were only exposed to the sodium chloride solution. Within each pair of specimens, one wire was cut in one specimen and two wires were cut in the companion specimen. After the environmental exposure, strain gages were attached along the length of the wires.

The measured elongation behavior of HC (10) in the first loading cycle is displayed in Figure 2.5. The continuous line represents the expected behavior of an undamaged strand and the dashed line represents the expected behavior of a strand with the appropriate number of broken wires without consideration of internal friction. The continuous plot of cross marks represents the measured response. The test results revealed that the elongation behavior of corroded strands with one or two wire breaks was linear within the range of applied stress, a maximum stress of approximately 190 ksi. Furthermore, the modulus of the damaged specimens was nearly identical to that of the undamaged strand.

The strain distributions of the lightly corroded strand (LC) with two wire breaks and the heavily corroded strand (HC 34) with two wire breaks are shown in Figure 2.6. The horizontal axis corresponds to distance from midspan of the specimens – wire breaks are located at midspan. The vertical axis represents the normalized strain values.



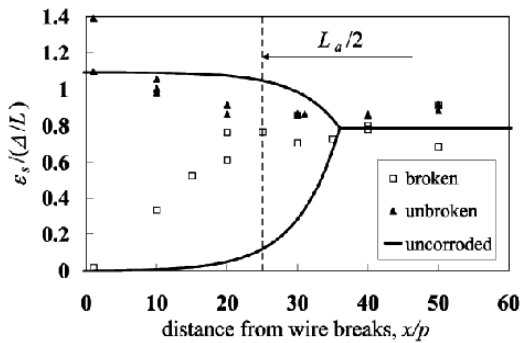
(a) Strand with one wire break



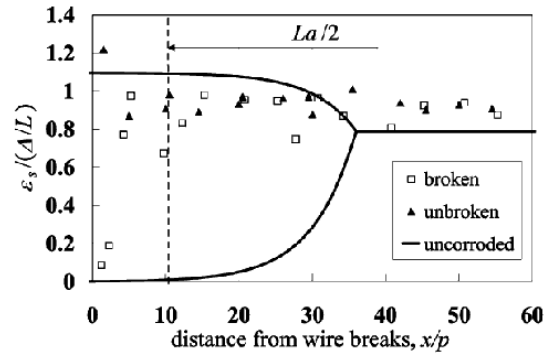
(b) Strand with two wire breaks

**Figure 2.5 Elongation Behavior of Corroded Strand**

The test results indicate that the cut wire recovered axial stress as the distance from the wire break increased. The researchers designated the distance from the point where the original capacity of broken wire was achieved to the location of wire break as a transfer length,  $L_a$ . Based on the results in Figure 2.6, the transfer length is significantly shorter for the heavily corroded strand.



(a) Lightly-corroded strand (LC)



(b) Heavily-corroded strand (HC 34)

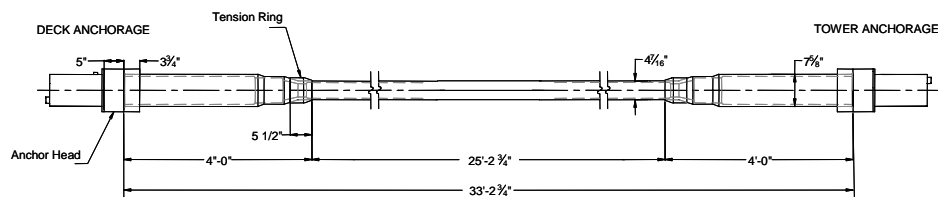
**Figure 2.6 Strain Distribution of Strand with Two Wire Breaks**

The test results suggest the corrosion products influence the elongation behavior of damaged strands. The internal friction due to the geometry of stands and corrosion products compensated for the capacity lost by the two broken wires. However, it should

be noted that wires in the test specimens did not unravel during the tests because the wires were broken before the tensile load was applied.

## 2.4 VARIATION OF LATERAL STIFFNESS WITH FATIGUE DAMAGE

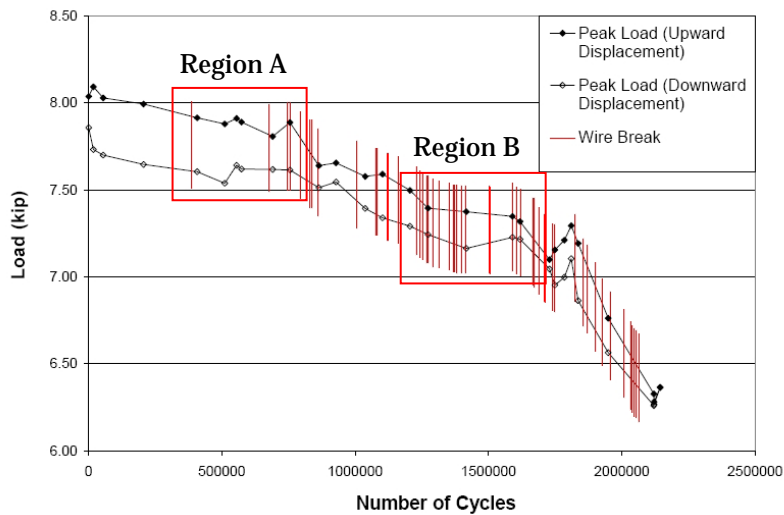
Poser (2001) and Ridd (2004) conducted twelve fatigue tests of full-scale stay cable specimens. The length of specimens was about 33 ft and most of specimens comprised nineteen, 0.6-in. diameter strands stressed to 40% of GUTS (Figure 2.7).



*Figure 2.7 Geometry of Cable Specimen 7*

In many aspects, the structural characteristics of the cable specimens are similar to those of an external tendon. The behavior of both systems is governed by applied prestressing. Also, the cable specimens were constructed using the same components as the external tendons (prestressing strands, cementitious grout, HDPE pipe, and an anchor system). Therefore, it was assumed that the behavior of the large-scale cable specimens was essentially the same as that of an external tendon.

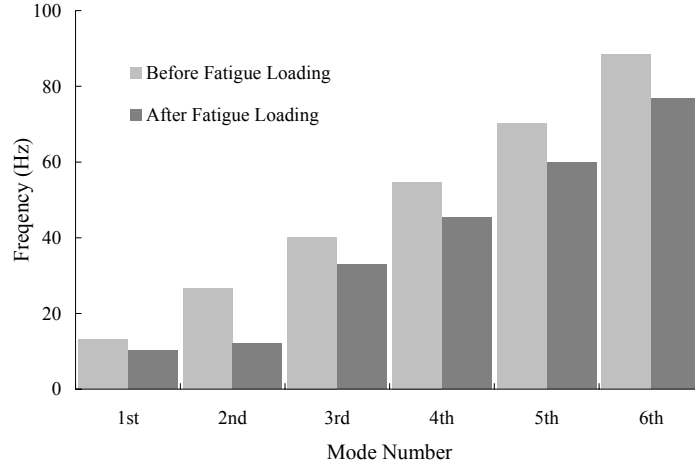
The specimens were subjected to constant-amplitude displacement cycles at midspan and were monitored continuously for wire breaks using acoustic sensors. In Figure 2.8, the peak loads applied to achieve the designated positive and negative displacements for Specimen 9 are shown. For the constant amplitude of  $\pm 1.6$  in., the required load decreased as damage accumulated. The variation of required load was interpreted as the variation of transverse stiffness. The vertical lines on this plot represent wire breaks reported by the acoustic sensors. During the test, wire breaks were concentrated at each end and near midspan of the specimen. The test was terminated after 76 wire fractures were reported over 2,566,000 cycles.



**Figure 2.8 Peak Load during Fatigue Test for Specimen 7 (Ridd 2004)**

The test results indicate that the transverse stiffness was not linearly related to the number of wire fractures. For example, numerous wire fractures occurred in region A and B, but transverse stiffness was nearly constant. The response of region A is particularly important because this region represents the structural behavior at the early stages of deterioration.

The natural frequencies of another specimen, which had nominally the same geometry as Specimen 7, were measured before and after the fatigue tests. The first six modes are plotted in Figure 2.9. During the fatigue tests, the natural frequencies decreased by approximately 20% in each mode, but the second frequency decreased nearly 55%. Because the mass and length of the specimen did not change during the fatigue tests, the differences in the natural frequencies were interpreted as a reduction in the applied tension.



**Figure 2.9 Variation of Natural Frequencies in Cable-Stay Specimen**

## **2.5 INSPECTION OF EXTERNAL POST-TENSIONED TENDONS**

The importance of inspection to detect corrosion damage in post-tensioned tendons was discussed in Section 2.2. Various approaches have been attempted; however, no single inspection technique consistently provides all the needed information. While numerous NDT techniques for civil engineering applications are discussed in documents from ACI Committee 228 (1998) and fib (2003), each method currently has distinct shortcomings for post-tensioned tendons such as significant signal attenuation or safety issues.

In order to conduct a direct investigation of the corrosion potential, electrical inspection technologies, such as the half-cell potential, require that the flow of electrons be measured. Direct contact to the prestressing steel is required to measure the half-cell potential. However, most post-tensioned tendons were not constructed with direct access to the strands. As a result, NDT technologies are generally designed to detect other relevant properties that can be used to infer the condition of the strand, rather than the presence of corrosion itself. Typical corrosion damage of strands (wire breaks and severe pitting) is shown in Figure 2.10.



(a) Fractured Wires



(b) Severe Pitting

***Figure 2.10 Degradation of Strand due to Corrosion (Corven Engineering 2001; Poston et al 2003)***

Inspection methods for post-tensioned tendons are generally designed to detect the presence of two major deficiencies within the tendons: wire breaks and grout voids. While significant loss of cross-sectional area can be caused by pitting corrosion, a wire break often represents the minimum resolution of NDT methods, such as the magnetic-flux method and remanent magnetism method. These methods generate a magnetic field in a discrete distance from the tendon and detect irregularities of the magnetic field caused by discontinuous strands. The tendon can also be scanned using X-ray or ultrasonic methods which are sufficient to identify severe pitting of the strand if the angle of image can be aligned properly with the damaged strands. In general, inspection technologies targeting the detection of wire breaks require precise and heavy equipment and advanced techniques to interpret the data. As a result, these technologies tend to require a long testing period and are quite expensive. Because post-tensioned bridges typically have a large number of external tendons, these methods are only used to evaluate specific tendons, which are suspected of having experienced corrosion damage.

Grout voids are often used as an alternative indicator of potential corrosion damage. The grout is the last barrier against corrosion; therefore, compromised grout implicates significant potential for corrosion damage. Practically, corrosion is not a

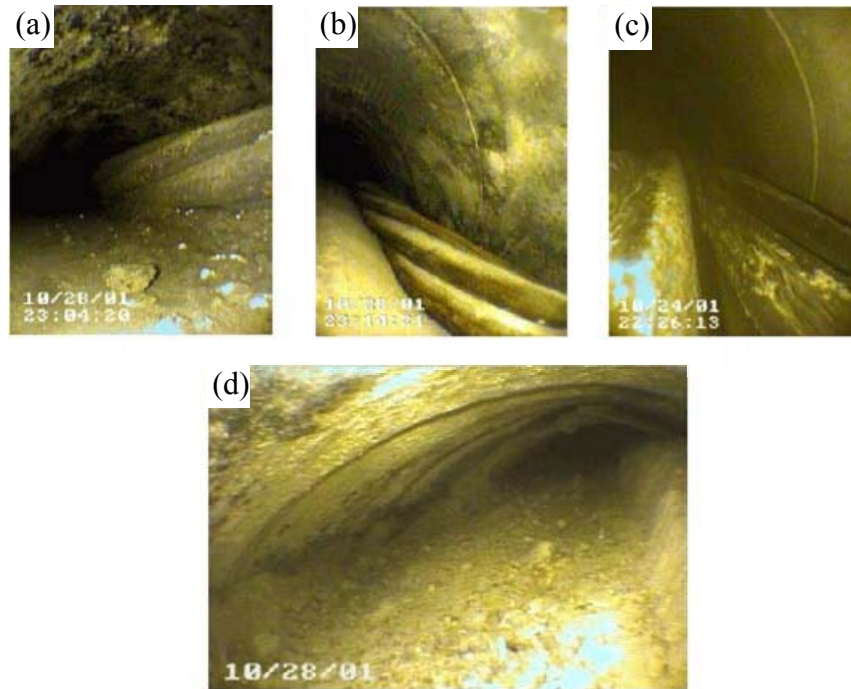


concern in solid grout. Stress wave methods, such as impact echo method, thermal scan or X-ray, can be used for this purpose. These methods idealize the grout as a medium for delivering an input signal, such as a stress wave, and discontinuities are detected in the reflected signals. As a result, these tests are only able to detect the presence of a grout void, but provide no quantitative information about location of the strand relative to the void. Therefore, evaluations based on the presence of a grout void tend to be conservative.

Four video images from an endoscope with different grout void conditions are displayed in Figure 2.11. In (a) and (b), the strands are partially exposed to the air in the duct. In (c), strands are completely exposed to the air. In (d), no strand is exposed within the void. While all images indicate the presence of severe grout voids, the corrective action is different. For example, immediate regrouting may be necessary for the case of (a), (b) and (c), but no action may be necessary for the case of (d). However, because the methods of detecting grout voids can only verify the existence of the grout void, the assessment of grout condition is made based on the worst case scenario.

In North America, the first attempt to identify appropriate NDT methods for detecting the presence of corrosion in post-tensioned tendons was funded by the National Cooperative Highway Research Program (NCHRP) (Ciolko et al. 1999). Fifteen NDT methods were reviewed to assess the feasibility of using the inspection methods to detect corrosion in post-tensioned construction. Each method was evaluated using a variety of criteria. After the assessment, it was concluded that none of the NDT techniques reviewed was sufficient to satisfy the intended criteria in terms of precision and accuracy.

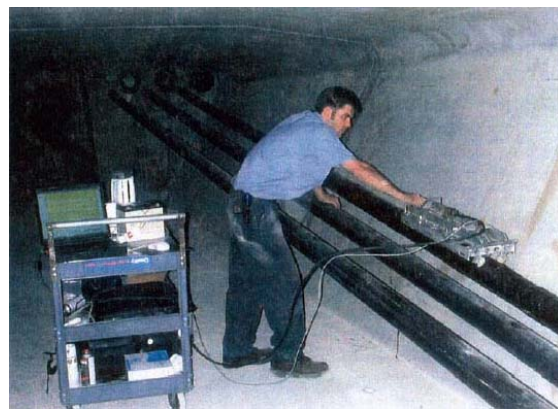
In 2001, the Florida Department of Transportation initiated a state-of-the-art inspection program for detecting corrosion damage in external tendons in the Mid-Bay Bridge (Corven Engineering 2001). Three techniques including the borescope inspection, the vibration technique, and the magnetic-flux method were used. In addition, visual inspection and soundings were used to identify tendons with likely corrosion problem (Figure 2.12).



**Figure 2.11 Visual Grout Void Results from Bore Scope: (a),(b) Partial strand exposure, (c) Complete strand exposure, (d) No strand exposure (DMJM Harris 2003)**



**(a) Vibration Technique**



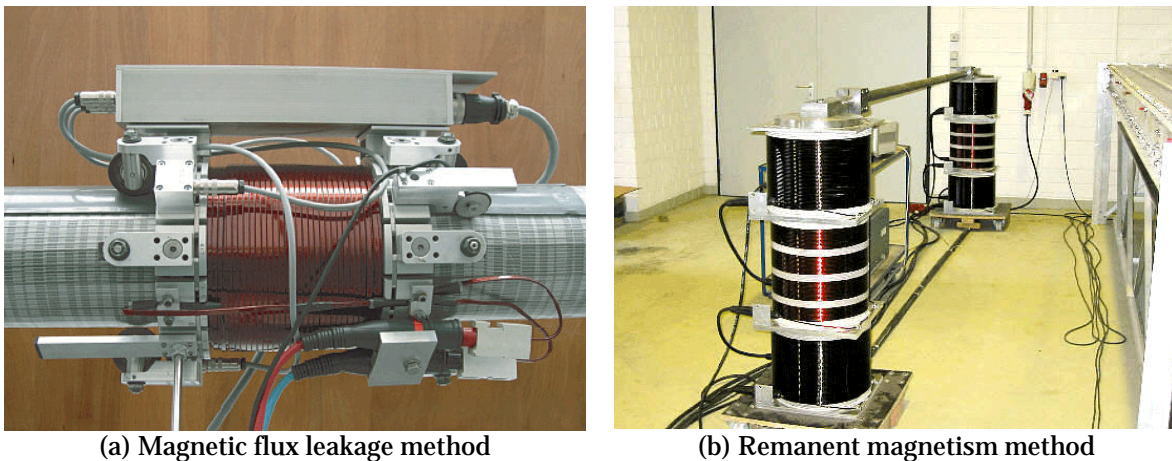
**(b) Magnetic-Flux Method**

**Figure 2.12 Mid-Bay Bridge Inspection Program (Corven Engineering 2001)**

The borescope inspection was considered as to be the only effective method for investigating anchorage regions due to congestion of the reinforcement and the presence

of large concrete diaphragms. Both vibration and magnetic-flux methods detected general corrosion damage, but the resolution and accuracy of the methods were still questioned.

At present, it appears that the reliability of NDT techniques for the evaluating external tendons is still not sufficient. Currently, each NDT technique provides partial information about the extent of damage within the tendon. Additional research to detect corrosion in the external tendons is underway. In 2003, various advanced technologies, such as the magnetic flux leakage method and remanent magnetism method, were suggested during an international symposium in Berlin (Figure 2.13). Time domain reflectometry techniques, where a probe is embedded in the external tendon during construction, are being developed by Chajes et al. (2003).



*Figure 2.13 Equipment used for NDT of Tendons  
(Bergamini et al 2003; Scheel et al 2003)*

## 2.6 VIBRATION TECHNIQUE

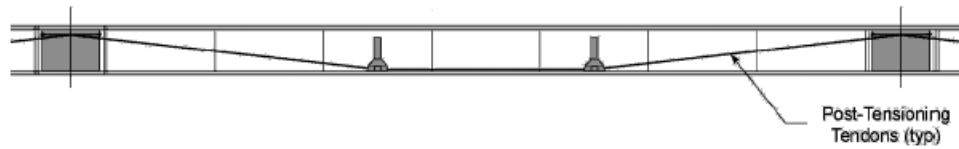
The vibration technique was selected for detailed study in this investigation. A distinct advantage of this method is the relatively low cost of the equipment needed and the relative ease of interpreting the measured response. The vibration technique is used to assess the global integrity of a structure by measuring the natural frequencies. Because

the natural frequencies are related to the mass and stiffness of the structure or component, a reduction in stiffness should be accompanied by a reduction in the natural frequencies (Eq. 2.1). Furthermore, it should be noted that the vibration technique is strictly only valid when the behavior of the structure is in the elastic range of response.

$$m\ddot{x} + kx = 0, \quad \omega = \sqrt{\frac{k}{m}} \quad (\text{Eq. 2.1})$$

where  $m$  = mass,  $k$  = stiffness,  $\omega$  = circular natural frequency (rad/sec)

In order to apply the vibration technique to post-tensioned tendons, assumptions must be made about the boundary conditions. As shown in Figure 2.14, a continuous tendon is often divided into multiple sections by deviators. The displacements at each end of the tendon and at the intermediate supports are typically assumed to be zero. Each segment of an external tendon may then be assumed to be an individual structural element. Therefore, the measured natural frequencies represent the response of the individual segments. Differences between the responses of nominally identical segments were used as an indication of the presence of damage within the tendon.



*Figure 2.14 Mid-Bay Bridge Span Layout (Corven Engineering 2001)*

### 2.6.1 Frequency-Domain Data

The acceleration response of the structure is measured in the time domain and transferred into the frequency domain to evaluate the natural frequencies. The discrete Fourier transform (DFT) was used in this investigation. The DFT is based on the principle of Fourier series which states that any arbitrary function can be equivalently

represented by the infinite summation of harmonic functions with various periods and amplitudes.

The definition of DFT is given in Eq. 2.2:

$$X_m = \sum_{t=0}^{N-1} x_t \exp(-2\pi i t(m/N)) \quad (\text{Eq. 2.2})$$

where  $x_t = [x_0, x_1, \dots, x_{N-1}]$ ,  $m = [0, 1, 2, \dots, N-1]$

where  $x_t$  represents a time series and  $N$  represents the number of total samples. The resolution of the transformed series in the frequency domain is determined by the number of samples and the sampling period:

$$\Delta f = 1/(N\Delta t) \quad (\text{Eq. 2.3})$$

where  $\Delta f$  = resolution in frequency domain,  $\Delta t$  = sampling period

It is important to use a sample rate that is sufficient to capture the desired frequency response. Sampling theory states that digital data can be reproduced if the frequency is less than the Nyquist frequency:

$$f_{Nyquist} = 1/(2 \cdot \Delta t) \quad (\text{Eq. 2.4})$$

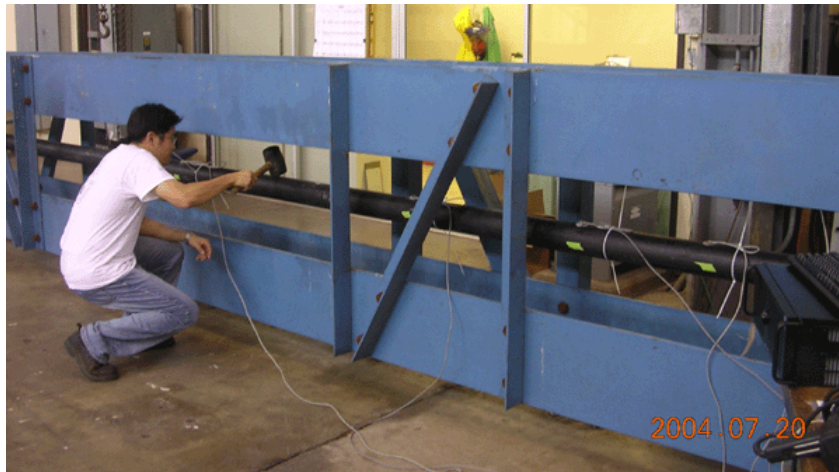
As a result, the Nyquist frequency is often used for the criteria to determine the capacity of DAQ system. The measured response of civil engineering structures often includes a considerable amount of noise. Therefore, it is customary to design the DAQ system conservatively. For example, Sansalone (1997) recommended using a sampling rate that is capable of capturing a maximum frequency that is 10 times the desired maximum frequency.

## 2.6.2 Vibration Technique Applied to External Post-Tensioned Tendons

Application of the vibration technique to external tendons is straight forward. External tendons are typically relatively simple structural systems. Continuous tendons are typically divided into multiple 30 to 50-ft long segments by deviators and diaphragms (Figure 2.14), and are typically stressed to 70 to 80% of GUTS. As a result of the relatively short length of each segment and high level of prestress, the initial position of

the tendon can typically be assumed to be straight. Therefore, the behavior of external tendon can be interpreted to be dominated by the applied tension without considering the geometric nonlinearities.

Because external tendons are enclosed within a concrete box girder, the inspector typically has access to the duct along the length of the external tendon. This provides flexibility in selecting the locations of sensors and the locations where the vibrations are induced (Figure 2.15). The measured natural frequencies are sensitive to the corresponding mode shapes; therefore, direct access permits the most efficient sensor locations to be selected.



***Figure 2.15 Preliminary Vibration Test for Cable Specimen***

The vibration technique was used during the detailed inspection of the Mid-Bay Bridge in northwest Florida in 2000 (Corven Engineering 2001). As shown in Figure 2.14, each tendon in the bridge is divided into three segments by the deviators, and each segment of each tendon was evaluated independently during the inspection. Vibrations were induced in the tendons by striking the duct with a hammer and the resulting acceleration response was recorded. The first two natural frequencies were extracted from the measured response and used to evaluate the condition of each tendon.

Each segment of tendon was idealized as having fixed boundary conditions at the ends and constant values of mass per unit length,  $m$ , and flexural stiffness,  $EI$ , along the length  $L$ . The governing differential equation corresponding to a stiff string (Eq. 2.5) was used to relate these parameters to the measured natural frequencies.

$$T \frac{\partial^2 y}{\partial x^2} - EI \frac{\partial^4 y}{\partial x^4} = m \frac{\partial^2 y}{\partial t^2} \quad (\text{Eq. 2.5})$$

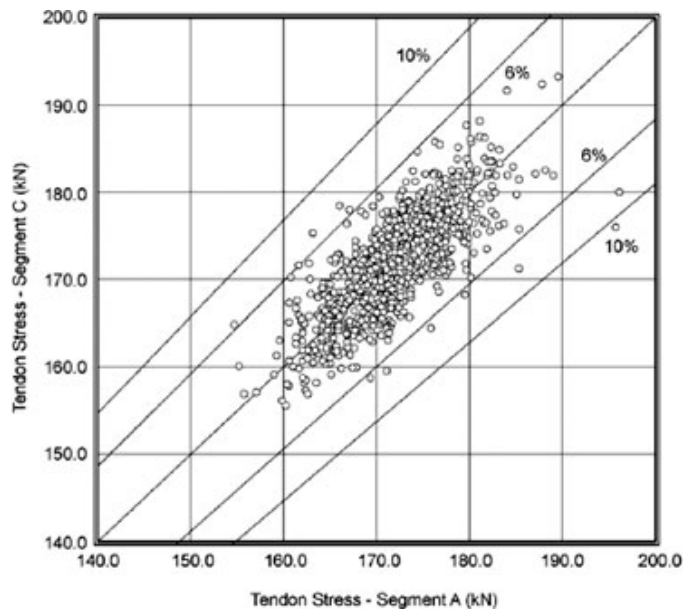
where  $T$  = applied tension,  $E$  = elastic modulus,  $I$  = moment of inertia, and  $m$  = mass per unit length

Additional information about this model and the corresponding natural frequencies is given in Chapter 6.

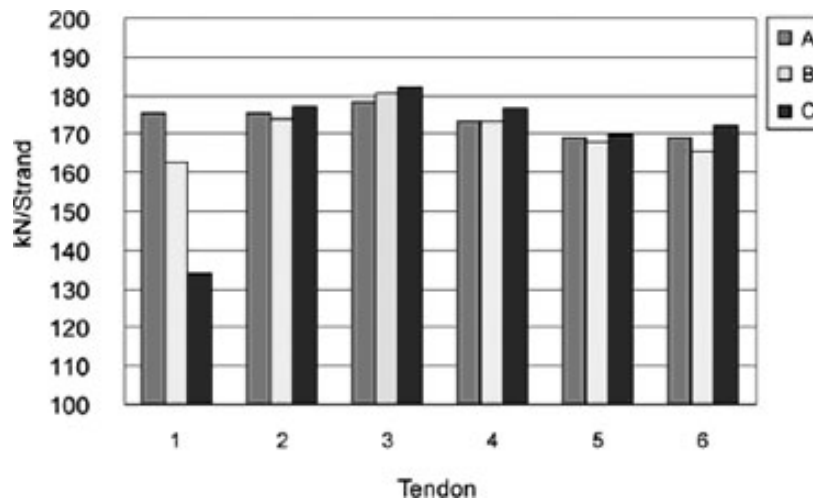
Values of  $m$  and  $EI$  were calculated based on the geometry of the tendon cross section and the specified material properties. The measured clear length of each segment was used. The values of  $T$  corresponding to both of the measured frequencies were calculated, and the average of these values was used in subsequent analyses.

In the absence of corrosion damage, the calculated value of the applied tension was expected to be equal in the three segments of each tendon. However, minor variations were observed. The results from 140 spans, each containing six tendons, are plotted in Figure 2.16. In all tendons, segment A corresponds to the section of tendon between the south diaphragm and the south deviator, segment B corresponds to the middle section of tendon, and segment C corresponds to the section of tendon between the north deviator and the north diaphragm (Figure 2.14). Variations in the calculated tension on the order of  $\pm 6\%$  were common, and interpreted to mean that significant damage had not occurred within the tendon. In contrast, differences on the order of 25% were observed in one tendon from Span 9 (Figure 2.17). Subsequent investigation of the north segment of this tendon indicated the presence of severe corrosion and wire breaks (Corven Engineering 2001).





**Figure 2.16** *Tensile Stress per Strand Extracted from Measured Frequencies in Tendons on the Mid-Bay Bridge (Corven Engineering 2001)*



**Figure 2.17** *Variations in Tensile Forces Calculated for Each Segment of Tendon in Span 9 of Mid-Bay Bridge (Corven Engineering 2001)*

The vibration technique is considered to be most appropriate for identifying tendons that have experienced significant levels of damage. Conducting vibration tests of all the tendons provides information about the expected variability of the measurements and detailed inspections can then be focused on the tendons that exhibited large



differences in the calculated tensile stresses. The primary limitation of the vibration technique is that the underlying analytical model is based on the assumption of fixed boundary conditions and uniform distributions of mass and flexural stiffness along the length of the tendon. These conditions are often not present in the actual tendon (Sagüés 2004).

### **Chapter 3: Uniaxial Tests of Individual Strand**

Prestressing strand is used as the primary structural component in post-tensioned tendons. During design, the strand is typically idealized as having a circular cross section with a cross-sectional area equal to the total area of the wires. However, the helical arrangement of the seven wires influences the axial response of the strand, especially when the strand has sustained damage. A series of uniaxial tests of strand are discussed in this chapter to obtain basic information about the stress-strain behavior of strand.

The results of nineteen tests are reported in this chapter. The specimens may be divided into four groups depending on the type of damage induced:

- (1) The prefix “UND” is used to identify the undamaged specimens. Five specimens were tested in this group.
- (2) The prefix “COR” is used to identify the specimens with uniform corrosion on the surface of the wires before the tension tests. The level of corrosion was varied by increasing the length of the time that the specimens were exposed to a saltwater environment. Two specimens were tested at each of three levels of corrosion.
- (3) The prefix “CUT” is used to identify the specimens where individual wires were cut before the tension tests. Two specimens were tested with one cut wire and two specimens were tested with two cut wires.
- (4) The prefix “DEF” is used to identify the specimens where an intentional defect in one wire was created before the tension tests. One wire was partially cut to measure the stress redistribution that occurs after a wire fractures. Four specimens with initial defects were tested.

Parameters measured during the tests included the tensile strength, modulus of elasticity, and apparent modulus of elasticity of the strand (Table 3.1). The tension tests were conducted in three phases and the testing procedures and instrumentation varied in each phase. All specimens, however, were taken from the same spool of strand. The

mechanical properties of the strand, as reported on the mill certificate, are summarized in Table 3.2.

The setup for each phase of testing is discussed in Section 3.1. The procedures used to induce damage in the test specimens are described in Section 3.2, and the test results from each phase are summarized in Section 3.3 through Section 3.5.

**Table 3.1 List of Single Strand Specimens**

	<b>Damage</b>	<b>Phase</b>	<b>Tensile Strength</b>	<b>Elastic Modulus</b>	<b>Apparent Modulus</b>
UND 1	None	1		x	x
UND 2	None			x	x
UND 3	None			x	x
UND 4	None	2	x		
UND 5	None		x		
COR 1	2-mo exposure			x	x
COR 2	2-mo exposure			x	x
COR 3	4-mo exposure		x	x	x
COR 4	4-mo exposure		x	x	x
COR 5	5.5-mo exposure		x	x	x
COR 6	5.5-mo exposure		x	x	x
CUT 1	1 wire cut		x		
CUT 2	1 wire cut		x	x	x
CUT 3	2 wires cut		x		
CUT 4	2 wires cut	x	x		
DEF 1	1 wire with initial defect	3			x
DEF 2	1 wire with initial defect				x
DEF 3	1 wire with initial defect				x
DEF 4	1 wire with initial defect				x

**Table 3.2 Mechanical Properties of Strand Reported on Mill Certificate**

<b>Grade</b>	<b>270</b>
Diameter	0.6 in.
Modulus of elasticity	28,300 ksi
Min. breaking strength	60.266 kip
Min. yield strength	53.973 kip
Nominal area	0.2204 in <sup>2</sup>

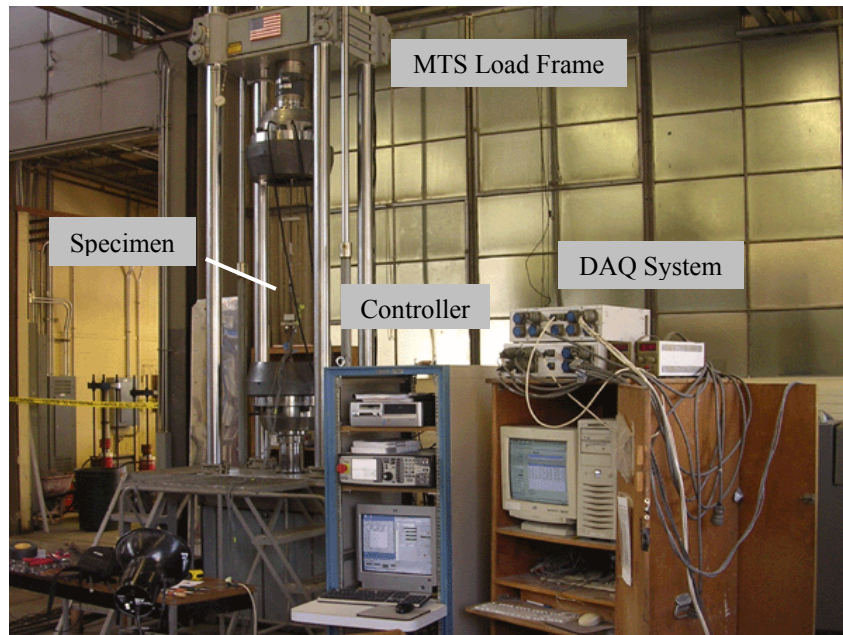
### **3.1 TEST SETUP**

The uniaxial tests were performed in three phases and the test setup was different in each phase. In the first phase, an MTS load frame was used. Details of these tests are summarized in Section 3.1.1. An SATEC load frame was used in the second phase of tests, and details are presented in Section 3.1.2. A steel frame with a hydraulic ram was used in the third phase. The configuration of these tests is discussed in Section 3.1.3.

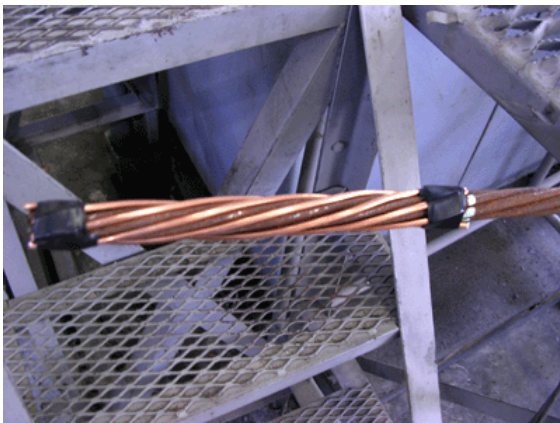
#### **3.1.1 Phase 1**

The 220-kip MTS load frame (model 311.31) was used for the first phase of uniaxial tests (Figure 3.1). Hydraulic grips were located in the top and bottom cross heads. The load frame was operated using PC-based software (MTS Flex Test<sup>TM</sup> Manager, version 3.50).

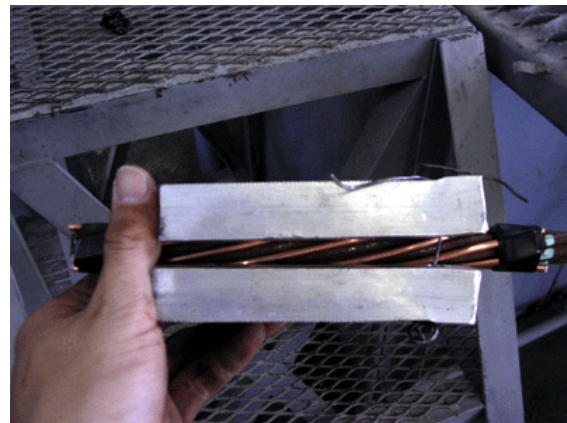
Aluminum blocks with six copper wires (Heller 2003) were used to grip the strand for the uniaxial tests (Figure 3.2). Two 8-in., smooth, aluminum blocks surrounded the copper wires and the strand at each end, and the assembled blocks were clamped in the cross heads. This method held the strand in the elastic range but the strand tended to slip before the specimen reached its tensile capacity. As a result, the aluminum blocks were not used in the later phases of the investigation.



*Figure 3.1 Load Frame for First Series of Strand Tests*



(a) Copper wires

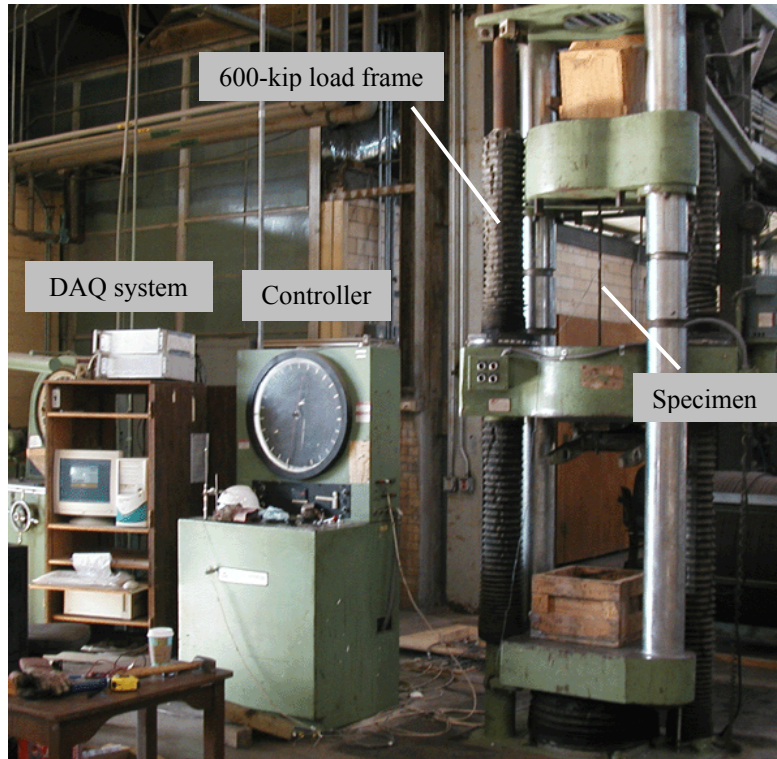


(b) Assembly of aluminum blocks

*Figure 3.2 Aluminum Block for Strand Grip*

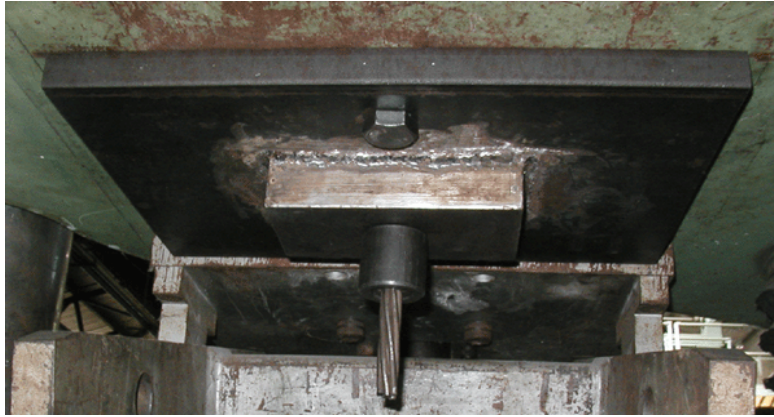
### 3.1.2 Phase 2

A 600-kip SATEC uniaxial test machine (model 600HVL) was used for the second series of tests (Figure 3.3). This testing machine has three cross heads and the top and bottom cross heads are linked rigidly.



*Figure 3.3 Load Frame for Second Series of Strand Tests*

Steel plates with a 5/8-in. diameter hole were positioned above the top and below the middle cross heads. The plates supported the mono strand anchors (Hayes Industries, Model F 5600), which were used to grip the strand (Figure 3.4). The details of the steel plates and the anchor heads are presented in Appendix A.



***Figure 3.4 Anchor below Middle Cross Head in Second Series of Tests***

The relative displacement between the top and middle cross heads was monitored using a linear potentiometer (Figure 3.5) which was located on the floor and measured the vertical displacement of the bottom cross head. The recorded displacement was equivalent to the relative displacement between the top and middle cross heads because the bottom and top cross heads are linked rigidly and the specimen was loaded by moving the top cross head only.

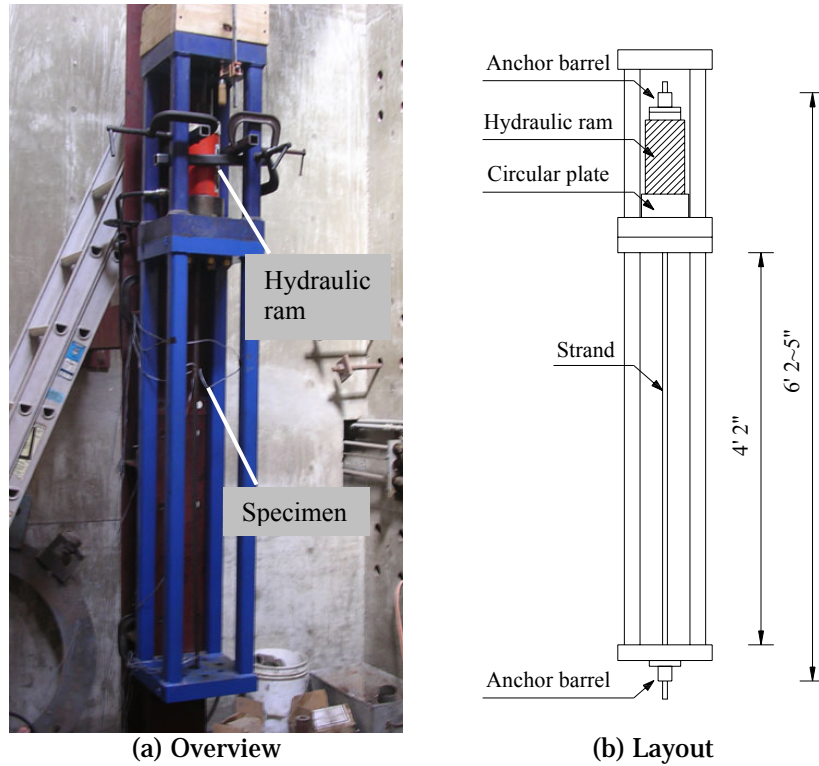


***Figure 3.5 Linear Potentiometer Used to Measure Relative Displacement between Cross Heads***



### 3.1.3 Phase 3

In phase 3, the strands were tested in an assembly comprising four steel plates supported by four posts (Figure 3.6). Each plate had a 1.5-in. diameter hole at the center to accommodate the strand and the posts were welded to the plates. The test frame consisted of two parts. A 60-kip hydraulic ram was positioned in the upper frame where a 3-in. thick circular plate was located to distribute stress evenly. The specimens were positioned in the lower frame, which accommodated a specimen free length of 50 in. The specimen was gripped using the mono strand anchors used in Phase 2 at each end.



**Figure 3.6 Test Setup Used in Phase 3**



## **3.2 PREPARATION OF DAMAGED SPECIMENS**

Damage of the strand was simulated using two methods: uniform corrosion on the surface of the strand and mechanical damage to individual wires. These techniques are discussed below.

### **3.2.1 Uniformly Corroded Strands**

A saltwater solution was used to induce corrosion on the surface of the strand. Six-ft lengths of strands were stored outside the Ferguson Structural Engineering Laboratory. On days when the surface of the strand was dry, a 3% solution by weight of sodium chloride was sprayed on the strand twice daily. If the strands were wet due to rain or high atmospheric humidity, saltwater was not sprayed on the surface.

The exposure test began on February 16, 2006. The first group of specimens was moved inside after two months, the second group were moved inside after four months, and the last group was moved inside on July 28, 2006 after 5.5 months of exposure. Once inside, the specimens were stored in an air-conditioned area within the laboratory and not exposed to moisture. The tests of all corroded strands were conducted in August 2006.

The uniformly corroded specimens were intended to provide information about how the structural properties were influenced by corrosion products and the corresponding reduction of cross-sectional area. Photographs of the test specimens and companion 6-in. specimens, which were exposed to the same environmental conditions, are shown in Figure 3.7.



(a) Specimens on February 16, 2006



(b) Specimens after first month exposed to salt water

***Figure 3.7 Uniformly-Corroded Specimens***

### 3.2.2 Estimated Weight Loss

A series of 6-in. sections of strand were also corroded by spraying the surface with salt water. These specimens were used to estimate the percentage of steel lost due to corrosion.

The ends of the specimens were restrained with tape and zip ties to protect the wires from unraveling (Figure 3.8) and a transparent plastic sealant was used to protect the ends of the wires from corrosion. The weight of each specimen was recorded before the exposure tests were started and at the end of the exposure tests.



*Figure 3.8 Specimen Preparation*

Before weighing the specimens, the corrosion products were removed using the chemical cleaning procedures described in ASTM G1-03 C.3.5 (2003), which are summarized in Table 3.3. The specimens were submerged in a 37.2% hydrochloric acid (SafeCote®, A114S-212). Due to the complex geometry of the strand, two modifications were made to the ASTM G1 procedures:

- (1) Corrosion products were removed from the surface of the strand using a brass, wire brush before soaking in the acid.
- (2) Specimens were submerged for 20 min, as the recommended interval of 10 min was insufficient to remove the corrosion.

***Table 3.3 Chemical Cleaning Procedures in ASTM G1 (2003)***

<b>Designation</b>	<b>Material</b>	<b>Solution</b>	<b>Time</b>	<b>Remark</b>
C.3.5	Iron and Steel	500 ml hydrochloric acid (HCl sp gr 1.19)	10 min	Longer time maybe required in certain instances

The final procedures are summarized below and photographs of the specimens are shown in Figure 3.9.

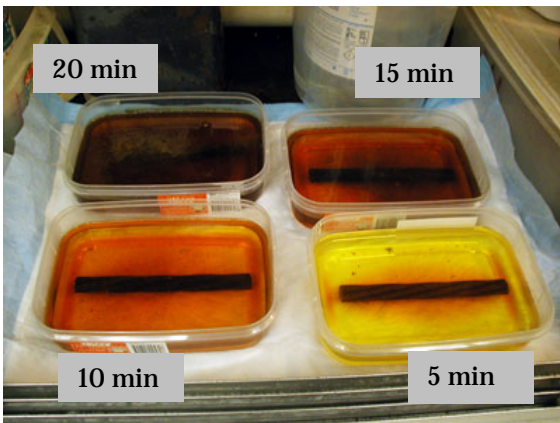
- Remove cable ties from ends of specimens
- Remove corrosion products from surface of strand using brass wire brush
- Submerge specimen in the hydrochloric acid for 20 minutes
- Rinse specimen with distilled water
- Rebrush if necessary
- Evaporate remaining water using heat gun
- Measure weight of specimen using electric balance



(a) Specimens after 2 mo exposure



(b) After cleaning with wire brush



(c) Acid immersion



(d) After acid immersion of 20 min

***Figure 3.9 Procedures Used to Remove Corrosion Products***

### **3.2.3 Mechanically Damaged Strands**

The reduction of cross-sectional area caused by completely corroded or fractured wires was simulated by cutting one or two wires before testing. Different techniques were used to cut the wires in Phase 2 and Phase 3. In Phase 2, the wires were cut completely before the tensile loads were applied. In Phase 3, a nick was formed in a single wire, but the damaged wire was still intact at the beginning of the tension test.



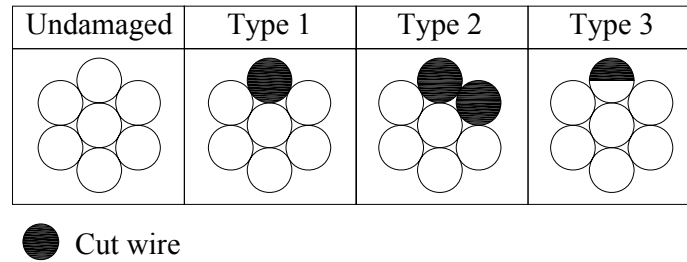
In order to avoid damaging adjacent wires when cutting wires in Phase 2, the specimens were supported in a vise and vise grips were used to unravel all outer wires along approximately one-half the length (Figure 3.10). A small steel plate was wedged between wires and the strand was retightened. A grinder was used to cut the desired number of wires, and then the steel plate was removed.



*Figure 3.10 Simulation of Broken Wires in Phase 2*

In phase 3, a portion of a single wire was cut, but the wires were not unraveled before grinding the wire. The cut was sufficiently small that the adjacent wires were not damaged.

As shown in Figure 3.11, four different cross sections were tested: undamaged (zero cut wires), type 1 (one cut wire), type 2 (two cut wires), and type 3 (one partially cut wire). Type 1 and 2 represented the possible reduction of cross-sectional area due to extensive corrosion damage. Specimens with these types of damage were tested during Phase 2. Type 3 specimens were selected to measure the stress redistribution caused by a wire fracture, and were tested during Phase 3.



**Figure 3.11 Cross Sections Tested in Phases 2 and 3**

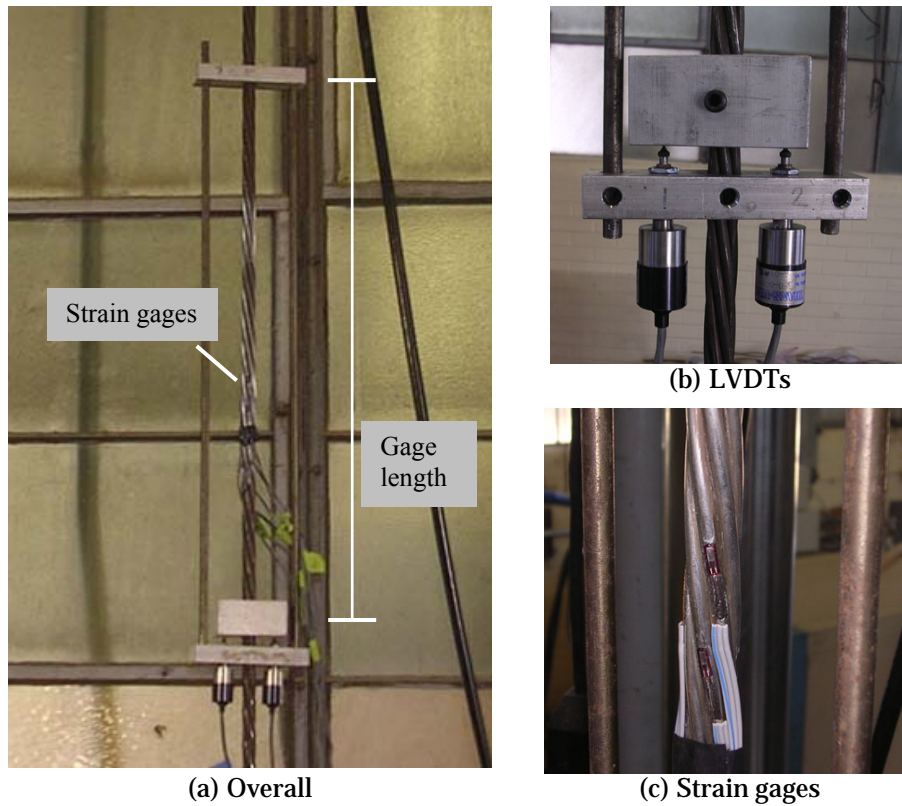
### 3.3 PHASE 1 TESTS

The tests in the first phase are described in Bean (2006) and were used to characterize the mechanical properties of the strand used to construct the cable specimens. The test specimens were subjected to two cycles of loading to a maximum of 30 kip in load increments of 2 kip. Data measured during the second loading cycle are plotted in this section.

#### 3.3.1 Elastic Modulus

The elastic modulus of specimens, UND 1 through UND 3 was determined from the measured axial load and axial displacement of the strand. Axial displacements were measured using the apparatus designed by Heller (2003). Two aluminum blocks were attached to the strand with a gage length of 24 in. Two displacement transducers with a range of  $\pm 0.05$  in. were threaded into a third aluminum block which was not attached to the strand, but was connected to the top block by two unstressed rods. The transducers measured the relative displacement between the two blocks attached to the strand (Figure 3.12).

The stress in the specimen was calculated by dividing the measured load by the area of the strand reported on the mill certificate (Table 3.2). The axial strain in the strand was calculated by dividing the average displacement from the two transducers by the gage length of 24 in.



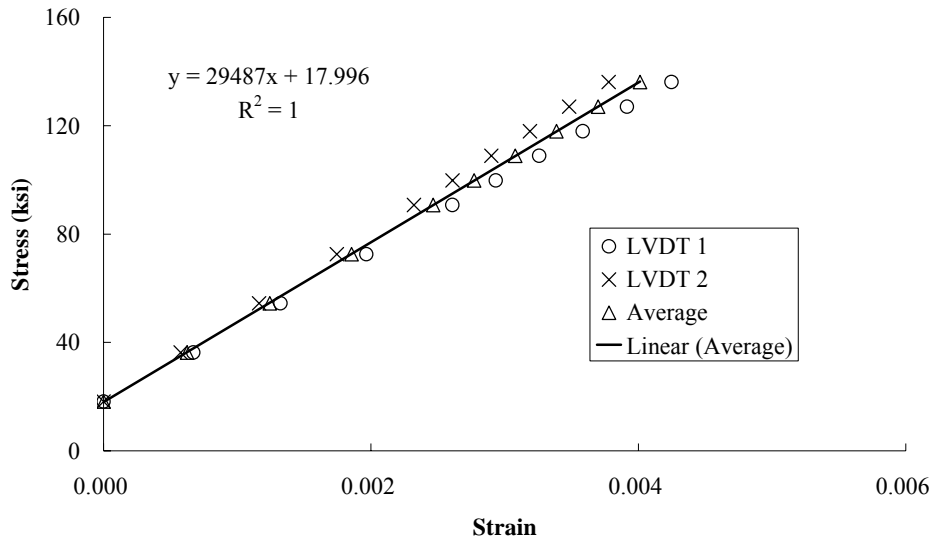
***Figure 3.12 Instrumentation Used to Measure Elongation and Strain in Phase 1***

Test results are summarized in Table 3.4 and displayed in Figure 3.13 through Figure 3.15. The elastic modulus was determined using a least-squares fit to the data. The measured displacements varied linearly with the applied load.

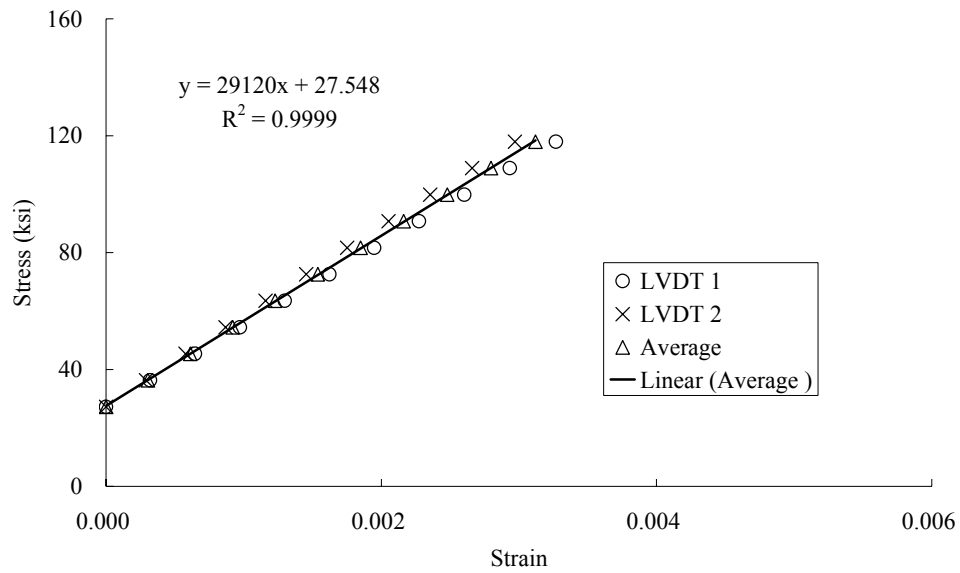


**Table 3.4 Elastic Modulus of Strand**

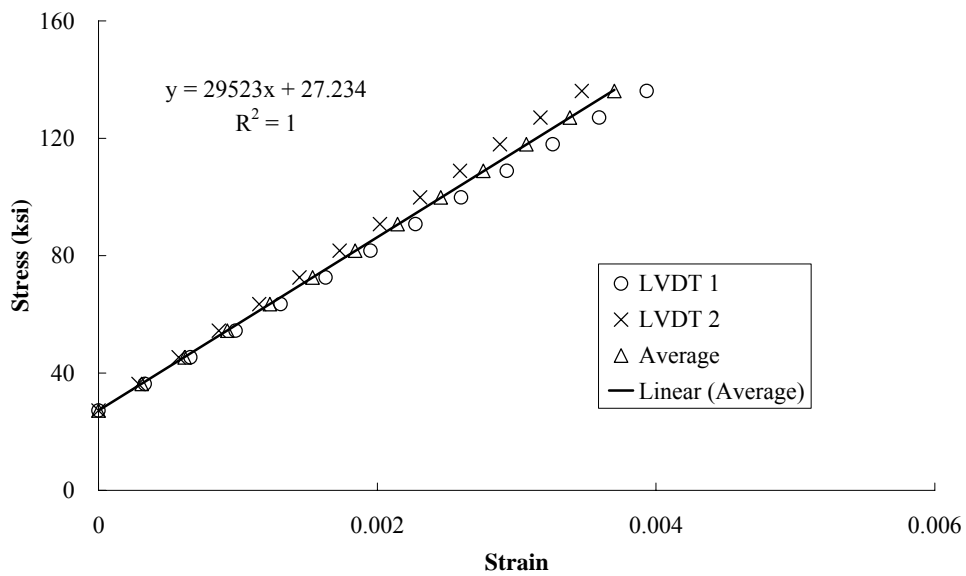
	Modulus of Elasticity (ksi)
UND 1	29,500
UND 2	29,100
UND 3	29,500
Average	29,400



**Figure 3.13 Stress-Strain Relationship for UND 1**



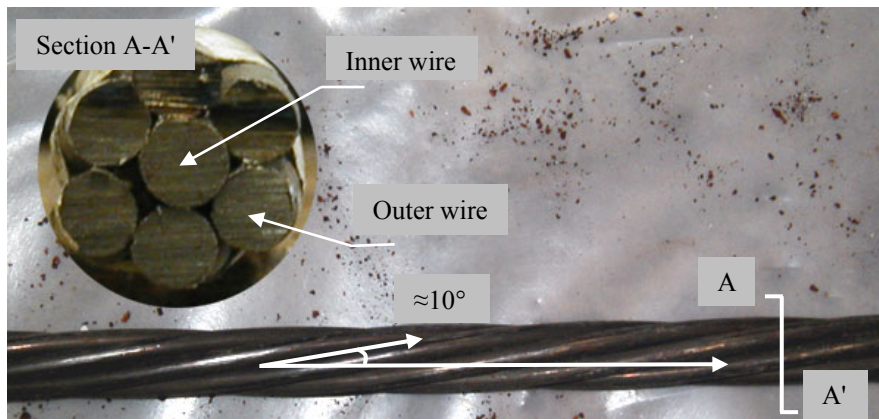
**Figure 3.14 Stress-Strain Relationship for UND 2**



**Figure 3.15 Stress-Strain Relationship for UND 3**

### 3.3.2 Apparent Modulus of Elasticity

For the 0.6-in. diameter strand used in this investigation, the longitudinal axes of the outer wires were rotated approximately  $10^\circ$  from the longitudinal axis of the strand (Figure 3.16). The strain gages were attached to the outer wires of the strand and aligned along the axis of the individual wires (Figure 3.12c, Figure 3.17). The number of strain gages varied from six for specimen UND 1 to two for specimen UND 2. The results are summarized in Table 3.5 and measured data are plotted in Figure 3.18 through Figure 3.20.



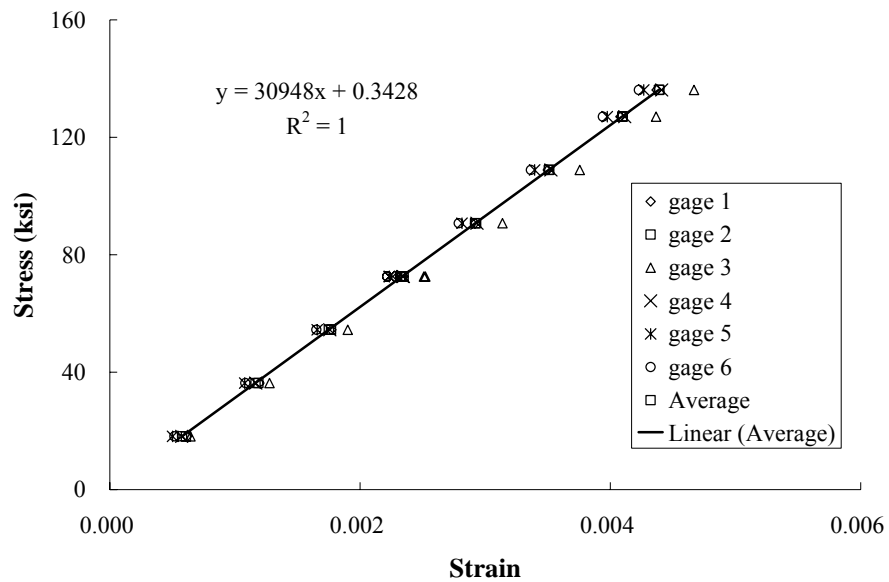
*Figure 3.16 Geometry of Strand Specimen*



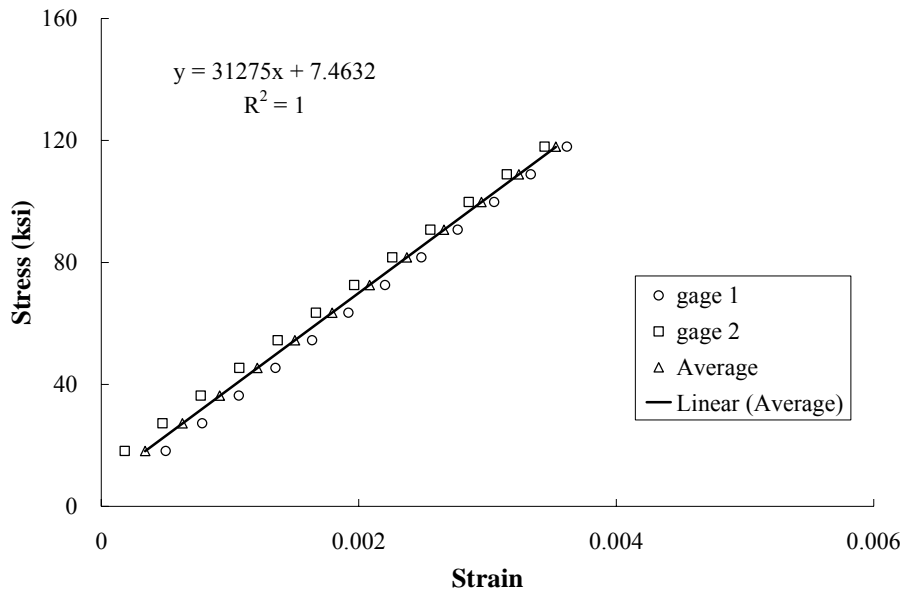
*Figure 3.17 Strain Gages Positioned along Longitudinal Axes of Wires*

**Table 3.5 Apparent Modulus of Elasticity of Strand**

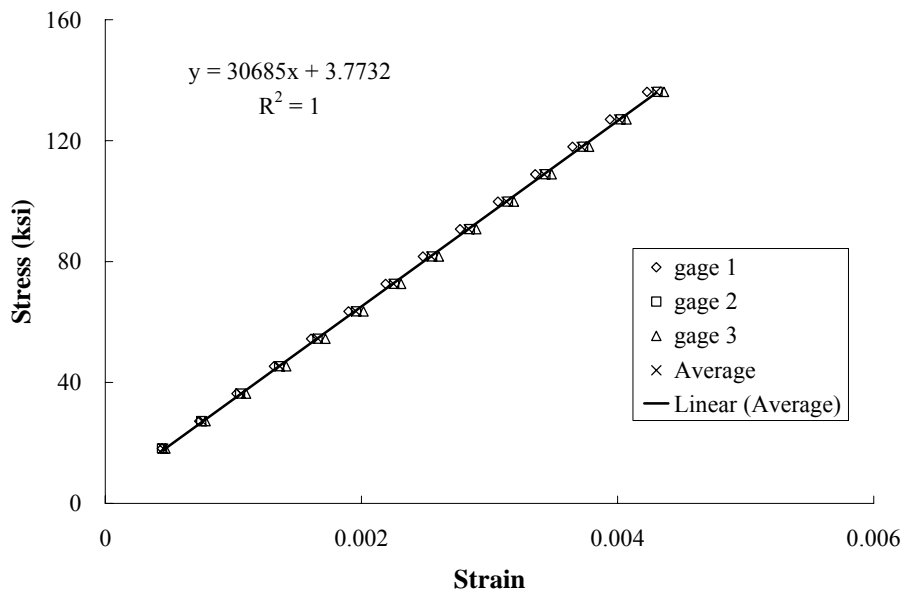
Strand	Gage	Apparent Modulus of Elasticity (ksi)
UND 1	1	31,030
	2	30,950
	3	29,500
	4	30,480
	5	30,880
	6	31,380
UND 2	1	32,020
	2	30,570
UND 3	1	31,140
	2	30,500
	3	30,430
Average		30,800



**Figure 3.18 Apparent Stress-Strain Relationship for UND 1**



**Figure 3.19 Apparent Stress-Strain Relationship for UND 2**



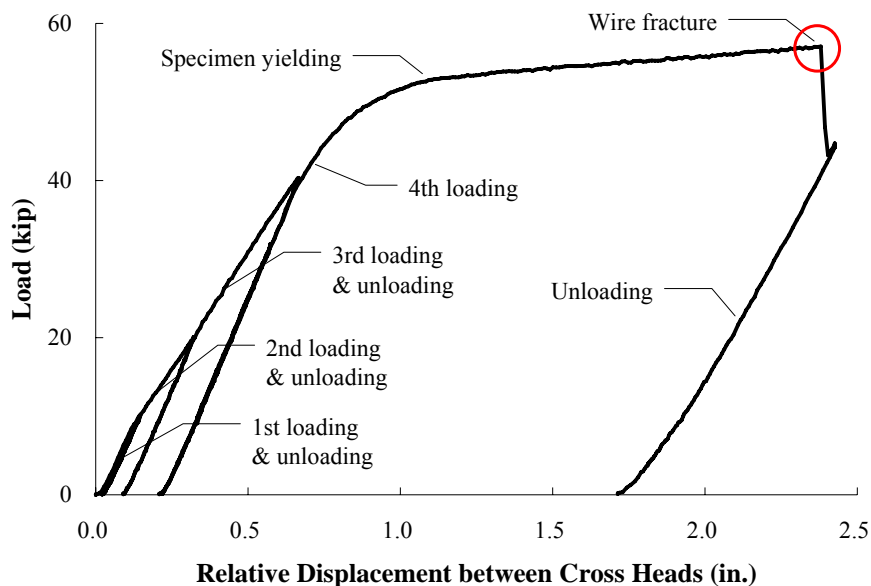
**Figure 3.20 Apparent Stress-Strain Relationship for UND 3**

Based on the test results from specimens UND 1 to UND 3, the modulus of elasticity was determined to be 29,400 ksi and the apparent modulus of elasticity was determined to be 30,800 ksi. The apparent modulus is approximately 5% larger than the modulus of elasticity, which indicates that higher stresses are likely to develop in outer wires of the strand than in an idealized solid bar at the same axial elongation.

Heller (2003) measured the elastic modulus and apparent modulus for twelve, 4-ft long sections of 0.5-in. diameter strands. He reported averaged values of 31,200 ksi for apparent modulus and 29,400 ksi for elastic modulus.

### 3.4 PHASE 2 TESTS

Unlike the tests in Phase 1, where hydraulic pressure was used to grip the specimens, which could be released without damaging the specimens, the anchors used in Phase 2 could not be released. Therefore, most of specimens in Phase 2 were tested to failure.

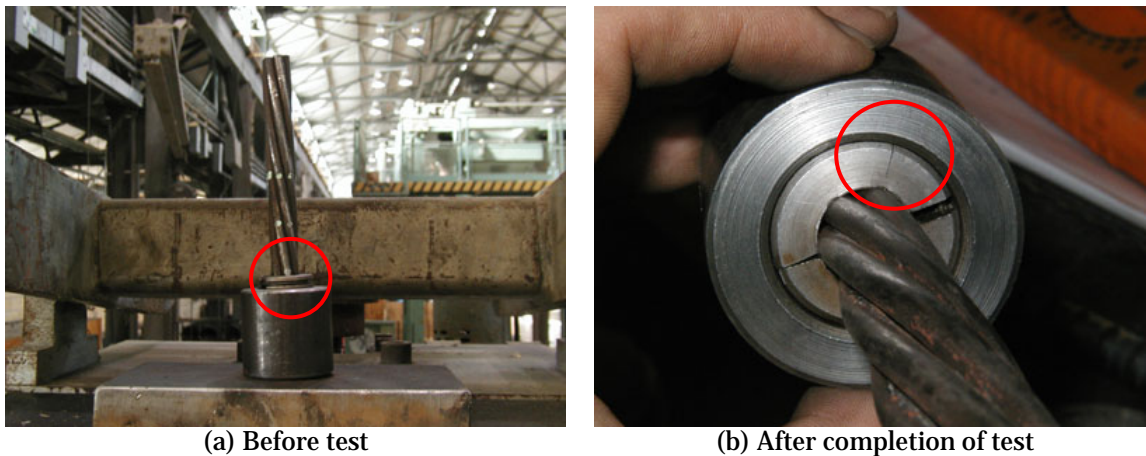


*Figure 3.21 Representative Load and Displacement Relationship in Test Series 2*

A representative load-displacement curve recorded by the linear potentiometer is shown in Figure 3.21. The specimens were typically subjected to four loading cycles. The maximum loads were 10 kip, 20 kip, and 40 kip in the first, second, and third cycles, respectively. The load was increased to the failure load in the fourth cycle. In most tests, the specimen was unloaded after the first wire fractured. The remaining wires were then cut, and the specimen was removed from the load frame.

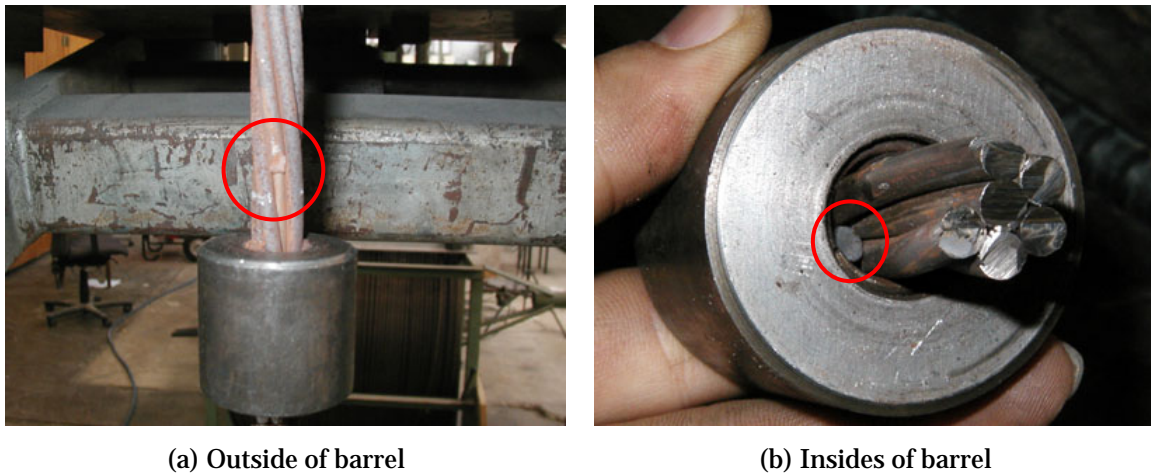
Multiple loading cycles were used to minimize the influence of slip of the specimen at the anchors. The strand was gripped at each end by the anchor barrels, but initially the wedges were not completely seated. The wedges were pulled into the cylinder as the applied load increased. As a result, the recorded displacement from the linear potentiometer included this slip of the anchor.

The wedges typically cracked before the specimen failed (Figure 3.22). Due to the slip of the anchors, the recorded data from the linear potentiometer were not used to calculate the elastic modulus but were used to monitor the overall behavior of the test specimens.



***Figure 3.22 Slip of Strand at Anchors***

The wire breaks typically occurred within the bottom barrel anchor. After the specimen yielded, one of the six outer wires fractured and then the applied axial load dropped due to slip of the specimen. The fractured surface was typically oriented approximately  $45^\circ$  from the longitudinal axis of the wire (Figure 3.23). This surface indicates that the fracture was influenced by shear stress, which probably developed due to friction between the wedges and the strand.



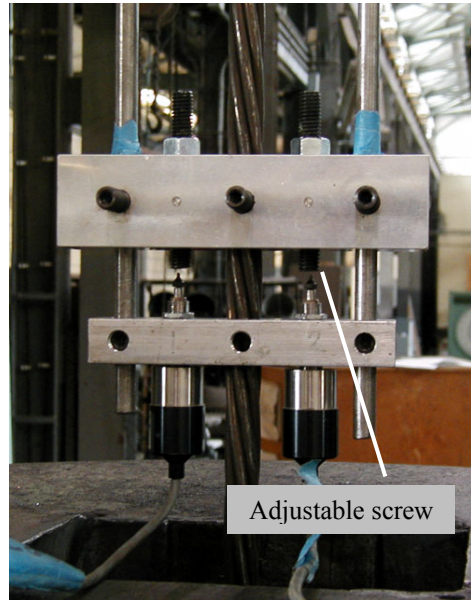
***Figure 3.23 First Wire Fracture***

The axial elongation of the strand was measured using the apparatus discussed in Section 3.3.1. In phase 2, however, the apparatus was modified by adding adjustable screws to the middle aluminum block to permit easier adjustment of the transducers (Figure 3.24). At the beginning of the test, the apparatus was attached to the strand without the transducers. The transducers were installed before the fourth loading cycle and were removed before the specimen yielded to prevent possible damage caused by the wire fracture. In general, the elongation of the strands was measured in the range of 10 to 30 kip.





(a) Apparatus for supporting displacement transducer



(b) Adjustable screws

***Figure 3.24 Instrumentation Used to Measure Elongation of Strand in Phase 2***

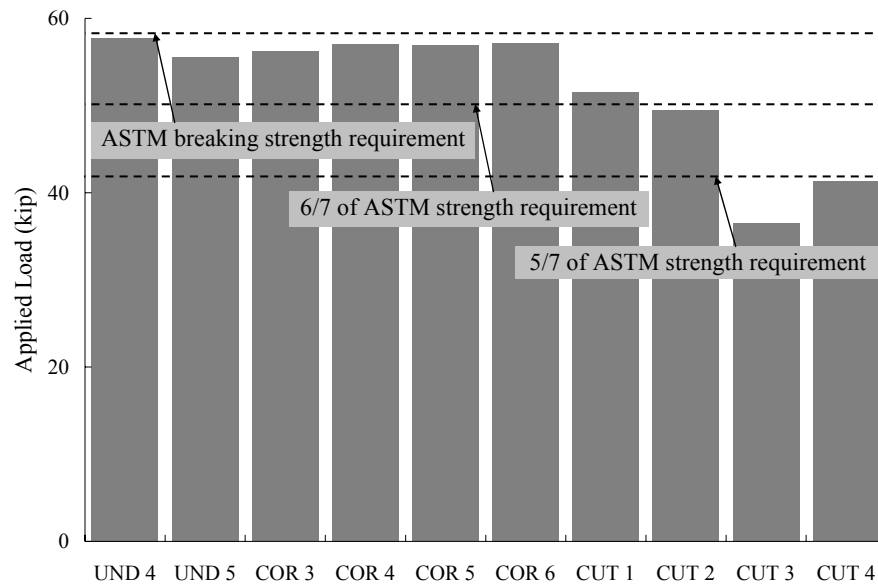
As in the phase 1 tests, the strain distribution in the outer wires was measured using strain gages. The axes of the gages were aligned along the longitudinal axes of the outer wires (Figure 3.25). The position and number of gages varied with the specimen. Most of gages malfunctioned after the first wire fractured.



***Figure 3.25 Strain Gages in Phase 2***

### 3.4.1 Tensile Strength

The measured tensile strengths of the specimens tested in Phase 2 are plotted in Figure 3.26 and summarized in Table 3.6. Due to stress concentrations at the ends of the specimens, the measured tensile strengths did not satisfy the minimum requirement in ASTM A 416. However, measured tensile strengths of the undamaged strands were within 1 to 3 kip of the ASTM limit.



*Figure 3.26 Measured Tensile Strength of Strands*

*Table 3.6 Tensile Strength of Specimens Tested in Phase 2 (kip)*

ASTM	UND4	UND5	COR3	COR4	COR5	COR6	CUT1	CUT2	CUT3	CUT4
58.6	57.7	55.6	56.2	57.1	56.9	57.2	51.6	49.5	36.5	41.3

The measured tensile strengths of the specimens were essentially proportional to the net cross-sectional area. The tensile strengths of corroded specimens were nearly identical to those of undamaged specimens. The tensile strengths of specimens with broken wires decreased as the number of broken wire increased. Specimens CUT 1 and CUT 2 failed at approximately  $6/7$  the breaking strength of the UND specimens. Also, specimen CUT 3 and CUT 4 failed at approximately  $5/7$  the breaking strength of the UND specimens. For specimens CUT 3 and CUT 4, the two cut wires unraveled before the specimen failed.

The CUT specimens unraveled violently after the wire fracture (Figure 3.27). Cut wire(s) separated from other wires along the full length of the specimen such that the initial geometry of strand was not maintained.



(a) Failure of CUT 1



(b) Failure of CUT 3

***Figure 3.27 Failure of Strand with Cut Wire(s)***

## **3.4.2 Response of Corroded Strand**

### **3.4.2.1 *Estimated Weight Loss***

As discussed in Section 3.3.2, 6-in. sections of strands were used to estimate the percent weight loss due to corrosion. After the first 2-month exposure period, tests were conducted to determine the appropriate procedures for removing corrosion products. A 20-min immersion period was selected and used in all subsequent tests.

Corrosion products were observed in the first week of the accelerated corrosion tests. The corrosion products were colored bright red-brown at the beginning. With time, the color of the products changed to dark-brown.

In spite of the visual evidence of corrosion damage, the maximum percentage of weight loss during the 5.5-month exposure was only 3.5%. Furthermore, estimated results indicated that amount of the corrosion did not increase between 4 months and 5.5 months. It is likely that accumulated corrosion products on the surface of the specimens interrupted the reaction between chloride ions and the steel. When corrosion products were removed by chemical cleaning procedure, mild pitting was evenly distributed on the surface. The test results are summarized in Table 3.7 and displayed in Figure 3.28.

**Table 3.7 Estimated Weight Loss due to Corrosion**

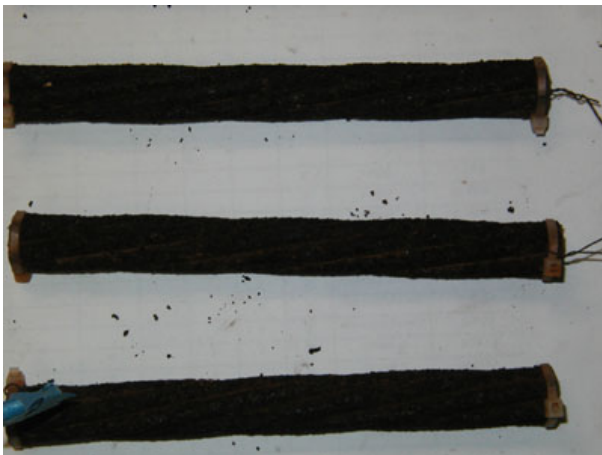
Specimen number	Exposure period (month)	Weight (g)			Percentage (%)	Average (%)	Immersion Time (min)
		Initial	After immersion in acid	Weight loss			
1	2	168.5	166.8	1.7	1.0	—	10
2		169.9	168.1	1.8	1.1	—	10
3		171.2	167.6	3.6	2.1	—	15
4		168.9	165.8	3.1	1.8	—	15
5		171.6	167.7	3.9	2.3	2.4	20
6		169.9	165.6	4.3	2.5		20
7		168.9	164.7	4.2	2.5		20
8	4	171.6	166.0	5.6	3.3	3.2	20
9		168.1	162.4	5.7	3.4		20
10		170.4	164.9	5.5	3.2		20
11		169.3	163.8	5.5	3.2		20
12		171.7	166.9	4.8	2.8		20
13	5.5	172.1	166.5	5.6	3.3	3.0	20
14		170.9	165.9	5.0	2.9		20
15		170.5	165.8	4.7	2.8		20
16		168.0	162.6	5.4	3.2		20
17		168.6	163.8	4.8	2.8		20



(a) 2-month exposure



(b) 4-month exposure



(c) 5.5-month exposure



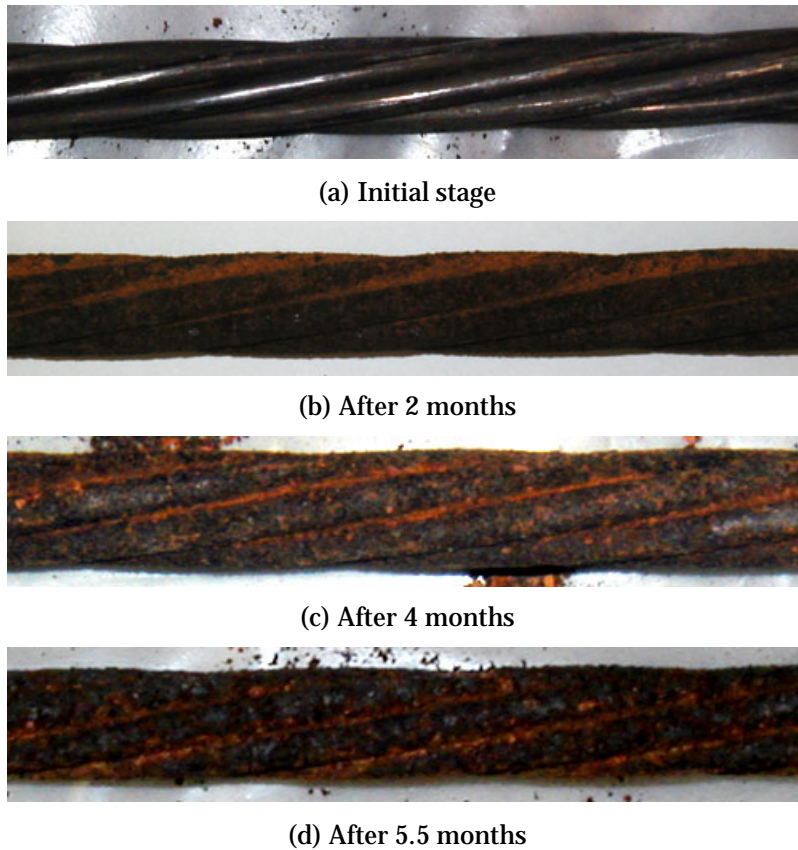
(d) After cleaning

***Figure 3.28 Observed Corrosion on Surface of 6-in. Specimens***



### 3.4.2.2 Elastic Modulus

The elastic modulus was measured for all corroded specimens. Corrosion products were visible on the surface of all specimens (Figure 3.29). The values of elastic modulus calculated from the measured stress-strain response are reported in Table 3.8. The applied stress was calculated using the cross-sectional area of the strand reported on the mill certificates, and no adjustment was made to reflect the 1 to 3% weight loss. The moduli for the corroded specimens ranged from 27,600 to 28,200 ksi, which were approximately 5% less than the modulus of undamaged specimens.



**Figure 3.29 Surface Conditions for Corroded Specimens**

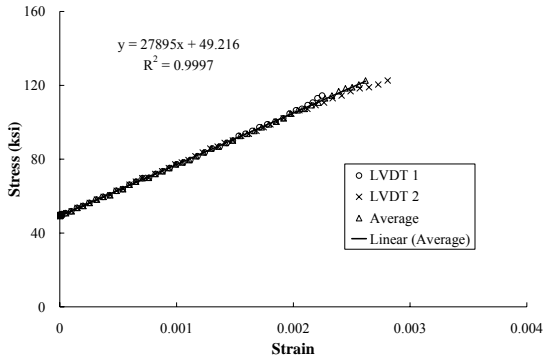
**Table 3.8 Measured Elastic Modulus of COR Specimens**

<b>Specimen</b>	<b>Elastic Modulus (ksi)</b>	<b><math>E_{COR} / E_{UND}</math></b>
COR 1	27,900	
COR 2	28,100	
Average	28,000	0.952
COR 3	27,600	
COR 4	28,200	
Average	27,900	0.949
COR 5	27,700	
COR 6	27,600	
Average	27,700	0.942

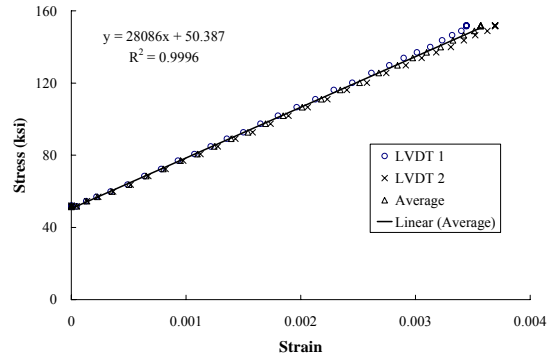
The differences between the moduli of the corroded specimens and the undamaged specimens may be attributed to two sources: the reduction in area of the wires and an increase in friction among wires due to the surface corrosion. However, the differences were small, and the instrumentation used to measure the response of the specimens may not have had sufficient precision to detect these changes. For example, the apparatus that was used to measure strains was attached to the strand using several screws. Minor pitting of the surface of the strand due to corrosion could have introduced systemic errors in these measurements. Therefore, the differences between the moduli of the two sets of strand were considered to be insignificant.

The recorded stress-strain relationships for the COR specimens are shown in Figure 3.30. Linear variations between stress and strain were observed in all cases.

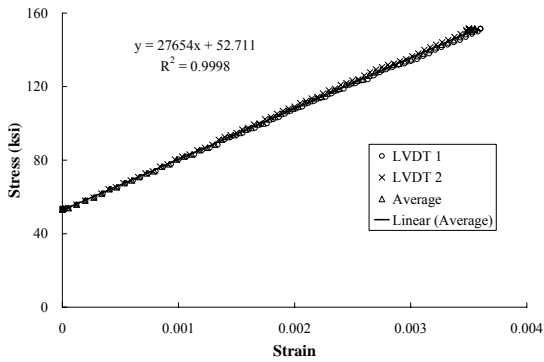




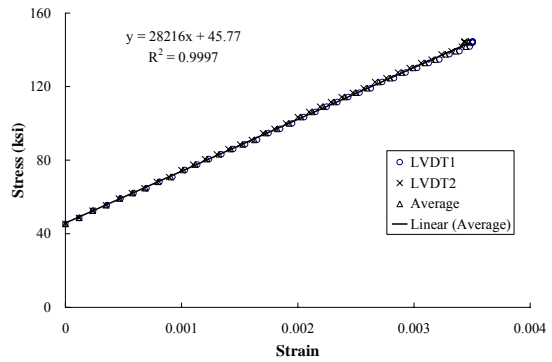
(a) COR 1



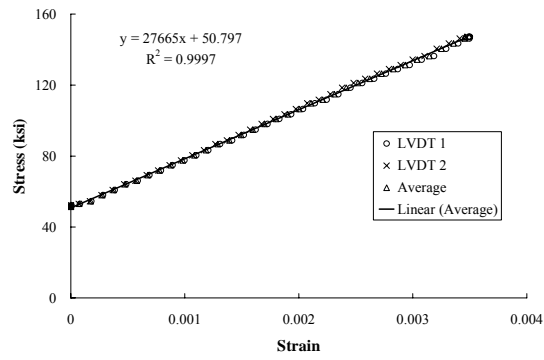
(b) COR 2



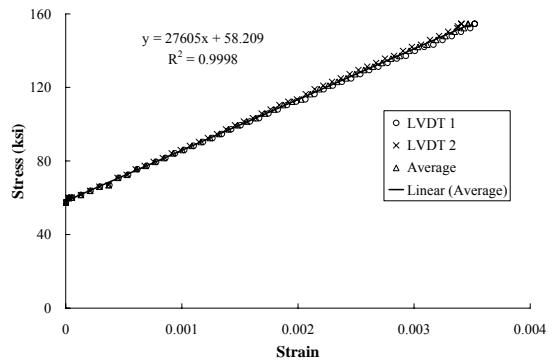
(c) COR 3



(d) COR 4



(e) COR 5



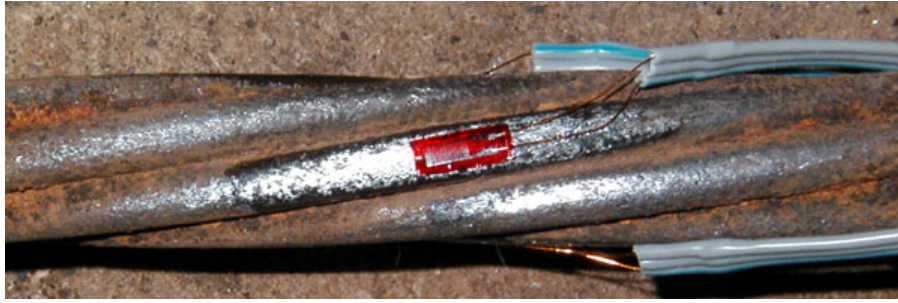
(f) COR 6

**Figure 3.30 Longitudinal Stress-Strain Relationship for COR Specimens**

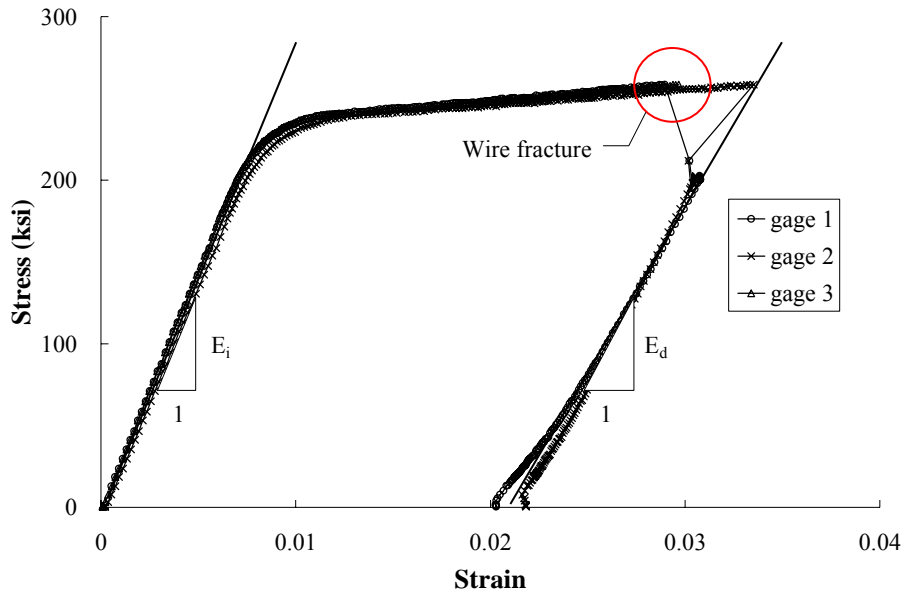
### ***3.4.2.3 Apparent Modulus of Elasticity***

Three strain gages were attached to the exterior wires at the midspan of each COR specimen (Figure 3.31). The elongation response of COR 4 is considered to be representative of all corroded specimens and is similar to that observed during phase 1 (Figure 3.32). Initially, the strains increased linearly with the applied load, and large inelastic deformations were observed after the specimen yielded. The calculated apparent modulus values in the elastic range of response are summarized in Table 3.9 and recorded stress-strain relationships for each specimen are presented in Figure 3.33.

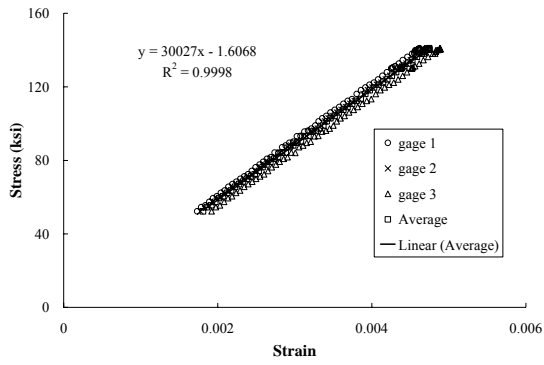
The values of apparent modulus for specimens COR 1 through COR 6 ranged from 29,100 to 30,000 ksi, which are 3 to 6 % less than the average value of apparent modulus determined for the undamaged strands. As before, these differences were considered to be minor and possibly attributable to instrumentation. For example, the roughness of the surface of the corroded strand can influence the response of the strain gages (Figure 3.31).



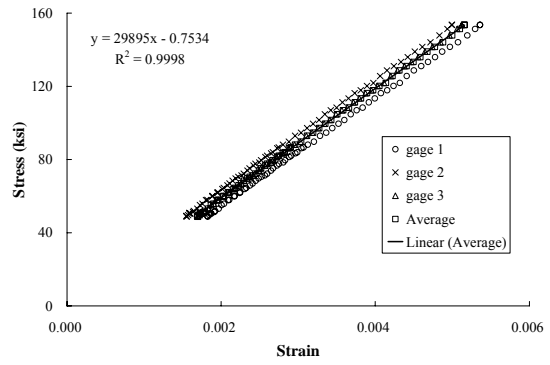
**Figure 3.31 Strain Gages Attached to Corroded Strand**



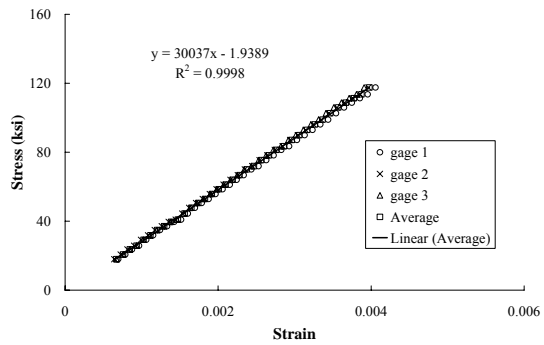
**Figure 3.32 Representative Apparent Stress-Strain Relationship (COR 4)**



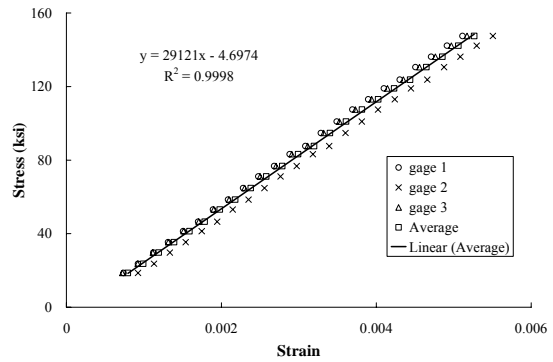
(a) COR 1



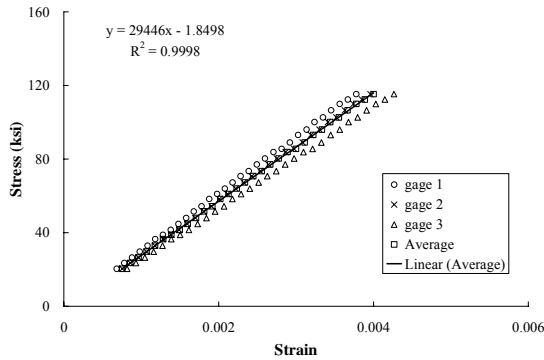
(b) COR 2



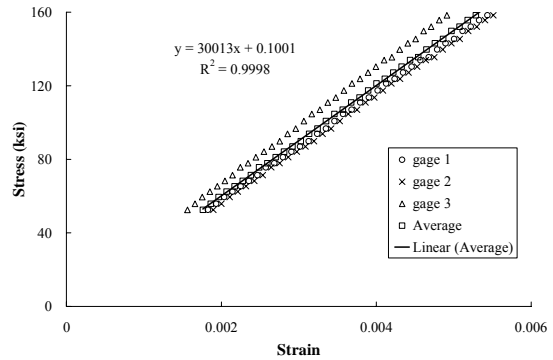
(c) COR 3



(d) COR 4



(e) COR 5



(f) COR 6

**Figure 3.33 Apparent Stress-Strain Response of Outer Wires (COR Specimens)**

**Table 3.9 Apparent Modulus of Elasticity of Corroded Strand**

	<b>Apparent Modulus (ksi)</b>	$E_{COR} / E_{UND}$
COR 1	30,000	
COR 2	29,900	
Average	30,000	0.974
COR 3	30,000	
COR 4	29,100	
Average	29,600	0.961
COR 5	29,400	
COR 6	30,000	
Average	29,700	0.964

Many of the strain gages malfunctioned when the first wire fractured but a few remained operational. The strains from these gages revealed that the strains in the outer wires varied linearly with the applied load after the first wire fractured, but the modulus was reduced by 20 to 35 %. These trends indicate that the strand behaves in the elastic manner after few wire fractures, which suggests the loss of prestressing due to the wire fracture may be not significant if the remaining axial capacity of the strand exceeds the level of applied prestressing. The apparent moduli determined from the gages that survived are summarized in Table 3.10.  $E_i$  refers to the initial apparent modulus before the wire fracture and  $E_d$  refers to the apparent modulus after the wire fracture.

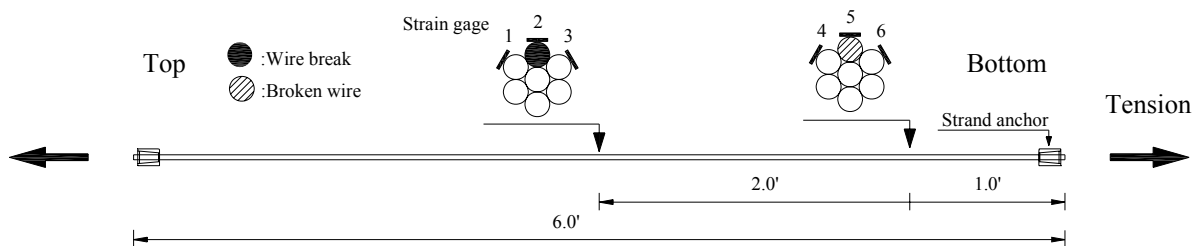
**Table 3.10 Change in Apparent Modulus after First Wire Fractured**

Specimen	Strain gage	Apparent Modulus (ksi)		$E_i / E_d$
		$E_i$	$E_d$	
COR 3	1	29,000	23,000	0.79
COR 4	1	29,000	20,000	0.69
	2	28,000	22,000	0.79
COR 5	1	28,000	20,000	0.71

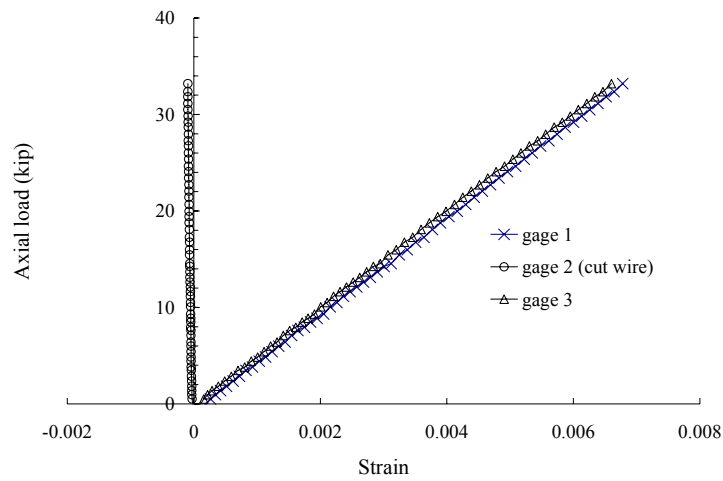
### 3.4.3 Response of Strand with Cut Wire(s)

#### 3.4.3.1 Stress Distribution within Strand

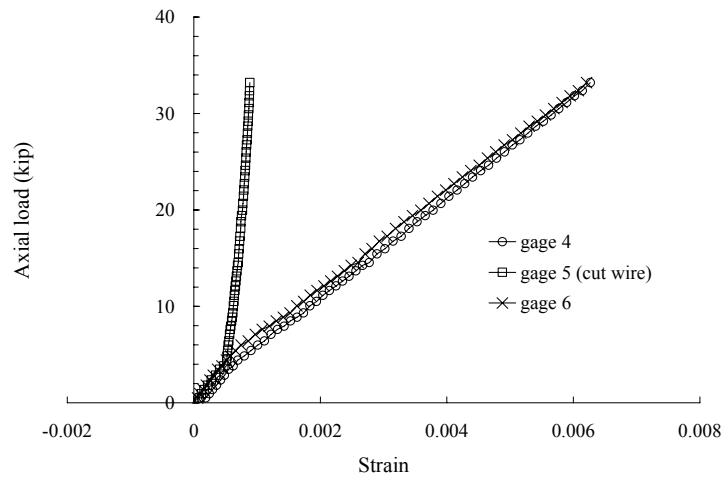
One wire in specimen CUT 2 was cut at midheight before the specimen was tested. The objective of this test was to determine the distribution of stress among the wires and the residual axial capacity of the strand. A total of six strain gages were attached to the specimens. Three strain gages were positioned at midspan where the wire had been cut, and the other three strain gages were positioned 2 ft from midspan. The arrangement of the strain gages is shown in Figure 3.34. The specimen was loaded to failure and the recorded data are presented in Figure 3.35.



**Figure 3.34 Arrangement of Strain Gages for Specimen CUT 2**



(a) Stress distribution at midspan



(b) Stress distribution 2 ft from midspan

**Figure 3.35 Strain Response of Specimen CUT 2**

**Table 3.11 Apparent Modulus of Outer Wires for Specimen CUT 2**

Location	Strain gage	Apparent Modulus (ksi)
At midspan	Gage 1	22,700
	Gage 3	22,900
2 ft from midspan	Gage 4	23,800
	Gage 6	23,300

Test results indicated the cut wire had partially recovered its ability to carry tensile stress 2 ft from the location of the cut. Tensile stress was transferred into the cut wire by friction from the intact wires. Immediately adjacent to the cut, the cut wire experienced small compressive (negative) strains. Both observations suggest that the spiral configuration of the seven-wire strand influenced the response of the strand.

The apparent modulus of the unbroken wires in specimen CUT 2 ranged from 22,700 ksi at midspan to 23,800 ksi a distance 2 ft from midspan, which are less than the average value of 30,800 ksi reported for undamaged strand (Table 3.11). The values of apparent modulus recorded 2 ft from midspan were slightly higher than those recorded at midspan, indicating that larger strains occurred in the continuous wires at midspan than 2 ft from midspan for a given level of axial load.

Test results indicate that tensile stresses in the strand redistribute among the continuous wires when a wire fractures. Also, friction between the wires has a significant influence on the tensile behavior. After the redistribution of stresses, the continuous wires exhibited elastic response in the CUT specimens. It should be noted, however, that the applied load was less than the level required to yield the continuous wires in these tests.

The influence of friction is expected to be greater in strand that has experienced corrosion damage than observed in the CUT specimens. The corrosion products increase the volume of the individual wires and roughen the outer surface of the wires, thereby increasing the internal friction among wires. This trend was expected for the COR specimens; however, the extent of corrosion was not sufficient to observe the expected response.

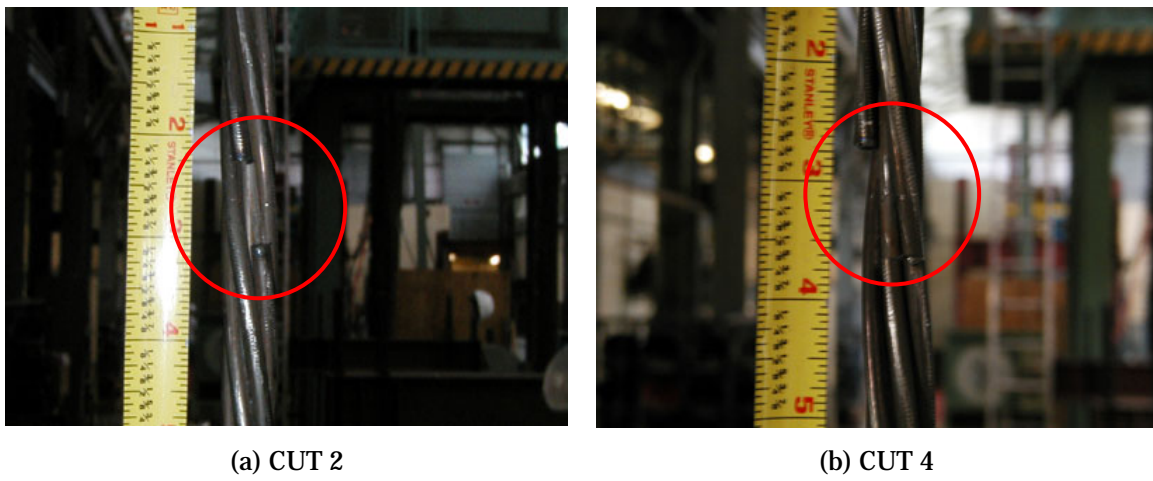
#### **3.4.3.2 *Elastic Modulus***

The elastic modulus of strands was determined from the longitudinal response of specimens CUT 2 (1 wire cut) and CUT 4 (2 wires cut). During the tests, the gap between the two discontinuous ends of the cut wire opened appreciably (Figure 3.36). After the



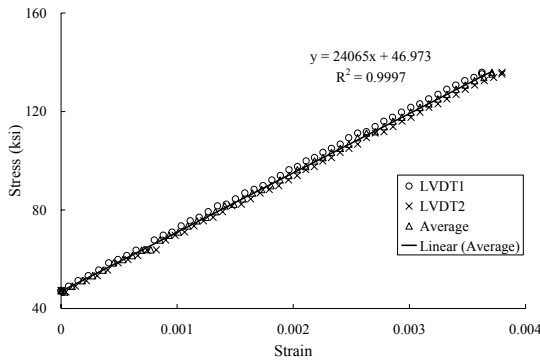
first loading cycle, this gap remained opened when the axial load was released. The gap between wire breaks was approximately 1.5 in. at the failure load.

As discussed previously, the apparatus used to measure axial elongation (Figure 3.24) was attached to the specimen using two screws. For the undamaged strand specimens, this method was effective because the stress and strain were uniformly distributed among the outer wires. Therefore, the position of the apparatus was not critical for the elongation measurement. However, for the specimens with cut wires, the stress was less in the cut wires. In addition, the cut wires moved relative to the other wires at midspan. Therefore, the location of the apparatus and placement of the screws influenced the recorded response.

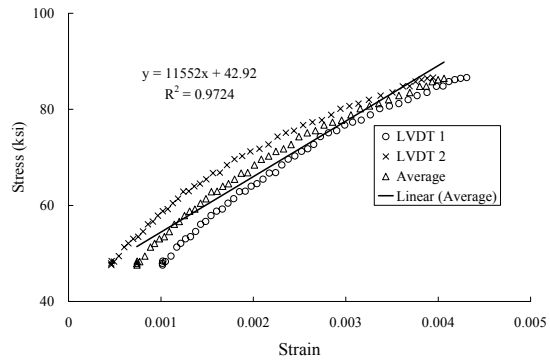


***Figure 3.36 Opening of Gap between Cut Wires***

The recorded relationships between applied load and strain for specimens CUT 2 and CUT 4 are shown in Figure 3.37 and summarized in Table 3.12. The stress-strain relationship for CUT 2 exhibited an elastic trend and the response between loading and unloading was identical. However, the axial stress-strain relationship for CUT 4 exhibited nonlinear trends. The relative movement of two broken wires to unbroken wires was significant such that the screws used to attach the apparatus to the specimen were influenced. Therefore, the measurement for CUT 4 was not considered to be repeatable.



(a) CUT 2



(b) CUT 4

**Figure 3.37 Stress-Strain Relationship**

**Table 3.12 Elastic Modulus for Specimens with Cut Wire(s)**

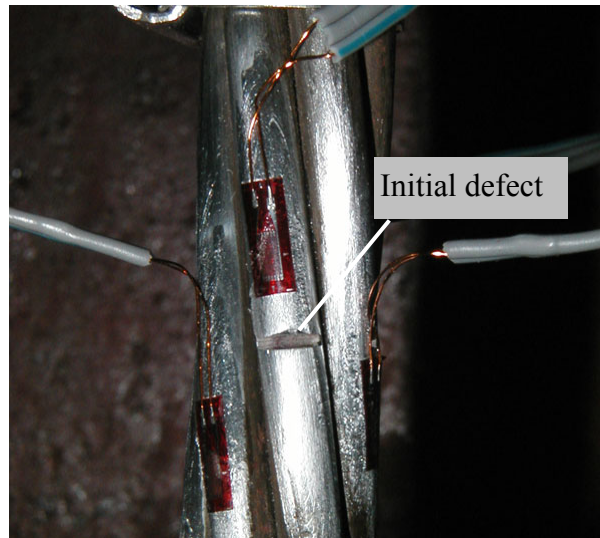
	Elastic Modulus (ksi)
CUT 2	24,000
CUT 4	—

### 3.5 PHASE 3 TESTS

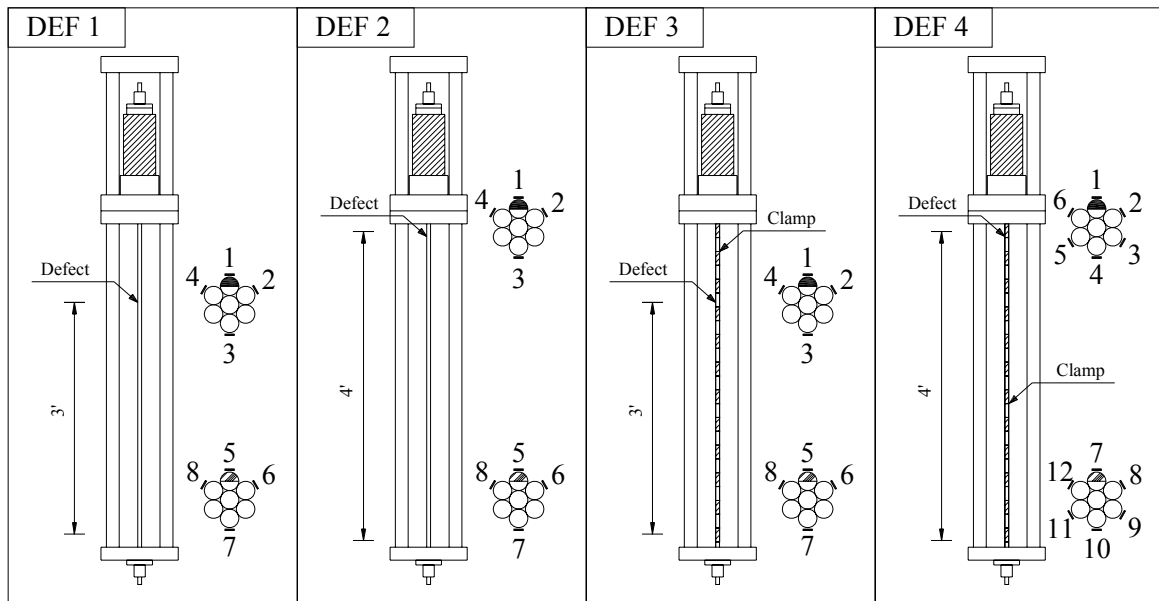
Four, 7-ft long, single strand specimens were tested to investigate the stress redistribution after a wire fractures. One of six outer wires had been partially cut using a grinder before the tests and this damaged wire failed during the test. The failure typically occurred at an axial load between 32 and 36 kip. After the fracture, the applied axial load dropped by 4 to 6 kip. The axial load was then increased to a maximum of 40 kip and released.

Eight strain gages were attached to each strand along the free length of the specimen (Figure 3.38). The location of the initial damage and the arrangement of strain gages are shown in Figure 3.39.

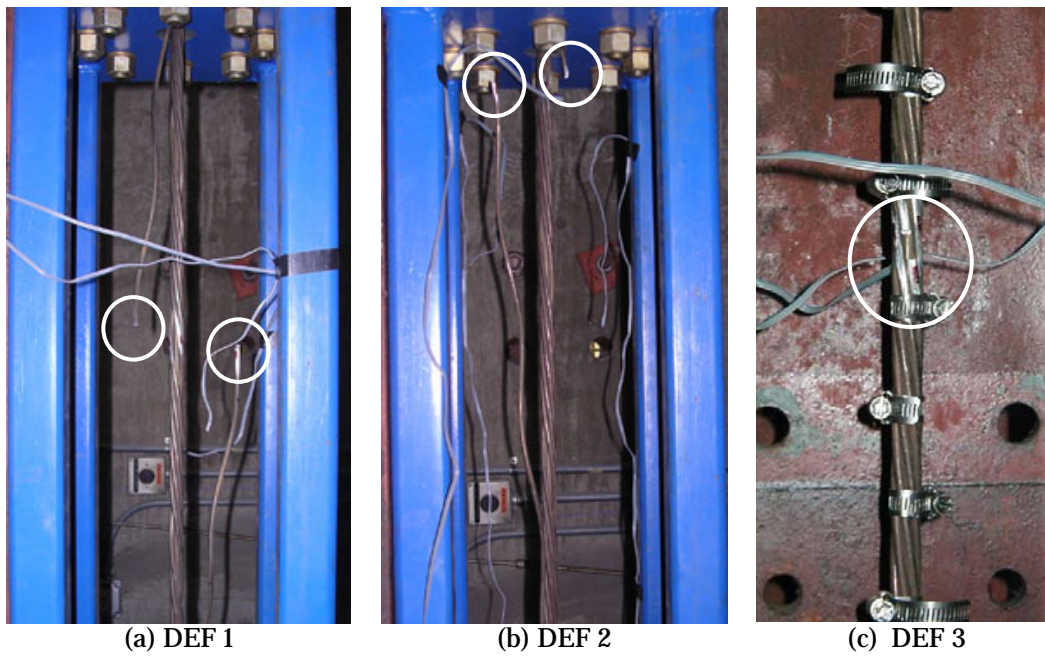
The sudden release of energy caused by fracture of the damaged wire in DEF 1 and DEF 2 caused the wires to unravel (Figure 3.40). The broken wire separated from the other six wires in the strand and broke the lead wires attached to all the strain gages positioned near the initial defect. In subsequent tests, metal hose clamps were positioned along the free length at a 2-in. spacing. The clamps prevented the broken wire from unraveling and simulated the restraint provided by the grout in external tendons. All the strain gages, except the gage attached the wire with the initial defect, survived the first wire fracture for specimens DEF 3 and DEF 4.



*Figure 3.38 Strain Gages in Phase 3*



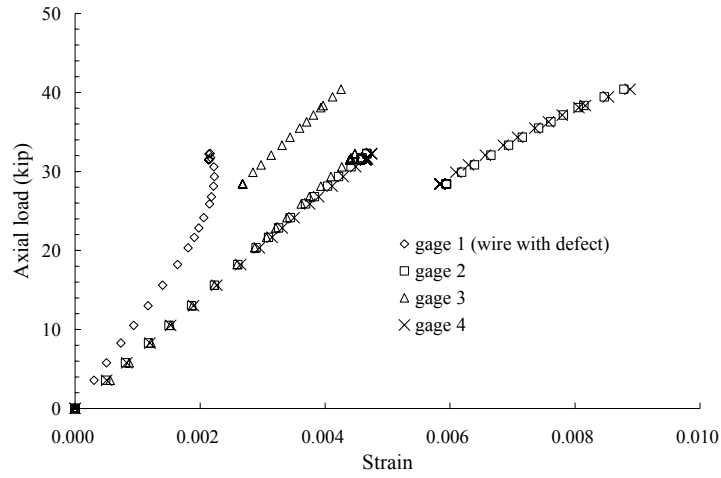
**Figure 3.39 Configuration of Specimens Tested in Phase 3**



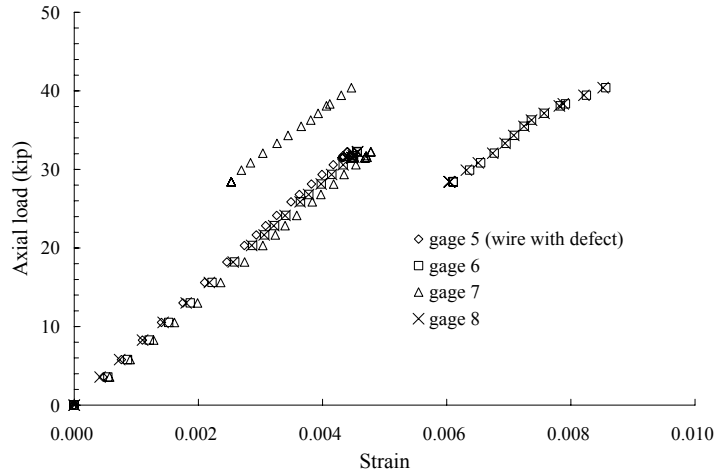
**Figure 3.40 Specimens after Initial Wire Fracture**

Representative strain response is shown in Figure 3.41. In specimen DEF 3, four strain gages were positioned at the location of the initial defect and four additional strain gages were positioned 3 ft below the initial defect. At the location of the initial defect, the damaged wire experienced less strain (gage 1) than the adjacent wires at a given level of applied load. Immediately before failure, the strain level started to drop in this wire. Before the damaged wire failed, strains were evenly distributed among the undamaged outer wires. However, the strains redistributed after the damaged wire fractured. Strains in adjacent wires (gages 2 and 4) increased after the damaged wire fractured, but the strain in the opposite wire (gage 3) decreased. As the applied load was increased, the wires adjacent to the damage wire exhibited inelastic response, while the wire on the opposite side of the strand exhibited elastic response.

The defect did not influence the initial distribution of strain 3 ft from the location of the initial defect – strains were uniformly distributed among the damaged and undamaged wires before the first wire fractured. However, after the damaged wire fractured, the distribution of strains was similar to that observed at the location of the initial defect. Strains in the adjacent wires (gages 6 and 8) increased after the damaged wire fractured while the strain in the opposite wire (gage 7) decreased. Recorded strains from all DEF specimens are presented in Appendix B.



(a) Stress distribution at midspan



(b) Stress distribution 3 ft from midspan

**Figure 3.41 Measured Strain Response of Specimen DEF 3**

The values of apparent modulus measured from the outer wires before the wire fractured are summarized in Table 3.13. The values were not the same for strains measured along the same wire. The variation at each location was approximately  $\pm 10\%$  from the average, but no specific trends were identified.

**Table 3.13 Apparent Modulus of DEF Specimens before Wire Fracture**

Specimen	Gage	Apparent Modulus (ksi)	Gage	Apparent Modulus (ksi)
DEF 1	1	-	5	32,000
	2	32,000	6	34,800
	3	34,600	7	30,700
	4	31,300	8	31,500
DEF 2	1	-	5	31,600
	2	30,800	6	32,000
	3	33,600	7	32,000
	4	31,900	8	31,000
DEF 3	1	-	5	33,000
	2	31,200	6	32,100
	3	32,800	7	30,700
	4	30,700	8	31,600
DEF 4	1	-	7	31,900
	2	31,500	8	31,300
	3	30,900	9	30,900
	4	30,900	10	31,300
	5	30,800	11	30,900
	6	31,500	12	31,600

### 3.6 SUMMARY

Nineteen 0.6-in. diameter strands were tested to investigate the variation of axial response at different levels of damage. Test results are summarized in Table 3.14. The elastic modulus and apparent modulus values for the strand were determined from the uniaxial response of three undamaged specimens. The average elastic modulus of strand was 29,400 ksi and the average apparent modulus was 30,800 ksi. The apparent modulus was higher than the elastic modulus by approximately 5%.

**Table 3.14 Average Test Results**

Specimens	Damage Type	Breaking Strength (kip)	Elastic Modulus (ksi)	Apparent Modulus (ksi)
UND 1 to 5	None	56.7	29,400	30,800
CUT 1,2	1 broken wire	50.6	24,000	23,500*
CUT 3,4	2 broken wires	38.9	-	-
COR 1,2	2-month exposure	-	28,700	30,700
COR 3,4	4-month exposure	56.7	28,800	30,500
COR 5,6	5.5-month exposure	57.1	28,500	30,600
DEF 1 to 4	1 wire w/ initial defect	-	-	31,800**

\* evaluated 2 ft from location of cut wire

\*\* evaluated 3 to 4 ft from location of initial defect

Six specimens with three different levels of corrosion damage were tested. Corrosion was induced by prolonged exposure to salt water and corrosion products were visible on the surface of the strands. However, no significant variations in the axial properties were identified. With respect to the undamaged strand, the tensile strength, the elastic modulus and apparent modulus were nearly identical. In spite of significant corrosion products, the measured weight loss was about approximately 3%.

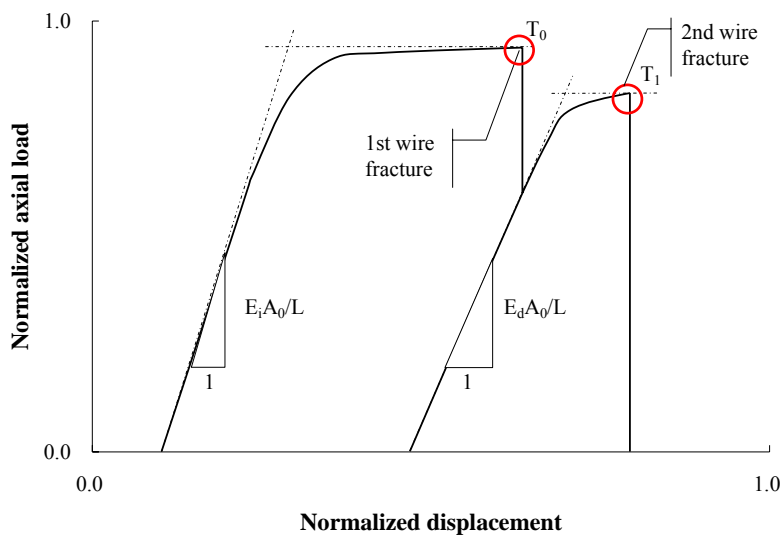
Four specimens with wire break(s) were tested. The broken wires were able to resist a portion of the applied load 2 ft from the location of the break. In each test, slip of the broken wires relative to the intact portions of the strand was observed. The elastic modulus of the strand with one broken wire was determined to be 24,000 ksi which is approximately 20% less than that of the undamaged strand. The apparent modulus of strand with one broken wire ranged from 22,700 to 23,800 ksi, which is 13 to 16% less than that of the undamaged strand.

Four specimens with an initial defect were tested. The wire with a defect fractured during the test. Before the fracturing, the wire with the defect deformed less than the adjacent wires at the location of the initial; but all wires deformed uniformly 3 ft from the



defect. After the fracture, the stress redistribution among wires caused an increase in strain in the adjacent wires, but caused a decrease in strain in the wires on the opposite side of strand.

Based on observations made in this chapter, an idealization of the elongation behavior of strand including the first and second wire fractures is shown in Figure 3.42. The overall behavior of strand is considered without including stress redistribution among wires. This figure suggests that the strand maintains a considerable portion of its original tensile strength and stiffness after the first wire fractures. Considering test results, the damaged elastic modulus ( $E_d$ ) is approximately 20% less than the initial elastic modulus ( $E_i$ ). Also, the tensile strength of the strand with one broken wire ( $T_1$ ) is approximately 6/7 of the tensile strength of undamaged strand ( $T_0$ ).



**Figure 3.42 Schematic Elongation Behavior of Strand**

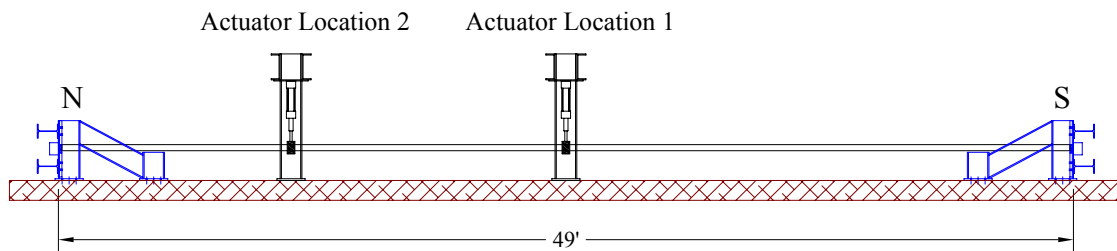
## Chapter 4: Fatigue Tests of Two-Strand Stay Cables

Three, 49-ft long stay cable specimens with two 0.6-in. diameter strands were constructed and subjected to fatigue loading until a significant loss of stiffness was detected. A series of the static and dynamic tests were conducted periodically during the fatigue tests to evaluate the condition of each specimen as damage accumulated. The specimens were also monitored continuously using acoustic sensors to detect wire breaks. In this chapter, the measured response of three cable specimens will be discussed.

### 4.1 BACKGROUND

The test specimens were designed by Bean (2006) to represent simplified stay cables. The specimens were 49 ft long (Figure 4.1). Two, 0.6-in. diameter strands were used to construct each specimen and were stressed to an initial tension of 50% of the tensile strength of the strand. The strands were parallel along the entire length and anchored in steel anchor heads at the ends of the specimen. The plastic duct was grouted after the strands were tensioned.

During the fatigue tests, the specimens were loaded transversely at one location along the length. Initially, the actuator was positioned at midspan (Location 1), but the actuator was positioned near the quarter-span (Location 2) for most of the cycles.



*Figure 4.1 Test Setup for Cable Specimens*

The structural characteristics of a stay cable are similar to those of an external tendon in many respects, and therefore, the cable specimens were evaluated in this dissertation. The global behavior of both systems is dominated by the applied tensile stress. A considerable amount of the external load is carried by the tension in the external tendons/stay cables and the preservation of this stress is critical for the durability of the overall structure. Both external tendons and stay cables have the similar corrosion protection systems. The high strength wires or strands are enclosed in a metal or plastic pipe and anchored using hardware. The pipe is usually filled with a cementitious grout.

Major differences between the two systems are the ratio of the applied initial prestress to the tensile strength of the strand and the typical dimensions of the member. A higher factor of safety is used for stay cables, where the initial prestress is limited to 50% of the guaranteed ultimate tensile strength (GUTS). In comparison, external tendons are often designed to be prestressed between 70 and 80% of GUTS.

The response of stay cables is complicated by geometric nonlinearities, which are caused by the long length relative to the diameter of the cross section. As a result, large deflections are often induced by the self-weight of stay cables. Therefore, small displacement theory is not valid for analyzing these cables, and advanced analysis techniques must be used to predict the response. However, because external tendons have a higher prestressing ratio and a relatively short length with respect to the cross-sectional diameter, the initial configuration of the tendon is typically assumed to be straight.

The test specimens were designed to study fatigue damage of stay cables under large-amplitude transverse deflections (Bean 2006). While the specimens were designed to simulate the behavior of stay cables, the structural characteristics were similar to those of an external tendon because geometric nonlinearities were negligible due to the relatively short length. A simple cross section with two parallel strands was also advantageous for investigating the distribution of strain along the length. Therefore, the cable specimens were considered to be identical to external tendons with a lower than normal level of prestressing. The construction process for the cable specimens is summarized in Appendix C and the hydraulic loading system is described in Appendix D.

## **4.2 OVERVIEW OF TESTING PROGRAM**

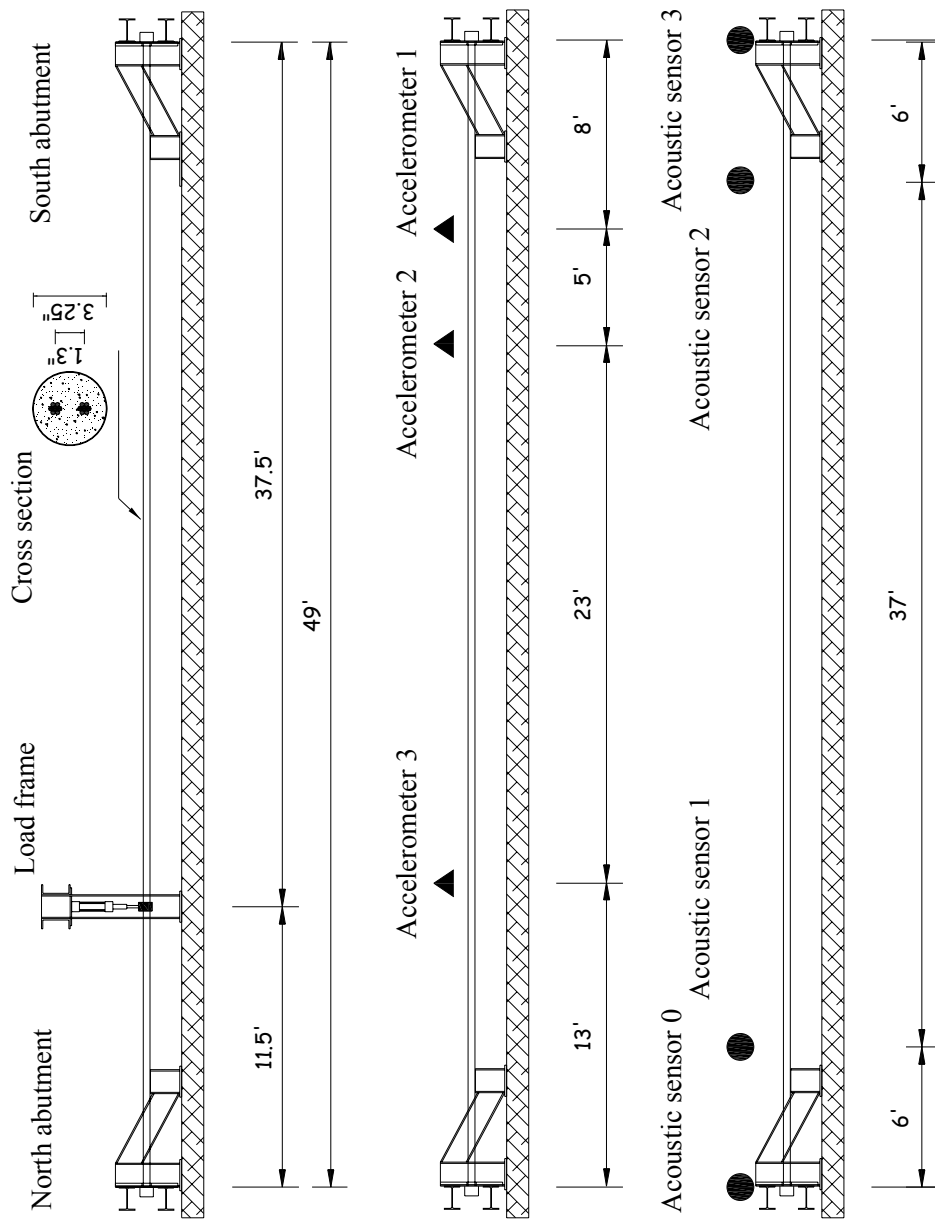
The primary objective of the testing program discussed in this chapter was to evaluate the fatigue performance of the cable specimens. An acoustic sensor system was used throughout the fatigue tests to detect wire breaks, which was used as an indication of damage within the stay cable. Periodically, the fatigue tests were stopped to conduct more detailed tests: static tests were conducted to evaluate the transverse stiffness and measure the distribution of strain in the strand, and free-vibration tests were conducted to determine the first six natural frequencies of the test specimens. These tests were designed to quantify how the structural characteristics of the cable specimens changed as damage accumulated.

The fatigue tests are summarized in Section 4.2.1 and the acoustic sensor system is described in Section 4.2.2. The periodic static tests are discussed in Section 4.2.3 and the associated instrumentation is presented in Section 4.2.4. The free-vibration tests are summarized in Section 4.2.5 and the instrumentation and procedures used to determine the natural frequencies are discussed in Section 4.2.6.

### **4.2.1 Fatigue Tests**

During the fatigue tests, a single transverse load was applied by a hydraulic actuator (Figure 4.2). For specimen Cable 01, the loading frame was initially positioned at midspan. However, the loading frame was moved closer to the north end, as shown in Figure 4.2, after approximately 40 days of testing. This position was used for the remainder of the tests.

In order to maintain the stability of the hydraulic actuator during the fatigue tests, the specimens were pulled upward from the initial position. Initially, the actuator was run in load control, but displacement control was used for the majority of the tests. The load applied by the actuator and the displacement of the actuator were monitored continuously during the fatigue tests. Additional details about the fatigue tests are available in the thesis by Bean (2006).

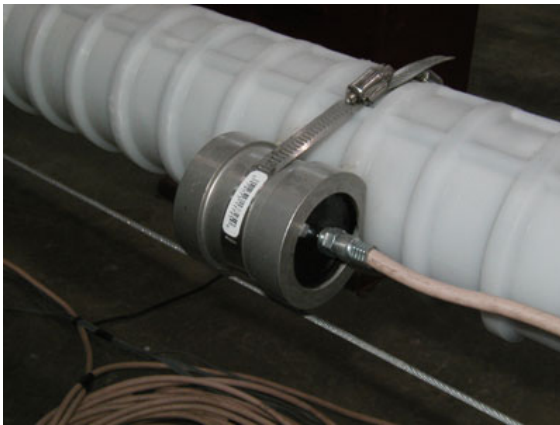


**Figure 4.2 Arrangement of Load Frame, Accelerometers, and Acoustic Sensors**

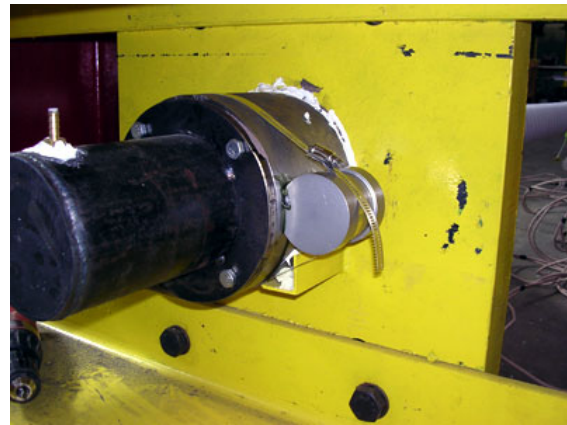
#### 4.2.2 Acoustic Sensors

Four acoustic sensors from Pure Technologies, Inc. (SoundPrint™ system) were positioned along the cable specimen to detect wire breaks during the fatigue tests (Figure 4.2). Two sensors were located on the plastic ducts and the other two sensors were located on the anchor head (Figure 4.3). Each sensor was attached to the specimen using a cyanoacrylate adhesive and then held in place by a metal clamp. These sensors were connected to the SoundPrint™ Watch Dog PS6 System in the Ferguson Structural Engineering Laboratory (Figure 4.4).

When the abrupt energy release caused by a wire fracture was detected by the sensors, the DAQ system triggered and captured the signal. These signals were stored on a local computer and transferred to Pure Technologies in Calgary once a day via an internet connection. Technical staff reviewed all signals, identified the records corresponding to wire breaks, and determined the locations of the wire breaks. Reports were available on a project website within two to four days.



(a) Sensor on Pipe



(b) Sensor on Anchor Head

*Figure 4.3 Acoustic Sensors Attached to Cable Specimens*



*Figure 4.4 Watch Dog-PS6 (SoundPrint™) Hardware*

### **4.2.3 Periodic Static Tests**

The fatigue tests were interrupted periodically to conduct static tests. As damage accumulated, the transverse stiffness of the specimens was expected to decrease. The testing protocols varied slightly for the three specimens, and are summarized briefly below.

Initially, Cable 01 was initially loaded at midspan and the fatigue tests were run under force control. During each static test, the specimen was loaded from 0 to 1.4 kip in 0.2-kip increments. After the load frame was relocated to the north end of the specimen, the static tests were discontinued.

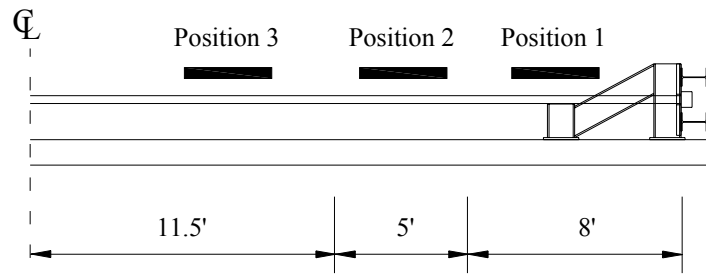
Cable 02 and Cable 03 were loaded near the north end and the fatigue tests were run under displacement control. During each static test, the specimen was pulled upward to a maximum displacement of approximately 2.5 in. in 0.4 to 0.6-in. increments.

#### 4.2.4 Instrumentation for Static Tests

The force applied by the actuator and the displacement of the actuator were recorded during the static tests. In addition, strain gages were attached to the outer wires of the strand during construction and were recorded during the static tests. The number and location of strain gages varied with each specimen. While strains were measured during all the static tests, the strain gages closest to the anchor heads malfunctioned after relatively few cycles of fatigue loading.

#### 4.2.5 Free-Vibration Tests

After each static test, the natural frequencies of the specimen were measured. The collar used to connect the hydraulic actuator to the specimen was removed and the ram was disconnected from the test specimen. Vibrations were induced by hitting the specimen with a rubber-headed hammer. During each free-vibration test, the specimen was struck at three different locations (Figure 4.5).



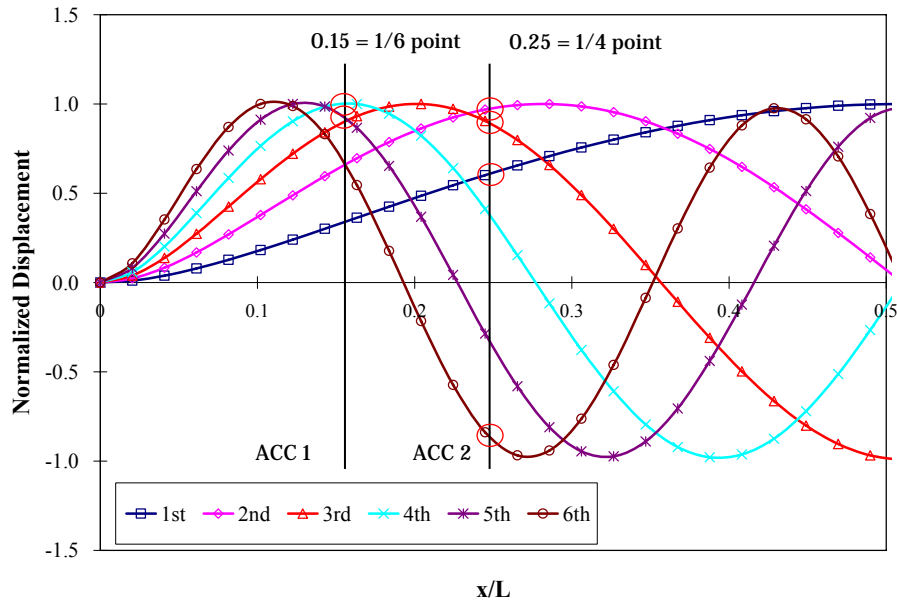
*Figure 4.5 Location of Impact for Cable Specimens*

#### 4.2.6 Instrumentation for Free-Vibration Tests

Three accelerometers were attached to each cable specimen to capture the free-vibration response. The locations of the accelerometers were selected based on the calculated mode shapes. The number of natural frequencies that can be detected from the free-vibration response depends on the location of the sensors. In order to identify a mode

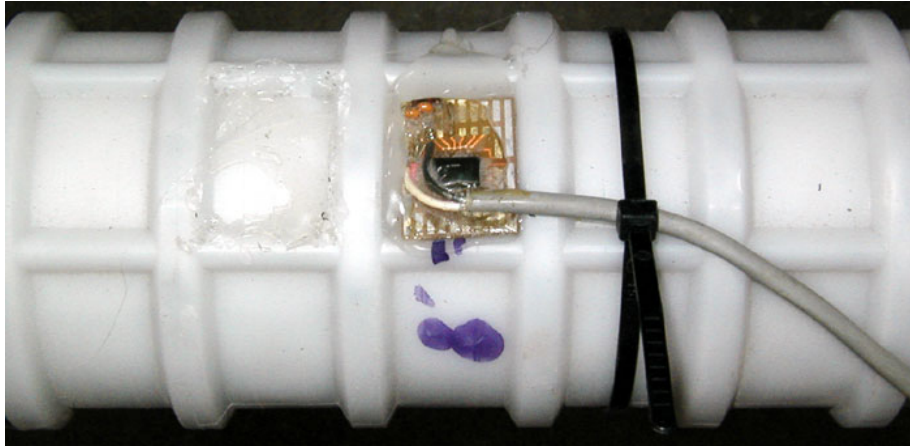


of vibration, an accelerometer must be positioned to capture the large-amplitude response of the mode shape. As shown in Figure 4.6,  $L/6$  and  $L/4$  were selected for the locations of the sensors, where  $L$  is the length of the specimen. These locations were sufficient to capture the first six modes of response.



**Figure 4.6 Normalized Mode Shapes for Cable Specimens**

Two accelerometers (Figure 4.2) were positioned 8 ft and 13 ft from the north end of the specimen and designated Acc 1 and Acc 2, respectively. A third accelerometer, Acc 3, was positioned 13 ft from the south end to verify the frequency response. Accelerometers were attached to the plastic ducts using hot-melt glue (Figure 4.7).



***Figure 4.7 Accelerometer Attached to Cable Specimens***

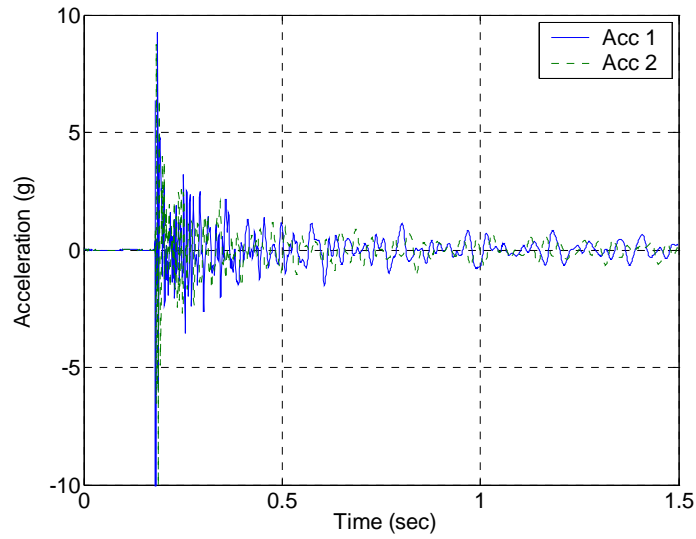
Micro machined accelerometers (model MMA 1220D) from Freescale Semiconductor™ were used for the dynamic measurements. The accelerometer had a bandwidth of 250 Hz and the DAQ system offered the maximum sampling frequency of 33,000 kS/sec (equivalent to a bandwidth of 16.5 kHz). Because the capacity of the equipment was higher than required to capture the frequency response, the signal was oversampled without filtering. Further information regarding the data acquisition system and the accelerometer is presented in Appendix E.

The accelerations measured during the free-vibration tests were converted into the frequency domain using the Fast Fourier Transformation (Figure 4.8). The measured vibrations indicated the same frequency components regardless of locations of sensor and impact; but the relative amplitude of each component varied. Recorded data in the frequency domain are presented in Appendix G.

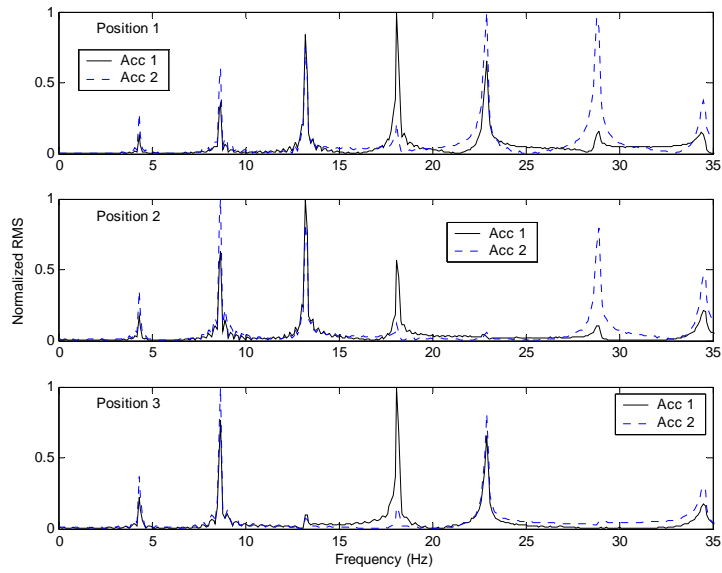
A resolution of 0.1 Hz was desired in the frequency domain. Therefore, a sampling rate of 1,000 Hz was selected in the time domain. Each sampling window was 10 sec long, providing a record with 10,000 data points for each accelerometer:

$$\frac{1}{N\Delta t} = \frac{1}{10,000 \times 0.001} = 0.1 \text{ Hz} \quad (\text{Eq.4.1})$$

where  $N$  = number of samples and  $\Delta t$  = sampling period



(a) Time domain



(b) Frequency domain

**Figure 4.8 Representative Free-Vibration Response**

### **4.3 MEASURED RESPONSE OF SPECIMENS**

In subsequent sections, the measured response of the three cable specimens is summarized. Damage accumulated in the specimens due to the fatigue loading. Static and dynamic tests were conducted periodically to observe the changes in structural behavior due to wire fractures and cracking of the grout. Once significant damage of the specimen was detected, the fatigue test was terminated and the specimen was disassembled to determine the extent of damage. The test schedules for the three cable specimens are summarized in Appendix H.

It is important to note that several key aspects of the testing program were not ideal. The amplitude and frequency of the displacement cycles were adjusted to accelerate fatigue damage for Cable 01 and Cable 02. The load frame was relocated during the test of Cable 01. The actuator position corresponding to zero load varied slightly during the tests of Cable 02, because the loading actuator was detached from the test specimen for each set of frequency measurements. In addition, the static and dynamic response of the specimen were not measured after each wire fracture because multiple wire breaks often occurred within a short period of time.

In spite of these limitations, fatigue damage accumulated in the specimen and the variation of the structural response in each set of tests did reflect induced damage. The acoustic sensors also provided a reasonable estimate of the number of wire breaks during the fatigue tests.

### **4.4 CABLE 01**

The response of Cable 01 is summarized in this section. The specimen was subjected to more than 5 million cycles over 61 days. The testing program for Cable 01 is summarized in Table 4.1. The test was terminated after the specimen collapsed due to fracture of all 14 wires.

The cyclic loading was initially applied at midspan in force control. However, this arrangement caused lower than expected levels of stress in the strand such that only two

wire breaks occurred during the first 40 days of the test. Therefore, the load frame was repositioned toward the north end to develop higher stresses as shown in Figure 4.9. At the same time, a new LVDT was attached to the actuator, which allowed the test to be operated in displacement control. The specimen failed after 13 days of additional cyclic loading.

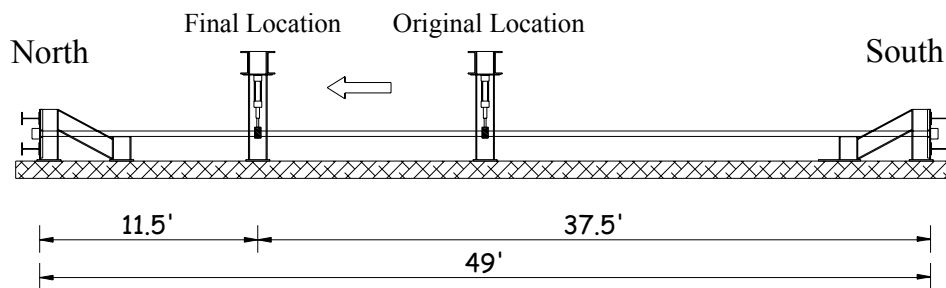
**Table 4.1 Overview of Testing Program for Cable 01**

Date and Time	Configuration		Remarks
	Force Control (kip)	Displacement Control (in.)	
9/01/05 3:15 pm	0.8 ± 0.5 at 0.6 Hz		Fatigue test started
9/12/05 4:30 pm	0.8 ± 0.5 at 1.25 Hz		
9/15/05 3:55 pm	0.8 ± 0.5 at 1.5 Hz		
10/14/05	Relocated load frame and replaced LVDT Changed from force control to displacement control		
10/17/05 12:10 pm		1.5 ± 1.25 at 1.5 Hz	Fatigue test restarted
11/01/05	Specimen failed		

The list of periodic measurements for Cable 01 is given in Table 4.2. At the beginning, the three types of measurements were performed at the same time. However, strain gages malfunctioned as the number of loading cycles increased, and the strain measurements were discontinued. The transverse stiffness was only measured before the load frame was relocated. While the natural frequencies were measured throughout the entire fatigue test, only two measurements were made between the third and sixteenth wire breaks. In this 5-day period, 9 of 14 wires fractured. After the test was completed, the autopsy was conducted to investigate the condition of the specimen.

**Table 4.2 Series of Tests for Cable 01**

Measurement	Date	Transverse Stiffness	Strains	Natural Frequency	Wire Breaks Reported
0		x	x	x	0
1	9/06/05	x	x		0
2	9/16/05	x		x	0
3	9/27/05	x			0
4	10/03/05	x			1
5	10/05/05	x		x	2
6	10/24/05			x	3
7	10/27/05			x	8



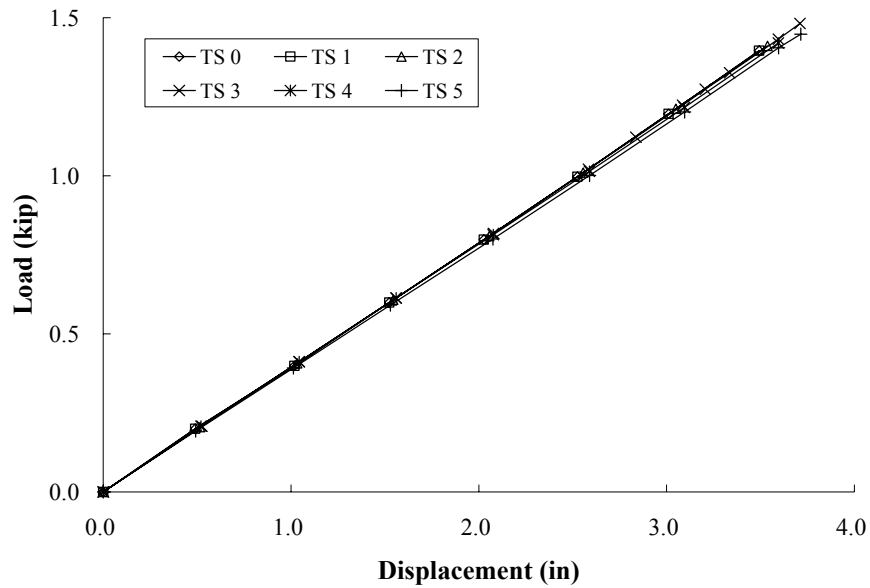
**Figure 4.9 Positions of Load Frame for Cable 01**

#### 4.4.1 Transverse Stiffness

Transverse stiffness was measured six times for Cable 01. The test results are displayed in Figure 4.10 and summarized in

Table 4.3. Tests are designated “TS X” where “TS” refers to transverse stiffness and “X” indicates the test number. TS 0 refers to the stiffness that was measured before the start of the fatigue tests. All transverse stiffness tests were conducted when the load frame was located at midspan.

The load-displacement relationship for Cable 01 was linear. The transverse stiffness decreased from 0.41 to 0.39 kip/in. as the number of the loading cycles increased. Two wires breaks were reported near midspan in the 47 days between test TS 0 and TS 5.



*Figure 4.10 Measured Transverse Stiffness of Cable 01*

*Table 4.3 Summary of Variation in Transverse Stiffness for Cable 01*

Measurement	Date	Stiffness (kip/in.)	Wire Breaks Reported
TS 0	8/30/05	0.41	0
TS 1	9/06/05	0.40	0
TS 2	9/16/05	0.40	0
TS 3	9/27/05	0.40	0
TS 4	10/03/05	0.39	1
TS 5	10/05/05	0.39	2

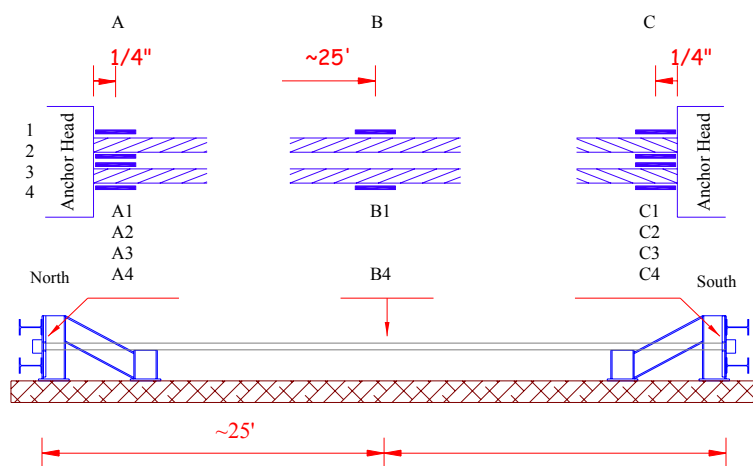
#### 4.4.2 Distribution of Strains

The first two sets of strain measurements were conducted at the initial stage and after the six days of cyclic loading. Tests are designated “SM X” where “SM” refers to strain measurements and “X” indicates the test number. The test schedule for the strain distribution measurements are given in Table 4.4. Recorded strains are presented in Appendix F.

**Table 4.4 Strain Measurements for Cable 01**

Measurement	Date	Wire Breaks Reported
SM 0	8/30/05	0
SM 1	9/06/05	0

Ten strain gages were positioned along the specimen, as summarized in Figure 4.11 and Table 4.5. Four strain gages were attached in the vicinity of each anchor head and two strain gages were attached at midspan. The gages were installed along the axes of individual wires. The measured strains represent the variation in strain due to the applied load and do not include the initial level of prestress.



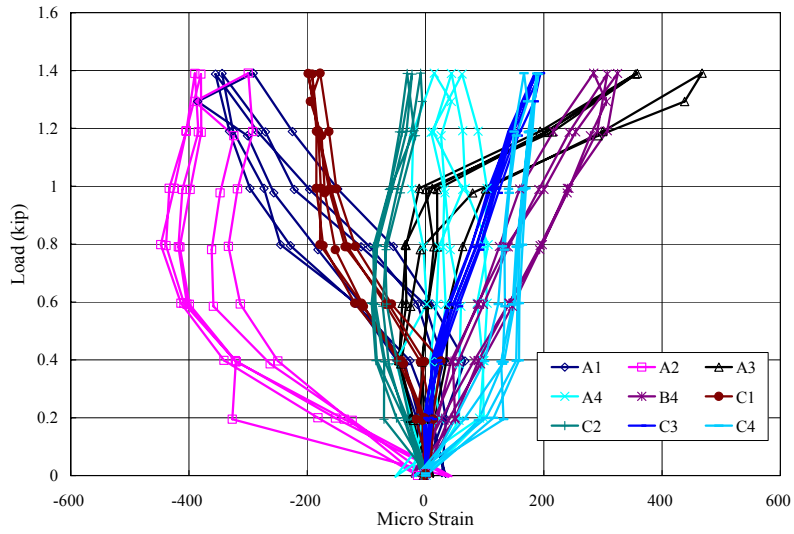
**Figure 4.11 Locations of Strain Gages for Cable 01**



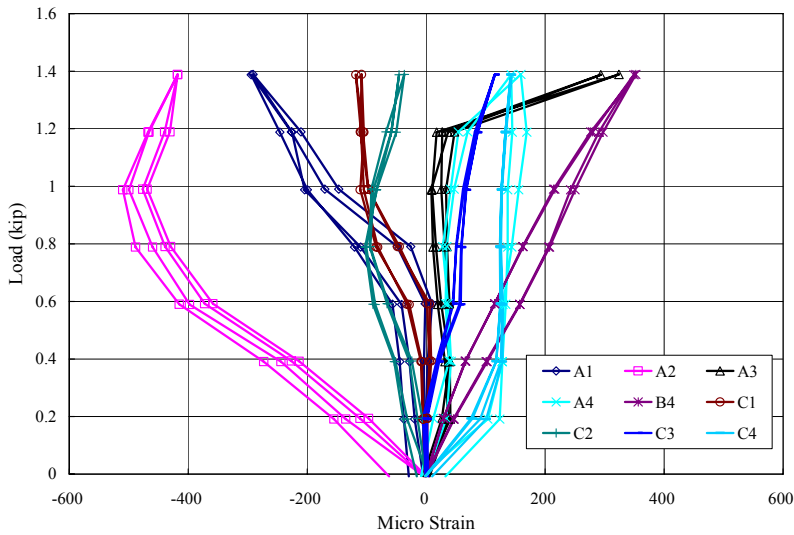
**Table 4.5 Locations of Strain Gages for Cable 01**

<b>Gage</b>	<b>Distance from North Anchor Head</b>	<b>Gage</b>	<b>Distance from South Anchor Head</b>
A1	1/4 in.	C1	1/4 in.
A2	1/4 in.	C2	1/4 in.
A3	1/4 in.	C3	3/16 in.
A4	5/16 in.	C4	5/16 in.
B1	Near center		
B4	Near center		

The measured distributions of strains are presented in Figure 4.12. The strains exhibited highly nonlinear trends. Loading paths did not coincide with the unloading paths. The strain gages positioned the same distance from the anchor heads did not exhibit a linear variation of strain with depth. The maximum strain was measured by gage A3, 470  $\mu\epsilon$ . Using the average apparent modulus of the elasticity discussed in Chapter 3, the maximum variation in stress was 14 ksi. Considering that the initial level of prestress was 50% of GUTS, the stress was estimated to vary from 135 to 149 ksi at the end of this specimen.



(a) Strain Measurement 0



(b) Strain Measurement 1

**Figure 4.12 Strain Distribution for Cable 01**

#### 4.4.3 Natural Frequencies

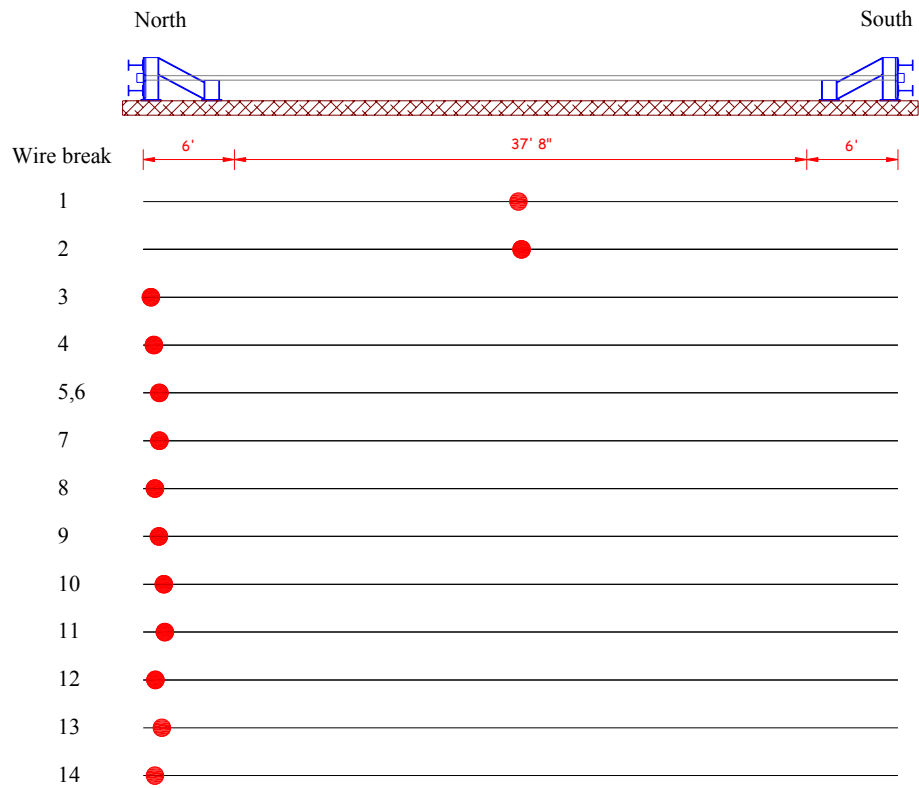
Natural frequencies were measured five times for Cable 01. Tests were performed after the acoustic sensors reported the second, third, and eighth wire breaks. The test results are presented in Table 4.6. Tests are designated “NF X” where “NF” refers to natural frequency and “X” indicates the test number. NF 0 represents a measurement at the initial stage. Three wire breaks were reported between NF 0 and NF 3, and the measured frequencies of the second through the sixth modes of vibration decreased slightly. During NF 4, significant changes in all six natural frequencies were observed.

*Table 4.6 Measured Natural Frequencies for Cable 01 (Hz)*

Mode of Vibration	NF 0	NF 1	NF 2	NF 3	NF 4
	7/14/05	9/16/05	10/05/05	10/24/05	10/27/05
1	4.6	4.6	4.6	4.6	4.2
2	9.4	9.3	9.2	9.1	8.6
3	14.5	14.3	14.2	14.0	13.2
4	20.0	19.7	19.5	19.4	18.3
5	25.6	25.1	24.9	24.5	23.6
6	32.2	31.7	31.2	30.7	29.7
Wire breaks reported	0	0	2	3	8

#### 4.4.4 Acoustic Sensor Monitoring

A total of 14 wire breaks were reported by the SoundPrint™ system. The location and dates of the wire breaks are reported in Figure 4.13 and summarized in Table 4.7, respectively. First two wire breaks were detected near midspan. All other wire breaks were detected near the north anchor head.



**Figure 4.13 Locations of Wire Breaks Reported for Cable 01**

**Table 4.7 Summary of Wire Breaks Detected by Acoustic Sensors for Cable 01**

<b>Number of Wire Break</b>	<b>Date and Time</b>	<b>Estimated Number of Loading Cycles</b>
1	10/03/05 11:42 am	3,106,000
2	10/04/05 6:10 pm	3,260,000
3	10/24/05 6:50 pm	4,126,000
4	10/25/05 1:22 am	4,365,000
5&6	10/25/05 6:43 pm	4,381,000
7	10/26/05 6:30 pm	4,431,000
8	10/26/05 9:56 pm	4,449,000
9	10/27/05 2:46 pm	4,521,000
10	10/27/05 4: 36 pm	4,531,000
11	10/27/05 8:28 pm	4,552,000
12	10/28/05 1:09 am	4,577,000
13	10/28/05 3:35 pm	4,595,000
14	11/01/05 3:15 am	5,044,194

#### **4.4.5 Autopsy of Cable 01**

The specimen was disassembled after the test was completed. The specimen collapsed after all the wires fractured (Figure 4.14). The failure occurred near the north anchor head. The top strand failed within 2-in. of the outside face of the anchor head and the bottom strand failed inside the anchor head. Thirteen wires at this section failed due to fatigue, but one wire yielded prior to failure.

A total of 16 wire breaks were identified during the autopsy. Two adjacent wires fractured near midspan and 14 wires fractured near the north anchor head (Figure 4.15). Two wire breaks at midspan appeared to occur before the load frame was relocated because the number and location of the wire breaks coincided with the SoundPrint™ system report.



(a) Overall collapse



(b) Separated section



(c) Collapsed section (toward duct)



(d) Collapsed section (toward anchor head)

**Figure 4.14 Specimen Collapse of Cable 01**

Grout at the north end of the specimen was fragmented. The energy generated by wire breaks appeared to pulverize the grout. Grout also cracked vertically at many sections. The crack developed from the top and bottom of the sections and continued through both of strands (Figure 4.15d). The relative movement between strands and grout during the cyclic loading probably resulted in compression and tension of the grout and caused the vertical crack.

A total of 16 wire breaks were observed in comparison to the 14 wire breaks reported by the acoustic sensors. The first two wire breaks at midspan were detected properly, but 2 wire breaks at the north end of the specimen were not detected. The transferred energy from wire breaks to the sensors was significant and 14 wire breaks

occurred in a narrow region in the vicinity of the anchor head. It is likely that the SoundPrint™ system was not able to distinguish between single and simultaneous wire fractures. However, the location of the wire fractures identified by the acoustic sensors was in general agreement with the observed wire breaks.



(a) Anchor head top strand



(b) Anchor head bottom strand



(c) Wire fracture at the midspan



(d) Typical section

***Figure 4.15 Wire Breaks and Typical Section for Cable 01***

#### 4.5 CABLE 02

The Cable 02 was subjected to 4.9 million loading cycles over 37 days. The testing program for Cable 02 is summarized in Table 4.8. The test was terminated after the sixth wire break was reported by the acoustic sensors. The cyclic loading was applied 11.5 ft from the north end of the specimen and operated in displacement control. The setpoint for the cyclic loading was increased from 1.52 to 1.96 in. to accelerate the fatigue damage but the variation of the setpoint for first 33 days of loading resulted from the detachment of the actuator from the specimen. The list of periodic measurements for Cable 02 is given in Table 4.9.

*Table 4.8 Overview of Testing Program for Cable 02*

Date and Time	Configuration		
	Setpoint (in.)	Amplitude (in.)	Frequency (Hz)
2/21/06 12:45 pm	1.52	1.25	1.5
2/24/06 10:15 am	1.58	1.25	1.5
3/03/06 10:17 am	1.55	1.25	1.5
3/06/06 12:57 am	1.42	1.25	1.5
3/15/06 1:43 pm	1.40	1.25	1.5
3/21/06 4:20 pm	1.54	1.25	1.5
3/24/06 10:40 am	1.81	1.25	1.5
3/27/06 4:20 pm	1.96	1.25	1.5
3/30/06 12:12 am	1.96	1.25	1.5
4/01/06 8:20 pm	Test terminated		

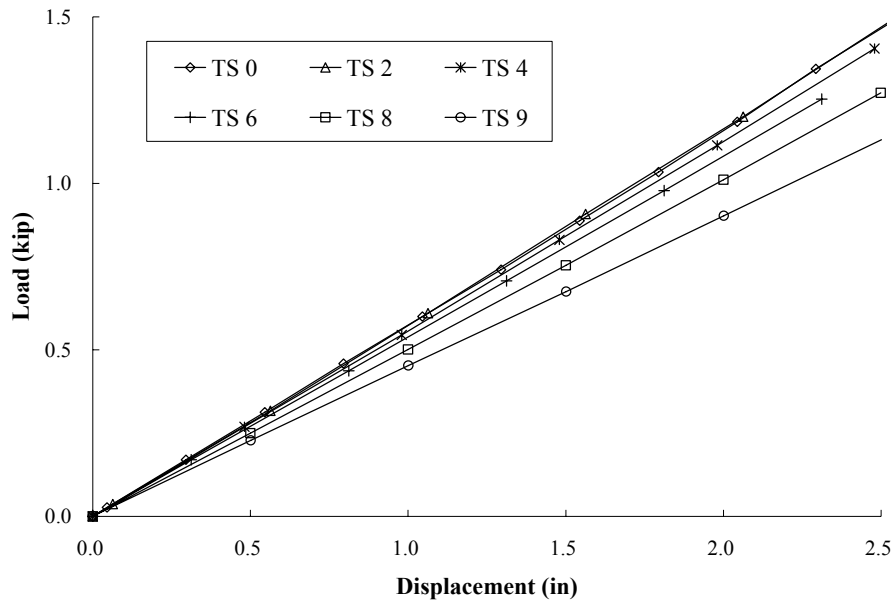


*Table 4.9 Series of Tests for Cable 02*

<b>Measurement</b>	<b>Date and Time</b>	<b>Transverse Stiffness</b>	<b>Strains</b>	<b>Natural Frequency</b>	<b>Wire Breaks Reported</b>
0	2/21/06	x	x	x	0
1	2/24/06	x		x	0
2	2/28/06	x	x		0
3	3/03/06	x		x	1
4	3/06/06	x		x	2
5	3/15/06	x	x	x	2
6	3/21/06	x	x	x	2
7	3/24/06	x	x	x	5
8	3/27/06	x	x	x	5
9	3/30/06	x	x	x	6

#### **4.5.1 Transverse Stiffness**

The transverse stiffness was measured ten times for Cable 02. The test results are displayed in Figure 4.16 and summarized in Table 4.10. The load-displacement relationships exhibited linear trends. The measured transverse stiffness decreased from 0.59 to 0.45 kip/in. from TS 0 to TS 9. The reduction between TS 0 and TS 5 was small, but increased after TS 6. In particular, the measured stiffness decreased from 0.51 to 0.45 kip/in. between TS 8 and TS 9.



*Figure 4.16 Measured Transverse Stiffness of Cable02*

*Table 4.10 Summary of Variation in Transverse Stiffness for Cable 02*

Measurement	Date	Stiffness (kip/in.)	Wire Breaks Reported
TS 0	2/21/06	0.59	0
TS 1	2/24/06	0.58	0
TS 2	2/28/06	0.59	0
TS 3	3/03/06	0.57	1
TS 4	3/06/06	0.57	2
TS 5	3/15/06	0.56	2
TS 6	3/21/06	0.54	2
TS 7	3/24/06	0.52	5
TS 8	3/27/06	0.51	5
TS 9	3/30/06	0.45	6

#### 4.5.2 Distribution of Strains

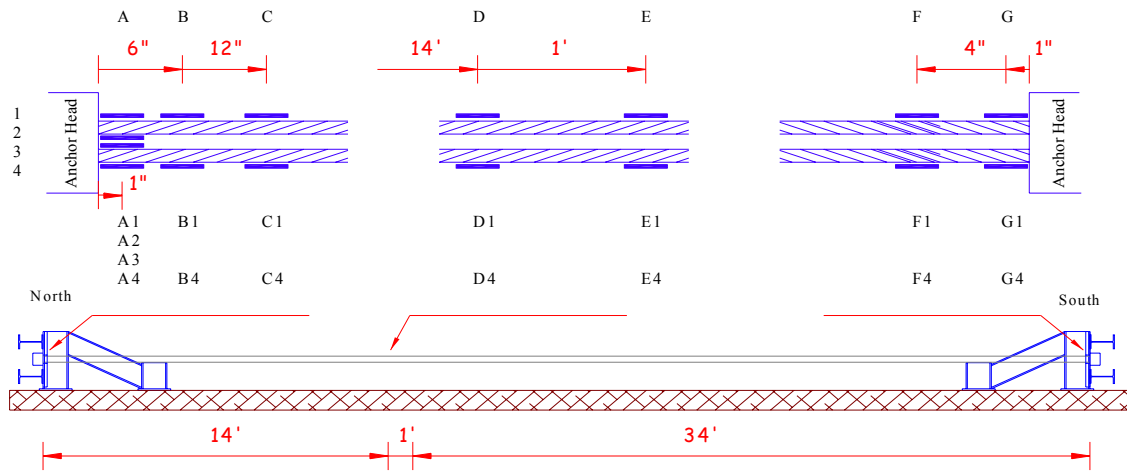
Seven sets of strain measurements were conducted for Cable 02. The schedule is given in Table 4.11. A total of 16 strain gages were attached to strands along the length. The location of strain gages is displayed in Figure 4.17 and summarized in Table 4.12. Recorded strains were presented in Appendix F.

*Table 4.11 Strain Measurements for Cable 02*

Measurement	Date and Time	Wire Breaks Reported
SM 0	2/21/06	0
SM 1	2/28/06	0
SM 2	3/15/06	2
SM 3	3/21/06	2
SM 4	3/24/06	5
SM 5	3/27/06	5
SM 6	3/30/06	6

The overall strain distribution exhibited highly nonlinear trends at the initial stage. The loading path did not coincide with unloading path. As the number of cyclic loading increased, the strain distribution gradually became linear. However, the strain gages located near the north anchor head malfunctioned after SM 0 (Figure 4.18).

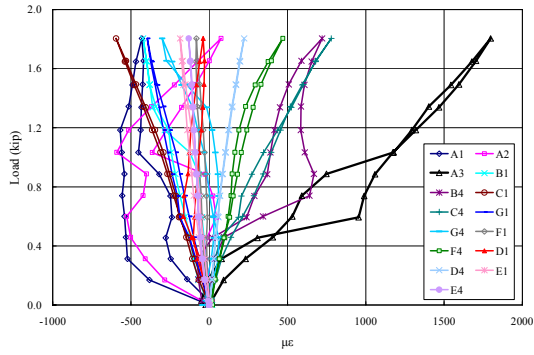
During SM 0, the maximum variation of  $1800 \mu\epsilon$  was recorded in A3 at a transverse displacement of 3.0 in. This strain was equivalent to the axial stress of 56 ksi in the wire. Considering that the maximum displacement of cyclic loading was 2.8 in. at the beginning of the fatigue tests, a similar amount of stress probably developed in the bottom strand at the north end.



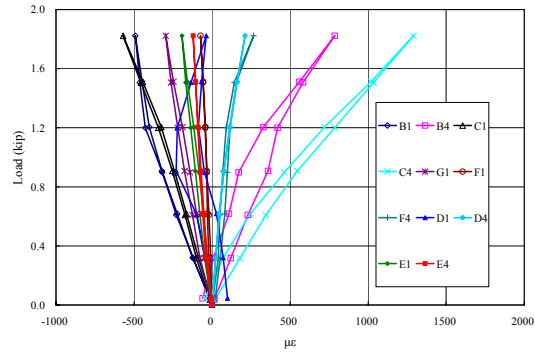
**Figure 4.17 Locations of Strain Gage for Cable 02**

**Table 4.12 Locations of Strain Gages for Cable 02**

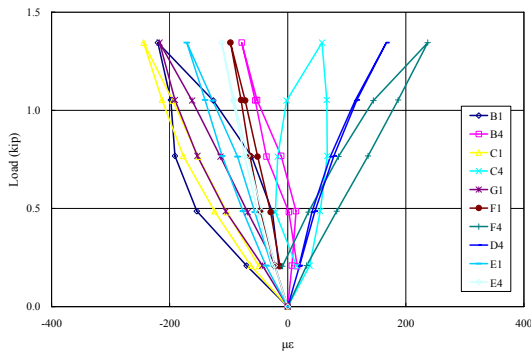
Gage	Distance from North Anchor Head	Gage	Distance from South Anchor Head
A1	1-1/16 in	F1	5 in
A2	2-1/16 in	F4	5 in
A3	1/2 in	G1	1-1/16 in
A4	1/2 in	G4	1/2 in
B1	6-1/8 in		
B4	5-7/8 in		
C1	12-3/8 in		
C4	12-1/2 in		
D1	~14 ft		
D4	~14 ft		
E1	~15 ft		
E4	~15 ft		



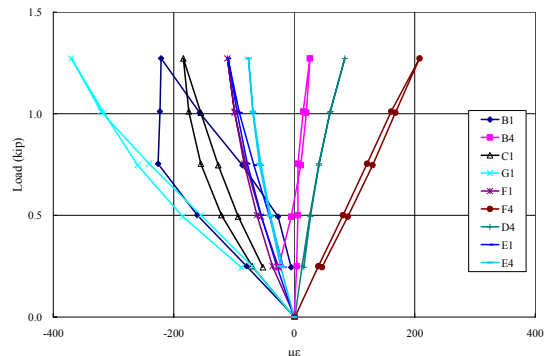
(a) SM 0



(b) SM 1



(c) SM 2



(d) SM 5

**Figure 4.18 Strain Distributions for Cable 02**

### 4.5.3 Natural Frequencies

Natural frequencies were measured nine times for Cable 02. The test results are presented in Table 4.13. The natural frequencies of all six modes decreased gradually from NF 0 to NF 8.

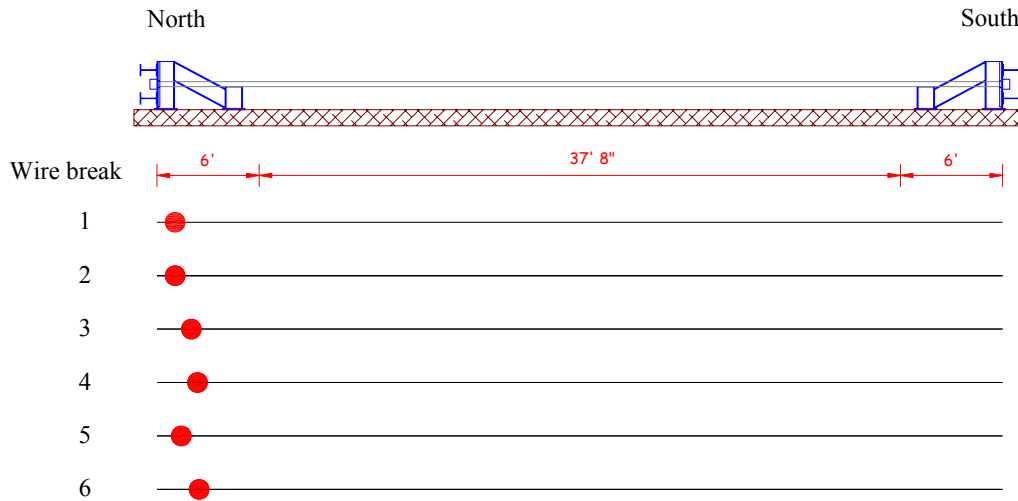
*Table 4.13 Measured Natural Frequencies for Cable 02 (Hz)*

Mode of Vibration	NF 0	NF 1	NF 2	NF 3	NF 4
	2/21/06	2/24/06	3/03/06	3/06/06	3/15/06
1	4.4	4.4	4.3	4.3	4.3
2	8.9	8.7	8.7	8.6	8.6
3	13.6	13.3	13.2	13.2	13.2
4	18.6	18.3	18.1	18.1	18.1
5	23.5	23.1	22.9	22.9	22.9
6	29.6	29.0	28.8	28.9	28.8
Wire breaks reported	0	0	1	2	2

Mode of Vibration	NF 5	NF 6	NF 7	NF 8
	3/21/06	3/24/06	3/27/06	3/30/06
1	4.2	4.1	4.1	3.9
2	8.5	8.3	8.2	7.9
3	13.0	12.9	12.8	12.4
4	18.0	18.0	17.9	17.4
5	23.0	23.1	23.2	22.6
6	29.1	29.1	29.2	28.9
Wire breaks reported	2	5	5	6

#### 4.5.4 Acoustic Sensor Monitoring

A total of six wire breaks were reported by the SoundPrint™ system. Wire breaks were concentrated near the north end of the specimen. Reported wire breaks are displayed in Figure 4.19 and summarized in Table 4.14.



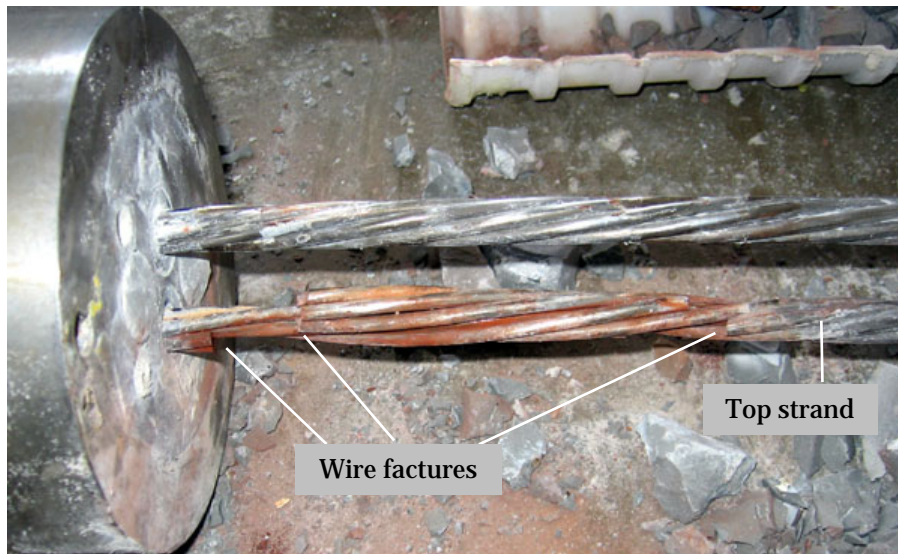
*Figure 4.19 Location of Wire Break Report for Cable 02*

*Table 4.14 Summary of Wire Breaks Detected by Acoustic Sensors for Cable 02*

Wire Break Number	Date and Time	Estimated Number of Cycles
Test started	2/21/06 12:45 pm	0
1	3/02/06 12:53 pm	1,125,000
2	3/03/06 5:32 pm	1,281,000
3	3/22/06 10:28 am	3,664,000
4	3/23/06 8:22 am	3,782,000
5	3/23/06 6:27 pm	3,836,000
6	3/28/06 5:32 pm	4,458,000

#### 4.5.5 Autopsy of Cable 02

The specimen was disassembled to investigate the extent of damage after the test was terminated. A total of eight wire breaks were identified along the top strand and no wire breaks were observed along the bottom strand. Six wires fractured within 8 in. of the outside face of the anchor head and two wires fractured inside the anchor head (Figure 4.20). The center wire fractured twice. Therefore, the top strand was completely separated from the anchor head. Mild corrosion was observed in the region where wires fractured. This corrosion indicated that severe abrasion and friction occurred at this region.



*Figure 4.20 Wire Fractures at North Anchor Head for Cable 02*

Grout near the north end was completely fragmented. Vertical cracks were also identified along the entire length as shown in Figure 4.21. The observed condition of the grout was similar to Cable 01.





(a) North anchor region



(b) Typical section

***Figure 4.21 Grout Condition of Cable 02***

A total of eight wire breaks was identified during the autopsy but the SoundPrint™ system only reported six wire breaks. Also, while three wire breaks were identified about 6 in. from the outer face of the anchor head at the north end, the SoundPrint™ system located the three wire breaks 2 to 2.5 ft from the outer face of the anchor head. The acoustic sensors appeared to not verify simultaneous wire fractures and the second wire break in the center wire could not produce large energy to be detected by the sensors. The presence of cracks in the grout could interfere with the signal delivery. In conclusion, the location and number of wire break report from the SoundPrint™ system was considered to be in general agreement with the findings from the autopsy.

#### 4.6 CABLE 03

The recorded response of Cable 03 is summarized in this section. The specimen was subjected to approximately 1.2 million loading cycles over 16 days. The test was terminated after the eighth wire break was reported by the SoundPrint™ system. The test program is summarized in Table 4.15.

The strain distribution was intensively investigated at the initial stage. A total of 32 strain gages were installed and the strains were measured eight times during the first 135,000 cycles with low-amplitude transverse displacements.

The cyclic loading was assigned an amplitude of 1.4 in. at a frequency of 1.5 Hz. While these parameters were similar to those of previous specimens, numerous wires fractured in a relatively short period of time.

***Table 4.15 Overview of Testing Program for Cable 03***

Date and Time	Loading Parameters		
	Setpoint (in.)	Amplitude (in.)	Frequency (Hz)
4/25/06	1.5	1.4	1.5
5/09/06 8:35 am	Test terminated		

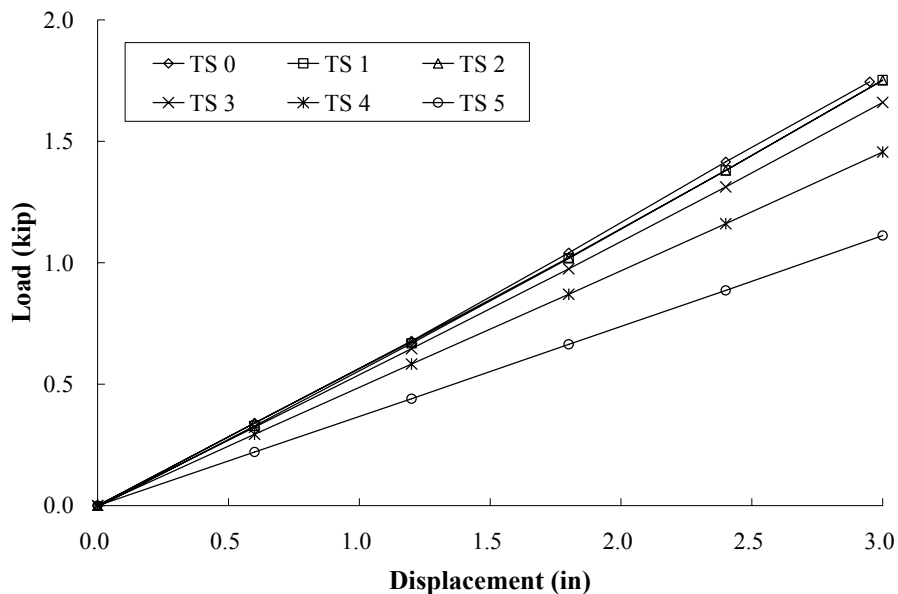
The transverse stiffness, strain distribution and natural frequencies were measured periodically throughout the test period. The list of periodic measurements for Cable 03 is given in Table 4.16.

**Table 4.16 Series of Tests for Cable 03**

<b>Measurement</b>	<b>Date</b>	<b>Transverse Stiffness</b>	<b>Strains</b>	<b>Natural Frequency</b>	<b>Wire Breaks Reported</b>
0	4/16/06			x	0
1	4/25/06	x	x		0
2	4/26/06	x	x		0
3	4/28/06	x	x	x	0
4	5/01/06	x	x	x	4
5	5/04/06	x	x	x	6
6	5/11/06	x	x	x	8

#### **4.6.1 Transverse Stiffness**

The transverse stiffness was measured six times for Cable 03 and test results are displayed in Figure 4.22 and summarized in Table 4.17. The load-displacement relationship exhibited a linear trend. From TS 0 to TS 5, the measured transverse stiffness decreased gradually from 0.59 to 0.48 kip/in. In this period, six wire breaks were reported by the SoundPrint™ system. The sudden reduction of stiffness was recorded from 0.48 to 0.37 kip/in. between TS 4 and TS 5.



*Figure 4.22 Measured Transverse Stiffness for Cable03*

*Table 4.17 Summary of Variation in Transverse Stiffness for Cable 03*

Measurement	Date	Stiffness (kip/in.)	Wire Breaks Reported
TS 0	4/25/06	0.59	0
TS 1	4/26/06	0.58	0
TS 2	4/28/06	0.58	0
TS 3	5/01/06	0.54	4
TS 4	5/04/06	0.48	6
TS 5	5/11/06	0.37	8

#### 4.6.2 Strain Distribution Measurement

The strain distribution along strands for Cable 03 was intensively investigated. A total of 32 strain gages were used to monitor the response of the specimen and strains were measured eight times at the initial stage. The overall test schedule is summarized in Table 4.18 and the test schedule at the initial stage is summarized in Table 4.19. Recorded strains were presented in Appendix F.

The strains measured in Cable 01 and Cable 02 exhibited nonlinear trends with the applied load during the initial series of tests. While these strains were measured before the start of the fatigue tests, the grout in the specimens was likely cracked, because the research team loaded the specimens while checking the performance of the hydraulic system. In contrast, Cable 03 was not preloaded before the first series of strain measurements and the amplitude of the applied displacements was low in the early tests to minimize the likelihood of cracking the grout.

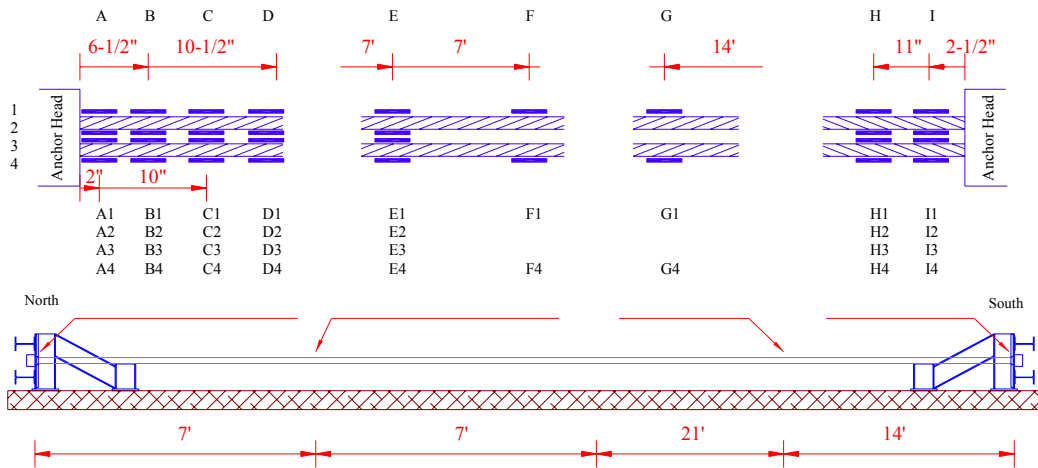
**Table 4.18 Strain Measurements for Cable 03**

Strain Measurement	Date	Wire Breaks Reported
SM 0-0~0-6	4/25/06	0
SM 1	4/26/06	0
SM2	4/28/06	0
SM3	5/01/06	4
SM4	5/04/06	6
SM5	5/11/06	8

**Table 4.19 Initial Strain Measurements for Cable 03**

Measurement	Maximum Displacement (in.)
SM0-0	0.4
SM0-1	0.8
SM0-2	1.2
1,000 loading cycles	
SM0-3	1.2
SM0-4	2.0
1,000 loading cycles	
SM0-5	3.0
10,000 loading cycles	
SM0-6	3.0
134,500 loading cycles	
SM1	3.0

The locations of strain gages are displayed in Figure 4.23 and summarized in Table 4.20. Sixteen gages were attached near the north end of the specimen to investigate the strain distribution with depth. Four of gages were positioned at locations A through E, H and I. Two gages were positioned at locations F and G.



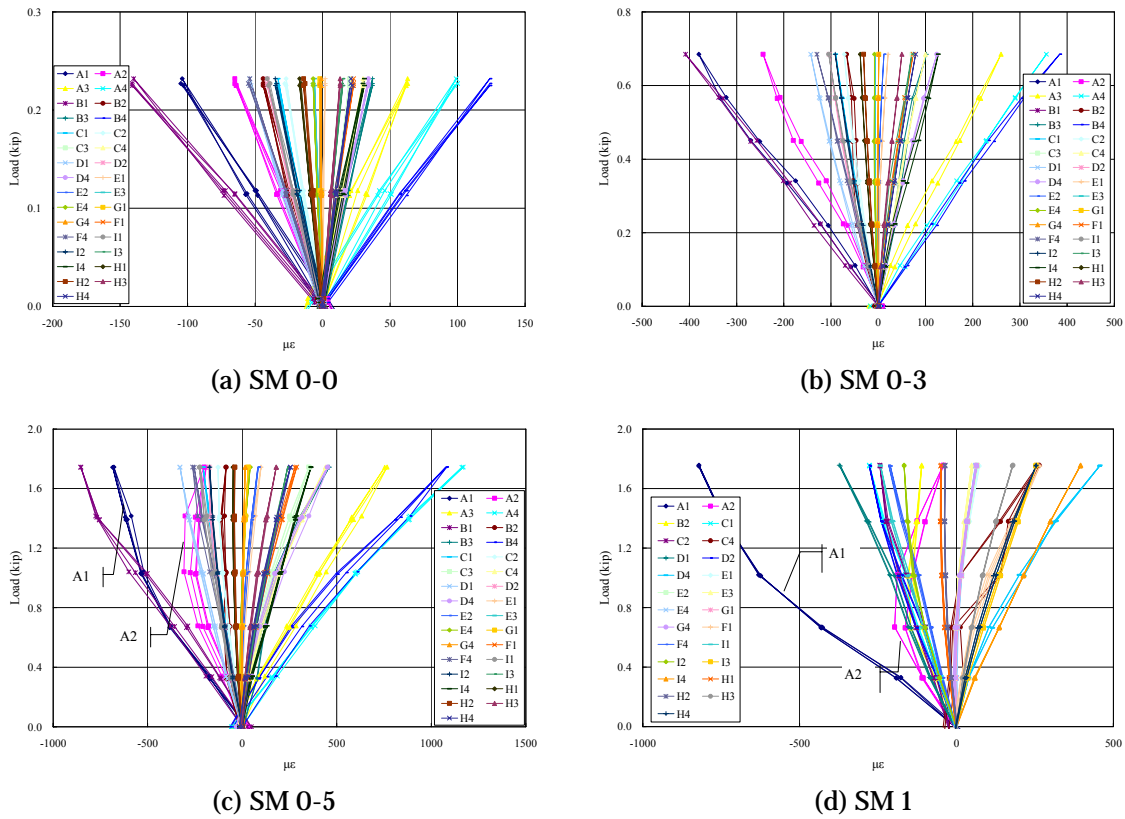
**Figure 4.23 Locations of Strain Gages for Cable 03**

**Table 4.20 Locations of Strain Gages for Cable 03**

<b>Gage</b>	<b>Distance from North Anchor Head</b>	<b>Gage</b>	<b>Distance from South Anchor Head</b>
A1	1-5/8 in	G1	14 ft 3 in
A2	2-1/2 in	G4	14 ft 3in
A3	2-1/8 in	H1	13-7/8 in
A4	2-3/8 in	H2	13-5/8 in
B1	6-1/2 in	H3	13-1/8 in
B2	6-1/2 in	H4	12-7/8 in
B3	6-1/4 in	I1	2-1/2 in
B4	6-5/8 in	I2	2 in
C1	12 in	I3	2-7/8 in
C2	12 in	I4	2-1/2 in
C3	12-1/4 in		
C4	12-1/4 in		
D1	16-3/4 in		
D2	17-5/8 in		
D3	16-3/4 in		
D4	17-1/2 in		
E1	7 ft 1 in		
E2	7 ft 1 in		
E3	7 ft 1 in		
E4	7 ft 1 in		
F1	14 ft 2 in		
F4	14 ft 2 in		

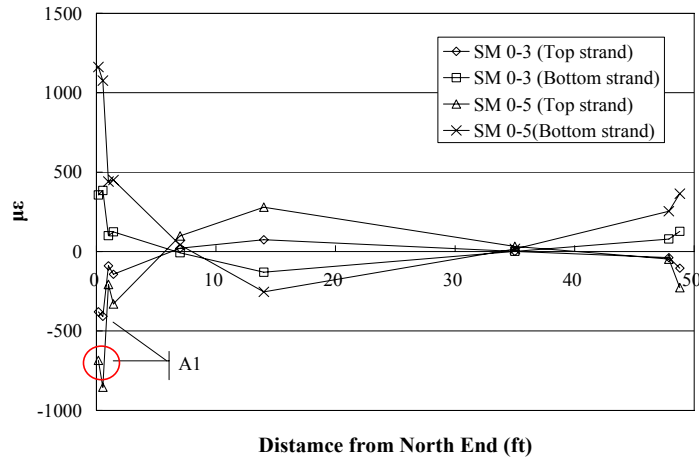
In Figure 4.24, four measured strain distributions are presented. The strain distributions from SM 0-0 to SM0-3 exhibited linear trends. However, when the displacement was increased to 2 in. during SM 0-4, nonlinear trends were observed in strain gages A1 and A2. As damage accumulated, more gages exhibited nonlinear behavior.

In Figure 4.24, the strain distribution along the length is presented. Measured strains exhibited steep gradients near the north end, which was likely caused by cracks in the grout. The highest strain measured during SM 0-6 was 1280  $\mu\epsilon$  by gage A4, which is equivalent to a stress of 40 ksi.



**Figure 4.24 Initial Stain Distributions for Cable 03**

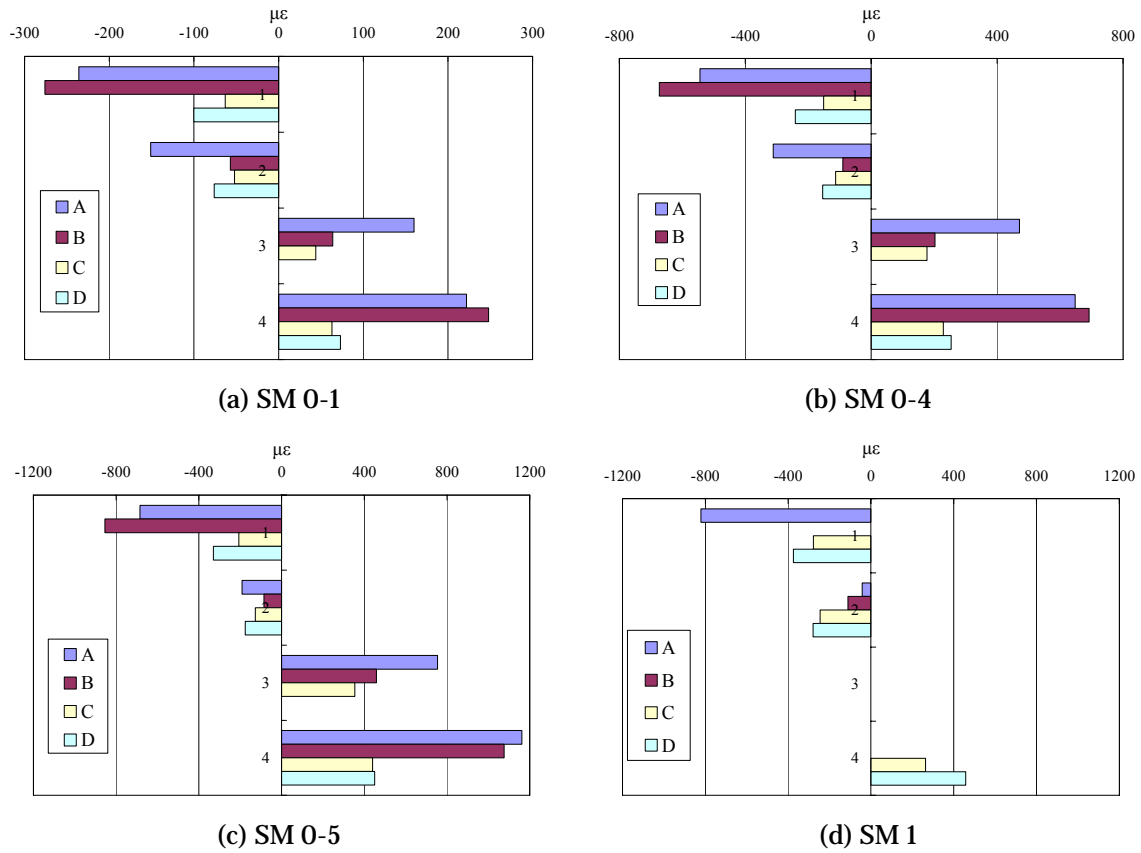




**Figure 4.25 Strain Distribution along the Length of Cable 03**

The strain distributions from the four sets of strain gages at the north end of the specimen are displayed in Figure 4.26. Strain values presented were obtained when the specimen was subjected to maximum transverse displacement.

The strain did not decrease linearly with distance from the end of specimen. The largest strains were measured in group B, rather than measured in group A. Recorded strains from group D were also higher than those from group C. Acquired strains from the top and bottom of the same strand also revealed considerable differences. For example, the amplitude of gage B2 was about one-tenth that of gage B1 during SM 0-1. This difference indicates that considerable shear stress developed along the strand and this shear stress probably contributed to debonding of the strands from the surrounding grout.



**Figure 4.26 Strain Distributions at North End of Cable 03**

### 4.6.3 Natural Frequencies

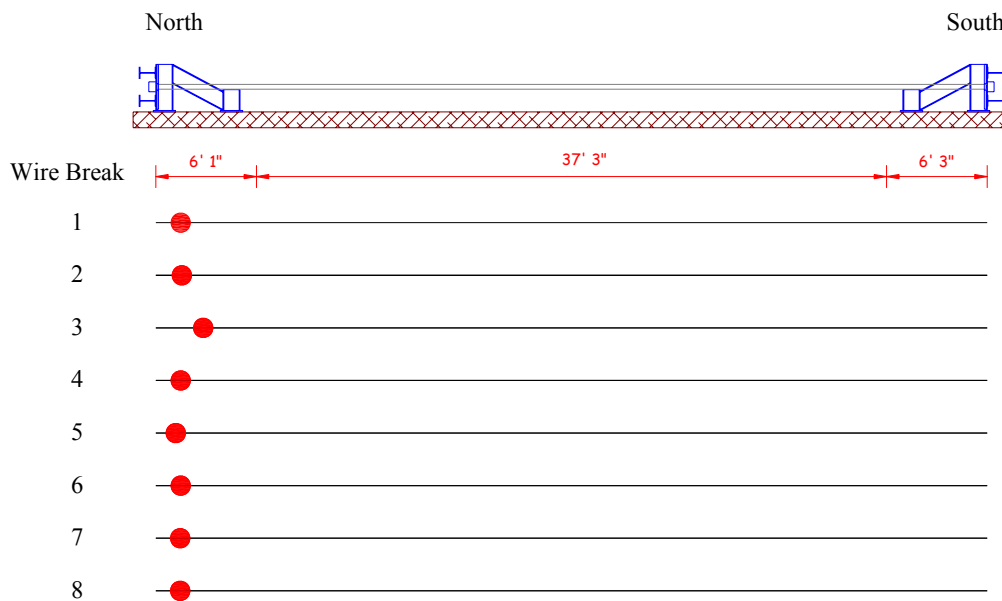
Natural frequencies were measured five times throughout the fatigue test and results are summarized in Table 4.21. The natural frequencies decreased gradually as the number of wire breaks increased. The variation of natural frequencies was observed first in NF 2.

**Table 4.21 Measured Natural Frequency for Cable 03 (Hz)**

Mode of Vibration	NF 0	NF 1	NF 2	NF 3	NF 4
	4/16/06	4/28/06	5/01/06	5/04/06	5/11/06
1	4.3	4.3	4.2	3.9	3.5
2	8.8	8.7	8.5	7.9	7.1
3	13.7	13.5	13.2	12.4	11.2
4	19.0	18.7	18.2	17.3	15.8
5	24.7	23.8	23.2	22.8	21.2
6	31.6	30.3	29.4	29.1	27.3
Wire breaks reported	0	0	4	6	8

#### 4.6.4 Acoustic Sensor Monitoring

A total of eight wire breaks were reported by the SoundPrint™ system. Reported wire breaks were concentrated at the north end of the specimen. The wire reports are displayed in Figure 4.27 and summarized in Table 4.22.



**Figure 4.27 Location of Reported Wire Break for Cable 03**

**Table 4.22 Summary of Wire Breaks Detected by Acoustic Sensors for Cable 03**

<b>Wire Break Number</b>	<b>Date and Time</b>	<b>Estimated Number of Cycle</b>
Test start	4/25/06	0
1	4/28/06 7:21 pm	415,000
2	4/29/06 6:40am	476,000
3	4/29/06 7:41 pm	546,000
4	4/29/06 7:52 pm	547,000
5	5/2/06 6:49 am	858,000
6	5/2/06 6:59 pm	924,000
7	5/8/06 6:23 am	1,510,000
8	5/8/06 6:38 pm	1,576,000

#### **4.6.5 Autopsy of Cable 03**

After the test was completed, the specimen was disassembled to determine the extent of damage. A total of twelve wire breaks were identified at the north end of the specimen. Six wires fractured within 1 in. of the outer face of the anchor head and six wires fractured inside the anchor head. Outside the anchor head, three wire breaks were identified in each strand (Figure 4.28a and b). Three wires fractured in the top strand but two wires fractured in the bottom strand – one outer wire experienced two wire breaks. Inside the anchor head, six wires fractured only in the bottom strand. Two wires including the center wire fractured within 0.25 in. of the outer face of the anchor head. Four wires fractured at the wedge (Figure 4.28c and d).



(a) Outside of anchor head (Top strand)



(b) Outside of anchor head (Bottom strand)



(c) Inside of anchor head (Bottom strand)

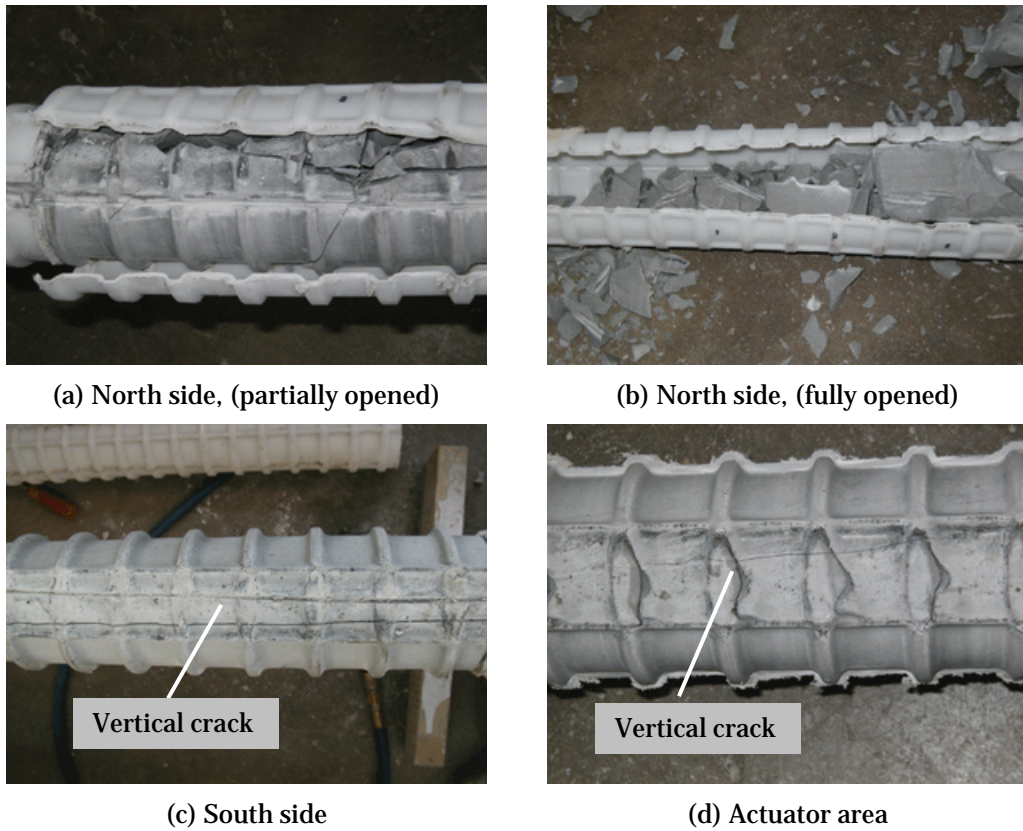


(d) Wire fracture at wedges (Bottom strand)

***Figure 4.28 Wire Fractures for Cable 03***

Grout at the north end was fragmented (Figure 4.29a and b). When the post-tensioning duct was opened, the grout surrounding the strands was pulverized. A vertical crack was observed along the entire length of the specimen (Figure 4.29c and d).

While a total of twelve wire breaks were identified, the SoundPrint™ system reported eight wire breaks. The SoundPrint™ system probably could not distinguish multiple wire fractures from single wire fracture or the secondary wire fractures in broken wire did not generate a considerable amount of energy. The location of wire breaks were in general agreement with findings from the autopsy.



**Figure 4.29 Crack Propagation for Cable 03**

#### 4.7 SUMMARY

Three, 49-ft long cable specimens with two 0.6-in. strands were constructed and subjected to cyclic loading. The static and dynamic responses of the specimens were measured periodically as damage accumulated.

The transverse stiffness decreased gradually throughout test period but did not change appreciably before the first few wire breaks were detected. The strain distributions indicated that the stresses along the strands varied significantly once the grout cracked. The strain distribution in Cable 03 behaved in an elastic manner when subjected to low-amplitude displacements; but behaved in an inelastic manner as the amplitude of the displacement increased and the grout cracked.

The natural frequencies of the specimens gradually decreased during the fatigue tests. In general, the variation was not sensitive to the first few wire breaks. When the tests were terminated, a top strand was completely fractured for Cable 02 and a bottom strand and three wires of top strand were fractured for Cable 03, respectively. While more than 50% of cross-sectional area of the strand had been lost, neither the transverse stiffness nor the natural frequencies decreased proportionally. The total variation of natural frequencies is summarized in Table 4.23.

The SoundPrint™ system monitored wire breaks and identified the locations during the test period. The report was in general agreement with the findings from the autopsy. However, the number of reported wire breaks was less than the number of actual wire breaks identified during the autopsy.

***Table 4.23 Variation of Natural Frequencies (Hz)***

<b>Mode of Vibration</b>	<b>Cable 01</b>		<b>Cable 02</b>		<b>Cable 03</b>	
	<b>Initial</b>	<b>Final</b>	<b>Initial</b>	<b>Final</b>	<b>Initial</b>	<b>Final</b>
<b>1</b>	4.6	4.2	4.4	3.9	4.3	3.5
<b>2</b>	9.4	8.6	8.9	7.9	8.8	7.1
<b>3</b>	14.5	13.2	13.6	12.4	13.7	11.2
<b>4</b>	20.0	18.3	18.6	17.4	19.0	15.8
<b>5</b>	25.6	23.6	23.5	22.6	24.7	21.2
<b>6</b>	32.2	29.7	29.6	28.9	31.6	27.3

## **Chapter 5: Response of Post-Tensioned Tendons**

Two, 36-ft external post-tensioned tendons were constructed and tested in this phase of the investigation. Two techniques were used to induce damage in the test specimens: Tendon 01 was subjected to fatigue loading, while the strands in Tendon 02 were exposed to acid. In both cases, the number of fractured wires increased with time, and the natural frequencies of the specimens were measured periodically during the tests. Measured data, including the frequency signatures and the results of the autopsies, are presented in this chapter. The relationships between the number of wire breaks and the measured frequencies are discussed in Chapters 6 and 7.

### **5.1 OVERVIEW OF TESTS**

Both test specimens were designed to simulate one section of a continuous external tendon between a diaphragm and a deviator or between two deviators in a post-tensioned bridge. The strands were anchored at each end in a concrete block using commercial post-tensioning hardware.

Tendon 01 comprised twelve, 0.6-in. diameter strands prestressed to 60% of GUTS, for a total applied prestressing force of 425 kip. Damage was induced in this specimen by fatigue loading in the transverse direction. The test setup was similar to that used by Poser (2001) and Ridd (2004) to evaluate the fatigue response of stay cables. The transverse load was applied near the quarter point of the specimen and 25 wire breaks were identified at the end of the fatigue tests. The wire breaks were monitored continuously during the fatigue tests using acoustic sensors and the natural frequencies were measured 13 times.

Tendon 02 comprised nine, 0.6-in. diameter strands prestressed to 80% of GUTS, for a total prestressing force of 425 kip. During construction, three 7-in. long grout voids were intentionally created along the length of the specimen. During the test, each void was filled with a hydrochloric acid solution to simulate hydrogen induced corrosion



(HIC) of the strand. At the end of the exposure test, 30 wire breaks were identified. Corrosion was monitored visually during the five-month exposure test, and the natural frequencies were measured 25 times.

The test schedule for specimens Tendons 01 and 02 is summarized in Table 5.1. The construction process was similar for the two specimens, and is discussed in Section 5.2, instrumentation is summarized in Section 5.3, the response of Tendon 01 is presented in Section 5.4, and the response of Tendon 02 is discussed in Section 5.5.

***Table 5.1 Test Schedule for Tendon Specimens***

***(a) Tendon 01***

<b>Stage</b>	<b>Date</b>
Stress strand	11/10/05
Grout specimen	11/16/05
Begin fatigue tests	1/4/06
End fatigue tests	1/26/06
Autopsy	1/27/06

***(b) Tendon 02***

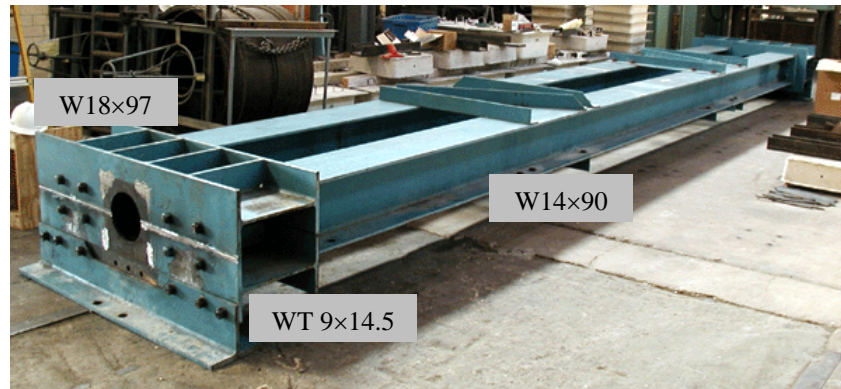
<b>Stage</b>	<b>Date</b>
Stress strand	2/14/06
Grout specimen	2/16/06
Begin acid exposure – Void 1	3/06/06
Begin acid exposure – Void 2	4/28/06
Begin acid exposure – Void 3	7/03/06
End exposure test	8/07/06
Autopsy	8/09/06

## 5.2 CONSTRUCTION OF TENDON SPECIMENS

The procedures used to construct the two tendon specimens are summarized below. The construction materials were nominally identical for the two specimens.

### 5.2.1 Reaction frame

A 32-ft, steel reaction frame was used to resist the prestressing force in the post-tensioned tendons (Figure 5.1). The frame was designed and constructed by Poser (2001) for fatigue tests of cable stays. Minor changes were made to accommodate the concrete anchor blocks and the location of the applied loads for Tendon 01.

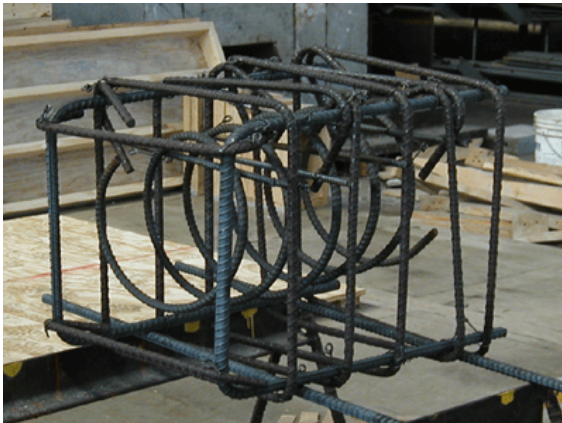


*Figure 5.1 Reaction Frame*

### 5.2.2 Concrete Anchor Blocks

Four concrete blocks were constructed to enclose the post-tensioning hardware used to anchor the strands (Figure 5.2). Each block was 24 in. long with an 18×18-in. cross section. The reinforcement in the blocks was designed to resist the prestressing forces and the corresponding local bursting stresses (Figure 5.2a). Two U-shaped bars were used as the longitudinal reinforcement. Closed hoops with 135° hooks were used as the transverse reinforcement. Spirals were positioned in the middle of the cage to resist bursting forces. Design calculations for the anchor blocks are presented in Appendix I.

Commercial, post-tensioning hardware was used. VSL Type E 6-12 is designed to accommodate twelve, 0.6-in. diameter strands and includes an anchor head, bearing plate, anchor cap, and high density polyethylene (HDPE) duct (Figure 5.2b). The HDPE duct extended 4 ft beyond the outer face of the concrete blocks (Figure 5.2c) to facilitate construction of the specimen. The measured compressive strength of the concrete (Figure 5.2d) was 4500 psi at 28 days.



(a) Reinforcement cage



(b) Anchor plate within reinforcement



(c) Concrete form



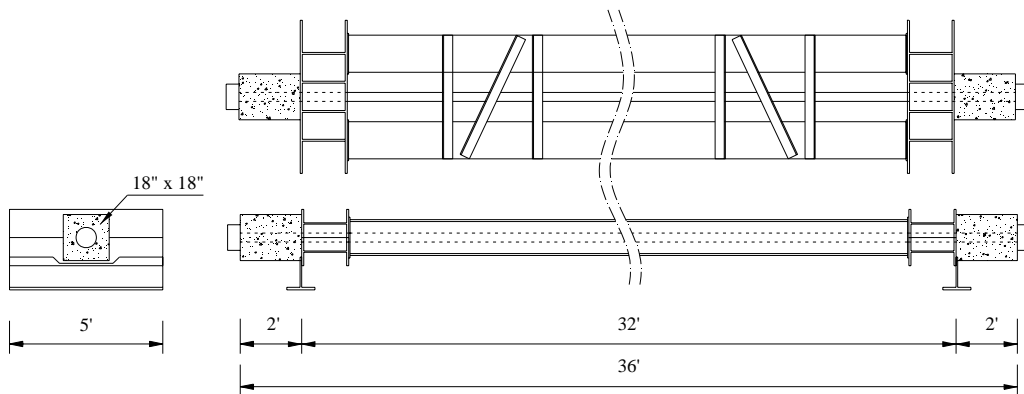
(d) Completed blocks

***Figure 5.2 Construction of Concrete Anchor Blocks***

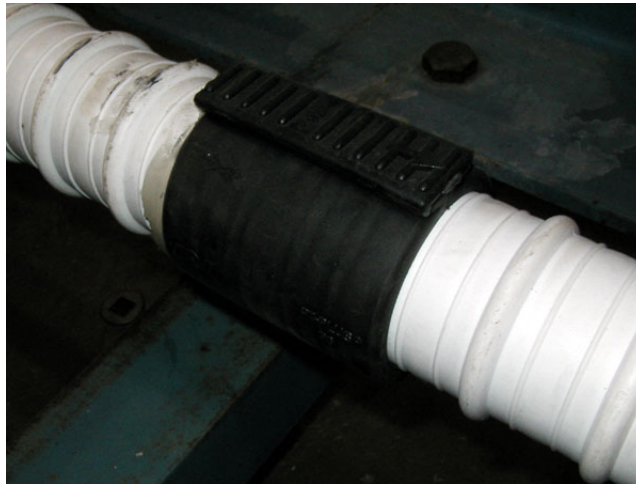
### **5.2.3 Assembly of Tendon Specimens**

After curing, a concrete anchor block was placed at each end of the steel reaction frame (Figure 5.3). Additional sections of duct were attached to the anchor blocks using

VSL plastic couplers (Figure 5.4). Each strand was pushed through the anchor head at one end, the HDPE duct, and the anchor head at the other end of the specimen. Care was taken to ensure that each strand entered and exited through corresponding holes in the anchor heads and that strands did not cross along the length of the specimens. The strands were positioned in the anchor head from bottom to top. As the strands became congested in the duct, the friction increased among the strands in the narrow cross-section of the duct, and higher forces were required to push the strands through the duct. Once positioned, the strands were held in place in the anchor heads using wedges.



**Figure 5.3 Configuration of Tendon Specimens**



*Figure 5.4 VSL Mechanical Coupler for HDPE Duct*

#### **5.2.4 Prestressing Procedure**

After the components were assembled, strands were prestressed in two stages. First, an axial force of approximately 5 kip was applied to each strand to align the strands with the anchor heads and seat the wedges. Then the desired level of prestressing was applied simultaneously to all strands.

##### **5.2.4.1 Initial Prestressing**

After assembly, the strands were loosely positioned and the wedges were not completely seated in the anchor heads. In order to prevent an uneven distribution of stress within the strands during the final stressing, the strands were first tensioned individually to about a force of approximately 5 kip using a mono hydraulic ram (Figure 5.5).

Due to the congestion of strands at the anchor head, a 2-ft long steel pipe with a tapered nose was used to transfer axial compression to the wedges. Two springs were positioned at the nose of the pipe to prevent the movement of wedges when the force was released.

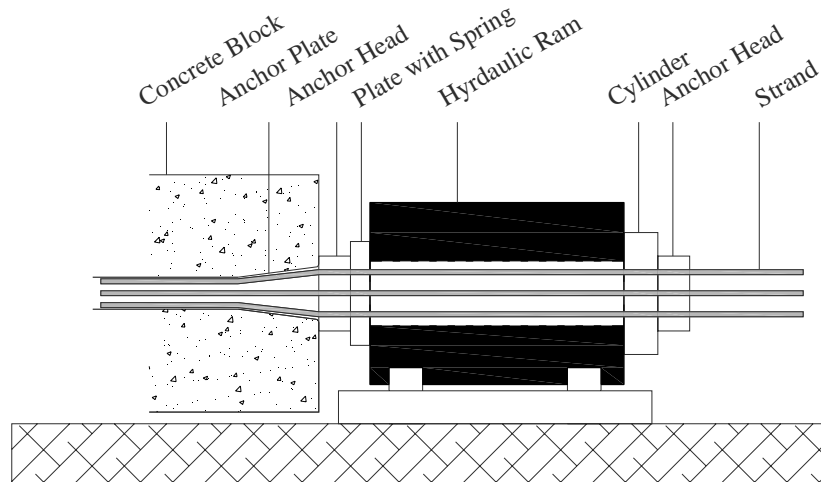




**Figure 5.5 Initial Prestressing Procedure**

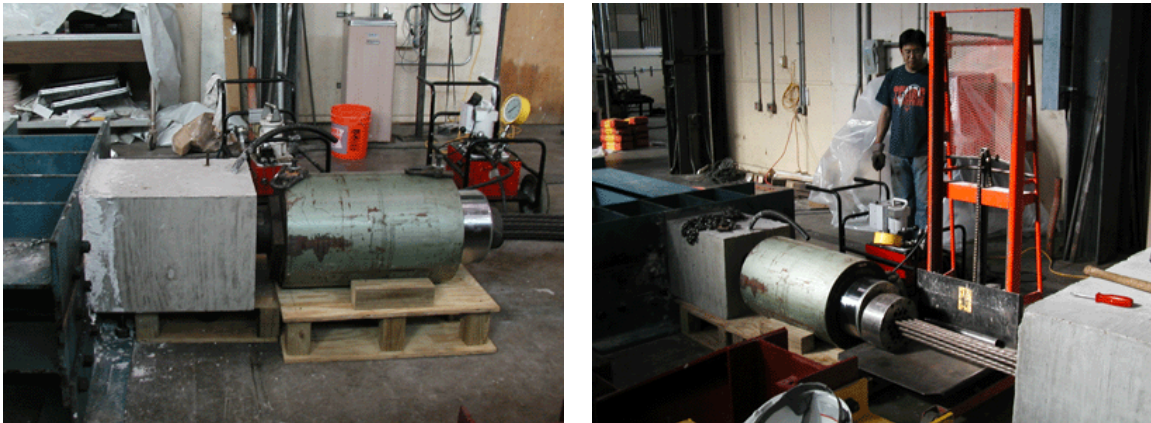
#### **5.2.4.2 Final Prestressing**

After each strand was stressed individually, a center-hole hydraulic ram was used to stress the strands simultaneously to the target force level (Figure 5.6). In Tendon 01, the twelve strands were stressed to 60% of GUTS and in Tendon 02, the nine strands were stressed to 80% of GUTS. The total prestressing force was the same in both specimens, 425 kip. In order to distribute the stress evenly among the strands, a plate with two springs along each strand was positioned between the ram and the anchor head.



**Figure 5.6 Arrangement of Equipment for Final Prestressing**

The stress was applied in three cycles to minimize seating losses. In the first cycle, the maximum force was 30% of the target force level. This force was released and increased to 60% of the target force in the second cycle. During the third cycle, the force was increased to 105% of the target force level to compensate for expected losses. The force in the hydraulic cylinder was monitored using a pressure gage during the stressing operation (Figure 5.7).



*Figure 5.7 Application of Final Prestressing*

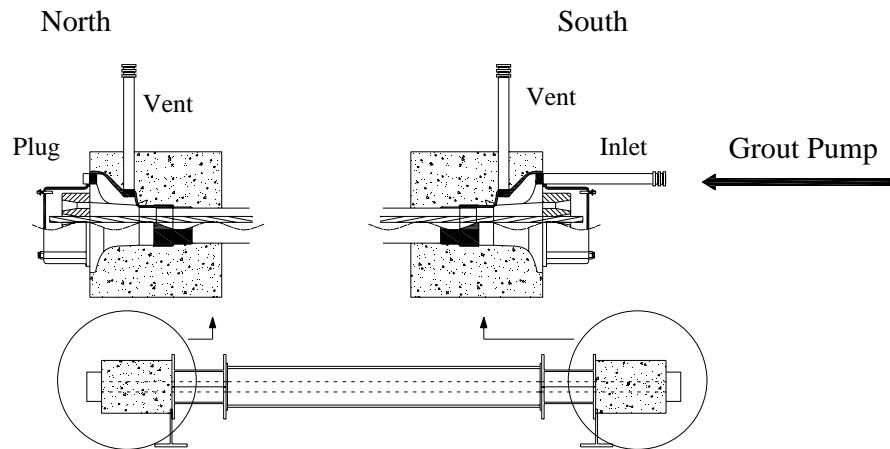
### **5.2.5 Grouting Procedure**

After the strands were stressed, the ducts were filled with a prepackaged cementitious grout, Sika 300 PT. The specimens were grouted in a horizontal position using the configuration recommended by VSL. Grout was pumped into the specimen through an inlet attached to the south anchor plate (Figure 5.8). The corresponding hole in the north anchor plate was plugged. A vent was also connected to the anchor plate at each end of the specimen.

### **5.2.6 Intentional Voids in Tendon 02**

Three, 7-in. long voids were intentionally created in Tendon 02 (Figure 5.9). To create the voids, pieces of cellulose sponge were attached to sections of HDPE duct

(Figure 5.10a) using epoxy and transparent tape. These sections of ducts were positioned along the length of the specimen using the plastic couplers (Figure 5.10b). Each section of duct was rotated such that the sponge was at the top.



(a) Arrangement of grout inlet and vents



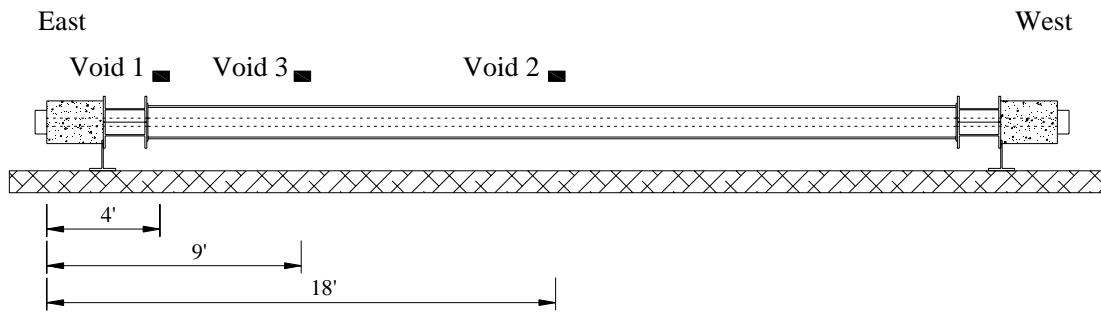
(b) North end



(c) South end

*Figure 5.8 Arrangement of Grout Inlet and Vents*





**Figure 5.9 Location of Grout Voids in Tendon 02**



**(a) Sponge attached to sections of duct**



**(b) Assembly of duct**



**(c) Sponge after grouting**



**(d) Strands after removal of sponge and grout**

**Figure 5.10 Construction of Grout Voids – Tendon 02**

After grouting, the top half of the sections of duct in the vicinity of the voids were removed (Figure 5.10c). The sponges were then removed, and the thin layer of grout that covered the strand was chipped away. Four to six strands were visible in each void (Figure 5.10d) at the completion of the process.

### **5.3 INSTRUMENTATION**

Two types of instruments were used to monitor the response of the tendon specimens. Acoustic sensors were positioned along Tendon 01 and were used to detect wire breaks during the fatigue tests. Accelerometers were used on both specimens to determine the natural frequencies. The locations of the instruments are shown in Figure 5.11 for Tendon 01 and in Figure 5.12 for Tendon 02.

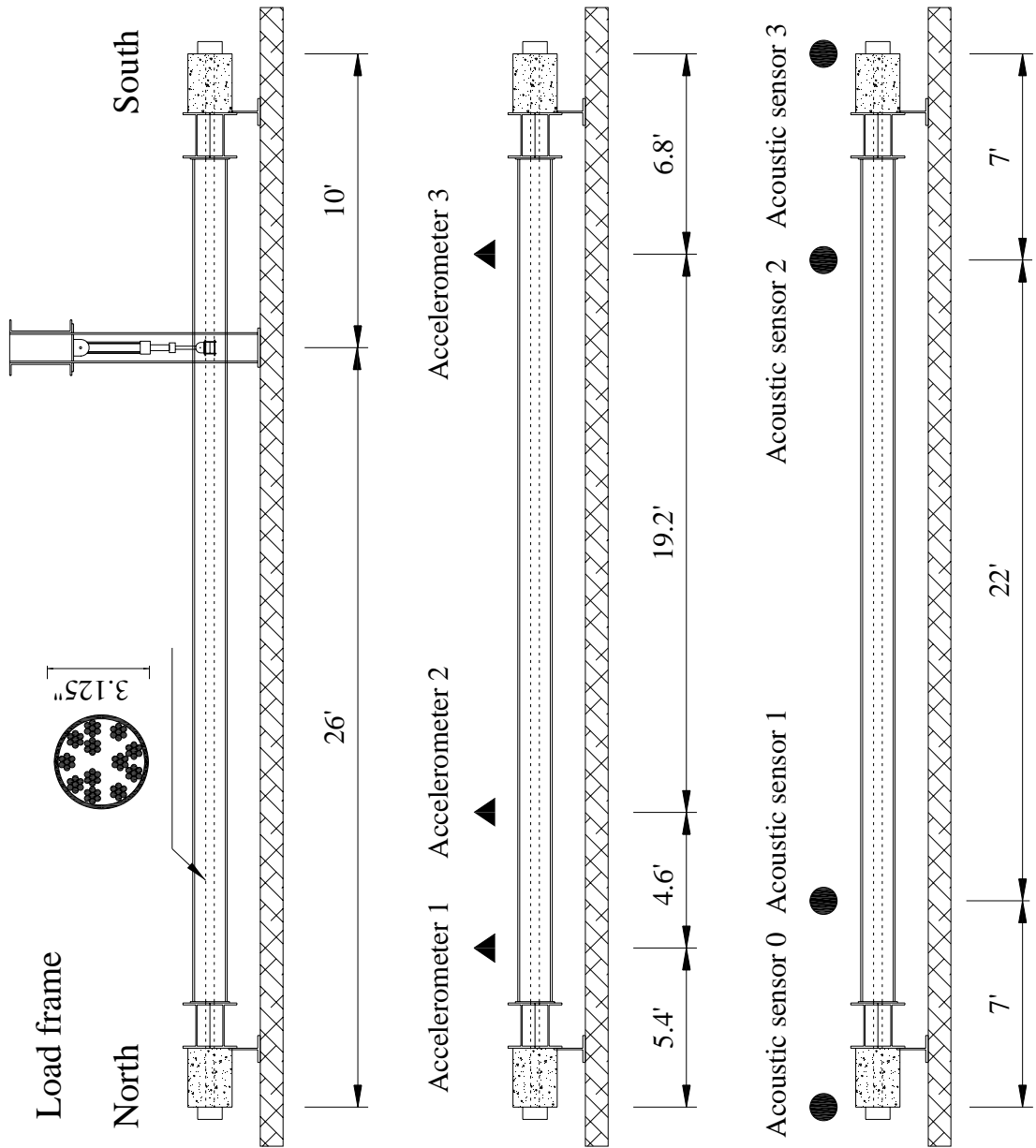
#### **5.3.1 Acoustic Sensors**

Four acoustic sensors were attached to Tendon 01. Two sensors were positioned 7 ft from each end and attached to the bottom of the duct using a cyanoacrylate adhesive and wrapped by a metal band (Figure 5.13a). The remaining two sensors were positioned on the outer faces of the concrete anchor blocks using a cyanoacrylate adhesive (Figure 5.13b).

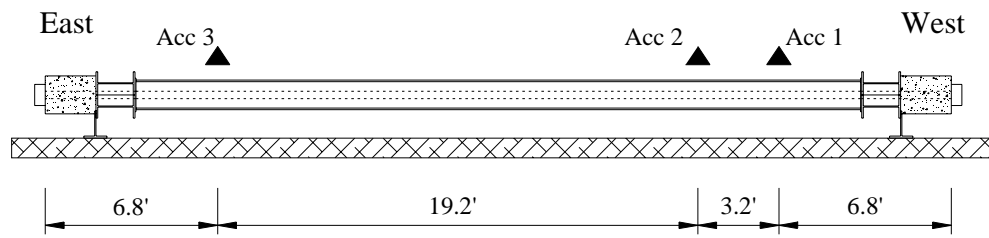
#### **5.3.2 Accelerometers**

Three, one-dimensional accelerometers were used to monitor the frequency response of Tendon 01 and Tendon 02. The accelerometers and DAQ system are described in Appendix E. The accelerometers were positioned 5.4 ft, 10 ft, and 29.2 ft from the north end of Tendon 01 and 6.8 ft, 10 ft, and 29.2 ft from the west end of Tendon 02.

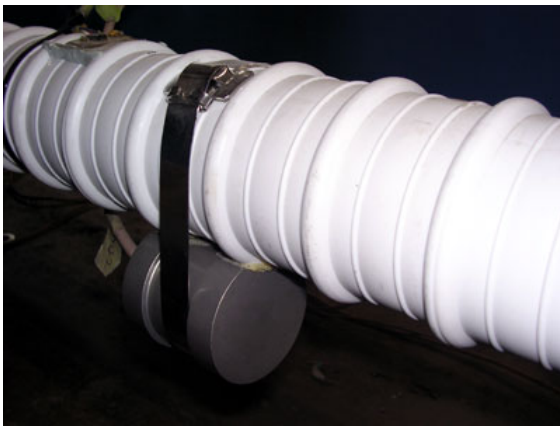
The accelerometers were attached to the post-tensioning ducts using hot-melt glue for Tendon 01 (Figure 5.14). Because Tendon 02 was outside during the exposure test, the accelerometers were potted and then attached to the post-tensioning duct for Tendon 02 (Figure 5.15).



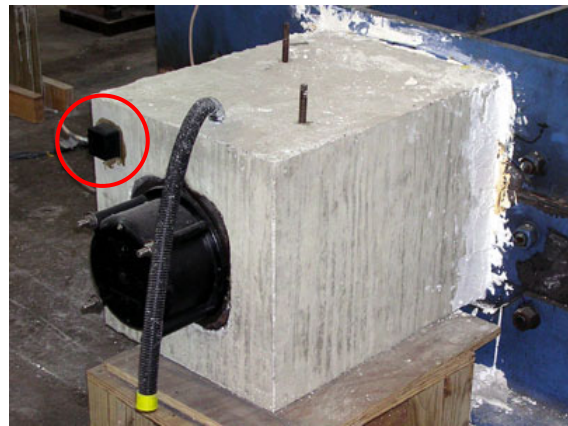
**Figure 5.11** Position of Load Frame, Accelerometers, and Acoustic Sensors for Tendon 01



**Figure 5.12 Position of Accelerometers for Tendon 02**



(a) At free length

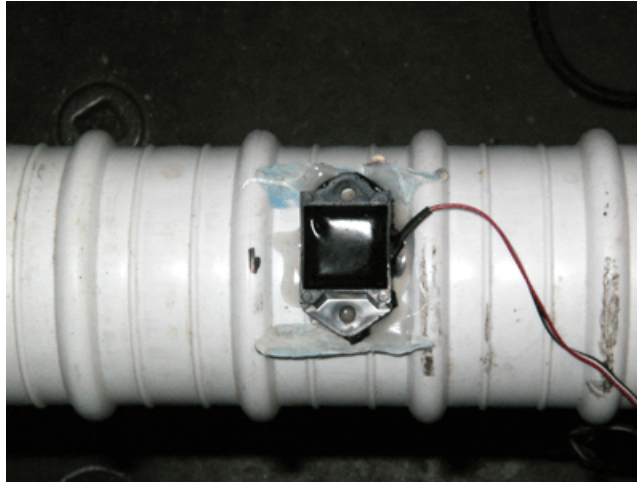


(b) At anchor block

**Figure 5.13 Acoustic Sensors used to Monitor Tendon 01**



**Figure 5.14 Accelerometer Attached to Tendon 01**



*Figure 5.15 Accelerometer Attached to Tendon 02*

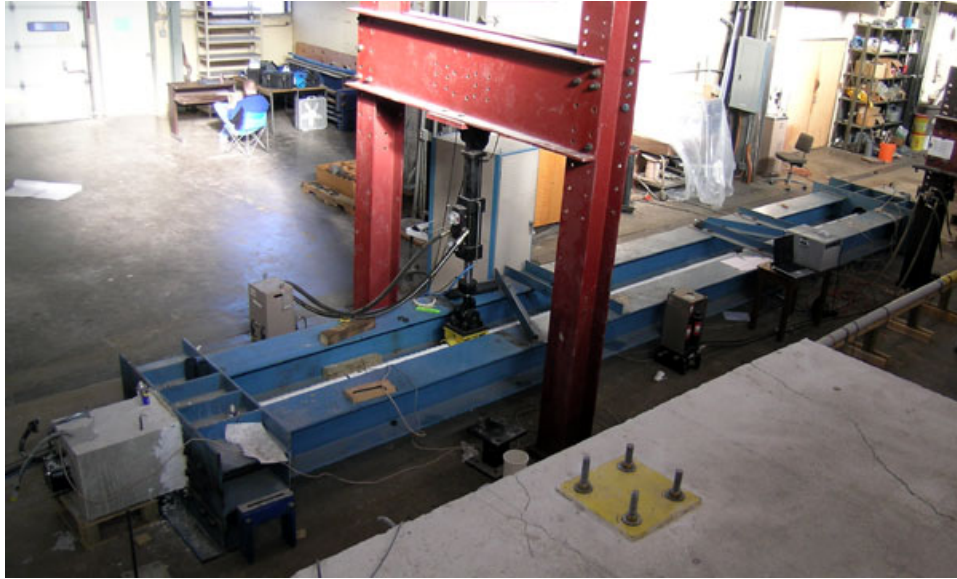
#### **5.4 TENDON 01**

The measured response of Tendon 01 is discussed in this section. The specimen was subjected to 3,900,000 loading cycles during a 22-day period. During the fatigue tests, damage accumulated in the form of wire breaks in the strand and cracks in the grout. The acoustic sensors were used to detect the wire breaks. Periodic measurements of the transverse stiffness and natural frequencies of Tendon 01 were made during the fatigue test (Table 5.2) to quantify changes in the global properties of the specimen.

The fatigue test (Figure 5.16) was operated in displacement control and the applied load was positioned 10 ft from the south end of the specimen (Figure 5.11). Initially, the specimen was excited upward and downward from the zero position. However, after 10 days the specimen was excited only upward to stabilize the hydraulic system. The span and frequency of the applied load were adjusted periodically to accelerate the fatigue damage. The hydraulic actuator and control system used for the fatigue tests are described in Appendix D. The overall test program for Tendon 01 is presented in Table 5.3 and the test schedule is summarized in Appendix J.

The measured transverse stiffness of Tendon 01 is discussed in Section 5.4.1 and the measured natural frequencies are summarized in Section 5.4.2. Wire breaks detected

by the acoustic monitoring system are documented in Section 5.4.3 and the condition of the specimen after the autopsy is presented in Section 5.4.4.



*Figure 5.16 Overview of Tendon 01*

*Table 5.2 Periodic Tests - Tendon 01*

<b>Date</b>	<b>Transverse Stiffness</b>	<b>Natural Frequency</b>	<b>Wire Breaks Reported*</b>
-	x	x	0
1/05/06	-	x	0
1/09/06	x	x	2
1/10/06	x	x	6
1/11/06	x	x	9
1/15/06	x	x	11
1/16/06	x	x	12
1/19/06	x	x	12
1/20/06	x	x	12
1/21/06	x	x	14
1/22/06	x	x	14
1/24/06	x	x	17
1/25/06	x	x	20
1/26/06	x	x	21

\* Wire breaks reported by acoustic sensors.



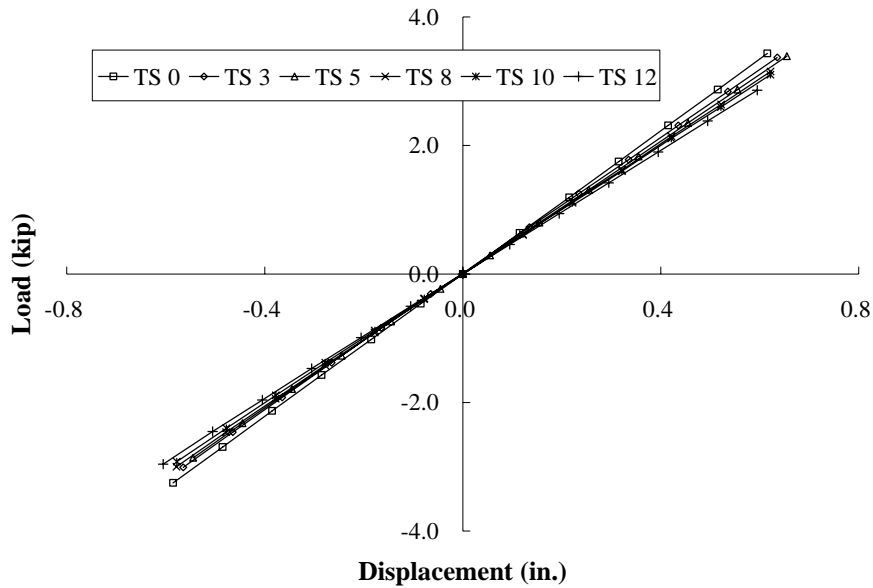
*Table 5.3 Fatigue Tests – Tendon 01*

Date	Cycle	Configuration		
		Set Point (in.)	Span (in.)	Frequency (Hz)
1/04/06	0	0	± 0.5	2.0
1/11/06	1,047,695	0	± 0.3	2.0
1/13/06	1,248,230	0.22	± 0.2	2.0
1/15/06	1,593,858	0.22	± 0.2	3.5
1/16/06	n/a	0.22	± 0.2	4.0
1/17/06	n/a	0.3	± 0.28	3.5
1/18/06	n/a	0.4	± 0.38	2.5
1/19/06	2,623,439	0.5	± 0.48	2.5
1/19/06	2,660,152	0.6	± 0.58	2.0
1/19/06	2,726,011	0.65	± 0.58	2.0
1/20/06	2,814,775	0.75	± 0.6	2.5
1/20/06	2,861,425	0.8	± 0.6	2.5
1/21/06	3,026,868	0.9	± 0.6	2.0
1/22/06	3,201,894	0.9	± 0.65	2.0
1/23/06	3,369,590	1.1	± 0.65	2.0
1/23/06	3,400,336	1.2	± 0.6	2.0
1/23/06	3,416,880	1.3	± 0.6	2.0
1/24/06	3,532,401	1.4	± 0.6	2.0
1/25/06	3,773,862	1.5	± 0.6	2.0
1/25/06	3,797,690	1.6	± 0.6	2.0
1/26/06	3,904,211	Test terminated		

#### 5.4.1 Transverse Stiffness

The transverse stiffness of Tendon 01 was recorded thirteen times during the fatigue test (Table 5.2). Tests are designated “TS X” where “TS” refers to transverse stiffness and “X” indicates the test number. Reported values of transverse stiffness correspond to the displacement at the location of the applied load. Initially, the specimen was pushed to displacement levels of ±1.5 in. during the static tests. However, two wire breaks were detected during these tests (the sixth wire fractured during TS 2 and the ninth wire fractured during TS 3). In all subsequent static tests, the displacement range was limited to ±0.6 in.

The variation of recorded stiffness is displayed in Figure 5.17 and summarized in Table 5.4. The load-displacement relationship was linear in all tests and the transverse stiffness decreased gradually from 5.6 to 4.8 kip/in. as damage accumulated.



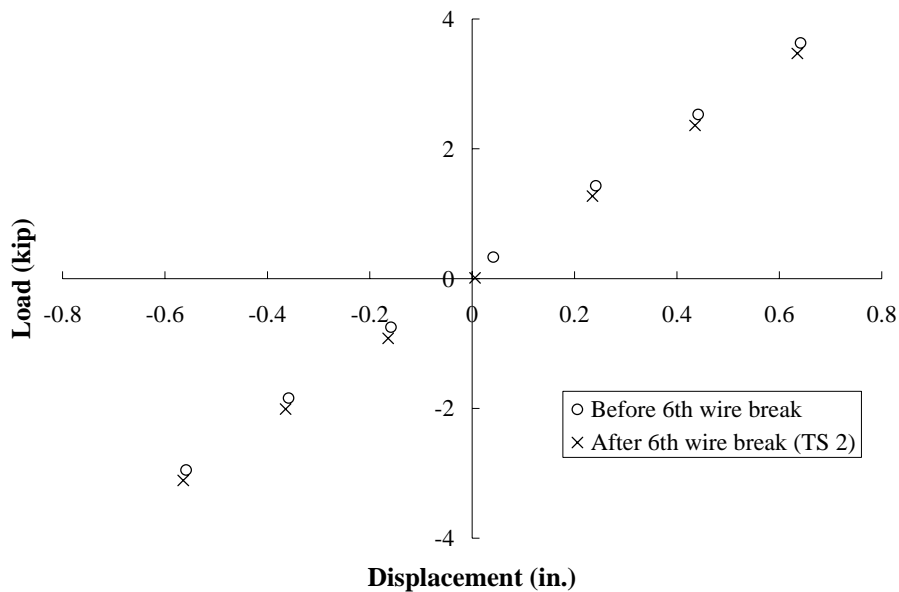
*Figure 5.17 Transverse Stiffness of Tendon 01*

*Table 5.4 Transverse Stiffness of Tendon 01*

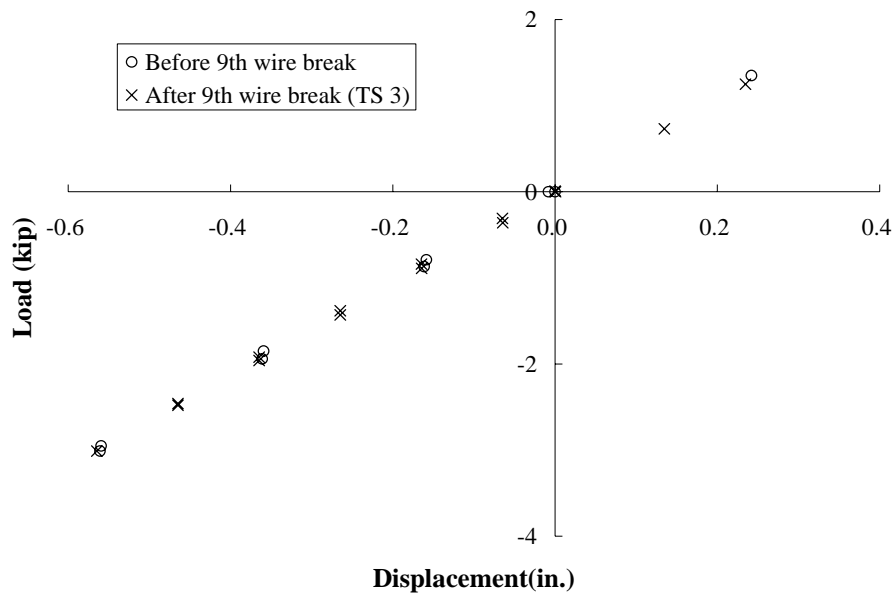
Measurement ID	Date	Stiffness (kip/in.)	Wire Breaks Reported
TS 0	1/04/06	5.6	0
TS 1	1/09/06	5.5	2
TS 2	1/10/06	5.5	6
TS 3	1/11/06	5.3	9
TS 4	1/15/06	5.4	11
TS 5	1/16/06	5.2	12
TS 6	1/19/06	5.2	12
TS 7	1/20/06	5.1	12
TS 8	1/21/06	5.1	14
TS 9	1/22/06	5.1	14
TS 10	1/24/06	5.0	17
TS 11	1/25/06	4.9	20
TS 12	1/26/06	4.8	21



Two wires fractured during static tests (TS 2 on 1/10/06 and TS 3 on 1/11/06). In both cases, the specimen was being loaded toward the maximum displacement of 1.5 in. The sound of the wire fracture was clearly audible and was detected by the acoustic sensors. However, these wire breaks did not influence the measured load-displacement response. Recorded data before and after the wire break indicated the same stiffness and no indication of nonlinear response was observed. Therefore, the data recorded immediately after the wire breaks are designated as TS 2 and TS 3, respectively. Recorded load-displacement relationships before and after the wire breaks are plotted in Figure 5.18 and Figure 5.19.



**Figure 5.18 Recorded Load-Displacement Response on January 10, 2006**



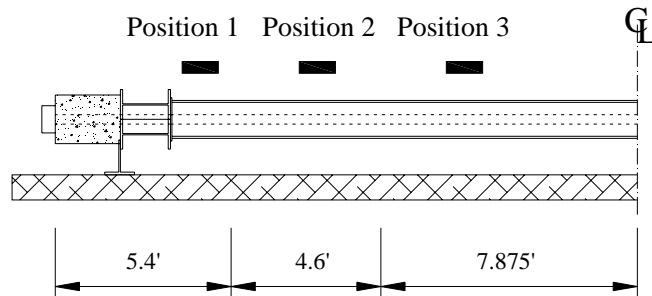
*Figure 5.19 Recorded Load-Displacement Response on January 11, 2006*

#### 5.4.2 Natural Frequencies

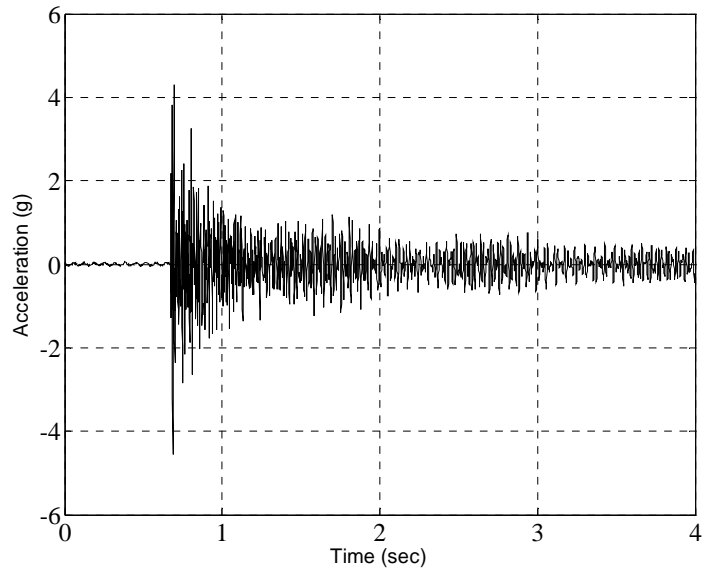
The natural frequencies of the Tendon 01 were measured fourteen times during the fatigue tests. Tests are designated “NF X” where “NF” refers to natural frequency and “X” indicates the test number. Vibrations were induced by striking the test specimen with a rubber hammer at three locations along the length (Figure 5.20). In most cases, this method was sufficient to capture the first six modes of vibration.

The measured response during test NF 4 was considered to be representative of the response of Tendon 01. Time-domain data are shown in Figure 5.21(a) and the corresponding frequency-domain data are shown in Figure 5.21(b). Unlike the cable specimens discussed in Chapter 4, a single peak was not observed in the frequency domain for most of the modes. Dual peaks may be observed for the second through the sixth modes of vibration in Figure 5.21(b). One possible explanation for the presence of the dual peaks is discussed in Chapter 6.

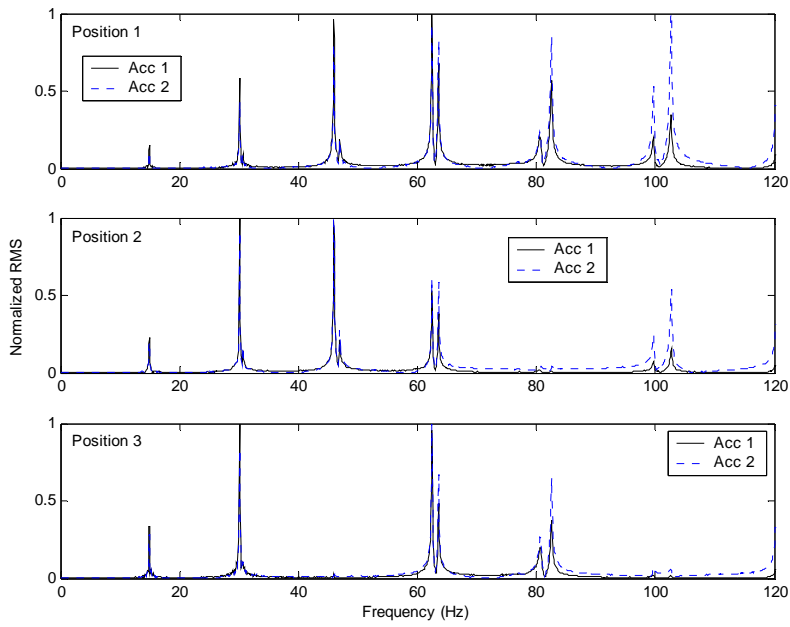
The values of the first six natural frequencies obtained from the free-vibration tests are summarized in summarized in Table 5.5. For cases where dual peaks were observed, the amplitude of one peak was generally two times larger than the amplitude of the second peak. The frequency of the stronger peak is reported in Table 5.5. However, in cases where the amplitudes of the two peaks were similar, the natural frequency of that mode of vibration is not reported. The complete set of frequency-domain data for Tendon 01 is presented in Appendix K.



**Figure 5.20 Location for impact for Tendon Specimens**



(a) Time domain



(b) Frequency domain

**Figure 5.21 Representative Response of Tendon 01 (NF 4)**

**Table 5.5 Measured Natural Frequencies for Tendon 01**

Mode of Vibration	NF 0	NF 1	NF 2	NF 3	NF 4	NF 5	NF 6
	12/22/05	1/05/06	1/09/06	1/10/06	1/11/06	1/15/06	1/16/06
1	15.4	15.2	15.2	15.1	15.0	14.9	14.7
2	31.0	30.6	30.7	30.4	30.1	30.0	29.7
3	47.4	46.8	46.8	46.4	45.9	45.7	45.3
4	64.4	63.9	63.7	63.2	62.5	62.2	61.7
5	84.8	83.3	83.7	83.3	82.5	82.3	-
6	105.7	104.1	104.4	103.6	102.7	102.3	101.6
Wire breaks reported	0	0	2	6	9	11	12

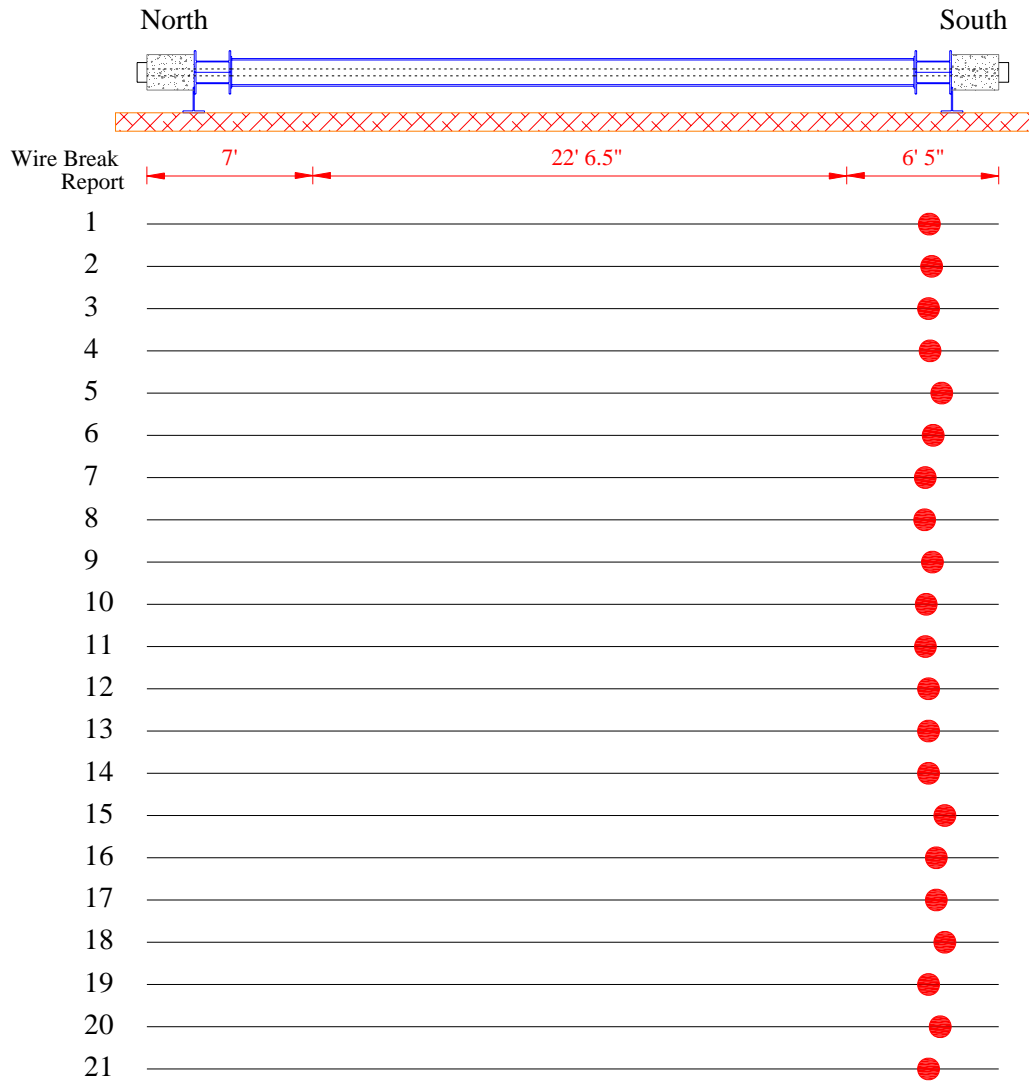
Mode of Vibration	NF 7	NF 8	NF 9	NF 10	NF 11	NF 12	NF 13
	1/19/06	1/20/06	1/21/06	1/22/06	1/24/06	1/25/06	1/26/06
1	14.7	14.7	14.6	14.6	14.5	14.3	14.2
2	29.6	29.5	29.5	29.5	29.2	28.8	28.7
3	45.3	45.2	45.0	45.0	44.6	44.0	43.8
4	61.6	61.5	61.3	61.3	60.8	59.9	59.7
5	-	-	81.1	81.0	80.5	76.9	76.7
6	101.5	101.2	100.9	100.8	100.2	99.2	98.9
Wire breaks reported	12	12	14	14	17	20	21

The reduction of natural frequencies observed between NF 0 and NF 1 was not due to wire breaks. During this period, fatigue cycles were only applied for 18 hours. The change in frequencies appeared to be caused by the formation of cracks in the grout, but similar trends were not observed in any of the cable specimens.

In spite of the fact that two wire breaks were reported between NF 1 and NF 2, the natural frequencies did not change. Variations in the natural frequencies were only observed after the sixth wire break was reported (NF 3). After NF 3, the frequencies of all modes decreased as damage accumulated.

### 5.4.3 Damage Detected by Acoustic Sensors

A total of 21 wire breaks was detected by the acoustic monitoring system. All 21 wire breaks were located near north end of the south anchor block. The reported locations of the wire breaks are displayed in Figure 5.22 and summarized in Table 5.6.



*Figure 5.22 Location of Wire Breaks Detected by Acoustic Sensors*

*Table 5.6 Summary of Wire Breaks – Tendon 01*

Wire Break Number	Date and Time	Estimated Number of Cycles	Location of Wire Break from South End (ft)
1	1/08/06 11:13 PM	731,000	2.9
2	1/09/06 7:31 AM	790,000	2.8
3	1/10/06 12:49 AM	901,000	3.0
4	1/10/06 7:46 AM	951,000	2.9
5	1/10/06 8:26 AM	955,000	2.4
6	1/10/06 10:00 AM	-	2.8
7	1/10/06 8:09 PM	1,020,000	3.1
8	1/10/06 8:43 PM	1,024,000	2.8
9	1/11/06 10:35 AM	-	3.1
10	1/13/06 10:59 AM	1,249,000	3.1
11	1/14/06 7:00 AM	1,394,000	3.0
12	1/16/06 3:36 AM	1,794,000	3.0
13	1/20/06 12:19 AM	2,739,000	3.0
14	1/20/06 4:47 PM	2,879,000	3.0
15	1/23/06 11:57 AM	3,382,000	2.3
16	1/23/06 8:06 PM	3,440,000	2.6
17	1/24/06 2:29 AM	3,480,000	2.6
18	1/24/06 4:23 PM	3,494,000	2.3
19	1/25/06 1:04 AM	3,642,000	3.0
20	1/25/06 9:49 AM	3,705,000	2.5
21	1/26/06 10:28 AM	3,875,000	3.0

#### **5.4.4 Autopsy of Tendon 01**

After the fatigue test was terminated, the specimen was disassembled to determine the extent of damage. The autopsy focused initially on wire fractures along the length of the specimen. However, extensive corrosion of the anchor heads was observed, and the scope was extended to include the post-tensioning anchorage system. The concrete anchor blocks were demolished and all the post-tensioning components were retrieved to assess the propagation of corrosion (Figure 5.23).

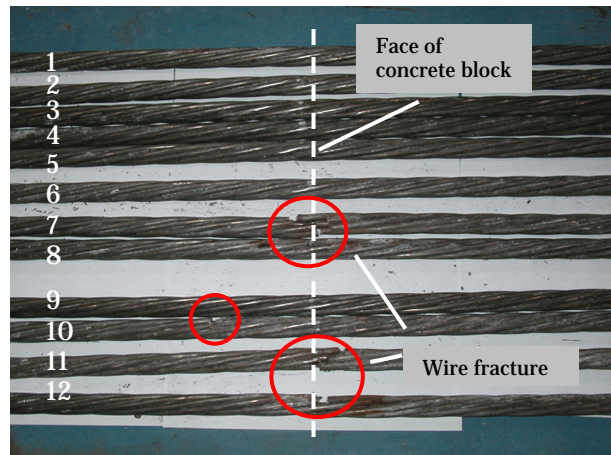


**Figure 5.23 Demolition of Concrete Anchor Block for Tendon 01**

After the autopsy, it was concluded that corrosion of the anchor head did not influence the response of Tendon 01. Findings related to the presence of corrosion in Tendon 01 are summarized in Appendix L.



**(a) Typical section**



**(b) Wire Fractures**

**Figure 5.24 Wire Fractures at Face of Concrete Block**



Twenty-five wire breaks was identified during the autopsy. All wire breaks occurred in strands positioned toward the bottom of the cross section near the north face of the south anchor block. The locations of wire fractures are shown in Figure 5.24. All seven wires fractured in strands 7, 11, and 12. Two wires fractured in the strands 8 and 10. The grout surrounding the fractured wires was severely fragmented, but no voids were observed in the grout (Figure 5.25).

Twenty-one wire breaks were reported by the acoustic sensors; but 25 wire breaks were identified during the autopsy. The location of the wire breaks identified by the acoustic sensors was in general agreement with the observed distribution of wire breaks.



(a) Condition of grout near fractured wires



(b) South anchor head



(c) Free length at north end of specimen



(d) North anchor block

**Figure 5.25 Condition of Grout – Tendon 01**

## 5.5 TENDON 02

The measured response of Tendon 02 is discussed in this section. Damage was induced in Tendon 02 by exposing the strand to acid over a five-month period (Figure 5.26). Wire breaks occurred at three locations along the length of the tendon where grout voids had been intentionally created. The natural frequencies of Tendon 02 were measured periodically during the exposure test.

Details of the acid exposure tests are given in Section 5.5.1 and the measured natural frequencies are summarized in Section 5.5.2. Non-destructive tests used to assess the likelihood of wire breaks are described in Section 5.5.3, and the condition of the specimen after the autopsy is presented in Section 5.5.4.

### 5.5.1 Corrosion Induced by Exposure to Hydrochloric Acid

As discussed in Section 5.2.6, three, 7-in. voids were created in the grout during construction of Tendon 02. Four to six strands were exposed in each void. Corrosion was induced in the strands at these locations by coating the exposed strand with a 15% solution of hydrochloric acid. The acid was applied to each void for several weeks until multiple wire breaks were detected by visual inspection. The void was then covered to prevent infiltration of water from the environment, and acid was applied to the next void (Table 5.7).

*Table 5.7 Schedule of Acid Exposure*

Location	Initiation	Completion	Exposure Period (day)
Void 1	3/09/06	4/12/06	37
Void 2	4/28/06	6/25/06	58
Void 3	7/03/06	8/07/06	35



*Figure 5.26 Overview of Tendon 02*

Most of the damage in Tendon 02 was detected by visual observation. Photographs taken when the acid was applied to Void 2 are shown in Figure 5.27 and are considered to be representative.

Before the acid was ponded in the grout void, the grout was intact and no corrosion was observed on the surface of the strand (Figure 5.27a). When the acid was poured into the void, the solution immediately reacted with the grout and formed green bubbles (Figure 5.27b). These bubbles turned dark brown within 2 to 4 hours (Figure 5.27c). The bubbles were only generated during the first two to three weeks of exposure to the acid. These bubbles were not produced during the preliminary tests discussed in Appendix M; therefore, it is believed that the bubbles were a byproduct of the reaction between the acid and the cement grout, which has a high pH. The residue of these reactions was observed on the surface of the strand (Figure 5.27d).





(a) Before acid attack



(b) Chemical reaction: phase 1

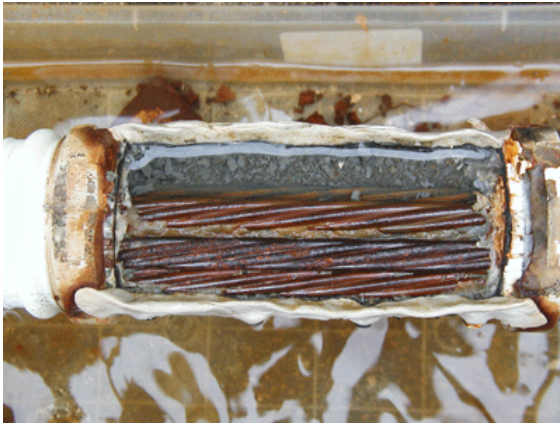


(c) Chemical reaction: phase 2



(d) Residue from bubble

***Figure 5.27 Observed Response of Tendon 02 during Exposure to Acid***



(e) After rainfall



(f) Corrosion products after rain evaporated



(g) Void filled with acid



(h) Visual observation of broken wire

***Figure 5.27 (cont.) Observed Response of Tendon 02 during Exposure to Acid***

Because the voids were exposed to the environment, rain water also accumulated in the ponding regions. After rainfall, acid was not poured into the void to avoid overflow (Figure 5.27e). After the surface of the strand dried, corrosion products were visible (Figure 5.27f).

After several weeks, pouring acid into the void did not generate green bubbles and the surface of the strand appeared to be cleaned (Figure 5.27g). When the acid dried, corrosion products were once again visible on the surface of the strand (Figure 5.27h). A screwdriver was wedged into the strand to detect the presence of broken wires.

Acid was only ponded in one void at a time. During the time that one void was exposed to permit ponding of the acid, the other two voids were covered with plastic to prevent infiltration of water from the environment. As a result, visual observations of damage in a void were only made during the portion of the test when the void was exposed. After the test, it was concluded that the number of wire breaks in Void 1 increased while acid was ponded in Voids 2 and 3, but no information is available about when those wire fractured.

### **5.5.2 Natural Frequencies**

The natural frequencies were measured 25 times before and during the acid exposure test. Four sets of readings were taken during the construction of the grout voids. These are numbered NF 0-0 (no voids) through NF 0-3 (after construction of Void 3). Twenty one measurements were made during the exposure test and are numbered NF 1 through NF 21. The test program is summarized in Table 5.8. The complete set of recorded signals in the frequency domain is presented in Appendix K.

#### ***5.5.2.1 Response before Exposure Test***

The natural frequencies were measured before and after each of the three voids was created (Table 5.9). The first grout void (Void 1) was created at the east end of the Tendon 02 and the void at midspan (Void 2) was created last. Therefore, the order in which the voids were constructed did not coincide with the order in which the voids were filled with acid.

The measured natural frequencies increased slightly as the voids were constructed. This result was not expected because removal of the grout in the vicinity of the voids was assumed to damage the specimen. However, the changes in frequency were modest compare with those observed during the exposure tests.

**Table 5.8 Summary of Test Program – Tendon 02**

<b>Date</b>	<b>Test / Remark</b>
3/06/06	Gout voids produced
3/06/06	NF 0-0, NF0-1, NF0-2, and NF 0-3
3/09/06	Begin ponding acid in Void 1
3/09/06	NF 1
3/15/06	NF 2
3/21/06	NF 3
3/29/06	NF 4
4/07/06	NF 5
4/12/06	First wire break observed in Void 1
4/12/06	NF 6
4/21/06	NF 7
4/28/06	Begin ponding acid in Void 2
4/28/06	NF 8
5/06/06	NF 9
5/12/06	NF 10
5/19/06	NF 11
5/26/06	NF 12
6/02/06	NF 13
6/06/06	NF 14
6/16/06	NF 15
6/25/06	First wire break observed in Void 2
6/25/06	NF 16
7/02/06	NF 17
7/03/06	Begin ponding acid in Void 3
7/10/06	NF 18
7/24/06	First wire break observed in Void 3
7/26/06	NF 19
8/01/06	NF 20
8/06/06	Second wire break observed in void 3
8/06/06	NF 21

**Table 5.9 Variation of Natural Frequencies in Tendon 02 before Exposure to Acid**

<b>Mode</b>	<b>Natural Frequencies, Hz</b>			
	<b>NF 0-0</b>	<b>NF 0-1</b>	<b>NF 0-3</b>	<b>NF 0-2</b>
1	15.9	16.0	16.0	16.0
2	31.7	31.8	31.8	31.8
3	48.8	48.8	48.9	49.0
4	65.8	65.8	65.9	65.8
5	84.0	84.0	84.0	84.1
6	102.8	102.8	102.9	102.9

### 5.5.2.2 Response during Exposure Test

The natural frequencies (Figure 5.28) of the test specimen were recorded twenty one times during the exposure test. The data are divided into three groups, based on the void where the acid was ponded at the time of the dynamic test. The test results are summarized in Table 5.10 through Table 5.12.



**Figure 5.28 Natural Frequency Measurement of Tendon 02**

**Table 5.10 Variation of Natural Frequencies (Void 1) (Hz)**

Mode of Vibration	NF 1	NF 2	NF 3	NF 4	NF 5		NF 6	NF 7
	3/09	3/15	3/21	3/29	4/07	4/12	4/12	4/21
1	16.4	16.4	16.5	16.5	16.5	Wire fracture identified in Void 1	15.2	15.2
2	32.3	32.2	32.1	32.0	32.1		31.4	31.6
3	48.9	48.7	48.6	48.4	48.4		47.5	47.6
4	65.9	65.6	65.4	65.0	65.0		63.8	63.9
5	83.8	83.3	82.8	82.3	82.3		80.9	81.1
6	102.3	101.6	101.1	100.4	100.5		98.8	98.9



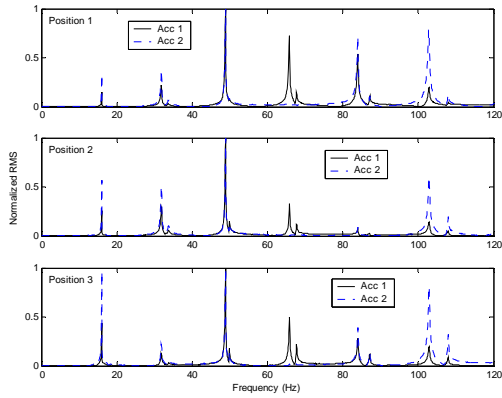
**Table 5.11 Variation of Natural Frequencies (Void 2) (Hz)**

Mode of Vibration	NF 8	NF 9	NF 10	NF 11	NF 12	NF 13	NF 14	NF 15		NF 16
	4/28	5/06	5/12	5/19	5/26	6/02	6/06	6/16	6/25	6/25
1	15.1	15.2	15.2	-	15.2	15.4	15.2	15.4	Wire fracture identified in Void 2	14.9
2	31.4	31.4	31.6	31.2	31.5	31.6	31.3	31.6		30.4
3	47.4	47.3	47.7	47.2	47.5	47.6	47.3	47.6		45.8
4	63.7	63.7	64.0	63.7	64.0	64.0	63.7	64.0		61.7
5	80.9	80.8	81.2	80.9	81.4	81.4	81.1	81.2		78.6
6	98.7	98.7	98.9	99.2	99.3	99.3	99.2	99.2		95.8

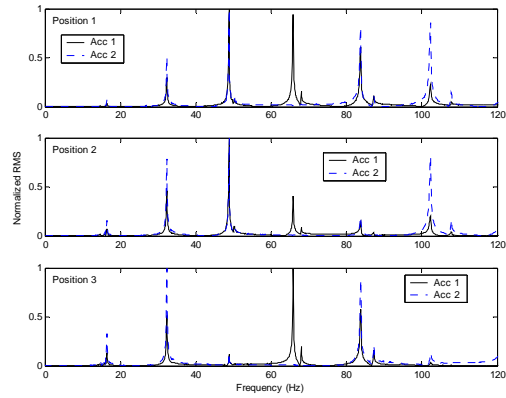
**Table 5.12 Variation of Natural Frequencies (Void 3) (Hz)**

Mode of Vibration	NF 17	NF 18		NF 19	NF 20		NF 21
	7/02	7/10	7/24	7/26	8/01	8/06	8/06
1	14.9	14.8	1st Wire Fracture Identified in Void 3	13.5	13.5	2nd Wire Fracture Identified in Void 3	13.2
2	30.5	30.3		26.8	26.9		26.3
3	45.9	45.6		41.3	41.3		40.4
4	61.7	61.4		55.7	55.7		54.5
5	78.7	78.2		71.7	71.0		69.5
6	96.0	95.5		-	86.6		84.9

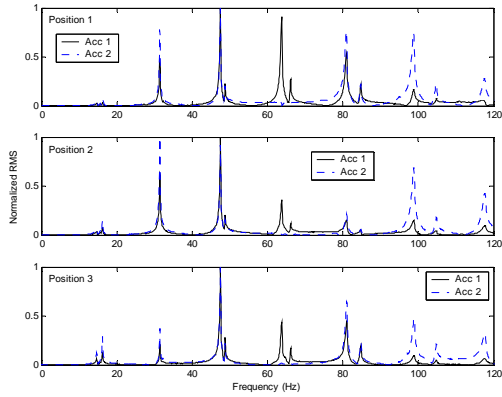
As discussed in Section 5.4.2, multiple peaks were observed in the frequency domain for Tendon 02 (Figure 5.29). This behavior was more pronounced in the fourth, fifth, and sixth modes of vibration, but was also observed in the lower three modes. In most cases, the relative amplitudes of the peaks were considerably different. Therefore, the frequency corresponding to the larger amplitude peak was selected and reported in Table 5.10 through Table 5.12. However, during NF 11, the first mode of vibration exhibited the dual peaks with comparable amplitude, and the frequency of this mode is not reported.



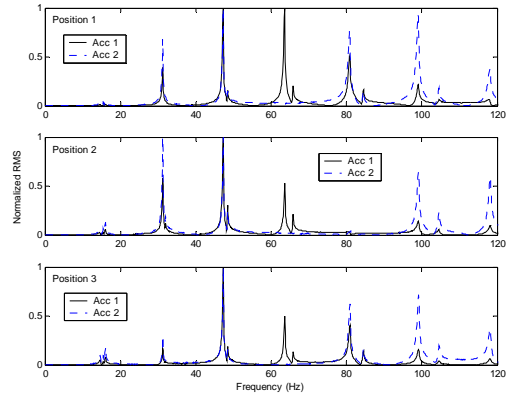
(a) NF 0-3



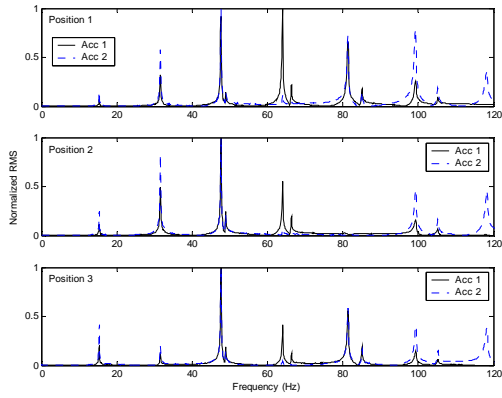
(b) NF 1



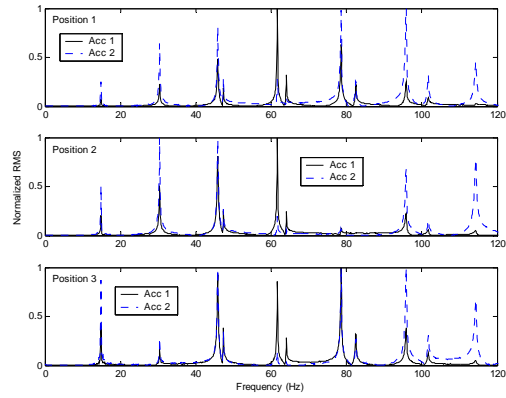
(c) NF 6



(d) NF 11



(e) NF 13



(f) NF 16

**Figure 5.29 Normalized Root Mean Square (RMS) of Tendon 02**

Between NF 0-2 and NF 1, Tendon 02 was moved from the south end of Ferguson Laboratory, where it had been constructed, to outside the north end of the laboratory, where it was located for the exposure test. The natural frequencies corresponding to the first, second, and fourth modes of vibration increased slightly after the specimen was moved, while the frequencies corresponding to the third, fifth, and sixth modes of vibration decreased slightly.

During the exposure test, the natural frequencies did not change appreciably until fractured wires were visually identified before NF 6, NF 16, NF 19, and NF 21. Due to congestion, only the strands in the top layer were visible. However, once a wire fractured, the broken wire unraveled with respect to the other wires within the void, and was easily detected. The number of wire breaks identified in the vicinity of each void at the conclusion of the ponding period for that void is summarized in Table 5.13.

***Table 5.13 Wire Breaks in each Void Detected by Visual Inspection***

<b>Date</b>	<b>Location</b>	<b>Number of Wire Breaks</b>	<b>Remark</b>
4/12	Void 1	3	Two fractures in one strand
6/25	Void 2	3	Two fractures in one strand
7/24	Void 3	1	-
8/6	Void 3	3	Two fractures in one strand
8/6	Void 1	10	Seven additional wire breaks occurred in Void 1 between 4/12 and 8/6
8/6	Void 2	8	Five additional wire breaks occurred in Void 2 between 6/25 and 8/6

Recorded natural frequencies exhibited slight variations between the wire fractures. For example, the natural frequencies increased and decreased two times between NF 12 and NF 15. These variations were not observed in any of the other specimens tested during this investigation and are likely attributed to thermal variations, since Tendon 02 was stored outdoors during the exposure tests.

Following the completion of the exposure test on 8/6/06, additional wire breaks were identified in the vicinity of Void 1 (Figure 5.30) and Void 2 (Figure 5.31). Because

these locations were only inspected while acid was ponded in these voids, nothing is known about when these wires fractured.

The condition of the strand in the vicinity of Void 3 is shown in Figure 5.32. Significant corrosion was observed on the surface of exposed strands in all voids and the surface of strands was blistered and roughened. Corrosion products were easily removed by tapping the strand with a screwdriver. In spite of the presence of severe corrosion products, severe pitting was not observed. Therefore, the strands appeared to fail by HIC.



(a) First observation (4/12/06)



(b) Second observation (8/06/06)

***Figure 5.30 Observed Wire Breaks at Void 1 at Conclusion of Exposure Test***



(a) First observation (6/25/06)



(b) Second observation (8/06/06)

***Figure 5.31 Observed Wire Breaks at Void 2 at Conclusion of Exposure Test***

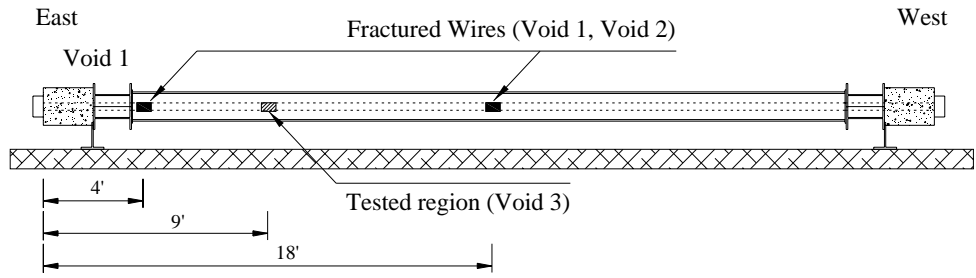


*Figure 5.32 Observed Wire Breaks at Void 3 at Conclusion of Exposure Test*

### **5.5.3 Screwdriver Penetration Test**

The screwdriver penetration test was originally developed to detect wire fractures in unbonded tendons. For this situation, the stress in the broken wire is released and the wire unravels from the strand. A screwdriver struck by a hammer can be pushed beneath the broken wire. The same approach was used to determine if stress in a broken wire in a grouted tendon recovers with distance from the wire break.

The tests were conducted by testing the soundness of the strand within in Void 3 (Figure 5.33). The first test was performed between NF 6 and NF 7 and the second test was performed between NF 16 and NF 17 (Figure 5.34). In spite of numerous wire fractures observed in Voids 1 and 2 at the time of these tests, broken wires were not identified using the screwdriver penetration test. The grout appeared to absorb the energy from the wire fractures and maintain the original geometry of strands. In the case of the grouted tendon, the broken wire is expected to recover a portion of the original axial stress, such that the screw driver cannot penetrate between wires several feet from the wire break.



***Figure 5.33 Tested Region and Location of Wire Breaks***



***Figure 5.34 Screwdriver Penetration Test***



#### 5.5.4 Autopsy of Tendon 02

Tendon 02 was disassembled at the end of the exposure test to determine the extent of damage. Thirty wire breaks were identified (Figure 5.35): 16 in the vicinity of Void 1, 11 in the vicinity of Void 2, and 3 in the vicinity of Void 3. Nine of these wire breaks occurred in the second layer of strands, which is why the breaks were not observed in the visual inspection conducted at the end of the exposure test. The grout was fragmented along nearly the entire length of the tendon. The grout in the vicinity of the voids was nearly completely pulverized (Figure 5.36).

While 30 wire breaks were identified in the three voids, it is expected that this number over-estimated the loss of cross-sectional area in the tendon. Because the same strand were exposed in each void, it is likely that wires in the same strand fractured in more than one void. Therefore, the loss of cross-sectional area of the strands was conservatively expected to higher than a maximum number of wire breaks in single void: 16 wire fractures in Void 1.



(a) Fractured wires



(b) Completely fractured strand

***Figure 5.35 Condition of Strand Observed during Autopsy***



*Figure 5.36 Condition of Grout in Vicinity of Void 1 after Autopsy*

## 5.6 SUMMARY

The response of two, grouted, 36-ft external tendons was discussed in this chapter. Fatigue loading was used to induce damage at one location in Tendon 01, while exposure to acid was used to induce corrosion at three locations along Tendon 02. The first six natural frequencies were used as an indicator of the global condition of the test specimens.

*Table 5.14 Variation of Natural Frequencies with Number of Wire Fractures*

	Tendon 01			Tendon 02		
	NF 1	NF 3	NF 13	NF 1	NF 6	NF 21
1	15.2	15.1	14.2	16.4	15.2	13.2
2	30.6	30.4	28.7	32.3	31.4	26.3
3	46.8	46.4	43.8	48.9	47.5	40.4
4	63.9	63.2	59.7	65.9	63.8	54.5
5	83.3	83.3	76.7	83.8	80.9	69.5
6	104.1	103.6	98.9	102.3	98.8	84.9
Estimated number of wire breaks	0	6	25	0	3	30



Twenty five wires breaks were induced in Tendon 01. Tendon 01 was constructed with twelve strands which were stressed to 60% of GUTS. The fatigue damage represented a 30% reduction in the area of steel at the south end of the specimen. The average difference in the first six natural frequencies of Tendon 01 before and after the fatigue test was 5% (Table 5.14).

Thirty wire breaks were induced in Tendon 02. Tendon 02 was constructed with nine strands, which were stressed to 80% of GUTS. The total number of wire breaks represents about 25% of the total area of steel. The average difference in the first six natural frequencies of Tendon 02 before and after the exposure test was 15%.

## **Chapter 6: Evaluation of Initial Response of Test Specimens**

The primary objective of this dissertation is to extract information about the condition of an external tendon from the measured frequency response. The approach is demonstrated in this chapter using the frequency response of the test specimens before damage was induced. The most promising techniques are then used in Chapter 7 to evaluate the condition of the damaged specimens.

Two analytical models are used to relate the measured frequencies to the unknown structural parameters: the taut string model and the stiff string model. These two models are presented in Section 6.1, and the difficulties associated with extracting the values of the structural parameters from the measured frequencies are discussed in Section 6.2. The initial estimates of the structural parameters are given in Section 6.3.

When extracting information from the measured frequencies, a unique solution is not obtained. The optimization procedure used to identify the best solution is discussed in Section 6.4. The initial responses of the cable specimens and the tendon specimens are evaluated in Sections 6.5 and 6.6, respectively.

### **6.1 ANALYTICAL MODELS**

Two simple analytical models were used to evaluate the initial response of the test specimens. The specimens were assumed to be straight and restrained against rotation and displacement at both ends. In addition, all structural parameters were assumed to be constant along the length.

The taut string model is often used to represent systems where the global behavior is dominated by the applied tension. The governing differential equation for a taut string is given in Eq. 6.1 and the corresponding natural frequencies are given in Eq. 6.2.

$$T \frac{\partial^2 y}{\partial x^2} = m \frac{\partial^2 y}{\partial t^2} \quad (\text{Eq. 6.1})$$

$$f_n = \frac{n}{2\ell} \sqrt{\frac{T}{m}}, \quad (n = 1, 2, 3, \dots) \quad (\text{Eq. 6.2})$$

where  $T$  = applied tension,  $m$  = mass per unit length,  $\ell$  = length,  $f$  = natural frequency (Hz), and  $n$  = mode number

Given the geometry and the cross-sectional dimensions of typical external tendons, the flexural stiffness of the tendon is also expected to influence the frequency response. The governing differential equation for the stiff string model is similar to Eq. 6.1, but includes the flexural stiffness of the cross section:

$$T \frac{\partial^2 y}{\partial x^2} - EI \frac{\partial^4 y}{\partial x^4} = m \frac{\partial^2 y}{\partial t^2} \quad (\text{Eq. 6.3})$$

where  $E$  = elastic modulus and  $I$  = moment of inertia

In 1948, Morse proposed an approximate solution to Eq. 6.3 for tendons that are restrained against translation and rotation at the ends. The corresponding frequencies are given in Eq. 6.4.

$$f_n \cong \frac{n}{2\ell} \sqrt{\frac{T}{m}} \left[ 1 + \frac{2}{\ell} \sqrt{\frac{EI}{T}} + \left( 4 + \frac{n^2 \pi^2}{2} \right) \frac{EI}{T\ell^2} \right], \quad (n = 1, 2, 3, \dots) \quad (\text{Eq. 6.4})$$

The two models described above include a total of five structural parameters: tension ( $T$ ), length ( $\ell$ ), mass per unit length ( $m$ ), moment of inertia ( $I$ ), and elastic modulus ( $E$ ). Because the product  $EI$  appears in both Eq. 6.3 and Eq. 6.4, these two parameters will be considered as a single coupled parameter in the analyses discussed in this chapter. The remainder of this chapter addresses methods for estimating the values of  $T$ ,  $\ell$ ,  $m$ , and  $EI$  from the measured frequencies.

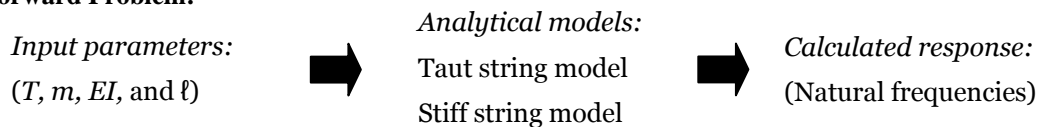
## 6.2 INVERSE PROBLEMS

During design, the engineer uses a model and assumed values of the structural parameters to calculate the natural frequencies of the structural system. For an external tendon, the engineer may use either Eq. 6.2 or Eq. 6.4 and values of  $T$ ,  $\ell$ ,  $m$ , and  $EI$  to calculate as many frequencies as desired. A unique solution is obtained for each frequency using a given model and a given set of parameters. This is known as the forward problem (Figure 6.1).

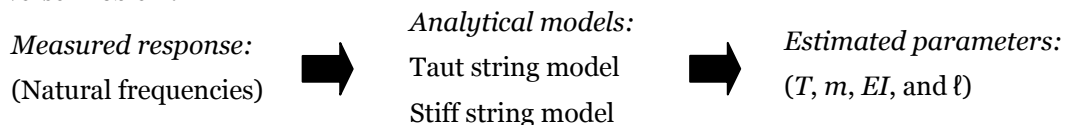
When evaluating an existing structure using the vibration signature approach, the engineer measures a discrete number of natural frequencies – the number depends on the limitations of the data acquisition system and the instrumentation. The values of  $T$ ,  $\ell$ ,  $m$ , and  $EI$  are then estimated from these frequencies. This is known as an inverse problem. Unlike the forward problem, a unique combination of the structural parameters can not always be identified to match the measured frequencies. There are several reasons for the lack of a unique solution: (a) the boundary conditions in the field may be different from those assumed in the analyses, (b) deterioration of the tendon is not expected to be uniform along the entire length, and (c) measurement errors are included in the measured frequencies.

In spite of these limitations, the measured frequencies do provide a basis for evaluating the condition of an external tendon. The optimization scheme proposed in Section 6.4 is used for this purpose.

### Forward Problem:



### Inverse Problem:



**Figure 6.1 Schematic Procedure of Forward and Inverse Problem**

### **6.3 INITIAL ESTIMATES OF STRUCTURAL PARAMETERS**

Three parameters ( $T$ ,  $\ell$ , and  $m$ ) are required to calculate the frequency of an external tendon using the taut string model and four parameters ( $T$ ,  $\ell$ ,  $m$ , and  $EI$ ) are required using the stiff string model. The initial values of these four parameters were estimated using the geometry of the test specimens and assumed material properties.

#### **6.3.1 Length**

The length of the cable specimens was assumed to be the clear distance between the anchor heads (49 ft). Because the degree of fixity provided by the concrete anchor blocks was not known, two lengths were considered for the tendon specimens: 32 ft, which represents the clear spacing between the anchor blocks, and 36.5 ft, which represents the overall length of the specimens, including the anchor heads.

#### **6.3.2 Tension**

The initial calculations were based on the target value of prestressing in the test specimens: 40% GUTS for the cable specimens (60 kip), 60% GUTS for Tendon 01 (425 kip), and 80% GUTS for Tendon 02 (425 kip).

#### **6.3.3 Mass per Unit Length**

In calculating the mass per unit length of the test specimens, the unit weight of the grout was assumed to be  $125 \text{ lb/ft}^3$  and the unit weight of HDPE duct was assumed to be  $60 \text{ lb/ft}^3$ . The cross-sectional area of the grout was calculated from the nominal inner diameter of the duct, and the area of the longitudinal and transverse ribs was approximated by adding an additional 5% of the area. Details of these calculations are given in Appendix N.

During the autopsy, the weight of a short length of each specimen, except Cable 01, was measured (Figure 6.2). The measured weight per unit length is compared with the calculated weight in Table 6.1. The calculated weight of the cable specimens was approximately 6% percent less than the measured unit weight, and the calculated weight

of the tendon specimens was within  $\pm 3\%$  of the measured weight. These variations were assumed to be related to the size of the ribs. The mass per unit length corresponding to the measured weight of the test specimens was used as the starting point for subsequent calculations.

**Table 6.1 Weight per Unit Length**

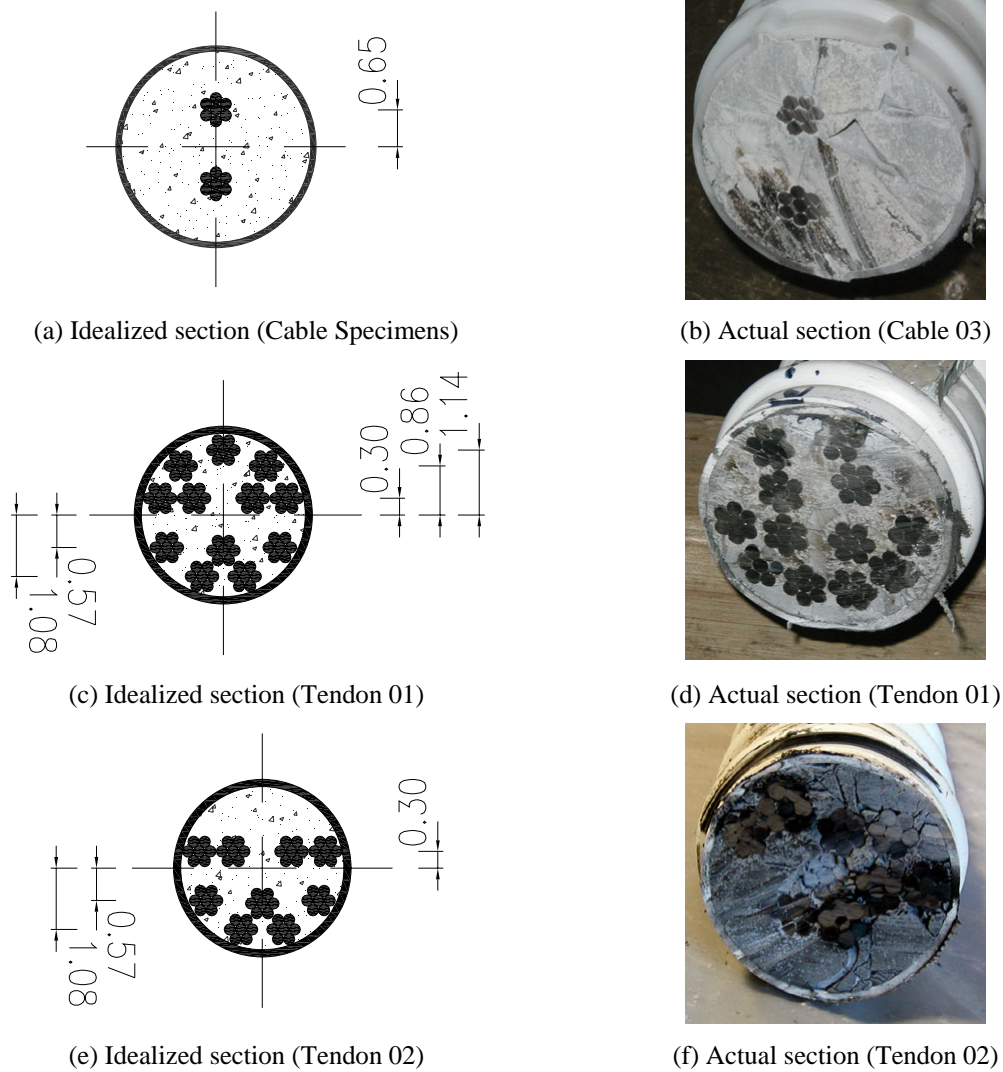
	Cable Specimens		Tendon Specimens	
	Cable 02	Cable 03	Tendon 01	Tendon 02
Measured unit weight (lb/ft)	10.10	10.24	13.23	11.82
Calculated unit weight (lb/ft)	9.53	9.53	12.87	12.11
Ratio	1.06	1.07	1.03	0.98



**Figure 6.2 Portion of Test Specimens used to Determine Weight per Unit Length**

### 6.3.4 Flexural Stiffness

The flexural stiffness is defined as the product of the transformed moment of inertia,  $I$ , and the modulus of elasticity,  $E$ . The cross-sectional dimensions at the anchor heads were assumed to represent the position of the strands along the entire length of the specimens (Figure 6.3).



**Figure 6.3 Idealized and Observed Locations of Strands within Cross Sections**

Details of the calculations are given in Appendix N, and the values reported in Table 6.2 and Table 6.3 are based on a modulus of elasticity for the grout of 3,500 ksi and a modulus of elasticity of the strand of 29,400 ksi. All values are reported in terms of the modulus of the strand.

The potential error in  $EI$  includes two components, one related to the arrangement of the strand and one related to the variation of material properties. Photographs taken of the cross sections during the autopsy, indicate that the locations of the strands did vary from the assumed positions (Figure 6.3). However, this observation was ignored in the

analyses because the value of  $EI$  was assumed to be constant along the length of the specimens. The modulus of the grout was not measured in the experimental program, therefore, the value of 3,500 ksi was assumed and used in all calculations.

**Table 6.2 Transformed Moment of Inertia for the Idealized Cross Sections**

	Cable Specimens	Tendon 01	Tendon 02
$I$ (in. <sup>4</sup> )	0.900	1.653	1.007

**Table 6.3 Flexural Stiffness**

	Cable Specimens	Tendon 01	Tendon 02
$EI$ (kip-ft <sup>2</sup> )	183.8	346.8	212.4

#### 6.4 OPTIMIZATION OF SOLUTIONS

As discussed in Section 6.2, a unique combination of structural parameters does not exist that corresponds exactly to the measured natural frequencies for each test specimen. Therefore, an optimization procedure was used to identify the best combination of parameters for each specimen. The ranges of each parameter considered in the analyses are summarized in Table 6.4.

**Table 6.4 Ranges of Structural Parameters Considered**

Parameter	Range Considered
$T$ (kip)	$0.9 T_o < T < 1.1 T_o$ ; $T_o$ = estimated tension
$l$ (ft)	Clear distance to overall length of specimens
$m$ (lb-sec <sup>2</sup> /ft <sup>2</sup> )	$0.9 m_o < m < 1.1 m_o$ ; $m_o$ = estimated mass per unit length
$EI$ (kip-ft <sup>2</sup> )	$E_s = 29,400$ ksi; $1000$ ksi $< E_g < 4000$ ksi, and $I_o$ = transformed moment of inertia;

For the tension,  $T$ , and mass per unit length,  $m$ , the feasible range was considered to be within  $\pm 10\%$  of the assumed values in Section 6.3. The range of lengths considered



was limited by the geometry of the test specimens. The minimum length was the clear distance between the anchor heads for the cable specimens and the clear distance between the anchor blocks for the tendon specimens. The maximum length was taken as the distance between the outer faces of the anchor heads. The flexural stiffness,  $EI$ , was calculated using the measured modulus of the strand and an elastic modulus of the grout that varied between 1000 and 4000 ksi. The transformed moment of inertia was calculated using the positions of the strands at the anchor head. Variations in the locations of the strands within the cross section were not considered.

The range of each parameter was divided by 10, and the first six natural frequencies were calculated for each combination of parameters. Therefore,  $10^3$  combinations of parameters were used with the taut string model and  $10^4$  combinations of parameters were used with the stiff string model.

For each combination of parameters, the error between the frequency of the  $i^{\text{th}}$  mode calculated using either Eq. 6.2 or Eq. 6.4 and the measured frequency for mode  $i$ ,  $\Omega_i$  was calculated using Eq. 6.5.

$$\Omega_i = \frac{f_{c,i} - f_{o,i}}{f_{o,i}} \quad (\text{Eq. 6.5})$$

where  $\Omega_i$  = error associated with mode  $i$ ,  $f_{c,i}$  = calculated frequency for mode  $i$ , and  $f_{o,i}$  = measured frequency for mode  $i$

The resulting values of  $\Omega_i$  were both positive and negative, because the calculated frequencies exceeded the measured frequencies in some cases and the measured frequencies exceeded the calculated frequencies in other cases. In order to determine the optimal combination of parameters, the total error,  $\Omega_{tot}$  was calculated as the sum of the square of the modal error terms, as indicated in Eq. 6.6. Each of the modes was weighted equally when calculating the total error.

$$\Omega_{tot} = \sum_{i=1}^6 \left[ \frac{f_{c,i} - f_{o,i}}{f_{o,i}} \right]^2 \quad (\text{Eq. 6.6})$$

where  $\Omega_{tot}$  = total error for combination of parameters

The combination of parameters corresponding to the minimum value of total error was then selected as the optimal combination. As discussed in Section 6.5 and Section 6.6, the values of the optimal parameters varied depending on the analytical model used to calculate the natural frequencies – taut string model using Eq. 6.2 or stiff string model using Eq. 6.4. The sensitivity of the error to the choice of parameters is also addressed in these sections.

## **6.5 RESPONSE OF CABLE SPECIMENS**

### **6.5.1 Initial Calculations**

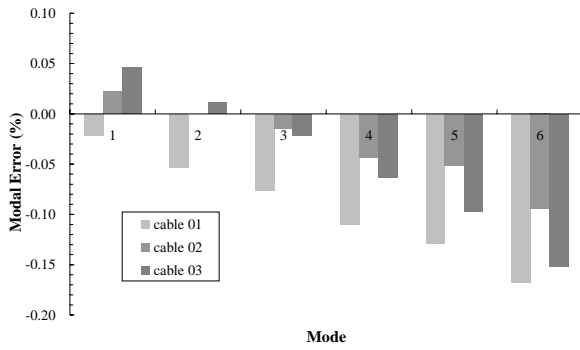
For the first set of analyses, the natural frequencies of the cable specimens were calculated using the values of the structural parameters discussed in Section 6.3 using both the taut string and stiff string idealizations. The measured frequencies for the lowest six modes of vibration before the start of the fatigue tests are summarized in Table 6.5, as are the calculated frequencies.

**Table 6.5 Natural Frequencies of Cable Specimens Corresponding to Initial Set of Parameters**

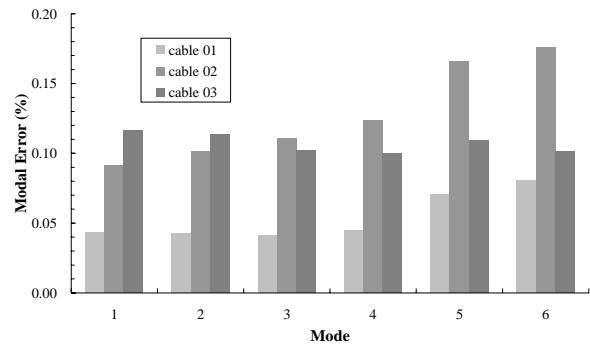
Mode		Measured Frequencies (Hz)			Calculated Frequencies (Hz)	
		Cable 01 NF 0	Cable 02 NF 0	Cable 03 NF 0	Taut String	Stiff String
1		4.6	4.4	4.3	4.5	4.8
2		9.4	8.9	8.8	8.9	9.8
3		14.5	13.6	13.7	13.4	15.1
4		20.0	18.6	19.0	17.8	20.9
5		25.6	23.5	24.7	22.3	27.4
6		32.2	29.6	31.6	26.8	34.8
Total Error	Taut string	0.0659	0.0141	0.0393		
	Stiff string	0.0189	0.1043	0.0691		

The measured natural frequencies for Cable 02 and Cable 03 for the first three modes were similar to the values calculated using the taut string model; however, the measured frequencies were higher than the calculated frequencies for the higher modes. The recorded natural frequencies for Cable 01 exceeded those calculated using the taut string model for all six modes. The calculated frequencies using the stiff string model exceeded the measured frequencies for all six modes in all three specimens.

The associated modal errors are displayed in Figure 6.4. The calculated frequencies vary considerably from the measured frequencies. The modal errors calculated using the taut string model varied as the mode number increased for all three cable specimens. In contrast, comparison, the modal errors calculated using the stiff model were relatively constant, except the fifth and sixth modes, which had experienced higher modal errors. The relative uniformity of the modal errors calculated using the stiff string model indicates that this model is likely to provide a better match to the measured frequencies when the optimized parameters are used in the analyses.



(a) Taut string model



(b) Stiff string model

**Figure 6.4 Modal Errors Corresponding to Initial Set of Parameters for Cable Specimens**

### 6.5.2 Optimized Parameters

The ranges of the parameters used to minimize the total error between the measured and calculated frequencies are listed in Table 6.6, and the combinations of parameters corresponding to the minimum total error are reported in Table 6.7. The taut string and the stiff string models were used independently, and results for both are reported.

**Table 6.6 Ranges of Parameters Considered in Evaluation of Cable Specimens**

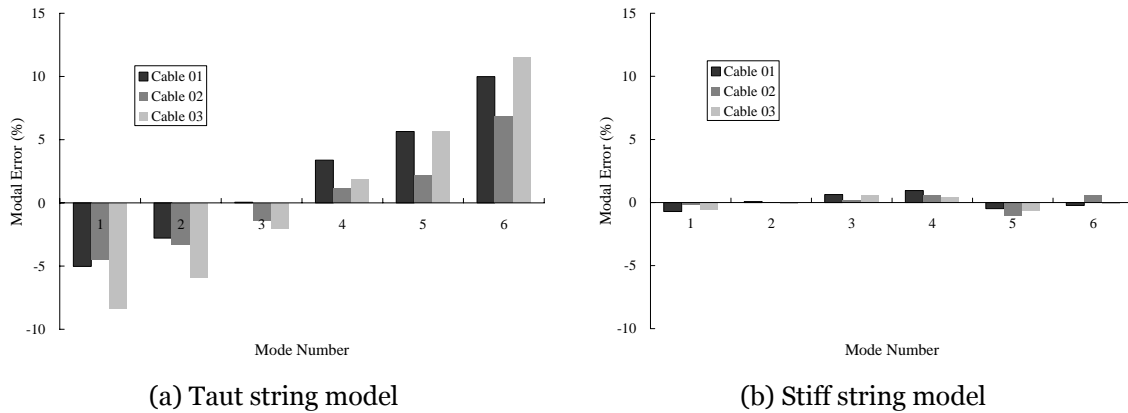
Parameter	Initial Estimate	Range Considered
$T$ (kip)	60	55 to 65
$l$ (ft)	49	49 to 50
$m$ (lb-sec <sup>2</sup> /ft <sup>2</sup> )	0.32	0.29 to 0.35
$EI$ (kip-ft <sup>2</sup> )	183.8	80 to 200

**Table 6.7 Parameters Corresponding to Minimum Total Error for Cable Specimens**

Parameter	Cable 01		Cable 02		Cable 03	
	Taut string	Stiff string	Taut string	Stiff string	Taut string	Stiff string
$T$ (kip)	65	63	64	55	63	55
$l$ (ft)	49	49.1	49.1	49.3	49.5	49.8
$m$ (lb-sec <sup>2</sup> /ft <sup>2</sup> )	0.290	0.350	0.314	0.326	0.296	0.350
$EI$ (kip-ft <sup>2</sup> )	-	152	-	92	-	188
<i>Total Error</i>	0.01700	0.00021	0.00855	0.00019	0.02776	0.00013

In many cases, the optimal value of a parameter was near the limits of the range considered. However, the optimal values were not the same for the two analytical models. For example, the tension corresponding to the minimum total error for all three specimens was near the upper limit of 65 kip using the taut string model, while the tension was near the lower limit of 55 kip for Cable 02 and Cable 03 using the stiff spring model. The total errors reported in Table 6.7 are significantly less than those calculated using the initial set of parameters (Table 6.5), and the total errors computed using the stiff string model were much less than those using the taut string model.

The modal errors corresponding to the optimal set of parameters are plotted in Figure 6.5 for both analytical models. The modal errors were also significantly less using the stiff string model than the taut string model for all three cable specimens. As a result, the stiff string model was considered to provide a better representation of the frequency response of the cable specimens than the taut string model. This suggests that the behavior of the cable specimens was influenced by bending, in addition to the applied tension. The measured natural frequencies are compared to the calculated frequencies using the optimized parameters in Table 6.8. The calculated frequencies are nearly identical to the recorded frequencies. This comparison demonstrates that the optimization scheme using the stiff string model can reproduce effectively the natural frequencies of the cable specimens before the specimens experienced damage.

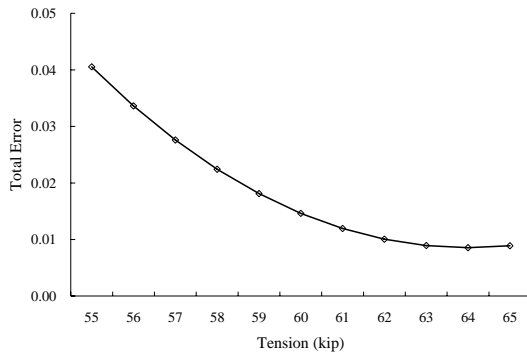


**Figure 6.5** *Distribution of Modal Errors Corresponding to Minimum Total Error for Cable Specimens*

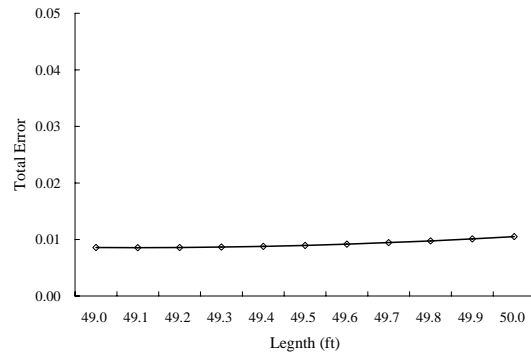
**Table 6.8** *Comparison of Measured Natural and Calculated Frequencies Using Optimized Parameters for Cable Specimens*

Mode	Cable 01		Cable 02		Cable 03	
	Measured Frequencies	Calculated Frequencies	Measured Frequencies	Calculated Frequencies	Measured Frequencies	Calculated Frequencies
1	4.6	4.6	4.4	4.4	4.3	4.3
2	9.4	9.4	8.9	8.9	8.8	8.8
3	14.5	14.4	13.6	13.6	13.7	13.6
4	20.0	19.8	18.6	18.5	19.0	18.9
5	25.6	25.7	23.5	23.7	24.7	24.9
6	32.2	32.3	29.6	29.4	31.6	31.6

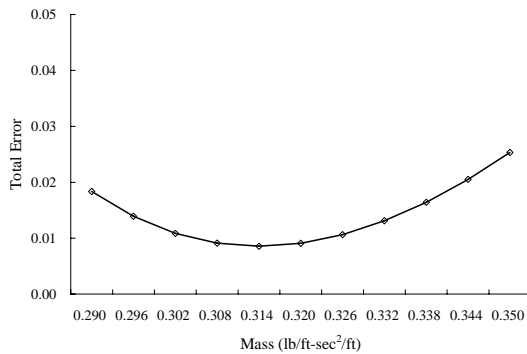
The sensitivity of the error to each parameter included in the analytical models is shown in Figure 6.6 and Figure 6.7 for Cable 02 for the taut string and stiff string models, respectively. One parameter is varied in each figure, while the values of the other parameters correspond to those listed in Table 6.7. Similar plots for Cable 01 and Cable 03 are given in Appendix O. The error was sensitive to variations in the tension, mass per unit length, and the flexural stiffness, but was almost independent of variations in the length. This is not surprising, because the range of lengths considered in the analyses was the smallest of the four parameters due to the geometry of the test specimens.



(a) Tension



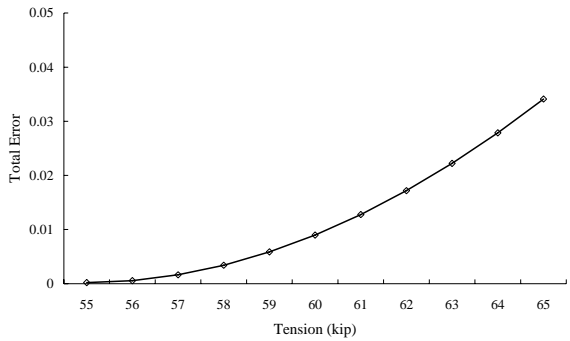
(b) Length



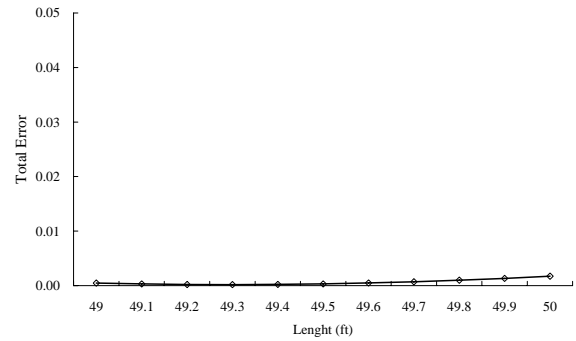
(c) Mass

**Figure 6.6 Sensitivity of Total Error to Structural Parameters using Taut String Model (Cable 02)**

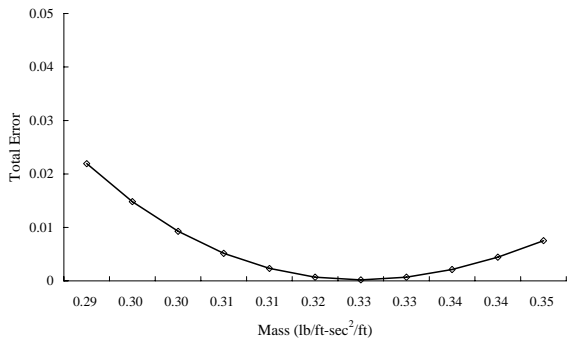
While specific combinations of structural parameters corresponded to the minimum total error between the measured and calculated natural frequencies for each test specimen, it is important to note that the values of the parameters do not necessarily have physical significance. For example, all three test specimens were constructed using the same procedures using the same hardware; therefore, it is reasonable to assume that the effective length of all specimens is the same. However, variations in the effective lengths may be observed in Table 6.7.



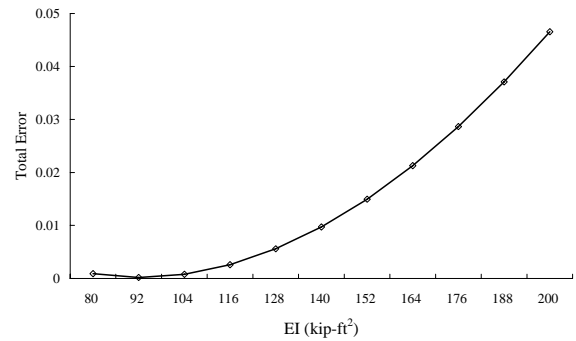
(a) Tension



(b) Length



(c) Mass



(d) EI

**Figure 6.7 Sensitivity of Total Error to Structural Parameters using Stiff String Model (Cable 02)**

The simplicity of the analytical models and total error function limit the ability to reproduce the measured response of the test specimens completely. Therefore, a number of combinations in the structural parameters results in an acceptable margin of error. The optimization scheme used in this chapter was intended to assess the possible errors due to variations in the structural parameters, rather than evaluating the physical meaning of each of the structural parameters.



## 6.6 RESPONSE OF TENDON SPECIMENS

### 6.6.1 Initial Calculations

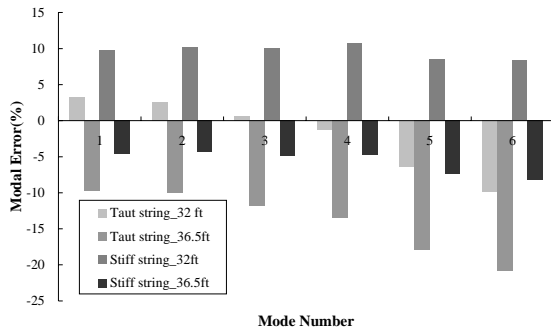
The tendon specimens were also analyzed using the initial values of the structural parameters discussed in Section 6.3 and both analytical models. As discussed, two lengths were used in the analyses. The shorter length corresponds to the clear distance between the concrete anchor blocks, while the longer length corresponds to the distance between the outside faces of the anchor heads. The measured and calculated frequencies for the first six modes of vibration are reported in Table 6.9 for Tendon 01 and Table 6.10 for Tendon 02.

*Table 6.9 Natural Frequencies for Tendon 01*

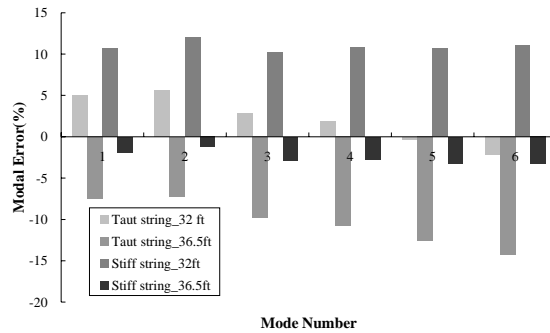
Mode	Measured Frequencies (Hz)	Calculated Frequencies (Hz)			
		Taut String		Stiff String	
	NF 0	32 ft	36.5 ft	32 ft	36.5 ft
1	15.4	15.9	13.9	16.9	14.7
2	31.0	31.8	27.9	34.2	29.6
3	47.4	47.7	41.8	52.2	45.1
4	64.4	63.6	55.7	71.3	61.3
5	84.8	79.4	69.6	92.0	78.6
6	105.7	95.3	83.6	114.5	97.0
Total Error	-	0.016	0.128	0.056	0.021

**Table 6.10 Natural Frequencies for Tendon O2**

Mode	Measured Frequencies (Hz)	Calculated Frequencies (Hz)			
		Taut String		Stiff String	
	NF 0	32 ft	36.5 ft	32 ft	36.5 ft
1	15.9	16.7	14.7	17.6	15.6
2	31.7	33.5	29.4	35.5	31.3
3	48.5	50.2	44.0	53.8	47.4
4	65.8	67.0	58.7	72.9	64.0
5	83.3	83.7	73.4	93.0	81.3
6	102.7	100.5	88.1	114.2	99.4
Total Error	-	0.0074	0.0686	0.0717	0.0042



(a) Tendon O1



(b) Tendon O2

**Figure 6.8 Modal Errors Corresponding to Initial Set of Parameters for Tendon Specimens**

The calculated frequencies were sensitive to the length used in the analyses. In general, the measured frequencies were between the two calculated values, however, the measured frequencies tended to be higher than the range of calculated frequencies when the taut string model was used to evaluate the frequencies of the higher modes. The tendon specimens exhibited trends similar to those observed for the cable specimens: modal

errors were nearly constant using the stiff string model, but varied by mode using the taut string model (Figure 6.8). These trends indicate that the behavior of the tendon specimens will be better represented by the stiff string model.

### 6.6.2 Optimized Parameters

As before, the values of the structural parameters corresponding to the minimum total error between the measured and calculated frequencies were estimated using the two analytical models. The ranges of each parameter considered in the optimization are summarized in Table 6.11 and Table 6.12 for Tendon 01 and Tendon 02, respectively. The combinations of parameters corresponding to the minimum total error are summarized in Table 6.13. Results are reported for both the taut string and stiff string models.

**Table 6.11 Ranges of Parameters Considered in Evaluation of Tendon 01**

<b>Parameter</b>	<b>Initial Estimate</b>	<b>Range Considered</b>
$T$ (kip)	425	400 to 460
$l$ (ft)	32	32 to 36
$m$ (lb-sec <sup>2</sup> /ft <sup>2</sup> )	0.41	0.37 to 0.45
$EI$ (kip-ft <sup>2</sup> )	337.4	310 to 350

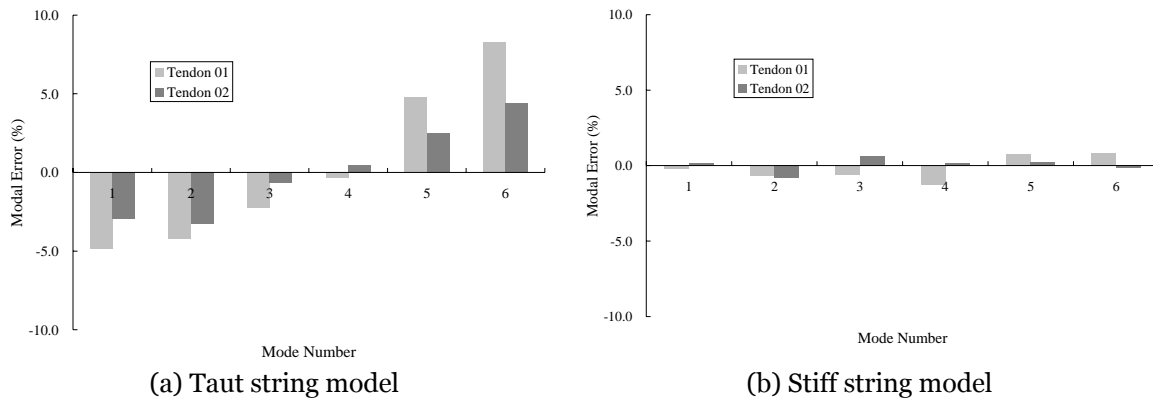
**Table 6.12 Ranges of Parameters Considered in Evaluation of Tendon 02**

<b>Parameter</b>	<b>Initial Estimate</b>	<b>Range Considered</b>
$T$ (kip)	425	400 to 460
$l$ (ft)	32	32 to 36
$m$ (lb-sec <sup>2</sup> /ft <sup>2</sup> )	0.37	0.33 to 0.41
$EI$ (kip-ft <sup>2</sup> )	212.4	160 to 220

**Table 6.13 Parameters Corresponding to Minimum Total Error for Tendon Specimens**

Parameter	Tendon 01		Tendon 02	
	Taut string	Stiff string	Taut string	Stiff string
$T$ (kip)	436	400	448	406
$l$ (ft)	33.6	32.8	33.6	33.2
$m$ (lb-sec <sup>2</sup> /ft <sup>2</sup> )	0.370	0.442	0.370	0.402
$EI$ (kip-ft <sup>2</sup> )	-	350	-	220
<i>Total Error</i>	0.01384	0.00039	0.00465	0.00012

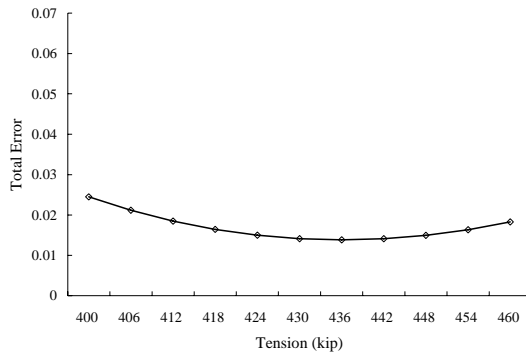
As before, the optimal value of each parameter was often near on of the limits of the range considered, and the optimal values parameters were not the same for the two models. The frequencies calculated using the optimized parameters and the stiff string model were closer to the measured natural frequencies of the tendon specimens than those calculated using the taut string model (Figure 6.9).



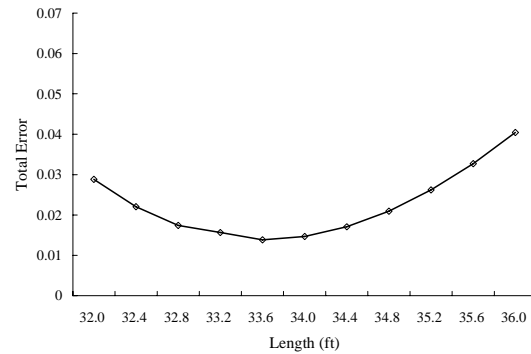
**Figure 6.9 Distribution of Modal Errors Corresponding to Minimum Total Error for Tendon Specimens**

The sensitivity of the total error to each parameter is shown in Figure 6.10 and Figure 6.11 for Tendon 01 for the taut string and stiff spring models, respectively. Similar

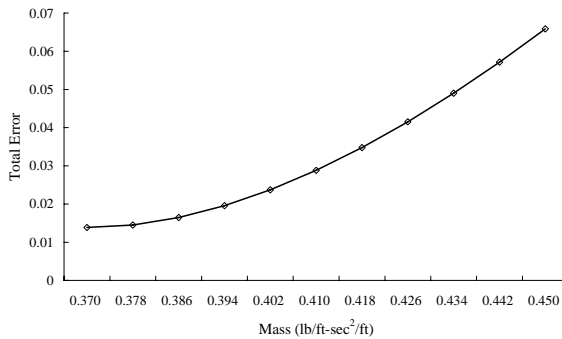
plots for Tendon 02 are given in Appendix O. The error was most sensitive to the length of the specimen,  $\ell$ , and the mass per unit length,  $m$ , and least sensitive to the flexural stiffness,  $EI$ . Surprisingly, the total error was not as sensitive to the tension,  $T$ , as  $\ell$  or  $m$  using either model.



(a) Tension



(b) Length

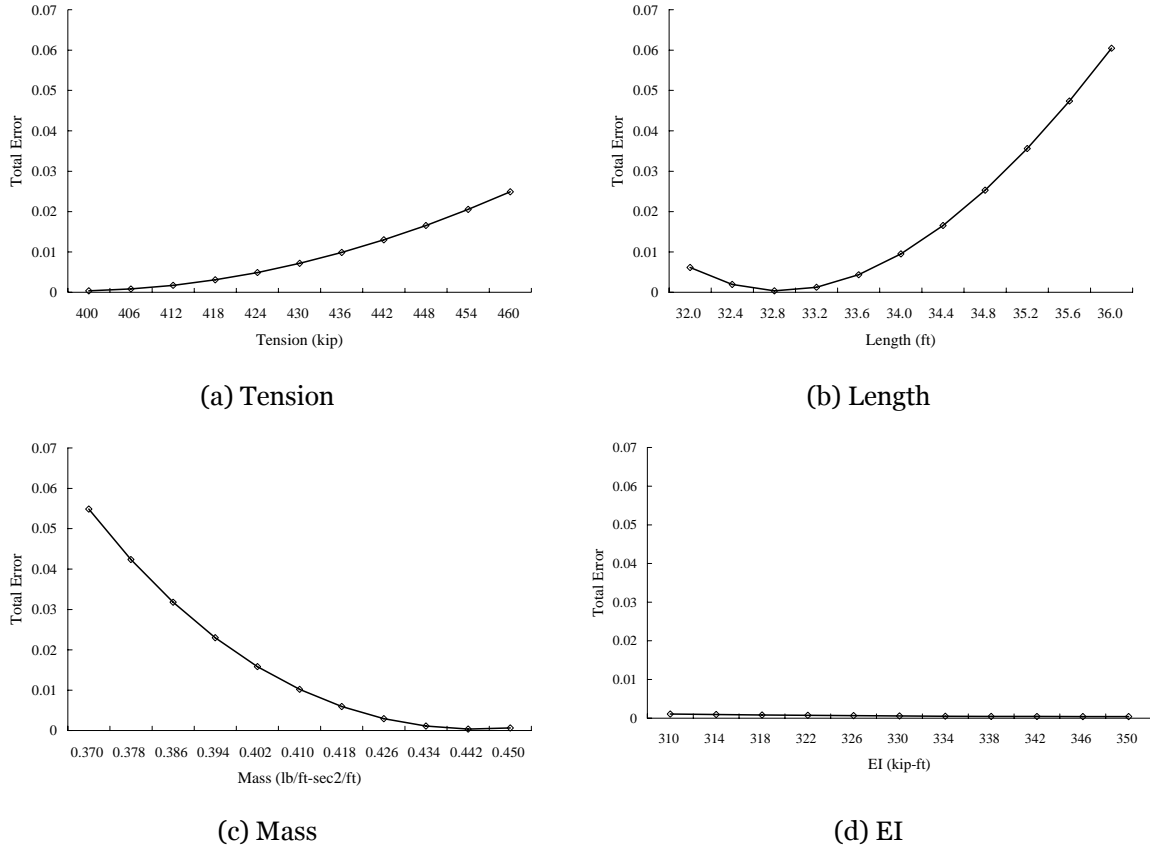


(c) Mass

**Figure 6.10 Sensitivity of Total Error to Structural Parameters using Taut String Model (Tendon 01)**

In all cases, the minimum total error corresponded to a length that was between the two extreme values. This indicates that the tendon specimens were not fixed at the inner face of the anchor block, but that the equivalent point of fixity was within the anchor block. This complicates the analysis of the tendon specimens, compared with the

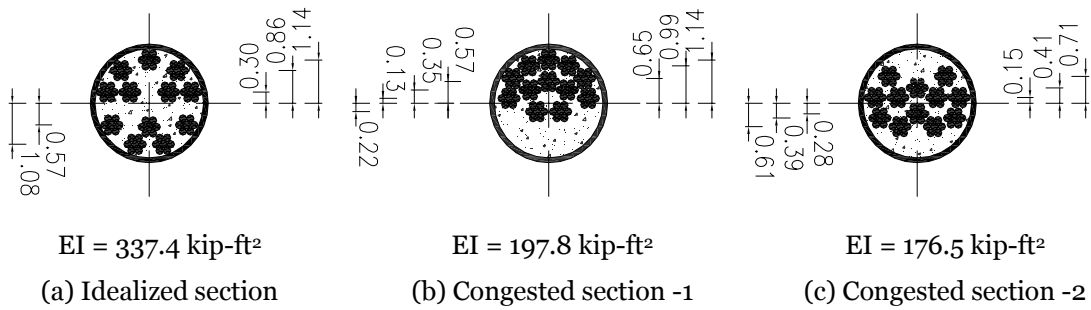
cable specimens, and represents an issue that must be addressed when evaluating external tendons in the field.



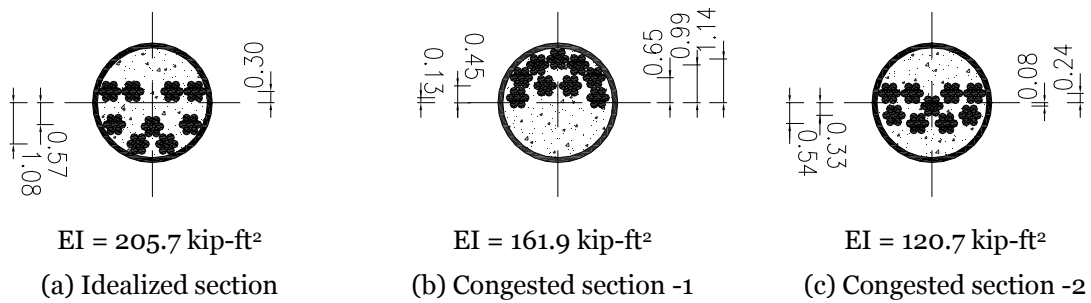
**Figure 6.11 Sensitivity of Total Error to Structural Parameters using Stiff String Model (Tendon 01)**

Larger variations in the flexural stiffness of the tendon specimens than those indicated in Table 6.11 are expected due to the observed differences between the locations of the strand in the idealized cross section and the actual locations observed during the autopsy (Figure 6.3). As shown in Figure 6.12 and Figure 6.13, the values of flexural stiffness change considerably when alternate arrangements of strand were considered. The fact that the total error was not sensitive to variations in the flexural stiffness implies that variations in the placement of the strands within the cross section of

the tendon do not influence the natural frequencies significantly. This is convenient, because the locations of the strands are expected to vary along the length and it is impossible to determine the geometry of the cross section in a nondestructive manner.



**Figure 6.12 Possible Arrangements of Strands in Tendon 01**



**Figure 6.13 Possible Arrangements of Strands in Tendon 02**

The measured natural frequencies are compared with the frequencies calculated using the optimized parameters in Table 6.14. The calculated frequencies are nearly identical to the measured frequencies. This comparison demonstrates that the optimization scheme using the stiff string model effectively reproduces the natural frequencies of the tendon specimens before damage has occurred.

**Table 6.14 Comparison of Measured Natural and Calculated Frequencies  
Using Optimized Parameters for Tendon Specimens**

Mode	Tendon 01		Tendon 02	
	Measured Frequencies	Calculated Frequencies	Measured Frequencies	Calculated Frequencies
1	15.4	15.4	15.9	15.9
2	31.0	31.2	31.7	32.0
3	47.4	47.7	48.5	48.5
4	64.4	65.2	65.8	65.7
5	84.8	84.2	83.3	83.8
6	105.7	104.8	102.7	102.9

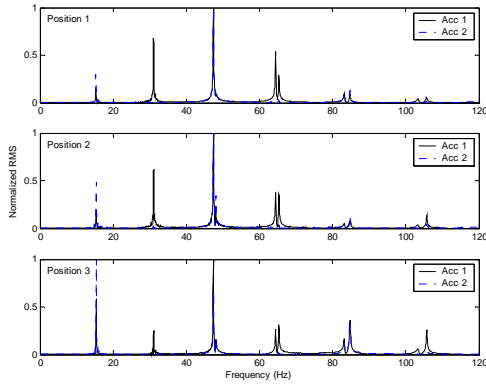
### 6.6.3 Presence of Multiple Peaks in Frequency Response

The response of the tendon specimens included multiple peaks for several modes of vibration (Figure 6.14). In most cases, the difference between the peaks was less than 5% of the frequency corresponding to the predominant vibration frequency.

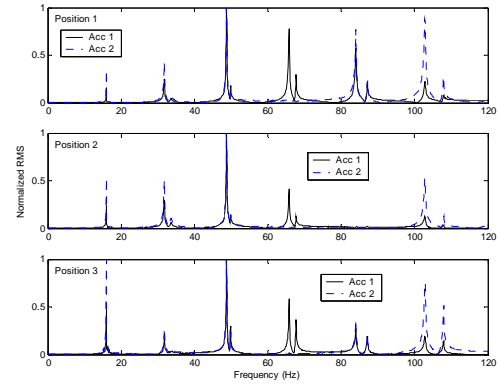
The measured frequencies for each peak are reported in Table 6.15, where  $f_1$  refers to the lower frequency and  $f_2$  refers to the higher frequency for each mode. These values are compared with the frequencies calculated using the stiff string model. Three values of length were used in the calculations:  $l_{\max}$  refers to the maximum considered length of 36.5 ft,  $l_{\min}$  refers to the minimum considered length of 32 ft, and  $l_{\text{opt}}$  refers to the length corresponding to the minimum total error (32.8 ft for Tendon 01 and 33.2 ft for Tendon 02). The values of  $EI$ ,  $m$ , and  $T$  corresponding to the minimum total error were used in all calculations.

The measured frequencies for all peaks were bounded by the frequencies calculated using the extreme values of the specimen length. In most cases, the measured frequency of the high-amplitude peak was similar to that calculated using the length corresponding to the minimum error. This is expected because the frequency with the higher amplitude peak was used in to identify the optimized structural parameters.





(a) Tendon 01 (NF 0)



(b) Tendon 02 (NF 0-0)

**Figure 6.14 Presence of Multiple Peaks in Frequency Response of Tendon Specimens**

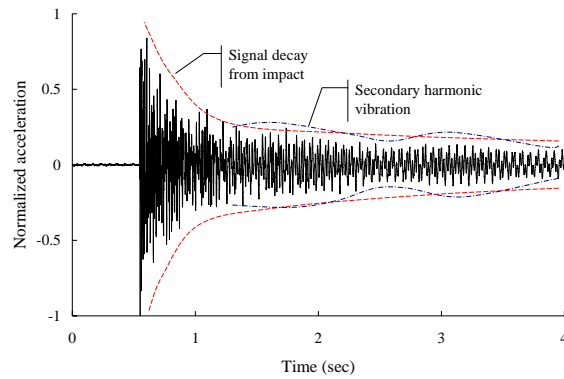
**Table 6.15 Frequencies of Multiple Peaks Observed for Tendon Specimens**

Mode	Tendon 01					Tendon 02				
	Measured Frequencies (Hz)		Calculated Frequencies (Hz)			Measured Frequencies (Hz)		Calculated Frequencies (Hz)		
	$f_1$	$f_2$	$l_{\max}$	$l_{\text{opt}}$	$l_{\min}$	$f_1$	$f_2$	$l_{\max}$	$l_{\text{opt}}$	$l_{\min}$
2	30.0*	-	28.7	31.2	32.1	31.7*	33.6	28.9	32.0	33.2
3	47.4*	48.0	42.3	47.7	49.0	48.8*	49.9	43.8	48.5	50.5
4	64.4*	65.3	57.6	65.2	67.1	65.8*	67.7	59.1	65.7	68.5
5	83.1	84.8*	73.9	84.2	86.8	84.0*	87.2	75.2	83.8	87.4
6	103.3	105.7*	91.5	104.8	108.2	102.8*	107.9	92.0	102.9	107.6

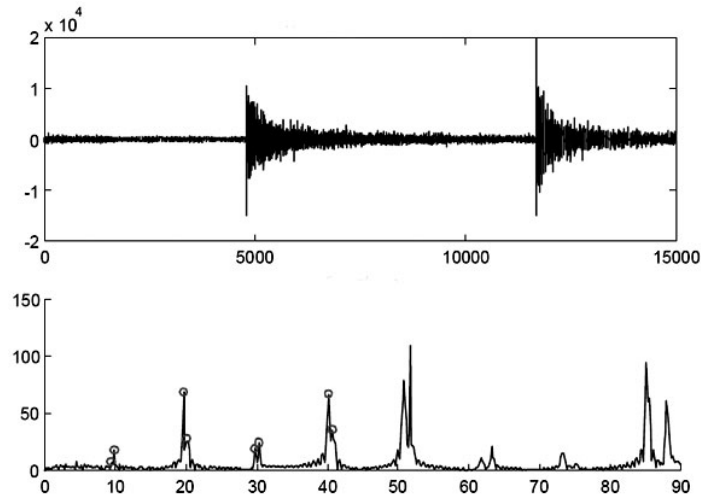
\*higher amplitude response

Based on these analyses, the presence of the dual peaks appears to be caused by the boundary conditions. The tendons are able to vibrate within the blocks, although most of the vibration occurs along the free length. The presence of closely-spaced modes of vibration is also evident in the time-domain response, as the beating phenomenon may be observed in Figure 6.15.

The boundary conditions may be even more complex in existing bridges, because external tendons are restrained by anchor blocks but pass through deviators along the length. In Chapter 2, it was assumed that each section of an external tendon could be evaluated separately, but the presence of dual peaks in the measured response of tendons in the Mid-Bay Bridge indicate that further consideration may be required for actual boundary conditions (Figure 6.16).



**Figure 6.15 Time-Domain Response of Tendon 01**



**Figure 6.16 Measured Frequency Response of External Tendons in Mid-Bay Bridge (Sagüés et al 2000)**

## 6.7 SUMMARY

A numerical scheme was developed to estimate the values of key structural parameters from the measured frequency response of the cable and tendon specimens. Two simple analytical models were selected to represent the frequency response of the five test specimens before damage was induced. The stiff string model provided a better representation of the measured frequencies in all cases.

The values of the parameters corresponding to the minimum error and the sensitivity of the error to these parameters varied with the type of specimen. The cable specimens were best represented using a length close to the clear distance between the anchor heads and the results were most sensitive to changes in the applied tension,  $T$ , and the flexural stiffness,  $EI$ . In contrast, the tendon specimens were best represented using an effective length between the clear spacing between anchor blocks and the overall length of the test specimens. The results for the tendon specimens were most sensitive to the length of the specimen,  $l$ , and the mass per unit length,  $m$ . The results were nearly independent of the flexural stiffness,  $EI$ .

The presence of dual peaks in the frequency response of the tendon specimens was attributed to vibration of the tendon within the concrete anchor blocks. Because the tendon was not fixed at the inner face of the anchor block, the restraint at the end of the specimens was distributed along the length of the anchor blocks. The flexibility of the boundaries permitted the specimens to vibrate in multiple modes within a narrow frequency range. This phenomenon has been observed in the measured response of external tendons in existing bridges and the frequencies may be bounded using the clear length of the section of tendon considered and the overall length.

## Chapter 7: Evaluation of Damaged Specimens using Vibration Signatures

The objective of this chapter is to summarize the observed response of the test specimens as damage accumulated and correlate the measured natural frequencies to a loss in the level of prestress. The damage induced during the investigation was intended to simulate deterioration in existing bridges due to corrosion. Accumulated damage in the form of wire breaks and grout cracking caused reductions in the measured natural frequencies of the test specimens.

Observations from the entire experimental program are summarized in Section 7.1. The stiff string model is used to evaluate the sensitivity of changes in the natural frequencies to changes in the tension and flexural stiffness in Section 7.2. The final set of frequencies from Cable 02, Cable 03, and Tendon 01 are evaluated in Section 7.3 to determine the best approach for extracting the residual tension from the measured frequency response. All sets of frequency data are used in Section 7.4 to track variations in tension and flexural stiffness with increasing damage. Several issues that may limit the application of the vibration technique for evaluating the condition of external tendons are summarized in Section 7.5.

### 7.1 MEASURED RESPONSE OF SPECIMENS

In this section, the frequency reduction ratio,  $\beta_n$ , is used as an indicator of damage:

$$\beta_n = \frac{f_{n,i}}{f_{n,o}} \quad (\text{Eq. 7.1})$$

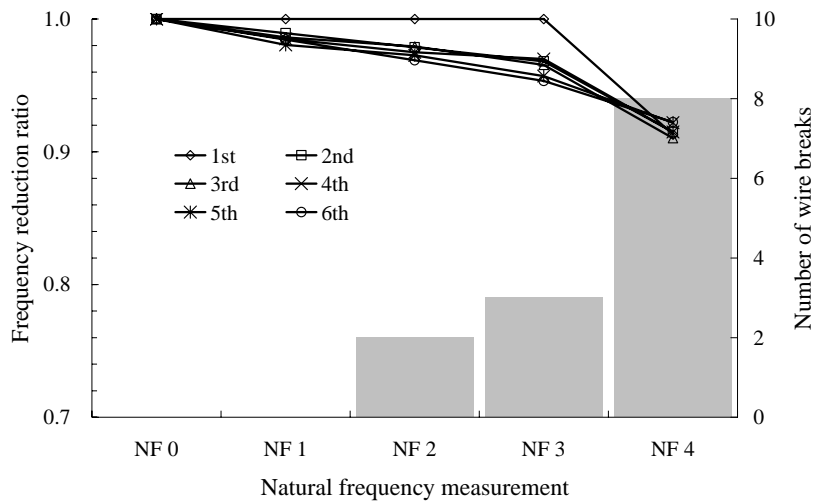
where  $\beta_n$  = frequency reduction ratio for mode  $n$ ,  $f_{n,i}$  = measured frequency of mode  $n$  during free-vibration test  $i$ , and  $f_{n,o}$  = measured frequency of mode  $n$  during initial free-vibration test.

Data from all six modes of vibration are used to determine the frequency reduction ratios. In this section, the frequency reduction ratios are compared with the number of wire breaks detected by the acoustic sensors and the condition of the test specimens during the specimen autopsies.

### 7.1.1 Cable Specimens

The frequency reduction ratios for Cable 01 are shown in Figure 7.1. The natural frequencies were measured until the eighth wire break was reported by the acoustic sensors. The first two wire breaks occurred at midspan and subsequent breaks occurred at the north end of the specimen. The natural frequencies, with the exception of the first mode, decreased gradually until three wire breaks were reported. The frequency of the first mode was essentially constant during these free-vibration tests.

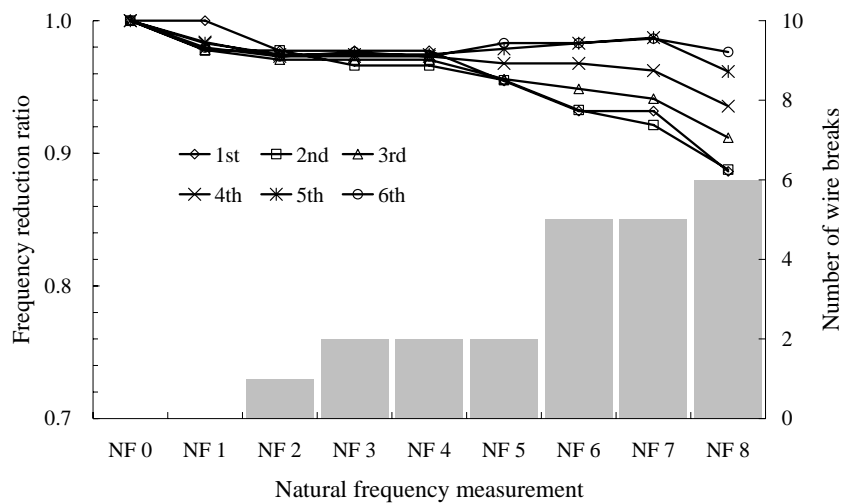
All six natural frequencies dropped in the next free-vibration test, after the eighth wire break was reported. The frequency reduction ratios varied between 91 and 92% for all modes during NF4.



**Figure 7.1** Frequency Reduction Ratio for Cable 01

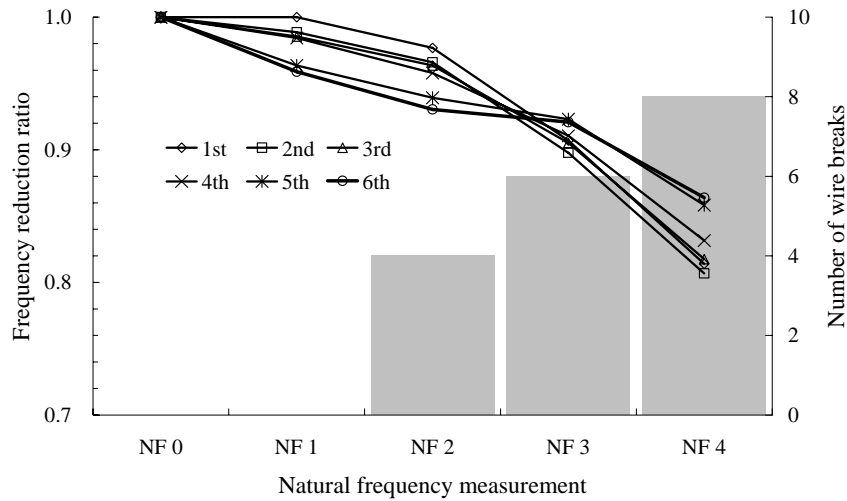
The frequency reduction ratios for Cable 02 are shown in Figure 7.2. The natural frequencies were measured until the sixth wire break was reported by acoustic sensors. From the autopsy, however, it is known that all seven wires in the top strand had fractured near the north anchor head at the conclusion of the fatigue test (one wire broke in two locations).

The natural frequencies did not vary appreciably until NF5. As damage continued to accumulate, the frequency reduction ratios decreased for most modes with the lower modes exhibiting larger variations. However, the frequency reduction ratios actually increased for modes 5 and 6 between NF4 and NF7. At the conclusion of the fatigue test, the frequency reduction ratios varied from 89 to 92%.



**Figure 7.2 Frequency Reduction Ratios for Cable 02**

The frequency reduction ratios for Cable 03 are shown in Figure 7.3. In the first few free-vibration tests, the frequencies of the higher modes changed more than the lower modes. This trend was reversed in NF3, and the lower modes exhibited lower frequency reduction ratios in the later tests.



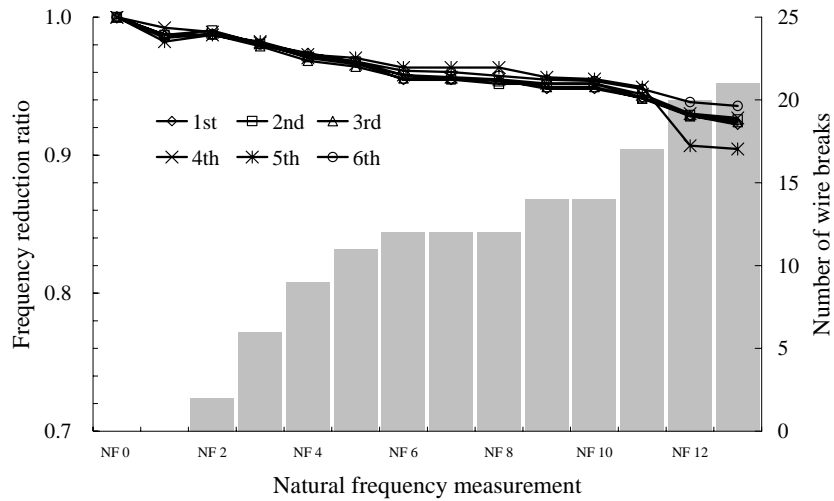
**Figure 7.3 Frequency Reduction Ratio for Cable 03**

During the autopsy, twelve wire breaks were observed at the north end of Cable 03. All seven wires in the bottom strand had fractured and three wires in the top strand had fractured. (Two wires in the bottom strand broke at two locations.) The minimum frequency reduction ratios varied between 80 and 86% at the conclusion of the fatigue test.

The changes in the frequency reduction ratios were minor – less than 5% – after the first two or three wire breaks were detected in the cable specimens. However, as the number of wire breaks increased, the rate of reduction in the frequency reduction ratios increased. The lower modes seemed to be more sensitive to damage than the higher modes.

### 7.1.2 Tendon Specimens

The variation in the frequency reduction ratio for Tendon 01 is shown in Figure 7.4. The natural frequencies in all six modes decreased gradually as damage accumulated in the tendon; however, the maximum variation in most modes was less than 6%. The natural frequencies for Tendon 01 were not as sensitive to individual wire breaks as the cable specimens.



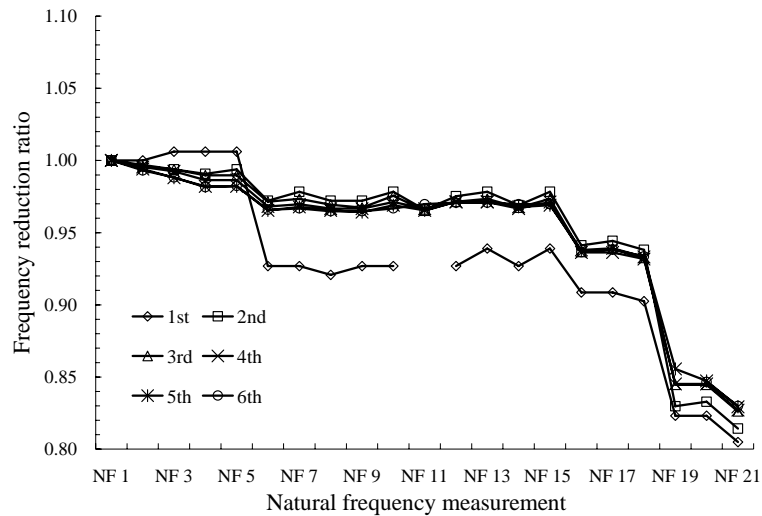
**Figure 7.4 Frequency Reduction Ratios for Tendon 01**

At the conclusion of the fatigue tests for Tendon 01, 25 wire breaks were observed approximately 2 ft from the north anchor head. All seven wires had fractured in three strands near the bottom of the cross section. Two other strands, also near the bottom, experienced two wire breaks each.

The frequency reduction ratio for Tendon 02 is shown in Figure 7.5. Acoustic sensors were not used to monitor the response of this specimen, so the number of wire breaks is not indicated. Four regions of response may be observed in Figure 7.5:

- (1) Between NF1 and NF5, the frequency reduction ratios varied by less than 2%. The frequency of the fundamental mode of vibration increased slightly, while the other five frequencies decreased.
- (2) An appreciable drop in the frequency reduction ratios was observed during NF6. The first wire breaks had been observed in Void 1 immediately before this test. The frequency reduction ratio for the first mode decreased to 93%, while the ratios for the other five modes were approximately 97%. The frequency reduction ratios remained essentially constant through NF15. The observed variations in frequency during this period were likely due to changes in temperature.





**Figure 7.5 Frequency Reduction Ratios for Tendon 02**

- (3) All six frequency reduction ratios dropped again during NF16. The first wire break had been observed in Void 2 immediately before this test. The frequency reduction ratio for the first mode dropped to 91%, while the ratios for the five higher modes were approximately 94%.
- (4) All six frequency reduction ratios dropped again during NF19. The first wire break was observed in Void 3 immediately before this test, and the change in frequencies was the largest observed. The frequency reduction ratios ranged from 82 to 85%. Another decrease in the frequency reduction ratios was observed during NF21, but the change was not as pronounced.

At the conclusion of the accelerated corrosion test, the frequency reduction ratios varied from 80 to 83% for Tendon 02. The lower modes experienced larger changes in frequencies than the higher modes.

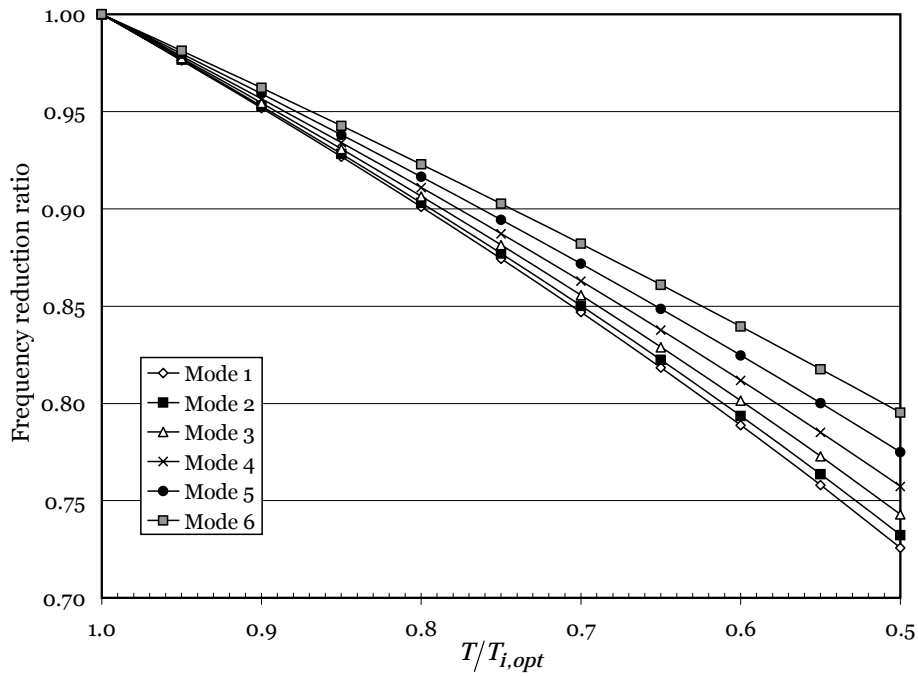
The tendon specimens exhibited many of the same trends as the cable specimens. In particular, the lower modes of vibration were more sensitive to damage than the higher modes.

## 7.2 CALCULATED SENSITIVITY OF NATURAL FREQUENCIES TO CHANGES IN TENSION AND FLEXURAL STIFFNESS

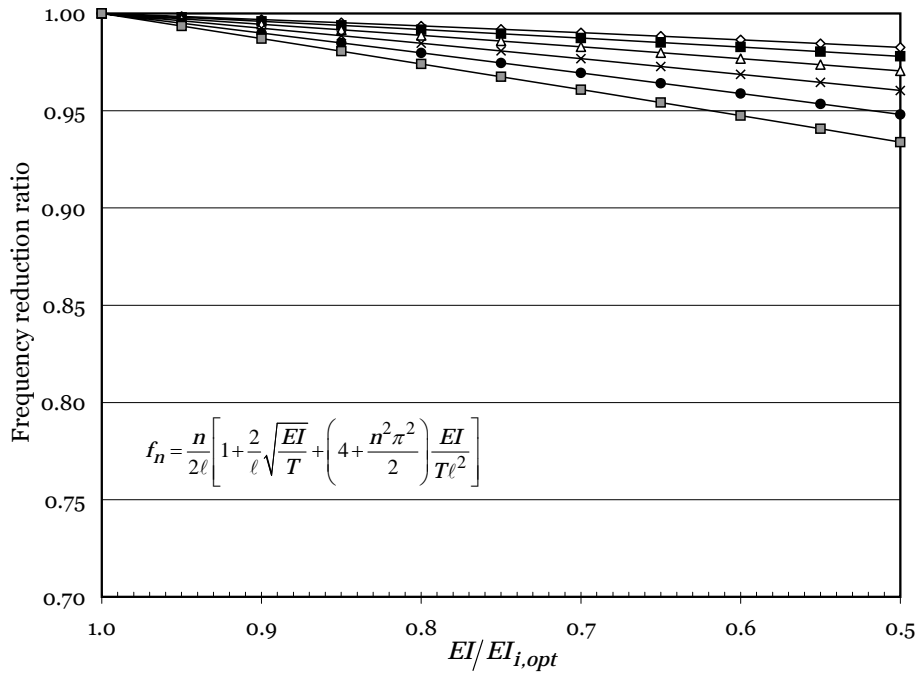
As discussed in Chapter 6, the stiff string model provided a better representation of the initial response of all five test specimens than the taut string model. Therefore, the approximate solution proposed by Morse (1948) was used to relate damage in the test specimens to the observed changes in the natural frequencies. Two sets of analyses are presented in this section. In both cases, the natural frequencies were calculated using Eq. 6.4 and the influence of damage was simulated by changing the value of a single parameter: either the tension,  $T$ , or the flexural stiffness,  $EI$ .

In the first set of analyses, the values of mass per unit length,  $m$ , length,  $\ell$ , and  $EI$  were set equal to those corresponding to the minimum total error for the undamaged specimens (Table 6.7 and Table 6.13) and were held constant in the analyses. The value of  $T$  was varied from  $1.0T_{i,opt}$  to  $0.5T_{i,opt}$ , where  $T_{i,opt}$  is the tension corresponding to the minimum total error for the undamaged specimens. In the second set of analyses, the values of  $m$ ,  $\ell$ , and  $T$  were held constant, while the value of  $EI$  was varied from  $1.0EI_{i,opt}$  to  $0.5 EI_{i,opt}$ , where  $EI_{i,opt}$  is the flexural stiffness corresponding to the minimum total error in the undamaged specimens. The results of the analyses for Cable 02 and Tendon 01 are presented in Figure 7.6 and Figure 7.7, respectively, and are considered to be representative of all five specimens.

When damage was simulated by decreasing the tension, the lower frequencies changed more than the higher frequencies. In contrast, when damage was simulated by decreasing the flexural stiffness, the higher frequencies changed more than the lower frequencies. In addition, the frequency reduction ratios were more sensitive to changes in  $T$  than in  $EI$ . A 50% reduction in  $T$  caused 25 to 30% reductions in the natural frequencies, while a 50% reduction in  $EI$  caused 1 to 11% reductions in the natural frequencies.

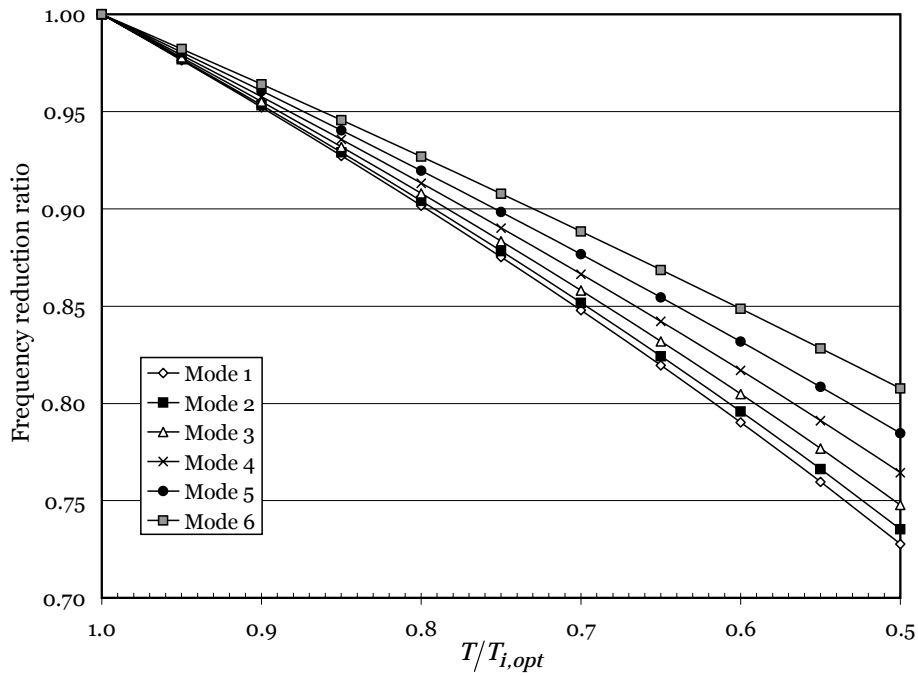


(a) Variations in Tension

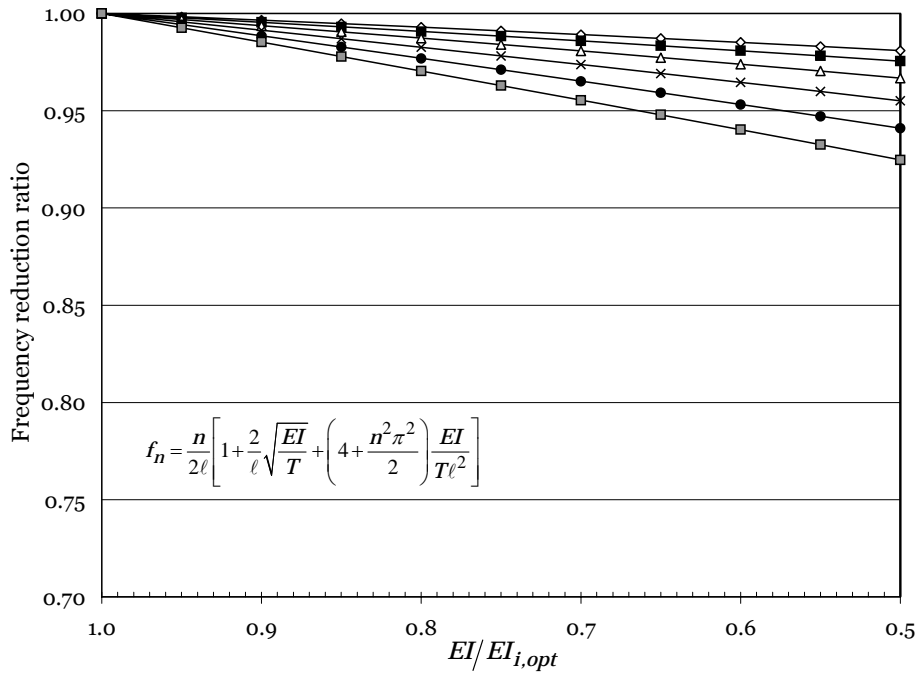


(b) Variations in Flexural Stiffness

**Figure 7.6 Sensitivity of Frequency Reduction Ratios to Changes in Tension and Flexural Stiffness for Cable 02**



(a) Variations in Tension



(b) Variations in Flexural Stiffness

**Figure 7.7 Sensitivity of Frequency Reduction Ratios to Changes in Tension and Flexural Stiffness for Tendon 01**

It should be noted that varying the values of individual parameters is an oversimplification of the manner in which damage accumulated in the test specimens. Changes in the flexural stiffness are expected to be located at the ends and near the point of the applied load, rather than being uniformly distributed along the length of the specimen. In addition, the presence of a wire break does not necessarily correspond to a loss in tension. As discussed in Chapter 3, the tensile stresses are redistributed to adjacent wires after wire fractures due to the spiral configuration of the strand.

The general trends exhibited in Figure 7.6 and Figure 7.7, however, are consistent with those observed in the measured data discussed in Section 7.1. For low levels of damage, the higher modes tended to exhibit lower frequency reduction ratios. This trend is consistent with a reduction in the flexural stiffness. As the number of wire breaks increased, the lower modes exhibited lower frequency reduction ratios, as is expected with a reduction in the tension.

### **7.3 ESTIMATED STRUCTURAL PARAMETERS AT CONCLUSION OF FATIGUE TESTS**

It is known from the results of the autopsies that each test specimen experienced significant damage during the fatigue or accelerated corrosion tests. The optimization procedures developed in Chapter 6 are used in this section to evaluate the residual tension in three of the test specimens: Cable 02, Cable 03, and Tendon 01. Cable 01 was not considered in this section because the specimen collapsed during the fatigue tests, and therefore, the residual tension was zero. In addition, the extent of damage at the time of the last free-vibration test was not known. Tendon 02 was also not considered in this section because the actual distribution of damage along the length of each strand was not known, even after the autopsy.

The observed conditions of the test specimens at the conclusion of the fatigue tests are summarized in Table 7.1. The estimated residual tension force,  $T_{min}$ , for each specimen is also listed as a multiple of the initial tension,  $T_o$ . In these calculations, all seven wires in the strand were assumed to have equal cross-sectional areas, the tensile stress was assumed to be uniformly distributed among the intact wires in the strand, the

tensile strength of the strand was taken as 270 ksi, and the yield strength of the strand was taken as 245 ksi. Given the initial level of prestress, individual strands in all three specimens were expected to be able to carry the initial tension force without yielding if one or two wires were broken (Table 7.2). If a strand experienced three wire breaks, the average stress was close to the yield strength of the strand for the cable specimens and fracture of the remaining wires in the strand was expected for Tendon 01. Therefore, at the conclusion of the fatigue tests, Cable 02 was estimated to be carrying 50% of its initial tension and Tendon 01 was estimated to be carrying 75% of its initial tension. Because the calculated average stress in the top strand of Cable 03 was close to the yield strength of the strand, the residual tension force was expected to be lower in Cable 03 than Cable 02, but a quantitative estimate was not made.

**Table 7.1 Condition of Test Specimens at Conclusion of Fatigue Tests**

Specimen	Final Frequency Test	Observed Damage	Estimated Residual Properties	
			$T_{min}$	$I_{min}$
Cable 02	NF8	Top strand: all 7 wires fractured Bottom strand: no damage	$0.5T_o$	$0.9I_o$
Cable 03	NF4	Top strand: 3 wires fractured Bottom strand: all 7 wires fractured	$< 0.5T_o$	$< 0.9I_o$
Tendon 01	NF13	All 7 wires fractured in 3 strands at bottom of cross section. Two other strands experienced 2 wire breaks per strand. No damage in remaining 7 strands.	$0.75T_o$	$0.55I_o$

**Table 7.2 Calculated Stress in Strand with Broken Wires**

Specimen	Initial Prestress		Residual Prestress (ksi)		
	% GUTS	ksi	1 Broken Wire	2 Broken Wires	3 Broken Wires
Cable Specimens	50	135	158	189	236
Tendon 01	60	162	189	227	*
Tendon 02	80	216	252	*	*

\* Calculated stress exceeds  $f_{pu}$ .

Using the reduced number of strands resisting tension at the conclusion of the fatigue tests, the transformed moment of inertia at the north end of the test specimens was calculated using the procedures described in Appendix N. These values are reported as  $I_{min}$  in Table 7.1.

An approach is developed in this section to estimate the values of the structural parameters that best match the measured frequency response at the conclusion of the fatigue tests. The physical significance of these parameters is also evaluated. Frequency data from all free-vibration tests of all specimens are evaluated using the same approach in Section 7.4.

### 7.3.1 Multi-Variable Optimization

As discussed in Chapter 6, the stiff string model provided a better match to the measured frequency response of the undamaged test specimens than the taut string model. Therefore, only the stiff string model is considered in this section. Four parameters,  $T$ ,  $EI$ ,  $\ell$ , and  $m$ , are needed to calculate the natural frequencies of an external tendon using the stiff string model. Similarly to Chapter 6, the best solution is taken as the set of parameters corresponding to the minimum total error between the measured and calculated natural frequencies,  $\Omega_{tot}$ , which is defined in Eq. 6.6. It is expected that the minimum total error for the damaged specimens will exceed the minimum total error for the undamaged test specimens, because the stiff string model assumes that all structural properties are uniformly distributed along the entire length of the tendon. However, the damage in the test specimens subjected to fatigue loads was concentrated near the north end. In spite of these limitations, the stiff string model was used to evaluate the damaged test specimens.

Three different approaches were used to determine the optimal combination of parameters from the natural frequencies recorded at the end of the fatigue tests. In the following discussion, the term “initial set of parameters” refers to the values of tension, flexural stiffness, specimen length, and mass per unit length corresponding to the minimum total error for the undamaged specimens. The notation  $T_{i,opt}$ ,  $EI_{i,opt}$ ,  $\ell_{i,opt}$ , and

$m_{i,opt}$  will be used to refer to these values, which are reported in Table 6.7 and Table 6.13. The term “updated set of parameters” refers to the values of tension, flexural stiffness, specimen length, and mass per unit length corresponding to the minimum total error for the specimens at the conclusion of the fatigue tests. The notation  $T_{f,opt}$ ,  $EI_{f,opt}$ ,  $\ell_{f,opt}$ , and  $m_{f,opt}$  will be used to refer to these values.

In the first series of analyses, the initial values were used for  $EI$ ,  $\ell$ , and  $m$ , and only the value of  $T$  was updated to reflect the fatigue damage. This analysis option is called a single-variable optimization. In the second series of analyses, the initial values were used for  $\ell$  and  $m$ , while the values of both  $T$  and  $EI$  were updated. This analysis option is called a two-variable optimization. In the third series of analyses, the values of all four parameters were updated. While the values of  $\ell$  and  $m$  did not change during the fatigue tests, this four-variable optimization was included for completeness.

The parameters used in the three series of analyses are summarized in Table 7.3, and the results are discussed in the following sections. In the analyses, the ranges of  $\ell$  and  $m$  considered were the same as those used in Chapter 6 for the undamaged specimens. However, no limits were placed on the values of  $T$  and  $EI$ .

**Table 7.3 Parameters used in Three Series of Analyses**

Parameters	Optimization Approach		
	Single Variable	Two Variable	Four Variable
$T$	Updated	Updated	Updated
$EI$	Initial	Updated	Updated
$\ell$	Initial	Initial	Updated
$m$	Initial	Initial	Updated



### 7.3.2 Cable 02

The results of the three sets of analyses for Cable 02 are summarized in Table 7.4. The total error decreased as the number of variables considered in the analyses increased. The values of residual tension,  $T_{f,opt}$ , ranged from 40 to 45 kip. These values are considerably higher than the estimated value ( $T_{min} = 0.5T_o$ ) based on the observed conditions during the autopsy.

**Table 7.4 Summary of Results of Multi-Parameter Optimization for Cable 02**

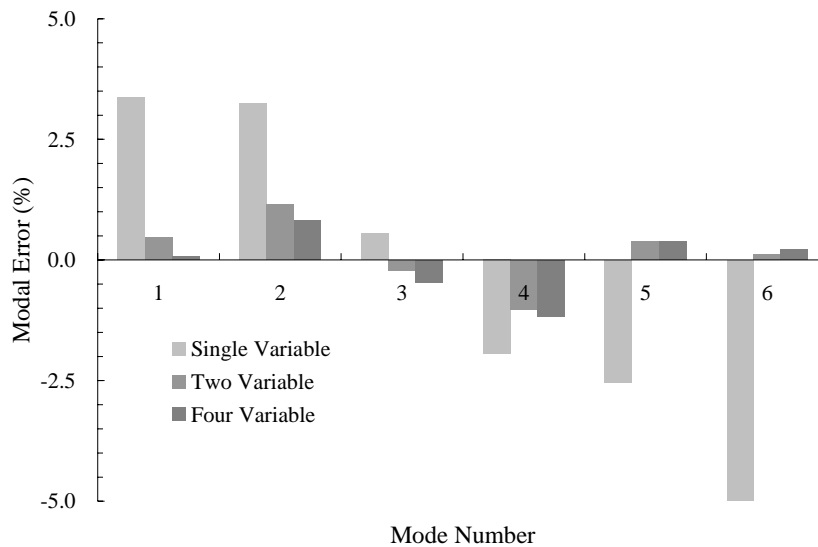
Optimization Approach	T (kip)	EI (kip-ft <sup>2</sup> )	ℓ (ft)	m (lb-sec <sup>2</sup> /ft <sup>2</sup> )	Total Error
Initial	55.0	92	49.3	0.330	0.00019
Single Variable	45.4	-	-	-	0.00573
Two Variable	41.0	145	-	-	0.00028
Four Variable	40.0	146	49.4	0.320	0.00024

When multiple parameters were considered in the optimization, the values of the residual flexural stiffness,  $EI_{f,opt}$ , were more than 50% larger than the value corresponding to the undamaged specimen,  $EI_{i,opt}$ . At first glance, this result appears to be incorrect. However, it should be noted that the value of  $EI_{i,opt}$  for Cable 02 was approximately one-half the value calculated for Cable 03 (Table 6.7). In addition, the values of  $EI_{f,opt}$  were approximately 20% less than the initial estimate, which was calculated using the geometry of the cross section and assumed material properties (Table 6.3). Based on these considerations, the value of  $EI_{i,opt}$  seems less reasonable than the value of  $EI_{f,opt}$ .

As expected, the values of  $\ell_{f,opt}$  and  $m_{f,opt}$  did not vary appreciably from the initial values. Calculated natural frequencies using the estimated parameters are summarized in Table 7.5 and the corresponding modal errors are plotted in Figure 7.8. The modal errors corresponding to the single-variable optimization were more than two times larger than those corresponding to the two-variable optimization. The modal errors were approximately the same for the two-variable and four-variable optimizations, where the modal errors were less than 1% for all modes.

**Table 7.5 Comparison of Natural Frequencies for Cable 02**

Mode	Measured Frequencies	Optimization Approach		
		Single Variable	Two Variable	Four Variable
1	3.9	4.0	3.9	3.9
2	7.9	8.2	8.0	8.0
3	12.4	12.5	12.4	12.3
4	17.4	17.1	17.2	17.2
5	22.6	22.0	22.7	22.7
6	28.9	27.5	28.9	29.0



**Figure 7.8 Modal Errors Corresponding to Multi-Variable Optimization for Cable 02**

### 7.3.3 Cable 03

The results of the three sets of analyses for Cable 03 are summarized in Table 7.6. As before, total error decreased as the number of variables considered in the optimization increased. The values of residual tension,  $T_{f,opt}$ , ranged from 32 to 33 kip. These values were less than those of Cable 02 but still larger than expected based on the results of the autopsy ( $T_{min} < 0.5T_o$ ). The values of residual flexural stiffness,  $EI_{f,opt}$ , ranged from 158 to 170 kip-ft<sup>2</sup>, which corresponds to 0.88 to 0.94  $EI_{i,opt}$ . These values are consisted with

the expectations summarized in Table 7.1. When the four-variable optimization was conducted, the value of  $\ell_{f,opt}$  was the same as  $\ell_{i,opt}$ , but  $m_{f,opt}$  was 7% less than  $m_{i,opt}$ .

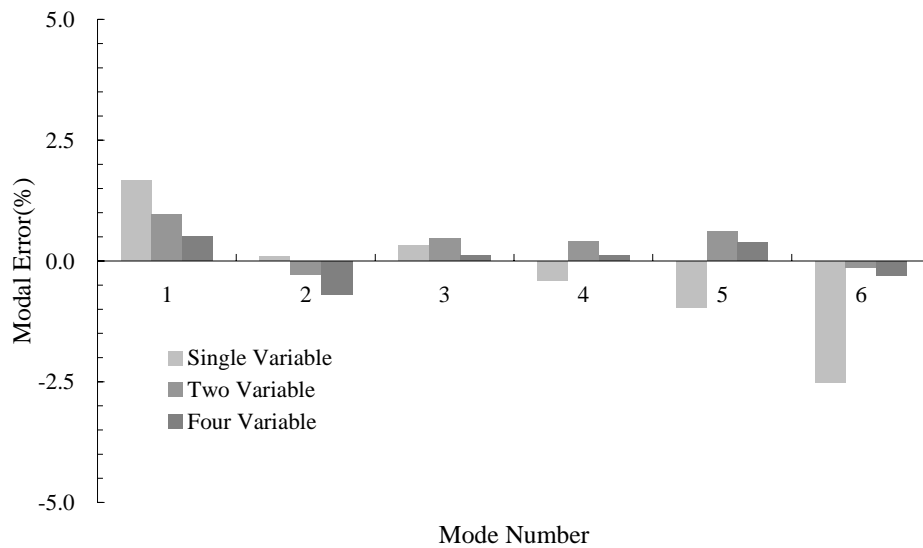
**Table 7.6 Summary of Results of Multi-Parameter Optimization for Cable 03**

Optimization Approach	T (kip)	EI (kip-ft <sup>2</sup> )	$\ell$ (ft)	m (lb-sec <sup>2</sup> /ft <sup>2</sup> )	Total Error
Initial	55	188	49.8	0.350	0.00013
Single Variable	33	-	-	-	0.00103
Two Variable	34	170	-	-	0.00018
Four Variable	32	158	49.8	0.326	0.00010

Natural frequencies calculated using the estimated parameters are summarized in Table 7.7 and the corresponding modal errors are plotted in Figure 7.9. The calculated frequencies from the analyses with two variables and four variables were nearly identical to the measured frequencies, where modal errors for all modes were less than 1%. Larger errors were calculated using the single-variable optimization.

**Table 7.7 Comparison of Natural Frequencies for Cable 03**

Mode	Measured Frequencies	Optimization Approach		
		Single Variable	Two Variable	Four Variable
1	3.5	3.4	3.5	3.5
2	7.1	7.1	7.1	7.2
3	11.2	11.2	11.1	11.2
4	15.8	15.9	15.7	15.8
5	21.2	21.4	21.1	21.1
6	27.3	28.0	27.3	27.4



**Figure 7.9 Modal Errors Corresponding to Multi-Variable Optimization for Cable 03**

### 7.3.4 Tendon 01

The results of the three sets of analyses for Tendon 01 are summarized in Table 7.8. Although the total error decreased as the number of variables considered in the analyses increased, the variation in total error was small. The values of residual tension,  $T_{f,opt}$ , ranged from 310 to 330 kip, which are close to the expected value based on the observed conditions during the autopsy ( $T_{min} = 0.75T_o$ ).

**Table 7.8 Summary of Results of Multi-Parameter Optimization for Tendon 01**

Optimization Approach	T (kip)	EI (kip-ft <sup>2</sup> )	ℓ (ft)	m (lb-sec <sup>2</sup> /ft <sup>2</sup> )	Total Error
Initial	400	350	32.8	0.442	0.00039
Single Variable	328	-	-	-	0.00059
Two Variable	330	340	-	-	0.00055
Four Variable	310	295	32	0.434	0.00054

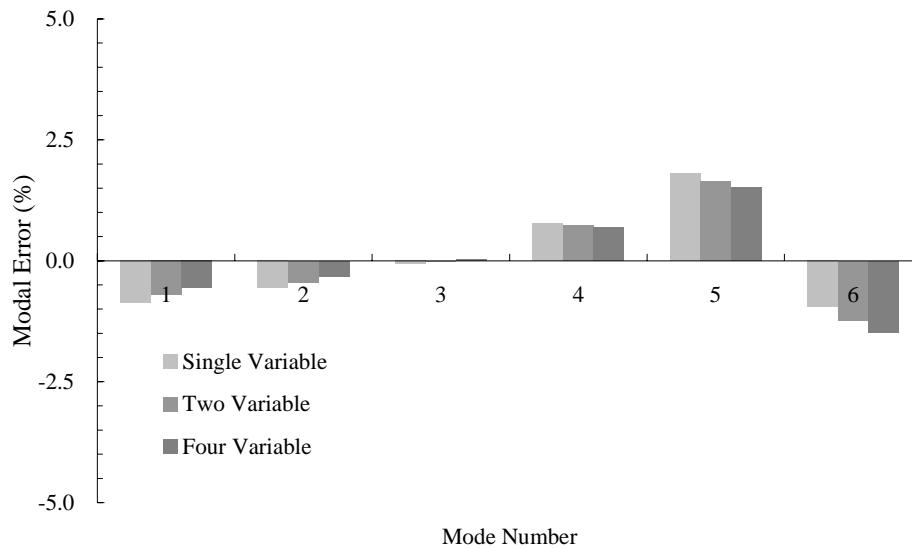
When multiple parameters were considered in the optimization, the values of residual flexural stiffness,  $EI_{f,opt}$ , ranged from 85 to 95% of  $EI_{i,opt}$ . These values are

considerably larger than the estimated value of  $EI_{min}$ , possibly because the damage was concentrated at the north end of the specimen and was not uniformly distributed along the entire length. The values of  $\ell_{f,opt}$  and  $m_{f,opt}$  did not vary appreciably from the initial values.

Calculated natural frequencies using the estimated parameters are summarized in Table 7.9. The corresponding modal errors are plotted in Figure 7.9. The modal errors corresponding to all three optimization approaches were nearly the same, but the modal errors decreased slightly as the number of parameters considered in the analyses increased.

**Table 7.9 Comparison of Natural Frequencies for Tendon 01**

Mode	Measured Frequencies	Optimization Approach		
		Single Variable	Two Variable	Four Variable
1	14.2	14.1	14.1	14.1
2	28.7	28.5	28.6	28.6
3	43.8	43.8	43.8	43.8
4	59.7	60.2	60.1	60.1
5	76.7	78.1	78.0	77.9
6	98.9	98.0	97.7	97.4



**Figure 7.10 Modal Errors Corresponding to Multi-Variable Optimization for Tendon 01**

### 7.3.5 Summary

The total error decreased as the number of variables included in the analyses increased and the values of the residual tension,  $T_{f,opt}$ , were lower than the initial values,  $T_{i,opt}$ , for all three sets of analyses. For Cable 03 and Tendon 01,  $T_{f,opt}$  was not sensitive to the number of variables considered in the optimization. However, for Cable 02,  $T_{f,opt}$  was approximately 10% larger using the single-variable optimization compared with the multi-variable optimizations. In all three cases, the values of  $T_{f,opt}$  were larger than expected based on the number of wire breaks detected during the autopsy (Table 7.1).

The values of flexural stiffness,  $EI_{f,opt}$ , were more variable than those of the residual tension. For Cable 02,  $EI_{f,opt}$  was larger than the initial value,  $EI_{i,opt}$ , which is inconsistent with expectations. The value of  $EI_{f,opt}$  for Tendon 01 was less than  $EI_{i,opt}$ , but larger than the expected value based on the number of observed wire breaks. In contrast, the value of  $EI_{f,opt}$  for Cable 03 was consistent with the autopsy results (Table 7.1). The results from this series of analyses indicate that the values of  $EI$  extracted from the measured frequencies need to be interpreted carefully, and that the values of  $EI$  do not necessarily decrease with increasing damage. The fact that  $EI$  is assumed to be constant along the length in the analyses, but the actual damage was localized, which may contribute to these inconsistencies.

The values of  $\ell_{f,opt}$  and  $m_{f,opt}$  did not vary appreciably from the initial values for any of the specimens. Based on the results of the analyses presented in this section, the two-variable optimization appears to be most appropriate for extracting the value of remaining tension from the frequency response of damaged external tendons.

## 7.4 VARIATION OF STRUCTURAL PARAMETERS WITH INCREASING DAMAGE

The two-variable optimization procedure was used to extract values of  $T$  and  $EI$  using all frequency measurements for all five test specimens. The results are summarized in this section.

### 7.4.1 Cable Specimens

The values of  $T$  and  $EI$  extracted from the measured frequencies of the cable specimens are presented in this section. For each optimization, the following ranges of parameters were considered:

- (1)  $T$  was constrained to vary between 35 and 65 kip using an increment of 1 kip.
- (2)  $EI$  was constrained to vary between 50 and 200 kip-ft<sup>2</sup> using an increment of 5 kip-ft<sup>2</sup>.
- (3)  $\ell$  was assumed to be equal to  $\ell_{i,opt}$  (49.1 ft for Cable 01, 49.3 ft for Cable 02, and 49.8 ft for Cable 03).
- (4)  $m$  was assumed to be equal to  $m_{i,opt}$  (0.350 lb-sec<sup>2</sup>/ft<sup>2</sup> for Cable 01, 0.326 lb-sec<sup>2</sup>/ft<sup>2</sup> for Cable 02, and 0.350 lb-sec<sup>2</sup>/ft<sup>2</sup> for Cable 03).

The values of tension and flexural stiffness extracted from the five sets of natural frequencies are summarized in Table 7.10 for Cable 01. Because the increment used in evaluating  $EI$  was larger in this set of analyses than the analyses of the undamaged specimens discussed in Chapter 6, the value of total error for NF0 is slightly larger in Table 7.10 than in Table 6.7.

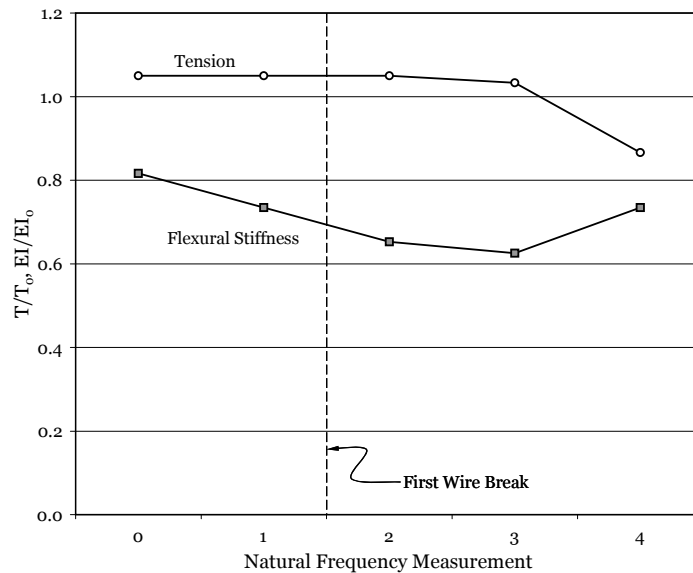
**Table 7.10 Optimized Parameters for Cable 01**

Parameter	NF0	NF1	NF2	NF3	NF4
$T$ (kip)	63	63	63	62	52
$EI$ (kip-ft <sup>2</sup> )	150	135	120	115	135
<i>Total Error</i>	0.00022	0.00798	0.00015	0.00045	0.00032
<i>Wire Breaks Reported</i>	0	0	2	3	8

The values of  $T$  decreased from 63 to 52 kip during the fatigue test; however, the tension did not change appreciably between NF0 and NF3. The residual tension decreased more than 15% between NF3 and NF4. The values of  $EI$  decreased from 150 to 115 kip-ft<sup>2</sup> between NF0 and NF3, and then increased to 135 kip-ft<sup>2</sup> in NF4.

The extracted parameters were normalized with respect to the initial values,  $T_o$  and  $EI_o$ , where  $T_o$  corresponds to the target level of prestress (50% GUTS) and  $EI_o$  corresponds to the idealized section and material properties discussed in Section 6.3.4. It was decided to use these values for normalizing the extracted data, rather than the values corresponding to the minimum total error during the first free-vibration test ( $T_{i,opt}$  and  $EI_{i,opt}$ ), because these are the values that the engineer is likely to be using when evaluating an existing bridge with external tendons. The normalized data are plotted in Figure 7.11

Early in the fatigue test, the flexural stiffness varied more than the tension. After the eighth wire break was reported (before NF4), the tension decreased abruptly, and the flexural stiffness increased. The increase in flexural stiffness is inconsistent with expectations.



**Figure 7.11** Variation of  $T$  and  $EI$  during Fatigue Test for Cable 01

The values of tension and flexural stiffness extracted from the nine sets of measured natural frequencies for Cable 02 are summarized in Table 7.11 and Figure 7.12. The values of residual tension decreased from 55 to 41 kip during the fatigue test. In

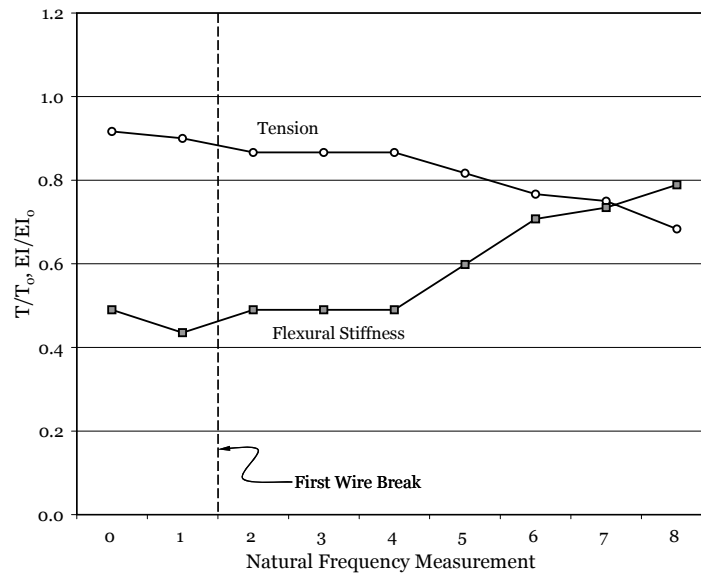


contrast, the values of flexural stiffness tended to increase from 90 to 145 kip-ft<sup>2</sup> during the fatigue test. This trend is inconsistent with expectations.

**Table 7.11 Optimized Parameters for Cable 02**

Parameter	NF0	NF1	NF2	NF3	NF4
<i>T</i> (kip)	55	54	52	52	52
<i>EI</i> (kip-ft <sup>2</sup> )	90	80	90	90	90
<i>Total Error</i>	0.00021	0.00041	0.00018	0.00026	0.00023
<i>Wire Breaks Reported</i>	0	0	1	2	2

Parameter	NF5	NF6	NF7	NF8
<i>T</i> (kip)	49	46	45	41
<i>EI</i> (kip-ft <sup>2</sup> )	110	130	135	145
<i>Total Error</i>	0.00012	0.00028	0.00033	0.00028
<i>Wire Breaks Reported</i>	2	5	5	6



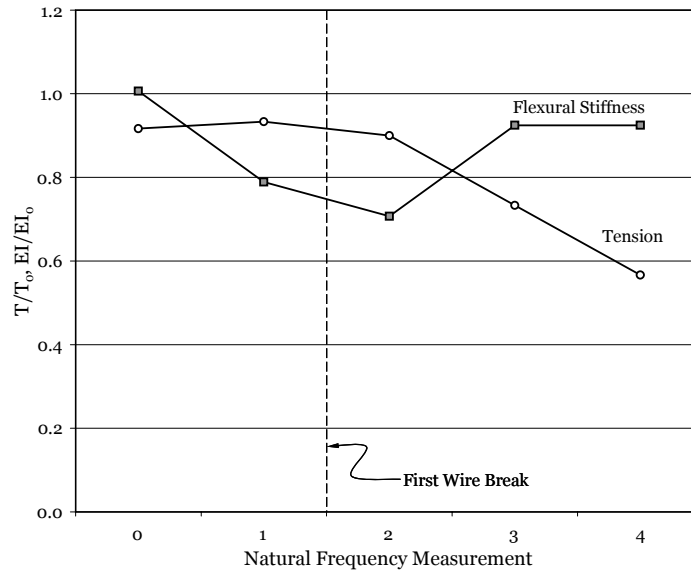
**Figure 7.12 Variation of *T* and *EI* during Fatigue Test for Cable 02**

The values of tension and flexural stiffness extracted from the five sets of measured natural frequencies for Cable 03 are summarized in Table 7.12 and Figure 7.13.

The values of residual tension decreased from 55 to 34 kip during the fatigue test. The tension corresponding to NF1 was slightly larger than the tension corresponding to NF0, but this difference may be attributed to numerical errors in the optimization, rather than an increase in the tension. The values of flexural stiffness decreased from 195 to 145 kip-ft<sup>2</sup> between NF0 and NF2; however, the flexural stiffness increased to 170 kip-ft<sup>2</sup> in NF3 and NF4.

**Table 7.12 Optimized Parameters for Cable 03**

Parameter	NF0	NF1	NF2	NF3	NF4
$T$ (kip)	55	56	54	44	34
$EI$ (kip-ft <sup>2</sup> )	185	145	130	170	170
<i>Total Error</i>	0.00014	0.00030	0.00028	0.00011	0.00018
<i>Wire Breaks Reported</i>	0	0	4	6	8



**Figure 7.13 Variation of  $T$  and  $EI$  during Fatigue Test for Cable 03**

For the cable specimens, the values of residual tension tended to decrease throughout the fatigue test. This result was expected and reflected the reduction in the measured natural frequencies as the extent of damage increased. However, the values of

flexural stiffness were more variable. Initially, the values of flexural stiffness tended to decrease slightly with an increasing number of fatigue cycles. This trend was expected because cracks formed in the grout at the beginning of the fatigue tests, which would reduce the flexural stiffness. However, the values of flexural stiffness increased after wire breaks were detected. This trend was not expected.

#### 7.4.2 Tendon Specimens

The values of  $T$  and  $EI$  extracted from the measured frequencies of the tendon specimens are presented in this section. For Tendon 01, the following ranges of parameters were considered:

- (1)  $T$  was constrained to vary between 300 and 450 kip using an increment of 5 kip.
- (2)  $EI$  was constrained to vary between 250 and 400 kip-ft<sup>2</sup> using an increment of 5 kip-ft<sup>2</sup>.
- (3)  $\ell$  was assumed to be equal to  $\ell_{i,opt}$  (32.8 ft).
- (4)  $m$  was assumed to be equal to  $m_{i,opt}$  (0.442 lb-sec<sup>2</sup>/ft<sup>2</sup>).

The values of tension and flexural stiffness extracted from the fourteen sets of measured natural frequencies for Tendon 01 are summarized in Table 7.13 and Figure 7.14. The values of residual tension decreased gradually from 390 to 330 kip. The total reduction in tension was less than estimated based on the number of wire breaks observed during the autopsy ( $T_{min} = 0.75 T_o$ ), but the trend is consistent with expectations.

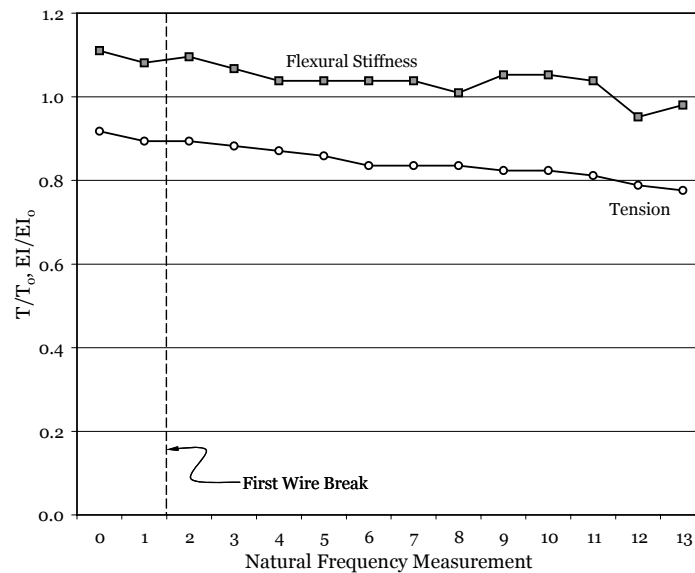
The values of flexural stiffness decreased gradually from 385 to 330 kip-ft<sup>2</sup> during the fatigue test. It is interesting to note that the value of flexural stiffness corresponding to the minimum error for most of the free-vibration tests exceeded  $EI_{i,opt}$  (Table 6.13). This is because the upper limit on  $EI$  was larger for the analyses discussed in this chapter than the analyses in Chapter 6 (350 kip-ft<sup>2</sup> in Chapter 6 and 400 kip-ft<sup>2</sup> in Chapter 7). However, based on the results presented in Figure 6.11, the total error was not sensitive to the flexural stiffness, so the trends should be similar if the same range of parameters had been used in the analyses.

**Table 7.13 Optimized Parameters for Tendon 01**

Parameter	NF0	NF1	NF2	NF3	NF4	NF5	NF6
$T$ (kip)	390	380	380	375	370	365	355
$EI$ (kip-ft <sup>2</sup> )	385	375	380	370	360	360	360
<i>Total Error</i>	0.00020	0.00007	0.00017	0.00021	0.00031	0.00031	0.00016*
<i>Wire Breaks Reported</i>	0	0	2	6	9	11	12

Parameter	NF7	NF8	NF9	NF10	NF11	NF12	NF13
$T$ (kip)	355	355	350	350	345	335	330
$EI$ (kip-ft <sup>2</sup> )	360	350	365	365	360	330	340
<i>Total Error</i>	0.00018*	0.00019*	0.00024	0.00022	0.00028	0.00060	0.00055
<i>Wire Breaks Reported</i>	12	12	14	14	17	20	21

\* Fifth mode not included in optimization.



**Figure 7.14 Variation of  $T$  and  $EI$  during Fatigue Test for Tendon 01**

Tendon 02 was moved after construction, and the natural frequencies shifted between the initial set of frequency measurements (NF0) and the first set of frequency measurements taken when the specimen was in the final position (NF1). Therefore, the

frequencies from NF1 were used to determine the values of  $\ell_{i,opt}$  and  $m_{i,opt}$  used in the analyses. For Tendon 02, the following ranges of parameters were considered:

- (1)  $T$  was constrained to vary between 260 and 425 kip using an increment of 5 kip.
- (2)  $EI$  was constrained to vary between 70 and 245 kip-ft<sup>2</sup> using an increment of 5 kip-ft<sup>2</sup>.
- (3)  $\ell$  was assumed to be equal to  $\ell_{i,opt}$  (32.8 ft).
- (4)  $m$  was assumed to be equal to  $m_{i,opt}$  (0.386 lb-sec<sup>2</sup>/ft<sup>2</sup>).

The values of tension and flexural stiffness extracted from the twenty-one sets of measured natural frequencies for Tendon 02 are summarized in Table 7.14 and Figure 7.15. The values of residual tension decreased from 405 to 265 kip. As discussed in Chapter 5, three abrupt changes in the natural frequencies were measured during the exposure test. The measured frequencies fluctuated slightly between these abrupt changes. Similar trends were calculated for the residual tension. The largest change in residual tension occurred between NF18 and NF19.

The variations in flexural stiffness were not consistent with the observed damage. Values of  $EI$  decreased from 130 to 75 kip-ft<sup>2</sup> between NF1 and NF4, and then increased to a maximum of 185 kip-ft<sup>2</sup> in NF12.

**Table 7.14 Optimized Parameters for Tendon 02**

Parameter	NF1	NF2	NF3	NF4	NF5	NF6	NF7
$T$ (kip)	405	405	410	410	410	365	365
$EI$ (kip-ft)	130	115	90	75	80	160	165
<i>Total Error</i>	0.00025	0.00033	0.00060	0.00074	0.00068	0.00047	0.00065

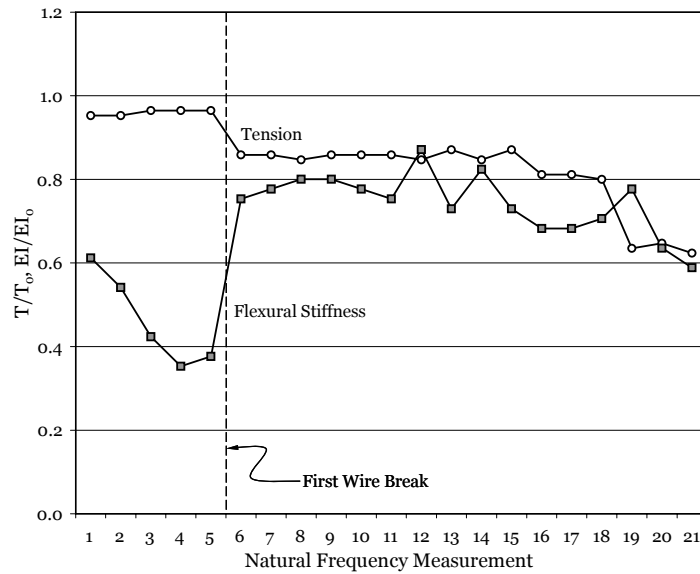
**Table 7.14 (cont). Optimized Parameters for Tendon 02**

Parameter	NF8	NF9	NF10	NF11	NF12	NF13	NF14
$T$ (kip)	360	365	365	365	360	370	360
$EI$ (kip-ft)	170	170	165	160	185	155	175
<b>Total Error</b>	0.00067	0.00042	0.00070	0.00001*	0.00052	0.00023	0.00032

\* First mode not included in optimization.

Parameter	NF15	NF16	NF17	NF18	NF19	NF20	NF21
$T$ (kip)	370	345	345	340	270	275	265
$EI$ (kip-ft)	155	145	145	150	165	135	125
<b>Total Error</b>	0.00023	0.00012	0.00017	0.00017	0.00017**	0.00011	0.00013

\*\* Sixth mode not included in optimization.



**Figure 7.15 Variation of  $T$  and  $EI$  during Exposure Test for Tendon 02**

For the tendon specimens, the values of residual tension tended to decrease throughout the fatigue/accelerated corrosion tests. This result was expected and reflected the reduction in the measured natural frequencies as the extent of damage increased. For Tendon 01, the residual tension extracted from the measured frequencies at the conclusion of the fatigue test was approximately 15% lower than the tension extracted

from the frequency response of the undamaged specimen. For Tendon 02, the residual tension at the conclusion of the exposure test was approximately 35% lower than the tension corresponding to the undamaged specimen. The values of flexural stiffness extracted from the measured frequency response of Tendon 01 decreased as damage increased, and the final value was approximately 12% lower than the initial value. However, the values of flexural stiffness extracted from the measured frequency response of Tendon 02 were highly variable and did not correlate with increasing damage.

It is believed that observed trends for the tendon specimens are more representative of the performance of external tendons than those from the cable specimens because the number of strands, level of prestress, and volume of grout in the tendon specimens were more representative of external tendons in post-tensioned bridge construction.

## **7.5 LIMITATIONS OF VIBRATION TECHNIQUE FOR EVALUATING EXTERNAL POST-TENSIONED TENDON**

Several issues were identified in the previous section that may limit the use of measured frequencies to extract information about the residual level of tension in an external tendon and may be attributed to two sources: model error and numerical uncertainty. Model error refers to the discrepancies between the test specimens and the idealized structural system, which is represented using the stiff string model. Of particular importance is the assumption that all structural parameters are constant along the length of the specimen, which introduces considerable error as damage accumulates at discrete locations. In addition, estimations of the parameters  $\ell$  and  $m$ , may introduce errors in the residual tension calculations if frequency measurements are not available for the undamaged tendon, as the errors for the undamaged specimens (Chapter 6) were sensitive to the length used in the analyses.

The numerical uncertainty refers to the inaccuracies related to the error function – the least squares function in this case. The least squares function is commonly used where the probability of error is normally distributed. However, the analyses discussed in

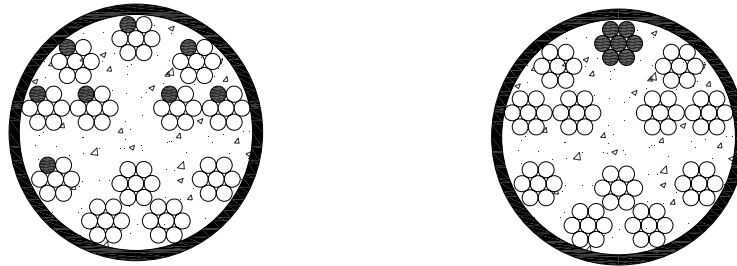
this chapter indicate that the least squares function can produce non-unique solutions. In general, the error function, also called objective function, restrains the numerical procedures to yield the optimum value of the unknown parameters. However, restraints were not suggested in this dissertation because information, such as the behavior of external tendons after damage and the appropriate values of structural parameters for recently constructed bridges, is rarely available.

The interpretation of damage in this dissertation has focused on the relationship between the remaining cross-sectional area of strands and the residual prestressing force. As discussed in Section 7.3, the calculated changes in tension at the conclusion of the fatigue tests were typically less than those calculated based on the number of wire breaks observed during the autopsy. Two factors may contribute to these differences:

- (1) As discussed in Chapter 3, the tensile stresses in the wires of a strand redistribute after a wire has fractured. In addition, the fractured wire is able to recover tensile stress due to the spiral configuration of the wires in the strand. Therefore, the remaining cross-sectional area of strands is not a direct indicator of the level of tension. For example, the two cross sections in Figure 7.16 have the same number of strands and the same number of wire breaks. However, the tension in Section A is expected to be larger than the tension in Section B due to the distribution of wire breaks.
- (2) All seven wires fractured in at least one strand for all five test specimens. Based on the calculations summarized in Table 7.2, the residual stress in these strands should be zero. However, the calculated values of residual tension,  $T_{f,opt}$ , exceeded the estimated values,  $T_{min}$ , for Cable 02, Cable 03, and Tendon 01. Although the actual number of broken wires in Tendon 02 is not known, it is reasonable to assume that all seven wires in the top three strands (the strands exposed to acid) fractured during the accelerated corrosion test. In that case, only two-thirds of the initial area of strand would be available to resist tension at the conclusion of the test. The ratio  $T_{f,opt}/T_{i,opt}$  was 0.65 for Tendon 02, which is close to the expected value based on the cross-sectional area. The primary difference



between Tendon 02 and the other test specimens is that the reaction frame for Tendon 02 was not tied to the strong floor in the Ferguson Structural Engineering Laboratory. It is possible that the additional axial stiffness caused by bolting the reaction frames to the strong floor provided a mechanism for stresses to redistribute among strands.



(a) Section A: scattered damage      (b) Section B: concentrated damage

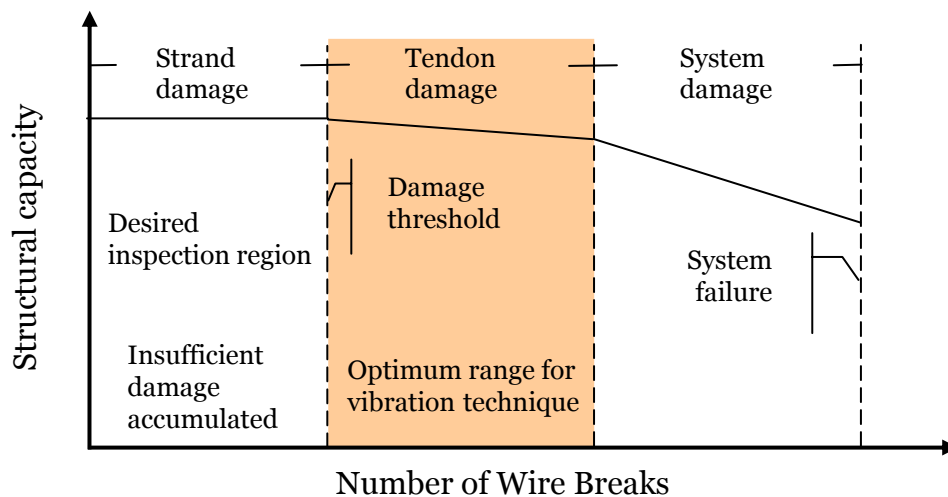
**Figure 7.16 Cross Section of External Tendon with Wire Breaks**

As discussed previously, external tendons in the post-tensioned bridge are designed to maintain applied prestressing force over the service life of the bridge. The preservation of this compressive force in the concrete section is the key guaranteeing the safety of the bridge. Because the prestressing force dominates the behavior of external tendon, determining the residual prestressing force is fundamental to assessing the condition of an external tendon.

External tendons typically contain 12 to 19 strands, and corrosion damage is expected to be distributed among tendons, but concentrated in a few strands within each tendon. Low levels of damage, such as few wire breaks, are not expected to influence the capacity of the entire structural system because the residual tension in the external tendons is not reduced. However, as damage in individual strands accumulates, considerable loss of tension may occur – two to three wire breaks in a given strand are likely to cause fracture of all wires in the strand (Table 7.2). In this case, the structural capacity of the system is reduced. If the damage to external tendons progresses such that

a number of tendons are compromised, the capacity of structure system could be severely limited.

Based on these assumptions, the structural capacity of an externally post-tensioned bridge is idealized as a function of the number of wire breaks in Figure 7.17. The level of damage has been separated into three phases: strand damage (individual wire breaks), tendon damage (loss of all seven wires in a strand), and system damage (loss of multiple strands in multiple tendons). The capacity of an individual strand is not assumed to decrease due to the presence of a single wire break, but the capacity of a tendon is assumed to decrease after the loss of a single strand. The capacity of structural system is assumed to decrease with increasing tendon damage.



**Figure 7.17 Idealization of Variation in Structural Capacity with Increasing Damage**

The vibration technique detects the presence of damage in a post-tensioned bridge by identifying shifts in the natural frequencies. Therefore, this technique is best suited for identifying damage in the second phase, as highlighted in Figure 7.17. The loss of three to four strands per tendon should be detectable using this approach. Although it is desirable to detect damage of individual strands, the influence on structural response is trivial, and therefore, can not be detected using measured natural frequencies.

## 7.6 SUMMARY

The objective of this dissertation is to correlate the recorded natural frequencies with levels of damage for external tendons. The vibration technique described in this chapter demonstrates that the two-variable optimization approach can be used to detect significant losses in the level of prestress from shifts in the natural frequencies. However, the optimization procedure should be viewed as a qualitative approach for identifying the most severely damaged tendons, rather than a means of determining losses in prestress quantitatively.

The measured natural frequencies decreased as damage accumulated in the test specimens. However, the changes in the natural frequencies were not proportional to the number of wire breaks. The residual values of tension also decreased with increasing damage, but in most cases the calculated values of tension exceeded expectations for a given level of damage. Using the two-variable optimization procedure, variations in flexural stiffness were also calculated. However, the calculated values were highly variable and often increased as the level of damage increased.

## Chapter 8: Summary and Conclusions

### 8.1 SUMMARY

The objective of the research program reported in this dissertation is to investigate the use of vibration signatures to detect the presence of damage in external, post-tensioned tendons. Although the types of damage induced in the test specimens during this investigation may not be representative of the most likely causes of damage in post-tensioned tendons during the service life of a bridge, the static and dynamic response of the specimens was measured periodically as damage accumulated. Therefore, the recorded data provide a means of evaluating the sensitivity of this nondestructive method of evaluation.

The experimental program may be separated into three phases, and different specimens were tested in each phase.

- A series of uniaxial tests of individual strands were conducted in the first phase. Structural properties, such as the tensile strength and elastic modulus, were determined. The variation of these parameters with increasing levels of damage was investigated. Damage was simulated in three ways: uniform corrosion on the surface of the strand, strands with cut wire(s), and strands with initial defects in one wire. Redistribution of stress and recovery of stress in broken wires were also investigated.
- Three, 49-ft long cable specimens were constructed and subjected to fatigue loading. These specimens comprised two strands stressed to 50% GUTS. As the fatigue tests progressed, damage in the form of wire breaks and cracks in the grout developed. The specimens were continuously monitored using acoustic sensors to detect energy released by wire breaks. Variations in the transverse stiffness and natural frequencies of the specimens were also measured periodically. After completion of the fatigue tests, the specimens were disassembled and the extent of the damage was determined visually.

- Two external tendon specimens were constructed. Damage was induced in Tendon 01 by fatigue loads and the strands in Tendon 02 were exposed to acid to induce corrosion. Tendon 01 comprised 12 strands stressed to 60% GUTS and Tendon 02 comprised 9 strands stressed to 80% GUTS. The specimens were constructed with commercial post-tensioning hardware and concrete anchor blocks were positioned at both ends. The transverse stiffness and natural frequencies were recorded periodically during the fatigue tests for Tendon 01. Natural frequencies were recorded periodically during the exposure test for Tendon 02. After completion of fatigue tests, the specimens were disassembled and the extent of the damage was determined visually.

The frequency response of the test specimens was evaluated to estimate the extent of the induced damage. An optimization scheme was developed to extract the residual tension in the test specimens from the measured natural frequencies.

- A numerical scheme was developed to evaluate the extent of damage in the test specimens. The stiff string model was considered to provide better approximation of the structural response than the taut string model. The feasibility of the numerical scheme was first evaluated using the frequency response of the undamaged specimens. The values of tension, flexural stiffness, mass per unit length, and specimen length corresponding to the minimum total error were calculated. The sensitivity of the total error to each of the four structural parameters was also evaluated.
- Measured natural frequencies for all five specimens recorded throughout the testing period were presented and compared with the induced damage. The numerical scheme was used to determine the values of the structural parameters in the damaged specimens that best matched the measured frequencies. A two-variable optimization procedure was considered to be the most appropriate for calculating the residual tension in the damaged specimens.

## 8.2 CONCLUSIONS

The conclusions from each phase of the investigation are summarized in this section.

### 8.2.1 Individual Strands

During design, prestressing strand is typically assumed to have a circular cross section with the same area as the area of the seven wires. However, the helical geometry has a significant influence on the behavior of strand as damage accumulates.

- The elastic modulus of the strand was determined to be 29,400 ksi and the apparent modulus of elasticity of the individual wires was determined to be 30,800 ksi. This indicates that higher stresses develop in the outer wires of the strand than in the idealized cross section at the same level of longitudinal elongation.
- The residual tensile strength of damaged strands was approximately proportional to the cross-sectional area of the intact wires. After the first wire break, the strand still behaved in an elastic manner.
- Minor uniform corrosion on the surface of the strand did not influence the structural properties appreciably. Changes in strength and stiffness were not significant in spite of the presence of corrosion products.
- When a wire fractures during a tension test, the sudden release of energy is sufficient to unravel the broken wire over a considerable length, if the wires are not restrained. In the larger-scale specimens, the grout restrained the wires. During Phase 3 of the individual strand tests, metal hose clamps were used to prevent unraveling of the wires.
- After fracture of a wire, stress in the strand redistributes to adjacent wires. In addition, if friction is present between the broken wire and the adjacent wires in the strand, the broken wire will be able to recover some of its initial stress a distance from the wire break.

The observations made during the uniaxial tests are sensitive to the length of the test specimens and the friction that develops in a strand within a grouted duct was not evaluated. However, the test results indicate that a strand with a few wire breaks can still resist the initial prestressing.

### **8.2.2 Cable Specimens**

When evaluating external tendons, it is often assumed that a loss of cross-sectional loss would lead to a proportional loss of prestressing. However, the test results from the cable specimens indicated that presence of wire breaks does not necessarily influence the static or dynamic response

- Transverse stiffness and natural frequencies decreased gradually as damage accumulated in the test specimens. However, neither parameter was sensitive to the first few wire breaks.
- The reduction in transverse stiffness and natural frequencies was not linearly related to the number of wire breaks. For example, all the wires fractured in one strand in Cable 02, while the other strand remained intact. Therefore, 50% of the cross-sectional area of the strand was lost during the fatigue tests. However, the transverse stiffness decreased by approximately 20% and the natural frequencies decreased by approximately 10% during the fatigue tests.

These trends suggest that the conventional idealization of damage accumulation is not sufficient to evaluate the response of a damaged external tendon.

### **8.2.3 Tendon Specimens**

The behavior of the tendon specimens was more complicated than the cable specimens due to two factors: restraint at the end of the specimens was distributed along the length of the concrete anchor blocks and the relative positions of the strand varied along the length of the specimens. These conditions are considered to be representative of conditions in external tendons in post-tensioned bridges because the strands are not

parallel along the length of the tendons, but are compressed near the anchor heads and as the tendon passes through deviators.

- The transverse stiffness and natural frequencies decreased gradually in Tendon 01 as the extent of damage increased. Twenty-five wire breaks, which corresponds to nearly 30% of the wires, were observed during the autopsy, but the natural frequencies changed by less than 10% and the transverse stiffness varied by less than 15%.
- The natural frequencies in Tendon 02 decreased in discrete jumps as wire fractures were observed in the different voids. The total decrease was larger than observed in the other test specimens. Thirty wire breaks were observed at the conclusion of the test and the natural frequencies changed by less than 20%. It was likely that wires fractured in the same strand at multiple locations along the length of the specimen. The high prestressing ratio of 80% GUTS also appeared to have influenced the response of this specimen.
- Recorded vibrations from the tendon specimens indicated that the concrete anchor blocks influenced the frequency response of the specimens. Because the strands were restrained along the length of the anchor blocks, rather than fixed at the anchor head, multiple peaks were observed in the frequency response of the specimens.
- Tendon 02 was stored outside during the 5-month exposure test. Temperature variations did cause fluctuations in the recorded natural frequencies; however, these variations were minor and easily distinguished from changes in frequency caused by the wire fractures.

The observed trends for the tendon specimens were similar to the cable specimens, but the frequency response was more complex due to the distributed restraint within the concrete anchor blocks.



#### **8.2.4 Evaluation of Natural Frequency Response**

The natural frequencies were recorded periodically during the fatigue and accelerated corrosion tests for all five test specimens. The residual tension was extracted from these data as damage accumulated. Observations from this phase of the research demonstrate the feasibility of using vibration signatures for nondestructive evaluation of external tendons.

- Two analytical models were proposed to relate the measured frequencies to the structural properties for the test specimens. The stiff string model provided a better match to the measured response than the taut string model, indicating that flexural stiffness influences the frequency response of the test specimens.
- Values of the four structural parameters used in the stiff string model were extracted from the measured frequency response of the undamaged specimens. The cable specimens were most sensitive to the tension and flexural stiffness, while the tendon specimens were most sensitive to the tension and the length of the specimen.
- Dual peaks were observed in the frequency response of the tendon specimens. It is believed that this phenomenon is caused by the non-rigid boundary conditions within the concrete anchor blocks. The frequency response of the tendon specimens was bounded using the clear length and the overall length of the specimens. Similar trends are expected in the post-tensioned bridges; therefore, care must be taken in evaluating the frequency response of external tendons.
- The natural frequencies of the specimens decreased as damage accumulated. However, reductions in frequencies were not proportional to the number of wire breaks. The following trends were similar in all five test specimens: (1) the changes in the frequencies were modest for the first few wire breaks, and (2) lower modes were more sensitive to damage than higher modes.
- Three specimens with well-defined damage at the end of the fatigue tests were used to evaluate the optimization procedure used to extract the structural

parameters from the measured frequency response of the damaged specimens. The results of the analyses indicated that (1) the values of residual tension were higher than expected based on the observed levels of damage, (2) the values of flexural stiffness varied with increasing damage and (3) the values of length of the specimens and mass per unit length were not sensitive to the optimization algorithm.

- The values of residual tension and flexural stiffness were extracted from the entire set of measured natural frequencies using the two-variable optimization procedure. The values of residual tension generally reflected the level of induced damage, but the values of flexural stiffness were variable.
- The vibration signatures technique was success in detecting significant losses in tension in external tendons using the two-variable optimization approach. Limitations of this technique are primarily related to insufficient information about the structural behavior of the external tendons after damage. Therefore, a comprehensive understanding of the behavior of external, post-tensioned bridges must be developed to utilize the full potential of this technique..

### **8.3 RECOMMENDATIONS FOR FUTURE RESEARCH**

The test results and observations made during this research program suggest that the ability to detect damage within an external tendon using the vibration signatures depends on the level of the initial prestress and the number of wires that fracture within individual strands. For example, the damage associated with seven wire breaks at one location in a single strand is much easier to detect than seven wire breaks in seven strands at one location or a total of seven wire breaks in a single strand that are distributed along the length of the tendon. However, within the limitations of this technique, it appears that further research is needed to enhance our understanding of the behavior of the external tendons with damage. This advanced understanding is critical for the applicability of the vibration method for the external tendon. As a result, it is recommended that the future research studies may be performed in four ways:

- Further studies of the behavior of strand after wire fracture(s) are required. The related topics may include the structural effects caused by the stress redistribution and stress recovery in the broken wires, the stress that can be recovered in a grouted tendon, and the energy released when a wire fractures. A better understanding of these phenomena is critical to quantifying the extent of damage in an external tendon.
- The sensitivity of frequencies to the actual boundary conditions should also be studied. All test specimens represented a single, straight section of an external tendon, but the presence of deviators may also influence the dynamic response.
- The analytical models used in this investigation were based on the assumption that the structural properties were uniformly distributed along the length of the tendon. More comprehensive models may be required to determine discrete changes in the structural properties along the length of the tendon.
- The application of the vibration technique to existing post-tensioned bridges is highly recommended. It should be noted that current procedures used to interpret the measured response include a number of uncertainties, and it may be necessary to measure the natural frequencies immediately after the bridge is completed to estimate the initial value of the parameters.

## Appendix A: Assembly of Anchor Barrel Assembly and Steel Plate

The specimen was gripped using an anchor barrel assembly at the top and intermediate cross head. The anchor barrel assembly consisted of a metal cylinder with a tapered hole and two wedges (Figure A.1). The strand specimens were positioned through the hole first and then gripped by two wedges.

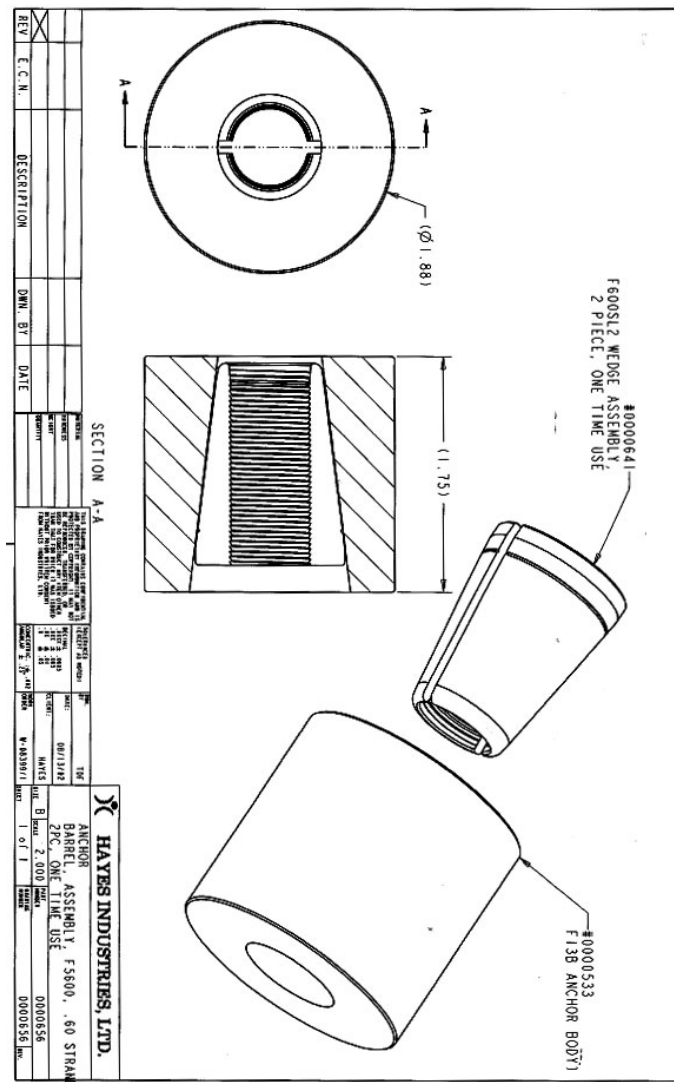
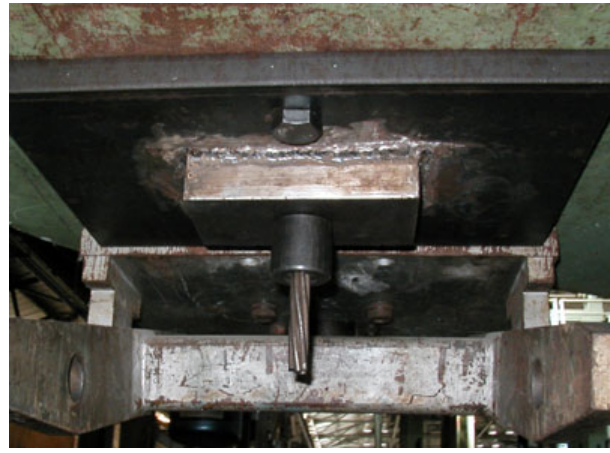


Figure A.1 Drawing of Anchor Barrel

In each cross head, the steel plate was positioned to accommodate the anchor barrel. A shim and jaw of the uniaxial machine was removed and replaced with the steel plate (Figure A.2). The steel plate was fabricated using two plates and attached by welding (Figure A.3). The plate had a 5/8-in diameter hole in center and a total thickness was 2.5 in. This steel plate was fixed to the cross beam by two bolts.

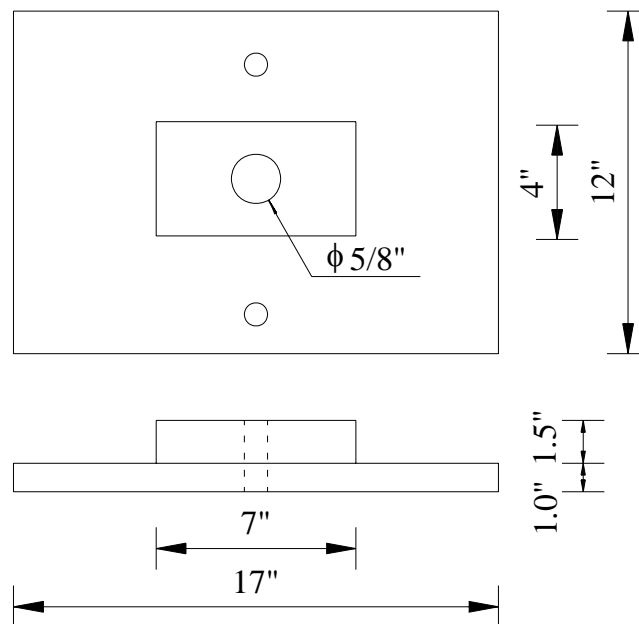


(a) Top cross head



(b) Intermediate cross head

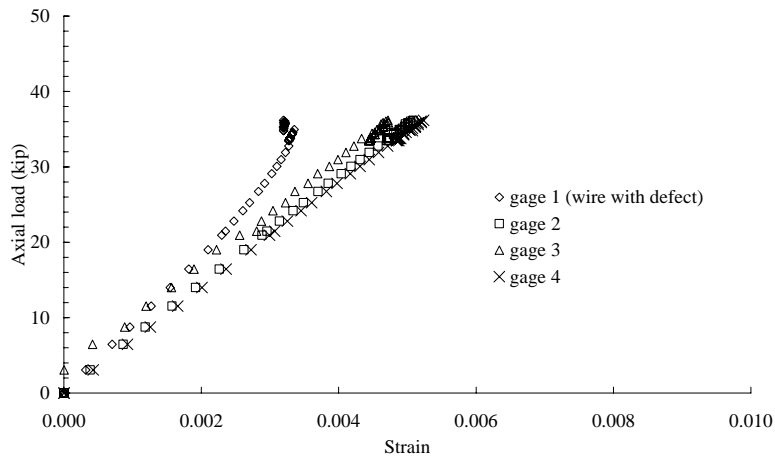
**Figure A.2 Assembly of Anchor Barrel and Steel Plate**



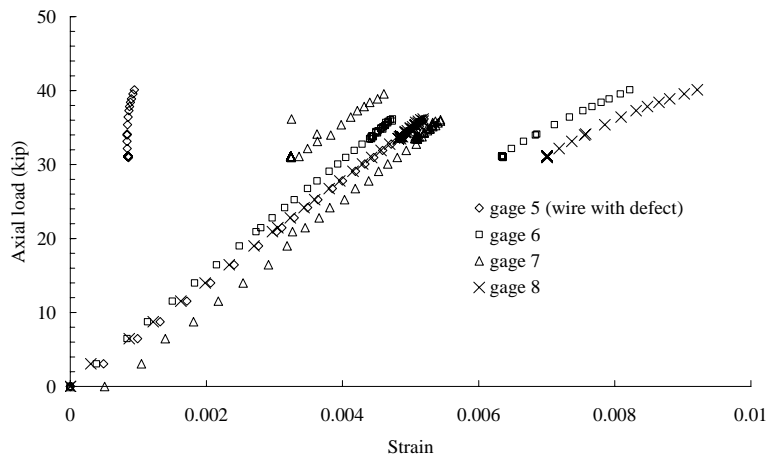
**Figure A.3 Drawing of Steel Plate**

## Appendix B: Strain Measurements from DEF Specimens

Recorded strains from DEF specimens are displayed in Figure B.1 through Figure B.4.

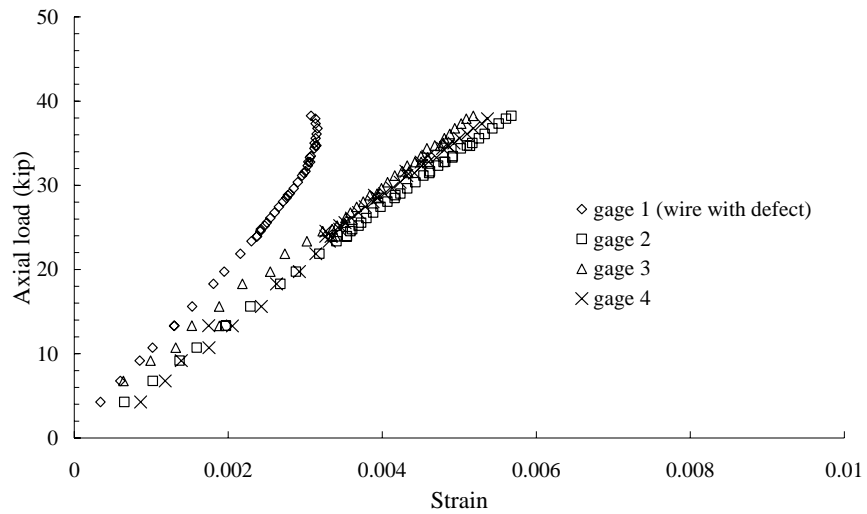


(a) Stress distribution at midspan

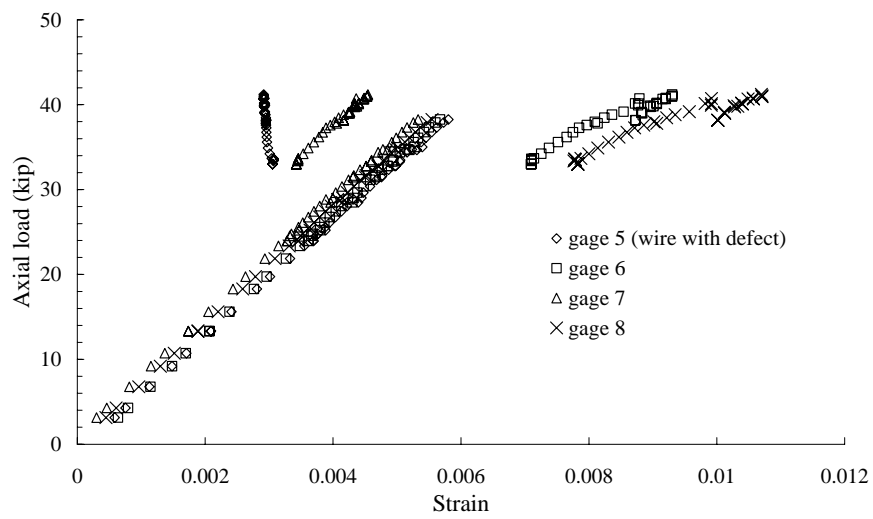


(b) Stress distribution 3 ft from midspan

**Figure B.1 Redistribution of Strain for Specimen DEF 1**

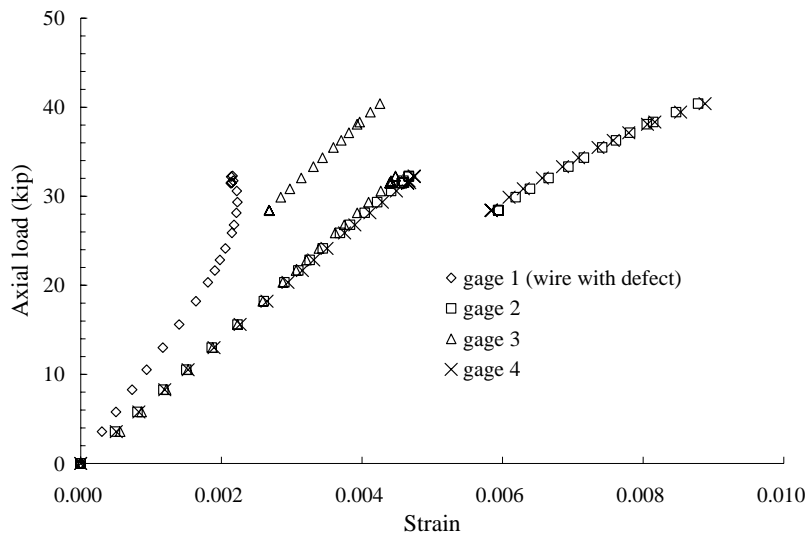


(a) Stress distribution at midspan

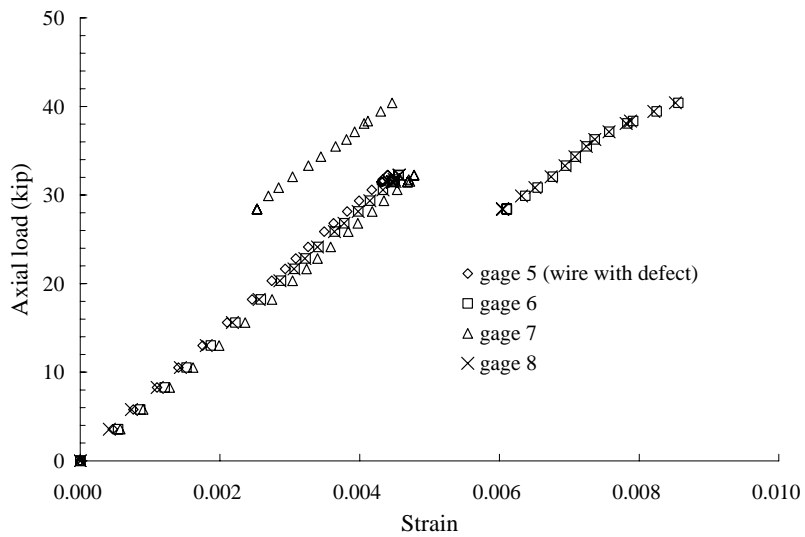


(b) Stress distribution 4 ft from initial defect

**Figure B.2 Redistribution of Strain for Specimen DEF 2**



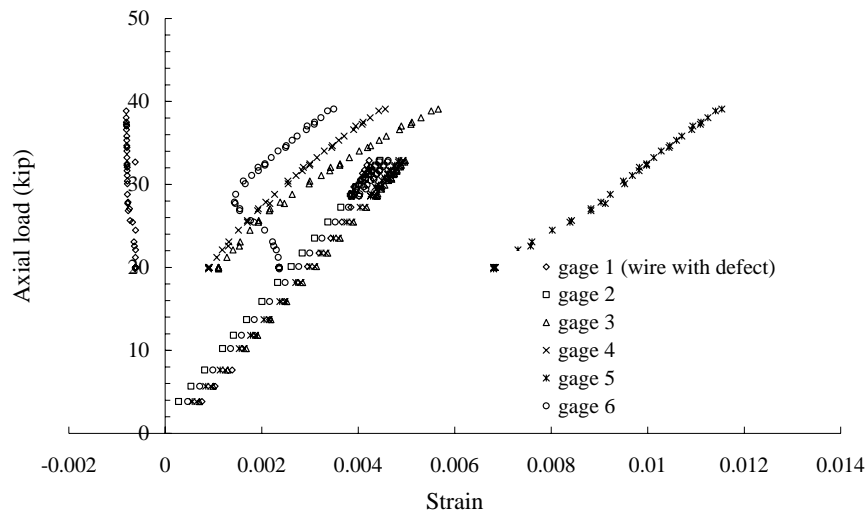
(a) Stress distribution at midspan



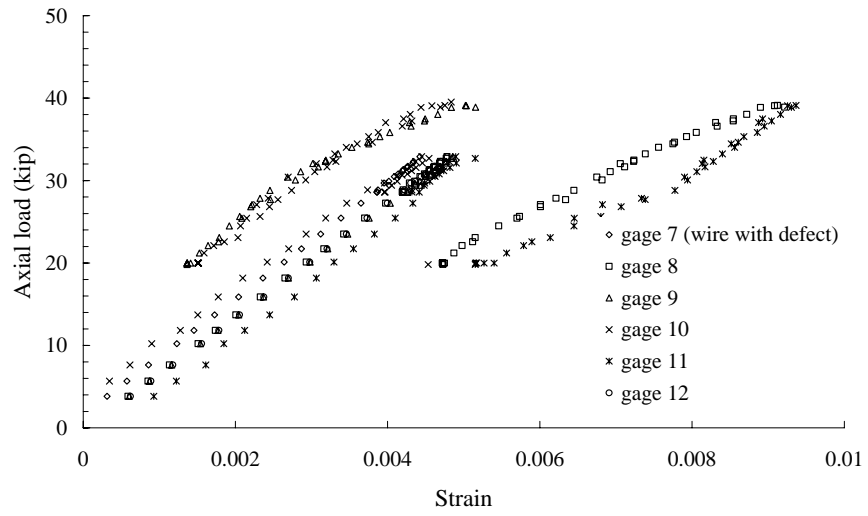
(b) Stress distribution 3 ft from midspan

**Figure B.3 Redistribution of Strain for Specimen DEF 3**





(a) Stress distribution at midspan



(b) Stress distribution 4 ft from initial defect

**Figure B.4 Redistribution of Strain for Specimen DEF 4**

## Appendix C: Construction of Cable Specimen

The process used to construct the cable specimen is summarized in this section. Additional information is presented by Bean (2006)

### C.1 ANCHORAGE SYSTEM

The anchor heads and the grout caps were manufactured to grip two, 0.6-in. strands and contain grout as shown in Figure C.1. The anchor head had 7-in. diameter and 5-in. thickness. The anchor head was originally designed with four holes. Later the two extra holes were sealed with an epoxy or silicone. The grout cap was fabricated from a steel plate and pipe. Grout vents were located near the end of each cap. The grout cap was connected to the anchor head by four bolts on the flange.



*Figure C.1 Anchor Head and Grout Cap*

### C.2 REACTION FRAME

The anchor heads were supported by two buttresses, which were constructed from W 12×40 sections. The buttresses were bolted to the laboratory floor and were positioned about 50 ft apart. Two beams spanned between the buttresses and a 2-in. plate spanned between the beams (Figure C.2).

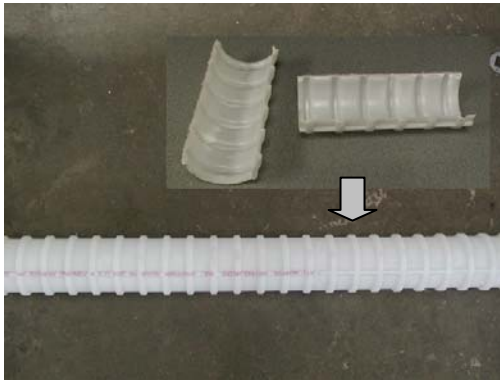


*Figure C.2 Reaction Frame and Anchorage Assembly*

### **C.3 ASSEMBLY OF STAY CABLE SPECIMEN**

Each specimen was constructed from two anchor heads, two 0.6-in. strands, and post-tensioning ducts. After the specimens were assembled and stressed, the duct was filled with grout. The duct had an inside diameter of 3.35 in. and was a blend of polyethylene and polypropylene. Because the semi-transparent duct had ribs and flow channels along the length the flow of grout was visually identified during the grouting procedure (Figure C.3a).

Three 20-ft long section of the post-tensioning ducts were used to construct each specimen. First, the strands were pushed through the sections of ducts. Then the strands were pushed through the holes in the anchor head and pulled taut the strands along the length. The strands were held with wedges. Finally, wood supports were positioned under the specimen to prevent excessive slack as shown in Figure C.3(b). The sections of duct were connected after the strands were stressed and strain gages attached to the strands.



(a) Post-tensioning duct



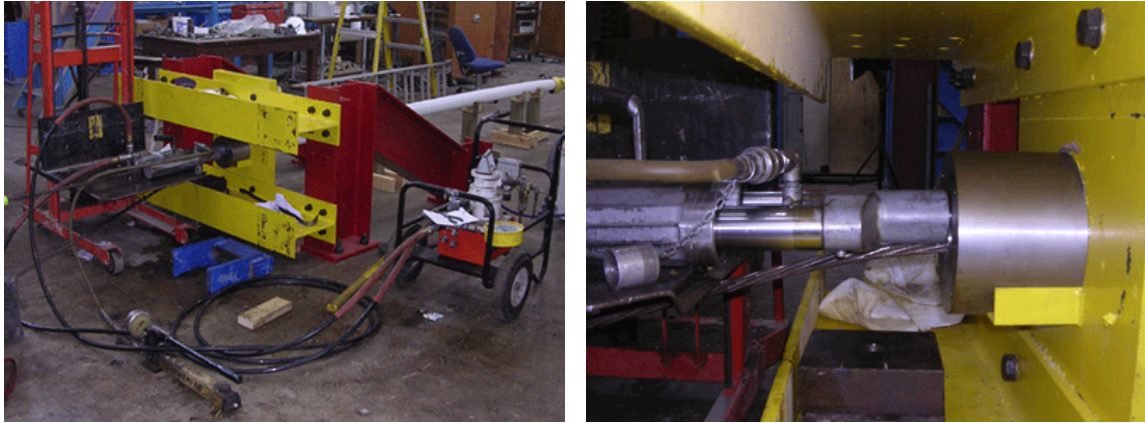
(b) Initial assembly of the specimen

*Figure C.3 Assembly of Cable Specimen*

#### **C.4 STRESSING PROCEDURE**

After the components of the cable specimens were assembled, the prestressing was applied to the strands. The strands were individually pulled using a hydraulic ram to a force of 30 kip, a total of 60 kip for the specimen.

A hydraulic pump was connected to the ram with a hydraulic hose and a pressure gage indicated the pressure level. The stressing was completed by the repeated cycles of pulling and releasing the strand for three times to minimize seating losses (Figure C.4). During each cycle, the maximum applied force was increased about 10, 20, and 30 kip. Two springs were positioned between the anchor head and the nose of hydraulic cylinder to minimize the movement of the wedges when the applied force was released. The strand was overstressed about 5% to compensate for expected losses.



*Figure C.4 Stressing Strand with Hydraulic Ram*

### **C.5 STRAIN GAGE INSTRUMENTATION AND PIPE CONNECTION**

After the stressing procedure was completed, strain gages were attached to the strand (Figure C.5). The strain gages were manufactured by the Tokyo Sokki Kenkyujo Company (model FLA-3-11-5LT). The gages were attached at desired locations using a cyanoacrylate adhesive and wrapped by an insulated tape. The strain gages were positioned along the longitudinal axes of outer wires. The number and location of gages varied for each specimen.

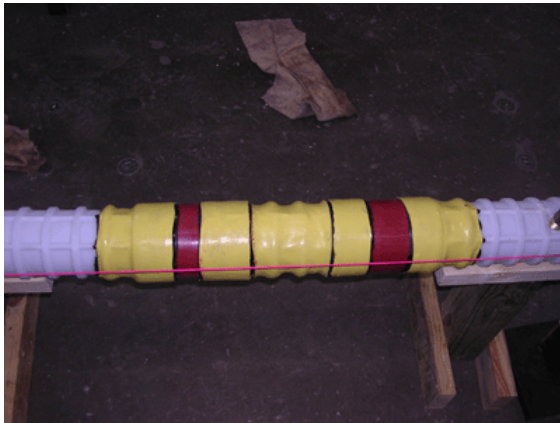


*Figure C.5 Strain Gage Installation*

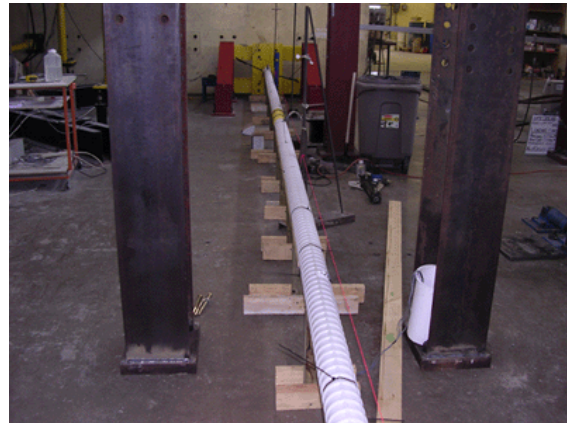


After all internal instrumentation were installed, adjacent sections of plastic ducts were connected using plastic couplers and then covered with the plastic heat shrink (Figure C.6a). Voided space between the plastic pipe and the steel plate in the buttress was sealed with an expanding foam.

After the sections of duct were connected, numerous wooden supports were placed under the specimen to set the elevation of the duct (Figure C.6b).



(a) Coupler and plastic heat shrink

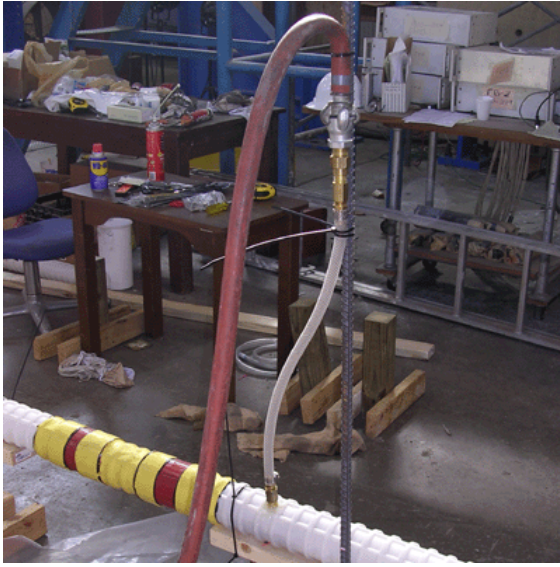


(b) Alignment and wooded supports

***Figure C.6 Completion of Pipe Connection***

## **C.6 GROUTING PROCEDURE**

The cable specimens were grouted with a prepackaged grout, SikaGrout 300PT. Four grout vents were placed along the length of specimen. Two vents were located at the grout caps. Other two vents were located 5 to 8 ft from the end. The grout inlet was positioned at midspan (Figure C.7a).



(a) Grout inlet



(b) Grout mixing and pumping

***Figure C.7 Grouting Procedure***

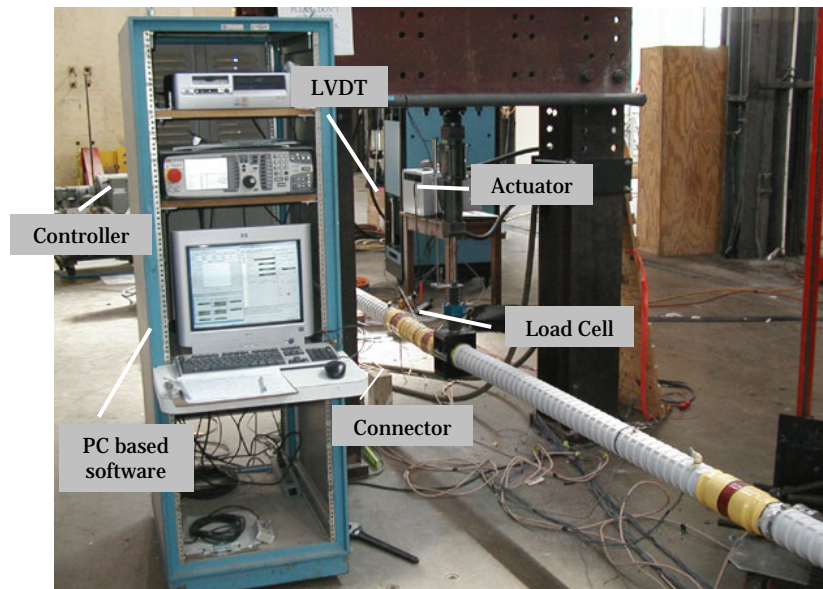
Grout was mixed 3 to 5 min with prescribed amount of water in a shear type mixer (Figure C.7b). The grout was then pumped into the specimen. After grout flowed through each of the vents, the vents were closed.

## Appendix D: Hydraulic Actuator System and Controller

The transverse loading of cable and tendon specimens were operated using the MTS controlling unit with a different configuration of the hydraulic actuator system.

### D.1 HYDRAULIC ACTUATOR CONFIGURATION FOR CABLE SPECIMEN

A 5-kip hydraulic actuator with an external LVDT was used to apply transverse loads to the cable specimen as shown in Figure D.1. Hydraulic pressure was supplied by an MTS hydraulic supply (model 506.02) and regulated by an MTS 293 hydraulic manifold. An external load cell manufactured by Interface (model 1010AF-5K-B) was installed at the end of the actuator to measure the applied force. The displacement transducer to monitor the hydraulic actuator was manufactured by G.L. Collins Corporation (model A5453).

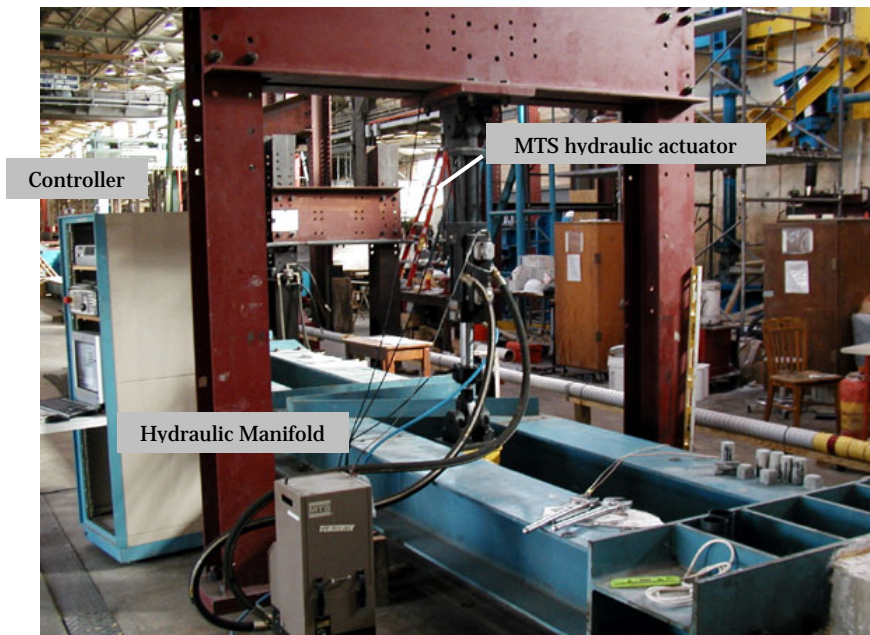


*Figure D.1 Hydraulic Actuator and Control Unit for Cable Specimen*



## D.2 HYDRAULIC SYSTEM FOR TENDON SPECIMEN

An MTS hydraulic actuator (Model 244.22-07) with the capacity of 22 kip was used to apply transverse loads to tendon specimen as shown in Figure D.2. The pressure was supplied by an MTS hydraulic power unit (Model 505.30) and regulated by an MTS 293 hydraulic manifold. The displacement and loading information were monitored by internal sensors of the actuator and transmitted to the control unit.

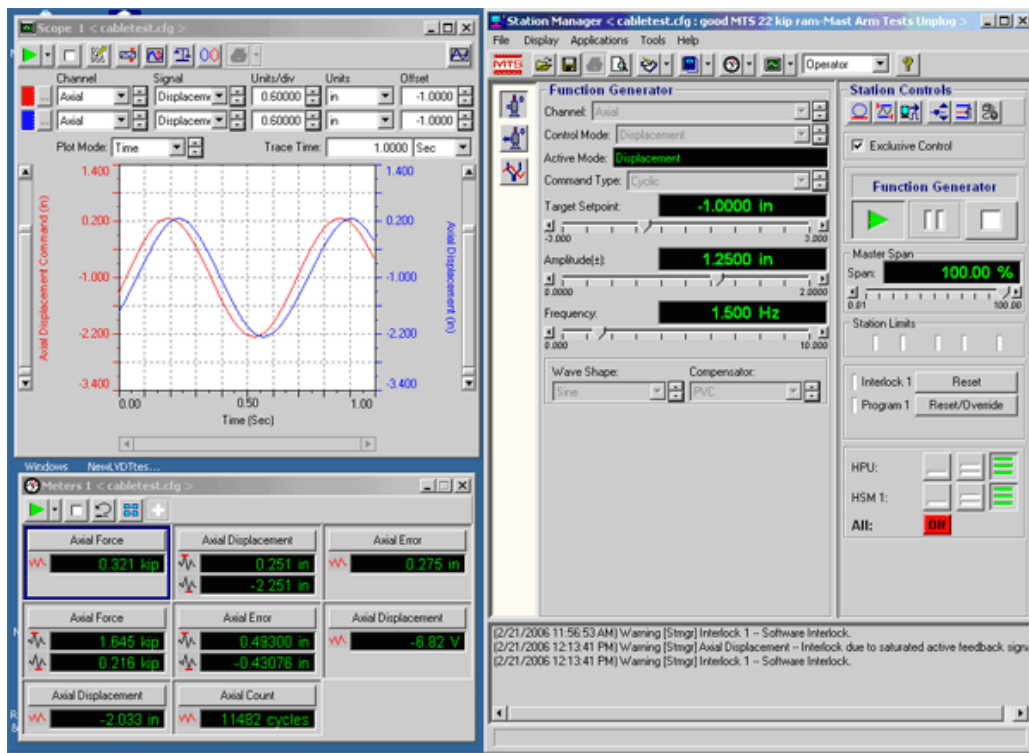


*Figure D.2 Hydraulic Actuator and Control Unit for Tendon 01*

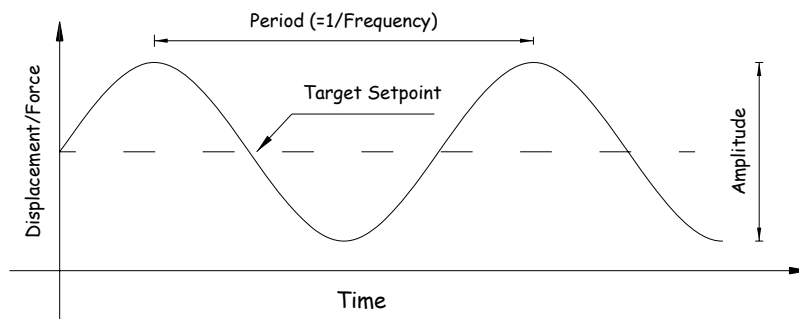
## D.3 OPERATION OF HYDRAULIC LOADING SYSTEM

The fatigue and static test were controlled by the MTS Flex Test<sup>TM</sup> SE system and operated by a PC based software (MTS Flex Test<sup>TM</sup> manager v 3.50). The interface of this software is displayed in Figure D.3(a). The input loading was assigned at the “Station Manager” window and the feedback was given in the “Meters” window located left bottom. The fatigue tests were run under displacement control and the input loading was operated by three parameters: target setpoint, amplitude, and frequency (Figure D.3b).

The target setpoint corresponds to the initial position for the cyclic loading. The cyclic movement of the actuator was initiated by defining the amplitude and frequency.



(a) Interface of software



(b) Cyclic loading parameters

**Figure D.3 Load Input Operation**

## Appendix E: Portable Data Acquisition System Development

A data acquisition (DAQ) system was composed for the vibration method in the Ferguson Structural Engineering Laboratory. The vibration test aims to assess the integrity of target structures in field; thus, the DAQ system needs to be portable. The DAQ system is also desired to be durable and low-cost.

### E.1 DATA ACQUISITION SYSTEM

The portable DAQ system consisted of a signal conditioning box manufactured by National Instruments<sup>TM</sup> and a laptop computer with a LabView 7.1 software. The signal conditioning box was composed of a chassis, an input module, and a terminal block (Figure E.1). The chassis (NI SCXI-1000) offered the sampling rate of 333 kS/sec. Inside of this box, the input module (NI SCXI-1520) was plugged to conduct signal conditionings such as filtering and signal amplification. At the end of this module, the terminal block (NI SCXI-1314) was connected to link an accelerometer to the signal conditioning box. The signal conditioning box was enclosed by a 2×2×1 ft metal box for protection against external impact. This system was connected a laptop using a USB cord and operated by a PC based software.



*Figure E.1 DAQ System*

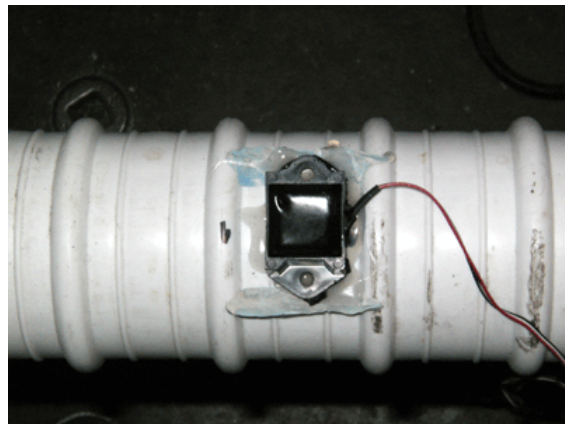
## E.2 ACCELEROMETER

The low G micro machined accelerometer (model MMA 1220D) from the Freescale Semiconductor<sup>TM</sup> was used for dynamic measurements. This sensor had various advantageous features for the vibration test. This sensor could measure a amplitude of acceleration to  $\pm 8g$  and hold without permanent damage against 1.2-m drop. This sensor offered the typical bandwidth of 250 Hz and valued about \$ 30.

The product was purchased in parts and assembled in the laboratory. After assembly and the sensor was covered with a transparent epoxy. This type of accelerometers was attached to all cable specimens and Tendon 01 using a hot-melting glue (Figure E.2a). Later, the dimension of the accelerometers was minimized by removing unused circuit plate. The sensors were also enclosed in a plastic cubic box and covered with a chemical compound (Figure E.2b). This type of sensors was applied for the outdoor test; Tendon 02.



(a) Original accelerometer (Tendon 01)

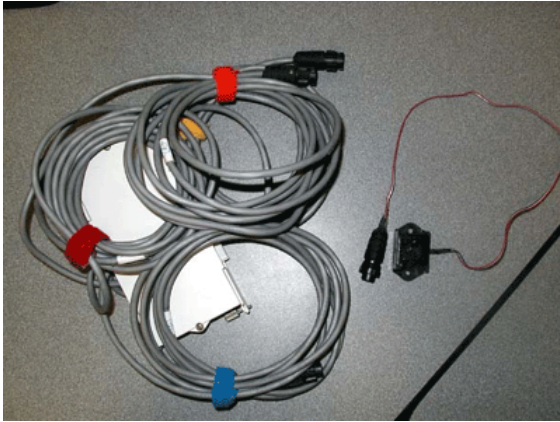


(b) Modified accelerometer (Tendon 02)

*Figure E.2 Modification of Accelerometer*

The modified accelerometers were connected to the terminal block via a plastic connector (Figure E.3a). Therefore, the sensors were attached to the plastic duct during the test period but connected to the DAQ system only when the test was conducted.

The portable frame with the accelerometer was fabricated using a light aluminum metal tubes and rods to offer a quick installation method in field. The vibration signal recorded by the sensor on the frame indicated the identical results with adjacent sensors.



(a) Terminal block and wire connector



(b) Portable frame

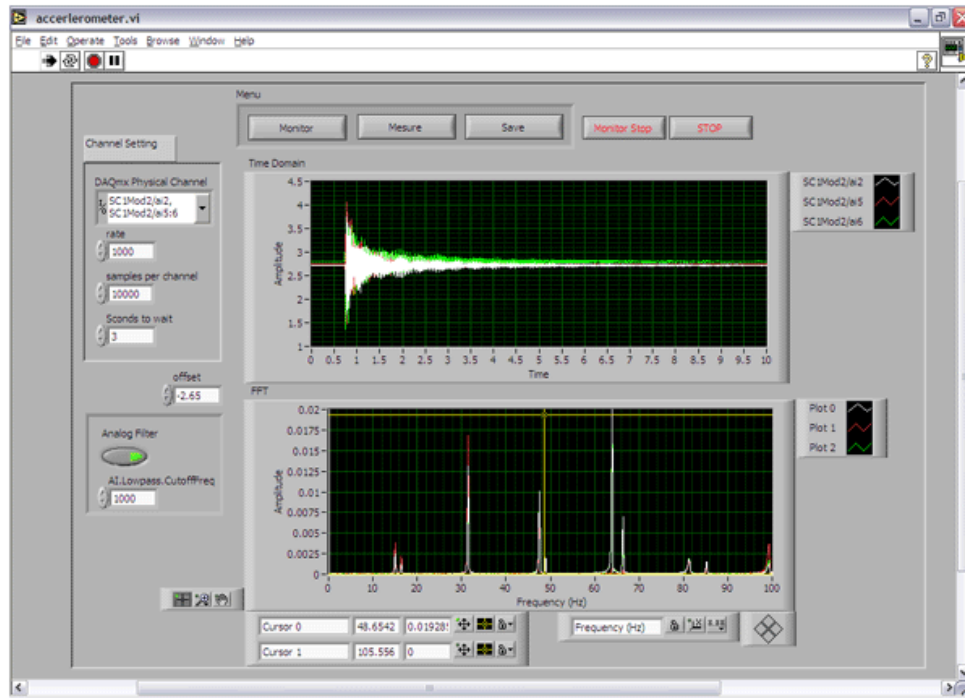
***Figure E.3 Portable Sensor and Connector***



### E.3 PC BASED SOFTWARE

The vibration signals were recorded by the program based on Lab-View 7.1. This program was designed to provide a user-friendly operational tool.

The interface of the software embedded required input parameters, operational menus, and test results in one front window. Upper graph displayed recorded signals in time domain and lower graph displayed converted signals into frequency domain (Figure E.4). Comments and required parameters are briefly described in Table E.1.



*Figure E.4 Interface of PC based Software*

*Table E.1 Description of Menu and Parameters*

	<b>Item</b>	<b>Description</b>
Menu	Monitor	Automatically update of acquired signal
	Measure	Initiate measurement
	Save	Save acquired signal
Setting	DAQ physical channel	Define channel of DAQ system
	Rate	Define sampling rate (sample/sec)
	Sampling per channel	Define sampling number
	Second to wait	Delay initiation of measurement (second)
Etc	Offset	Offset acquired signal
	Analog filter	Operate built-in analog filter in DAQ system

# Appendix F: Distribution of Strains for Cable Specimen

## F.1 CABLE 01

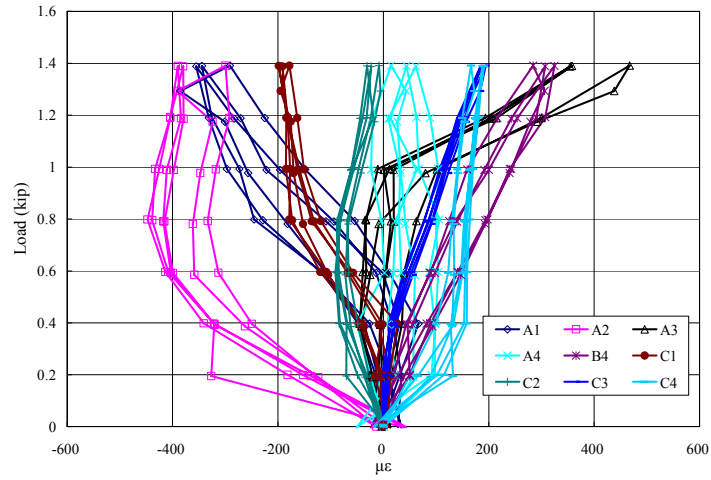


Figure F.1 Strain Distribution of SM 0

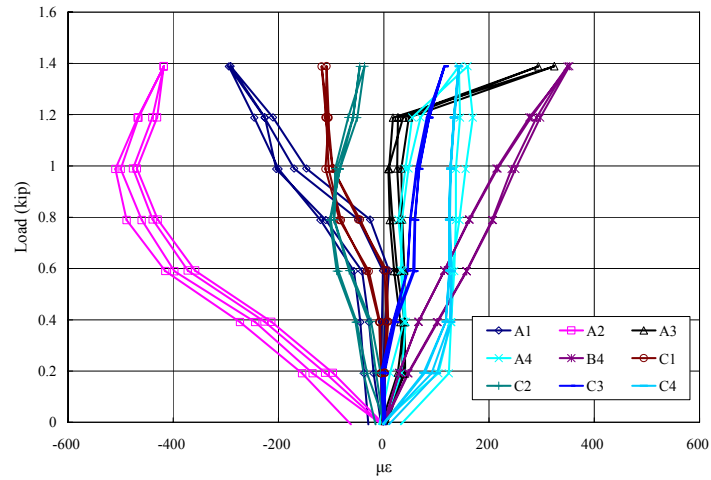
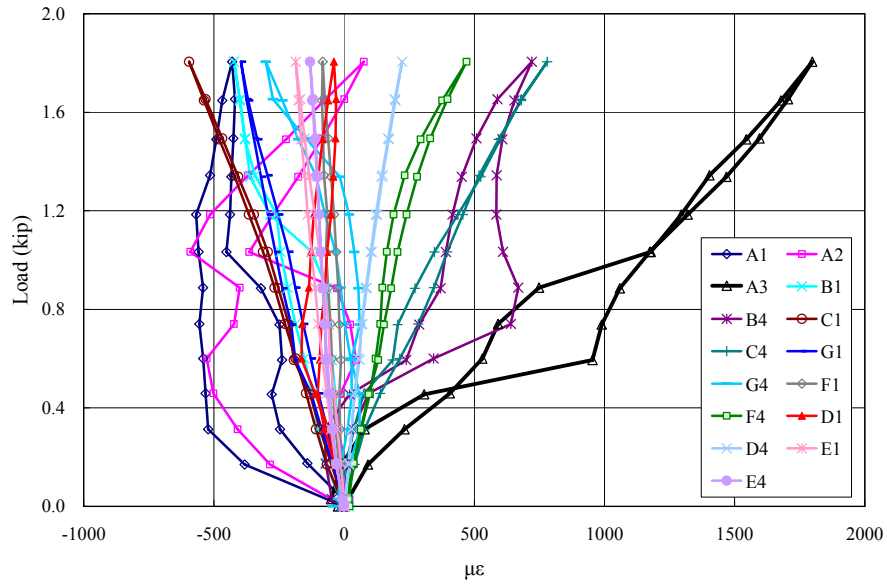


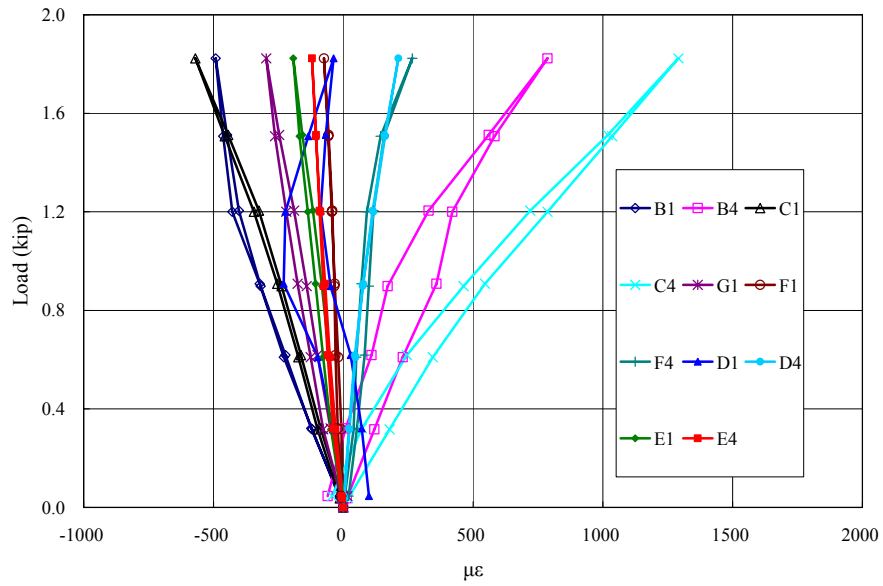
Figure F.2 Strain Distribution of SM 1



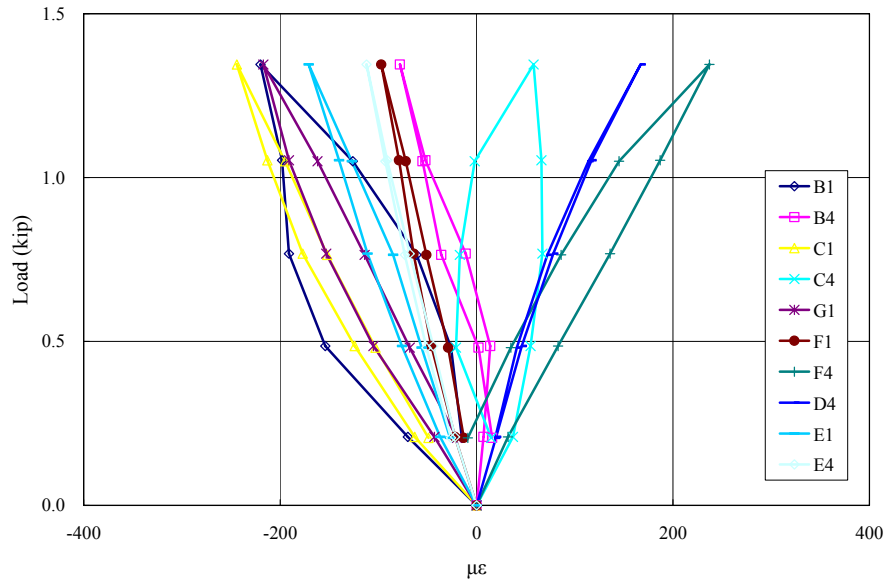
## F.2 CABLE 02



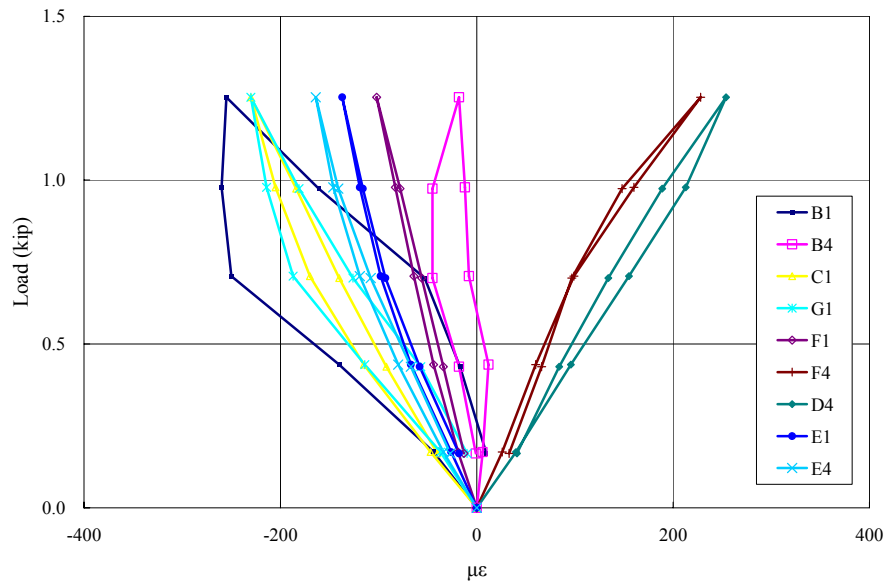
*Figure F.3 Strain Distribution of SM 0*



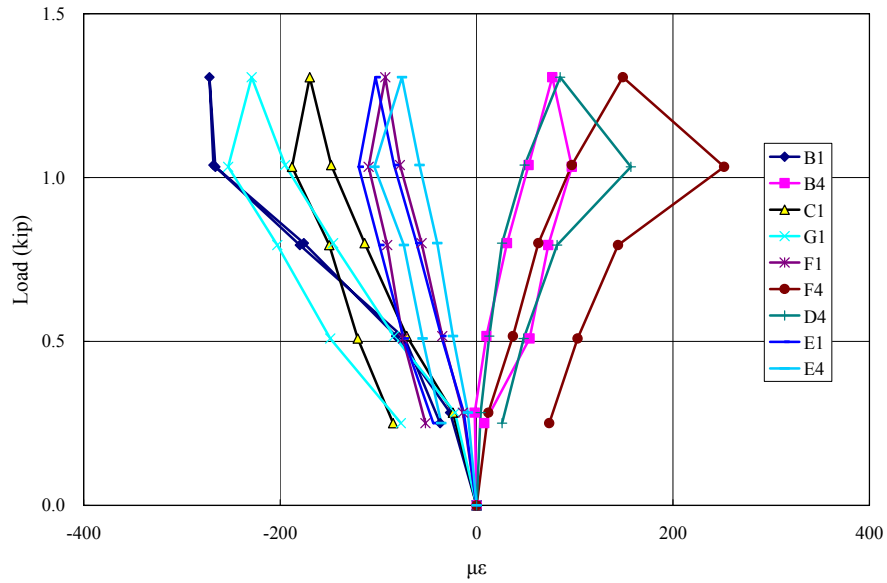
*Figure F.4 Strain Distribution of SM 1*



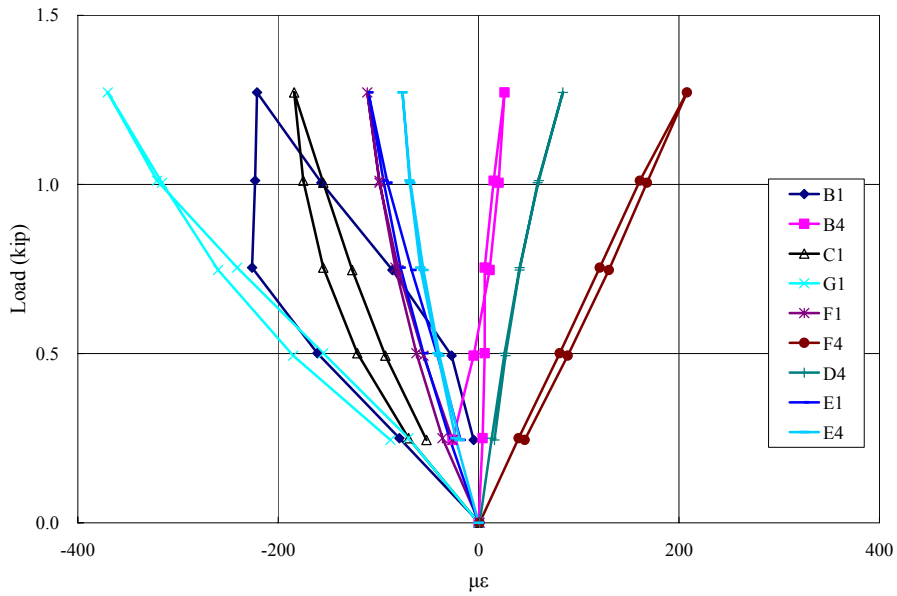
**Figure F.5 Strain Distribution of SM 2**



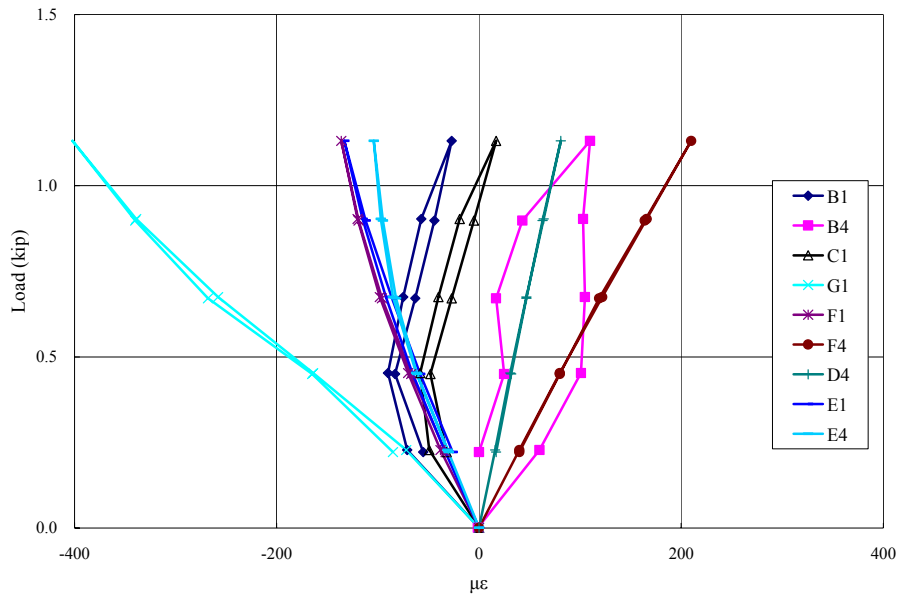
**Figure F.6 Strain Distribution of SM 3**



**Figure F.7 Strain Distribution of SM 4**

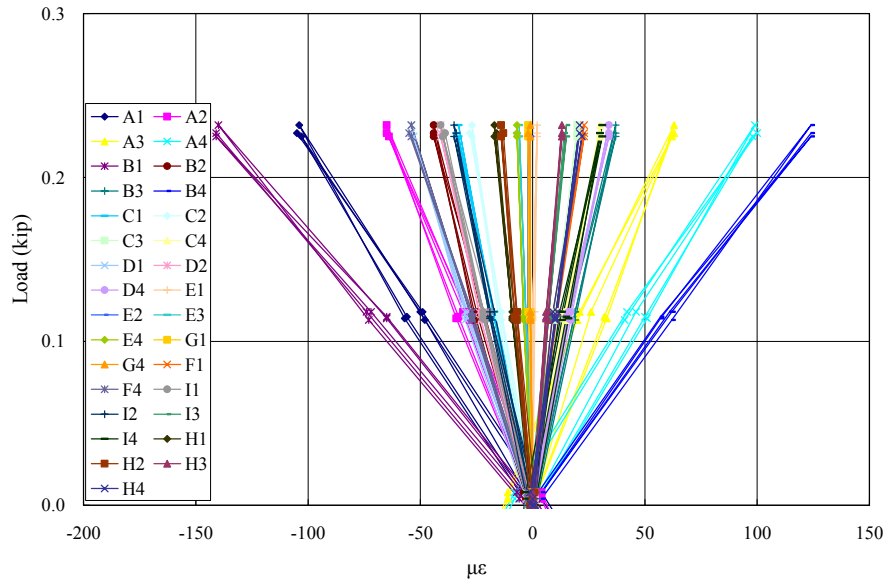


**Figure F.8 Strain Distribution of SM 5**

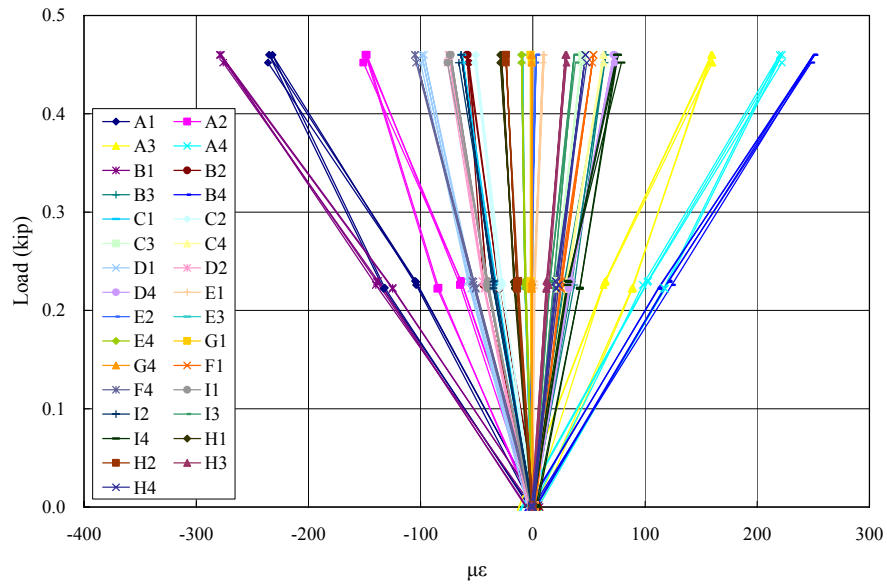


**Figure F.9 Strain Distribution of SM 6**

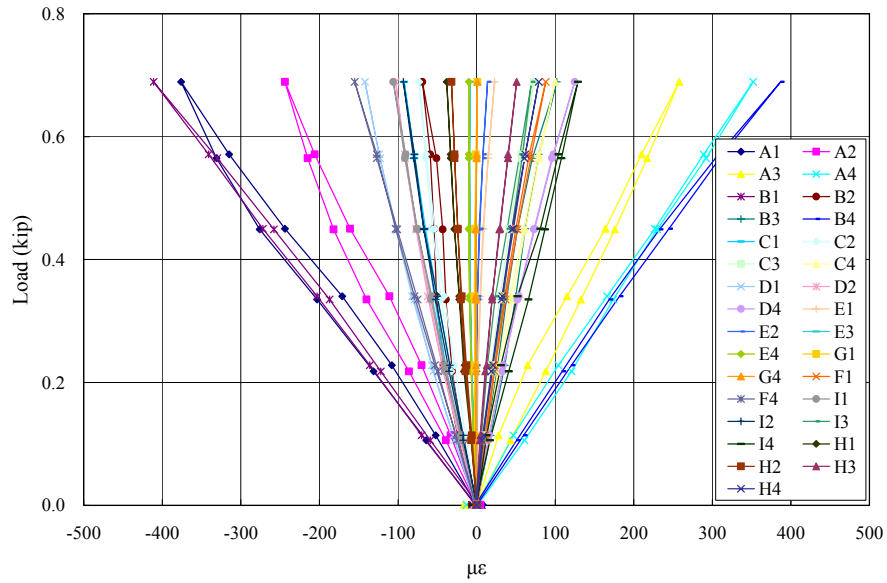
### F.3 CABLE 03



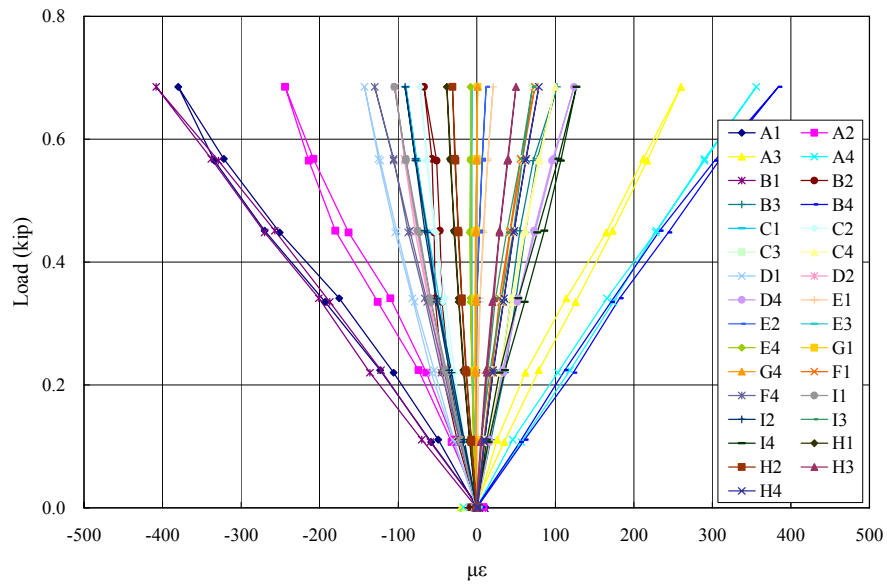
*Figure F.10 Strain Distribution of SM 0-0*



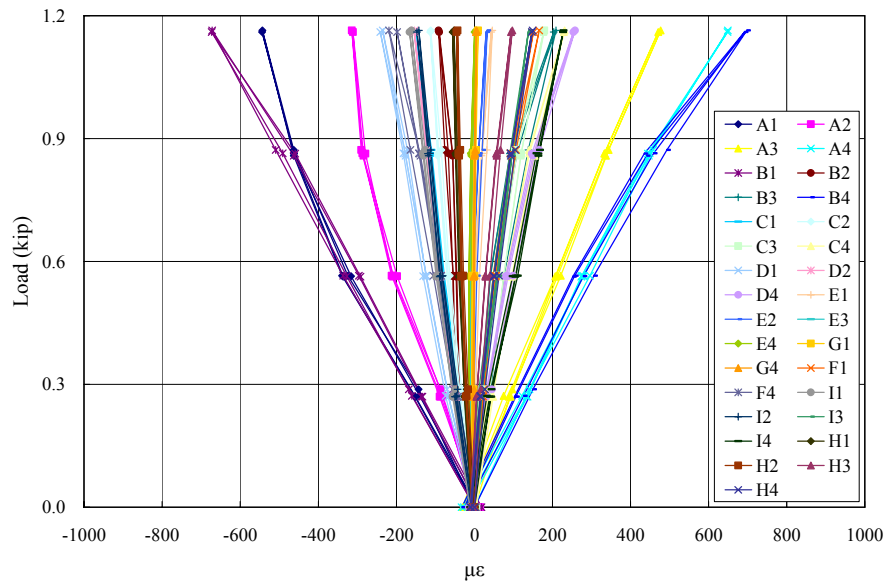
*Figure F.11 Strain Distribution of SM 0-1*



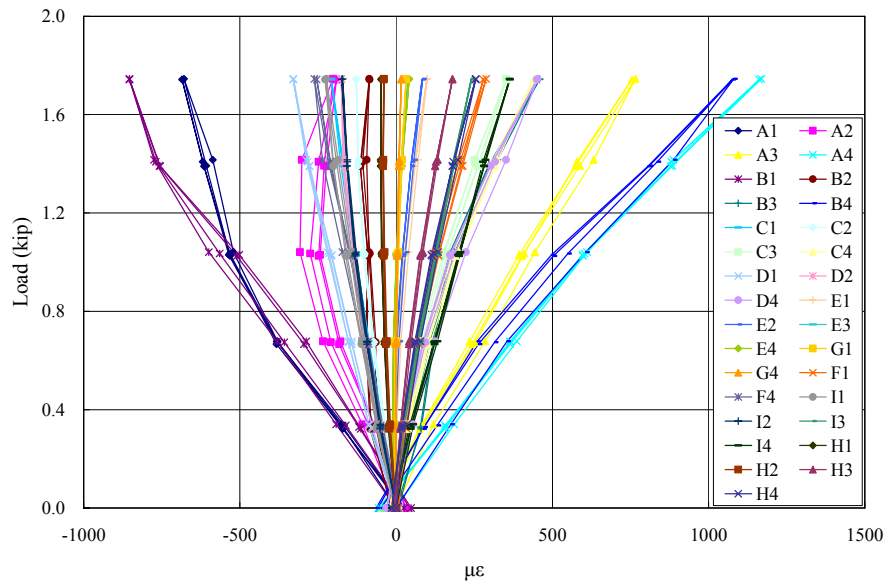
**Figure F.12 Strain Distribution of SM 0-2**



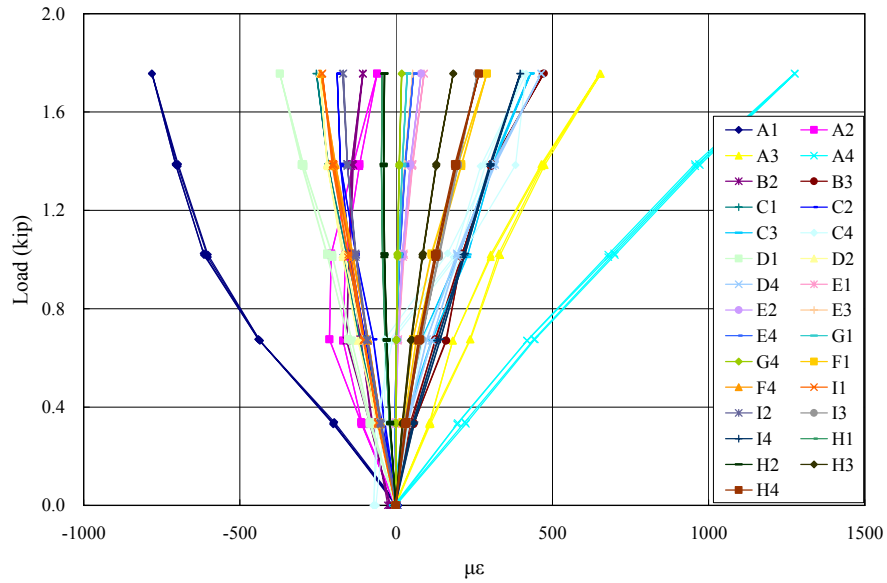
**Figure F.13 Strain Distribution of SM 0-3**



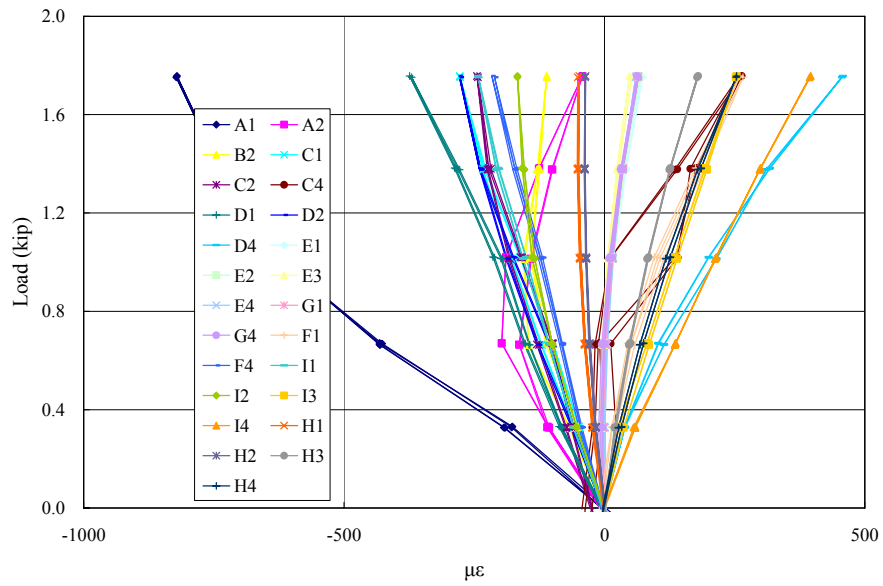
**Figure F.14 Strain Distribution of SM 0-4**



**Figure F.15 Strain Distribution of SM 0-5**

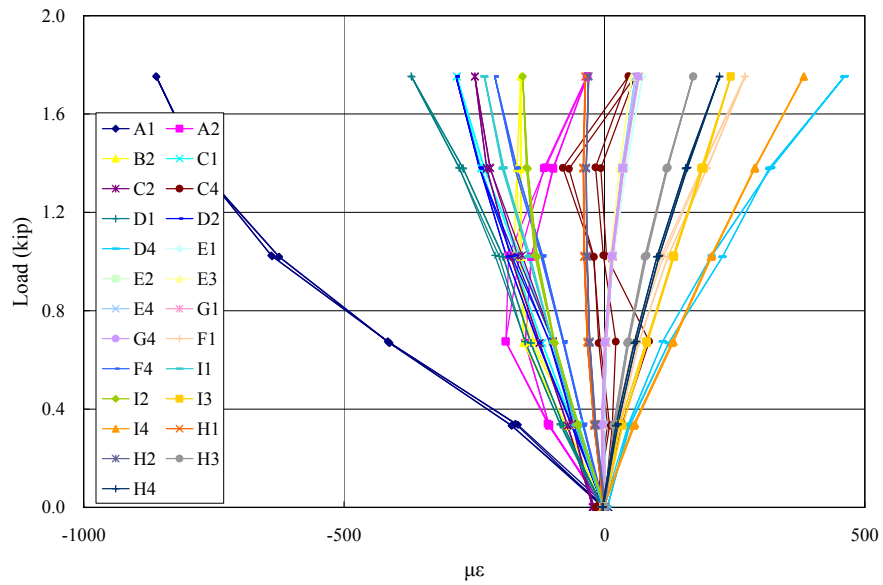


**Figure F.16 Strain Distribution of SM 0-6**

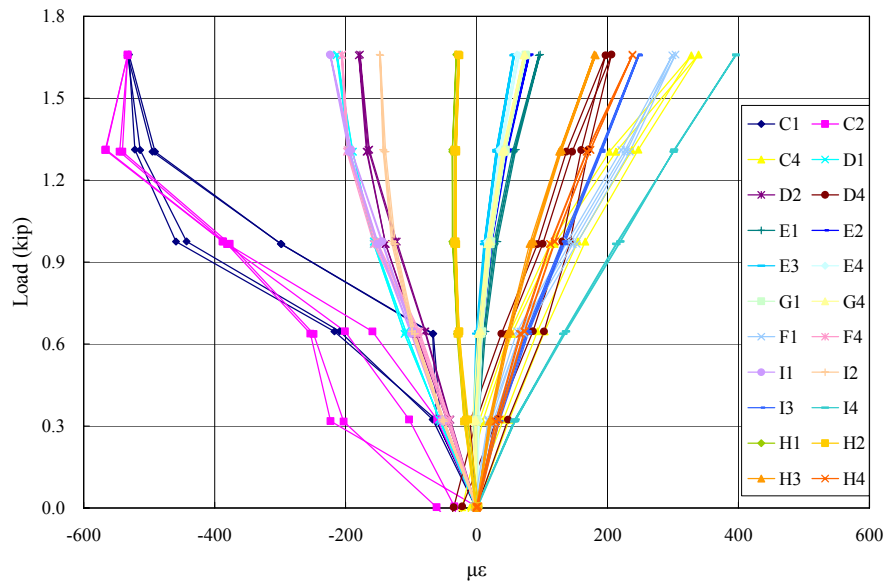


**Figure F.17 Strain Distribution of SM 1**





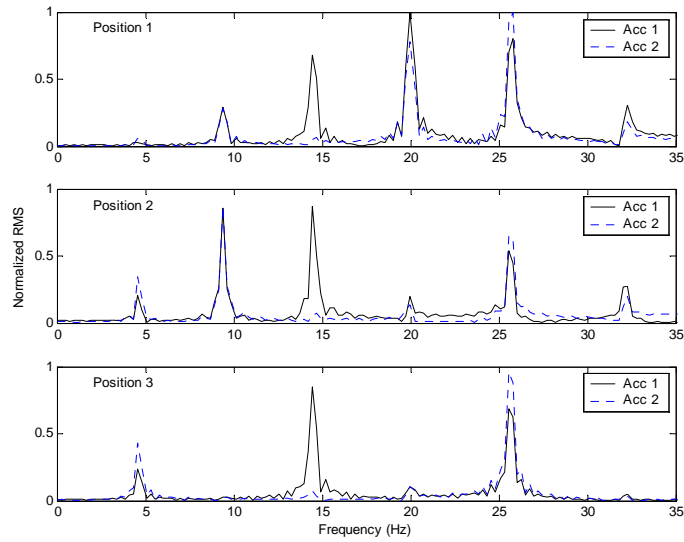
**Figure F.18 Strain Distribution of SM 2**



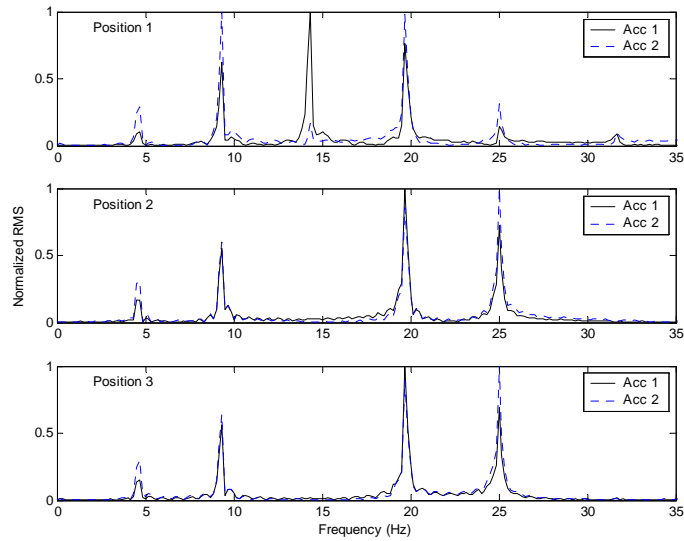
**Figure F.19 Strain Distribution of SM 3**

# Appendix G: Natural Frequencies of Cable Specimens

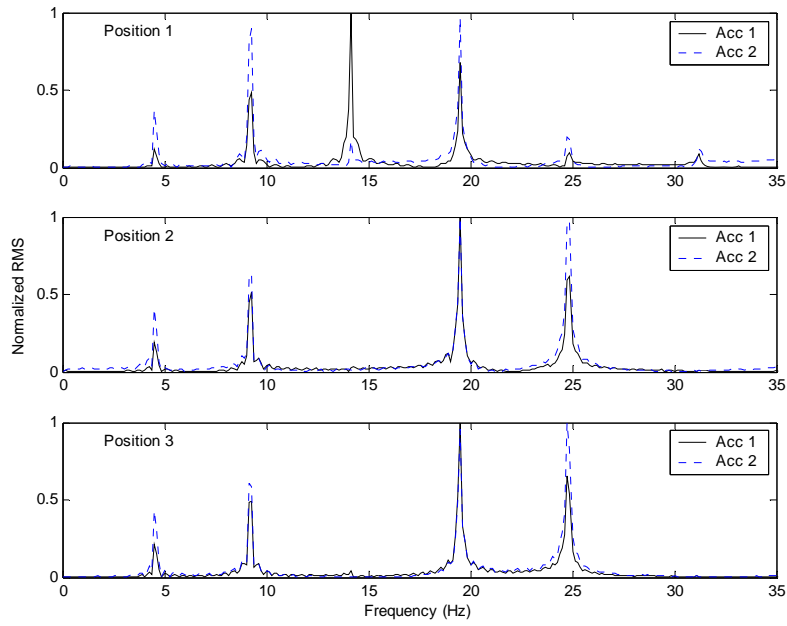
## G.1 CABLE 01



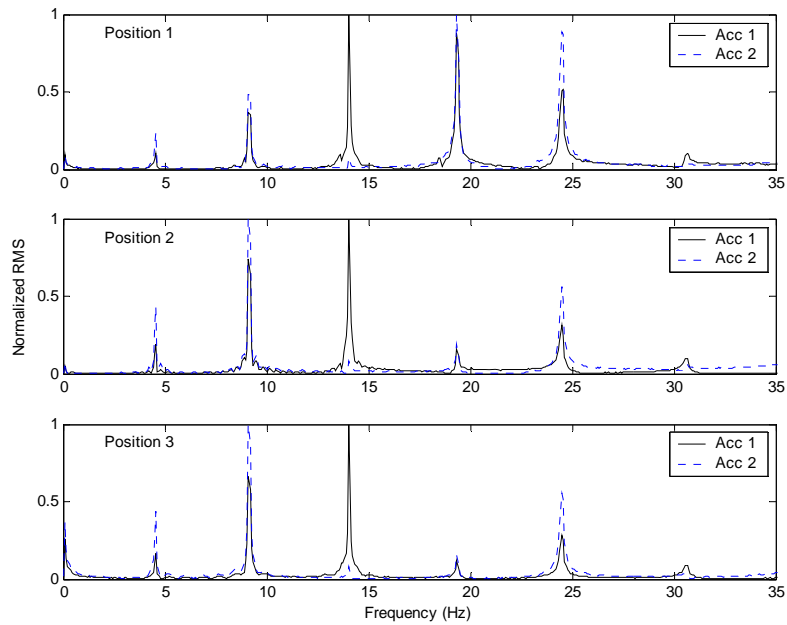
**Figure G.1 Normalized Root Mean Square (RMS) of NF 0**



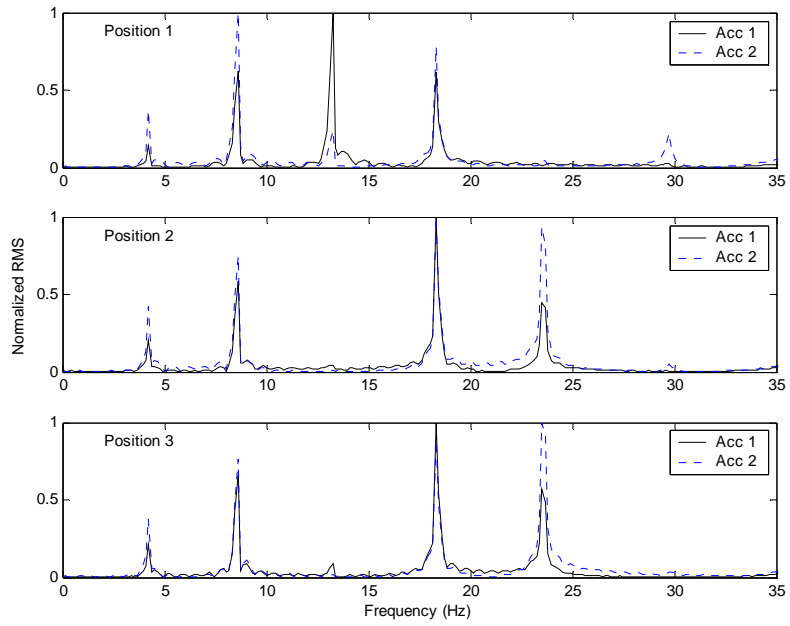
**Figure G.2 Normalized Root Mean Square (RMS) of NF 1**



**Figure G.3 Normalized Root Mean Square (RMS) of NF 2**

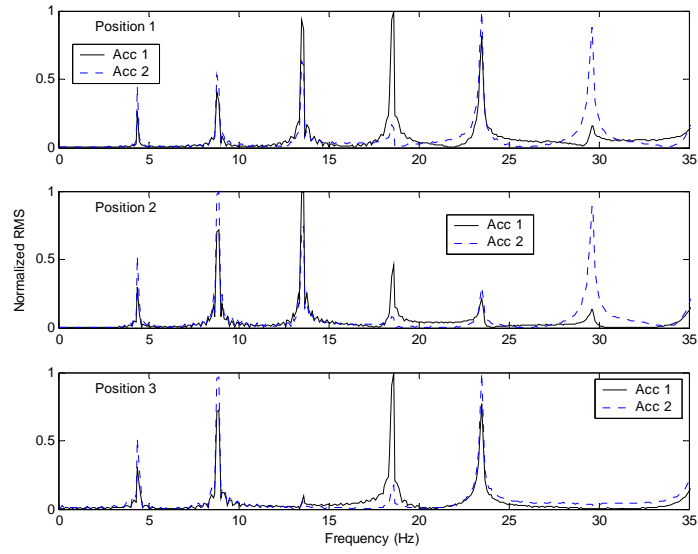


**Figure G.4 Normalized Root Mean Square (RMS) of NF 3**

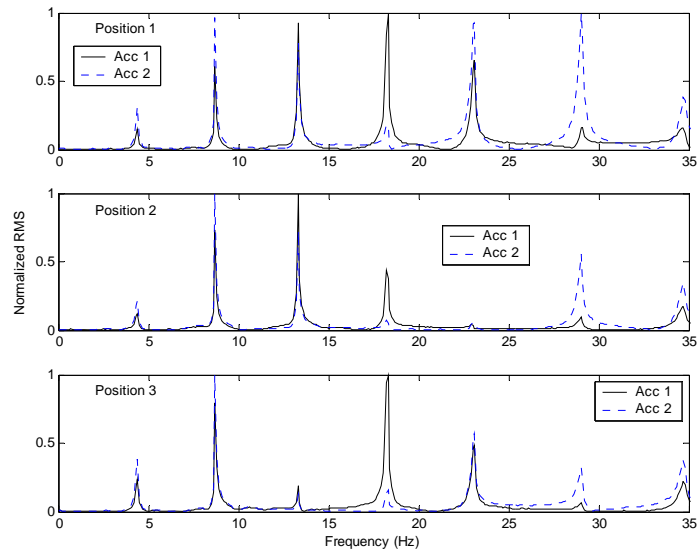


**Figure G.5 Normalized Root Mean Square (RMS) of NF 4**

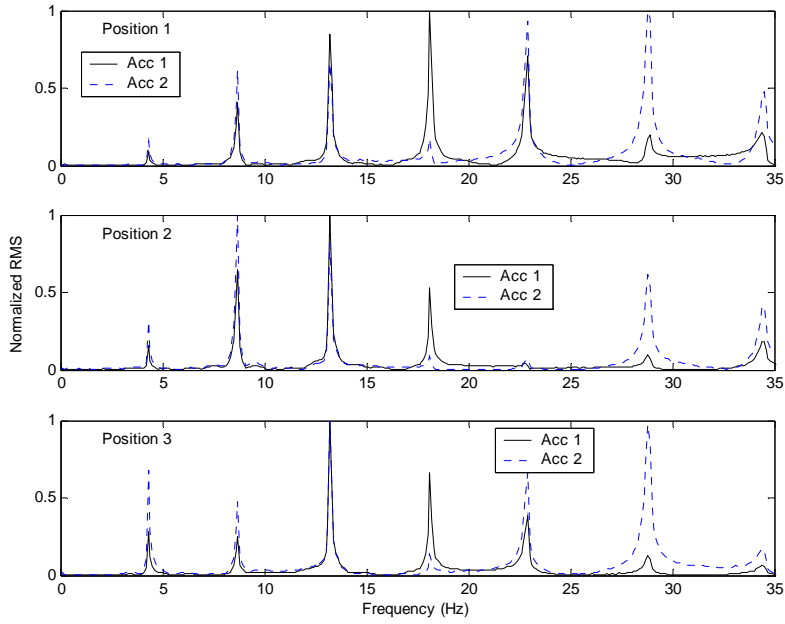
## G.2 CABLE 02



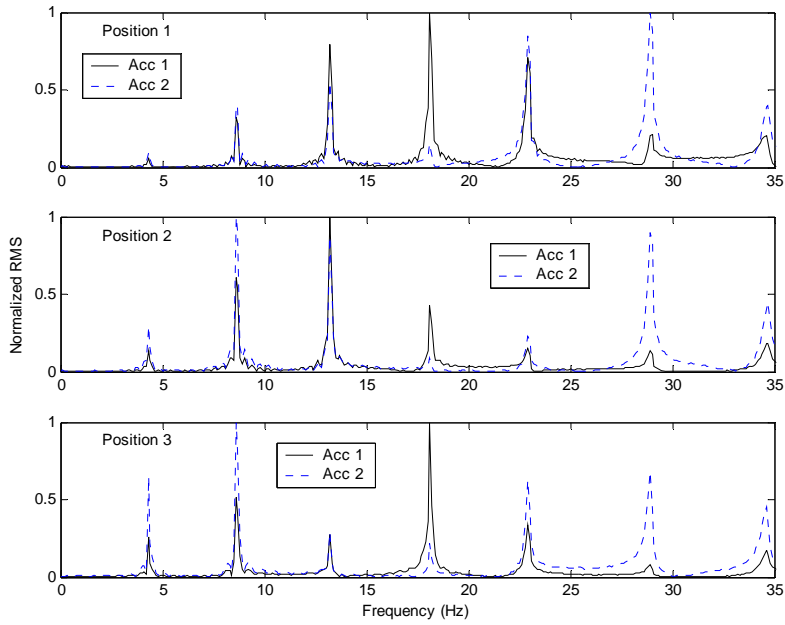
*Figure G.6 Normalized Root Mean Square (RMS) of NF 0*



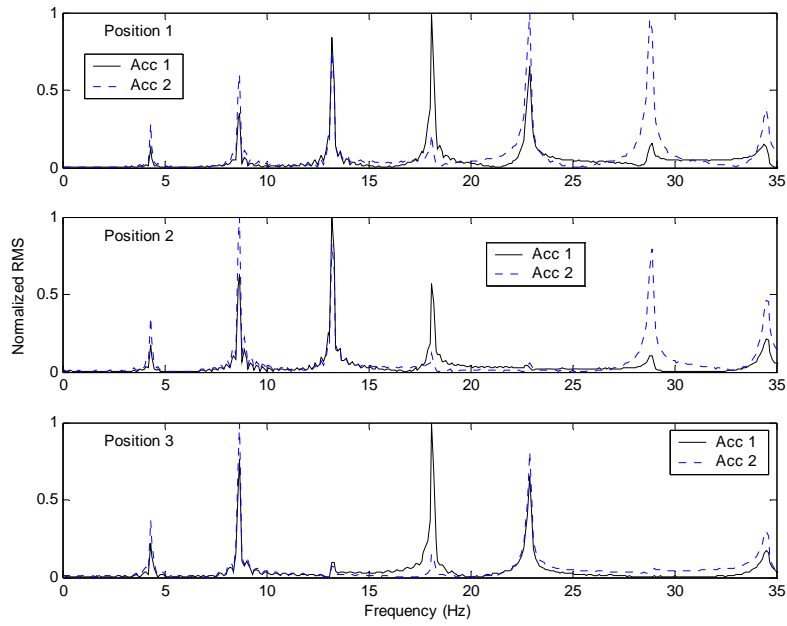
*Figure G.7 Normalized Root Mean Square (RMS) of NF 1*



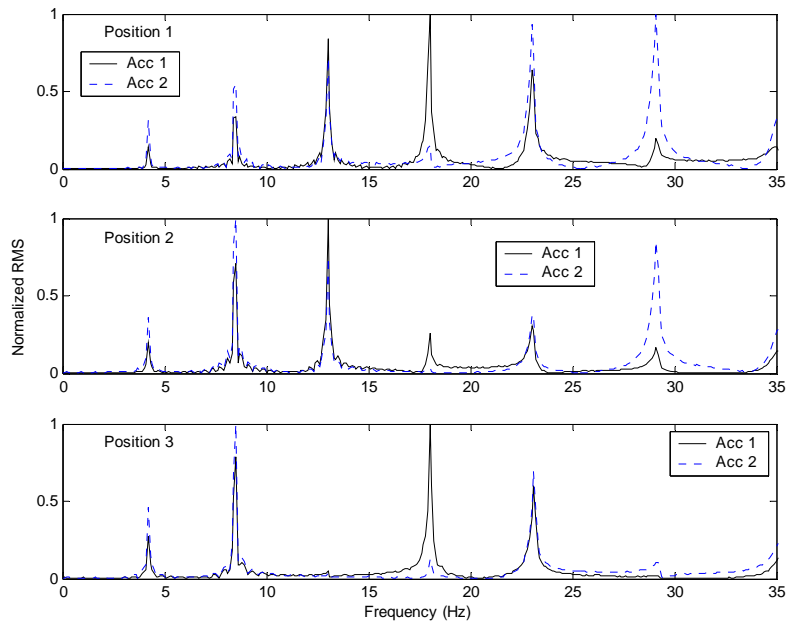
**Figure G.8 Normalized Root Mean Square (RMS) of NF 2**



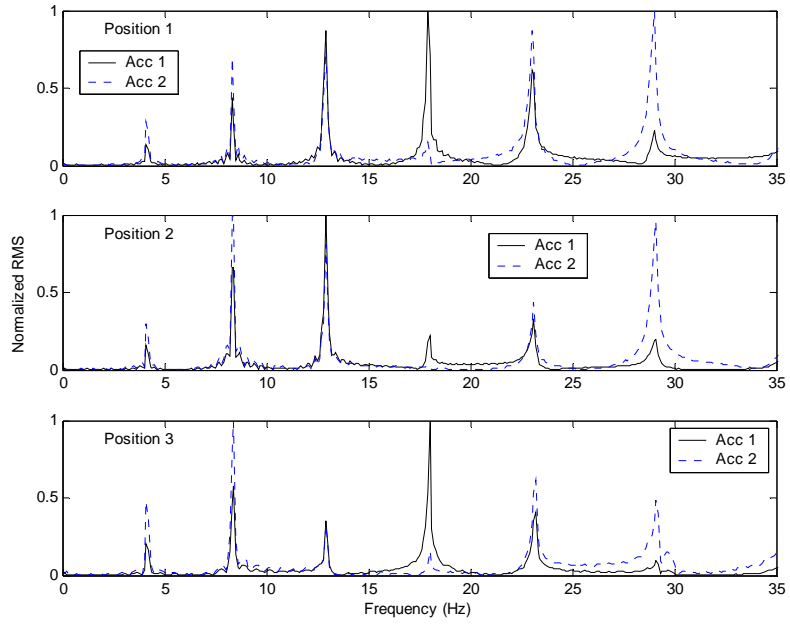
**Figure G.9 Normalized Root Mean Square (RMS) of NF 3**



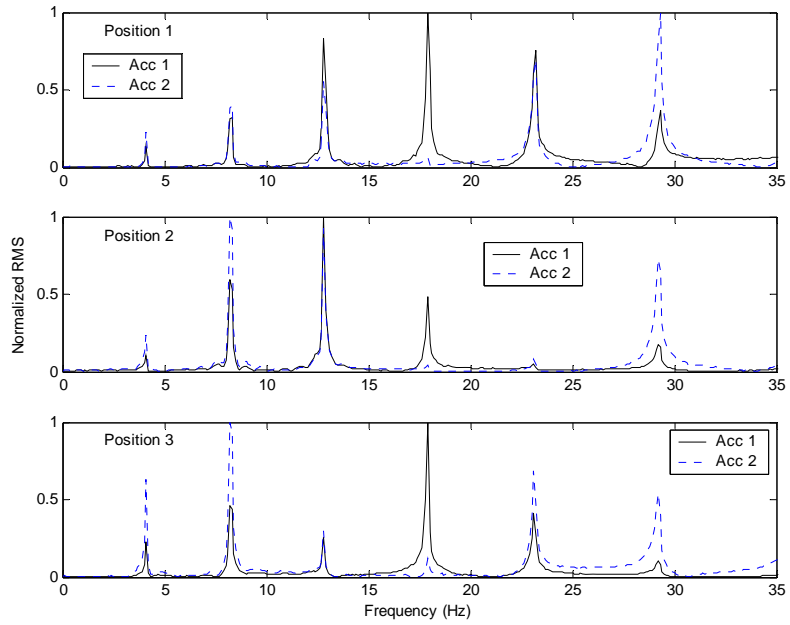
**Figure G.10 Normalized Root Mean Square (RMS) of NF 4**



**Figure G.11 Normalized Root Mean Square (RMS) of NF 5**

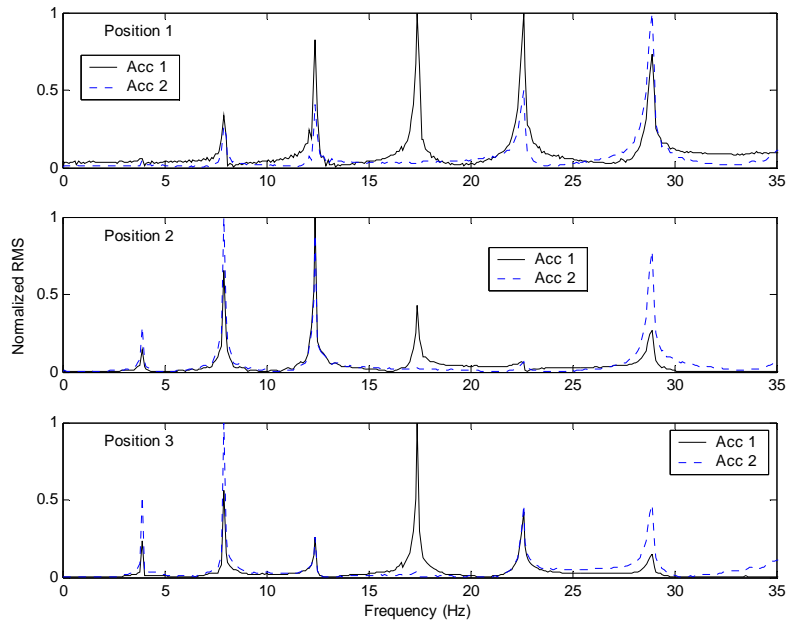


**Figure G.12 Normalized Root Mean Square (RMS) of NF 6**



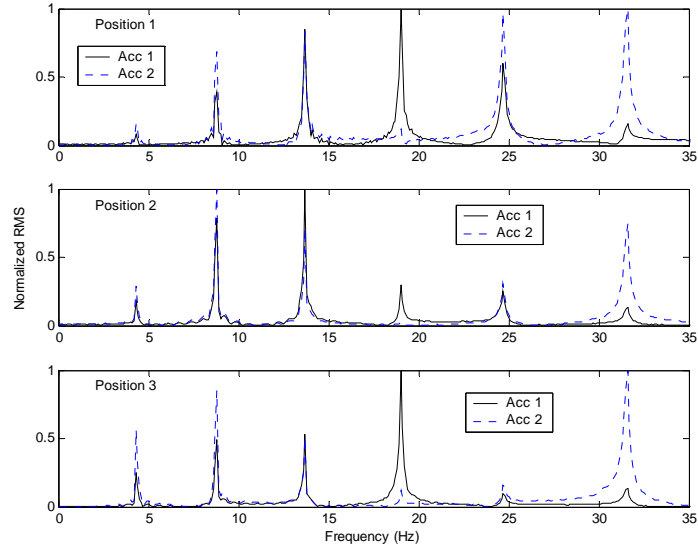
**Figure G.13 Normalized Root Mean Square (RMS) of NF 7**



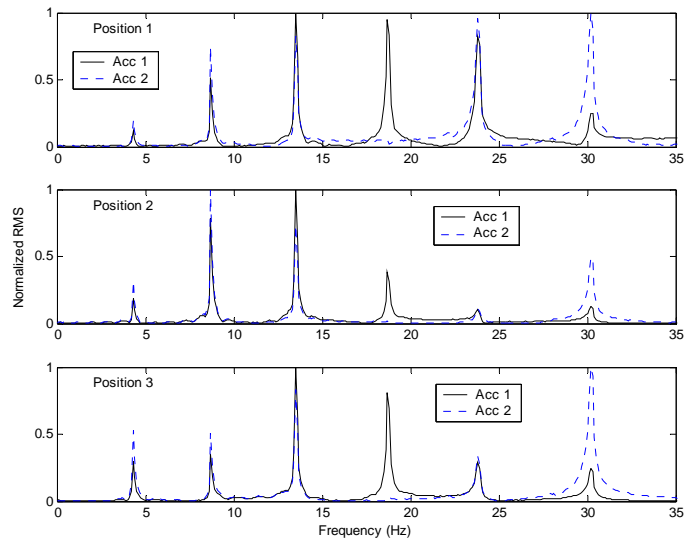


**Figure G.14 Normalized Root Mean Square (RMS) of NF 8**

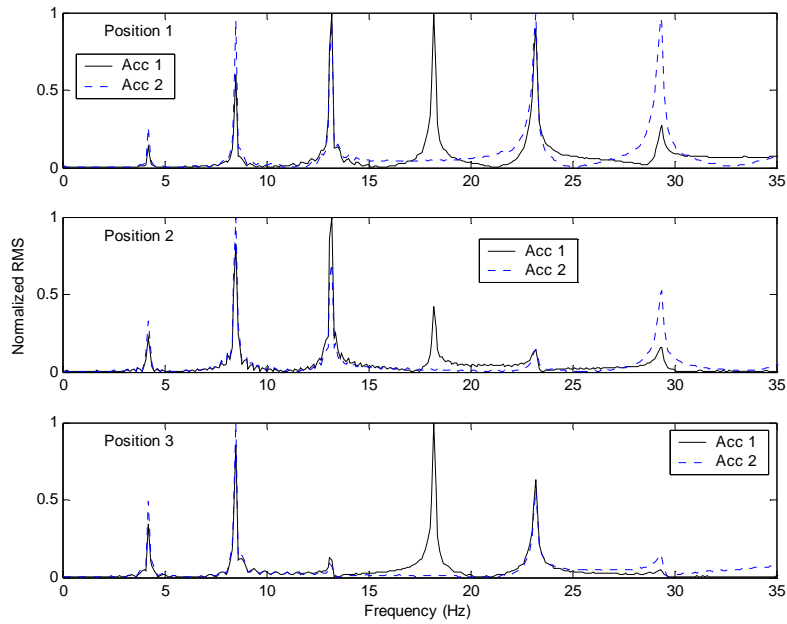
### G.3 CABLE 03



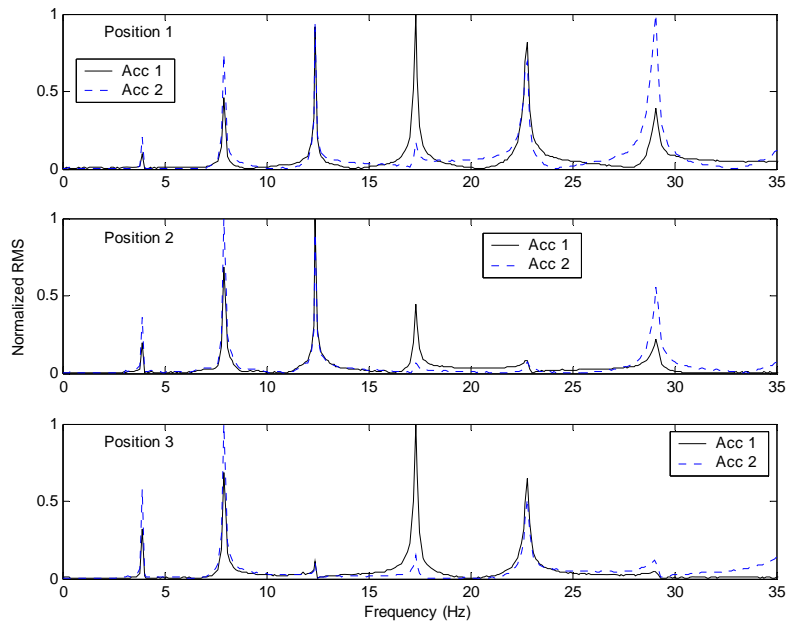
**Figure G.15 Normalized Root Mean Square (RMS) of NF 0**



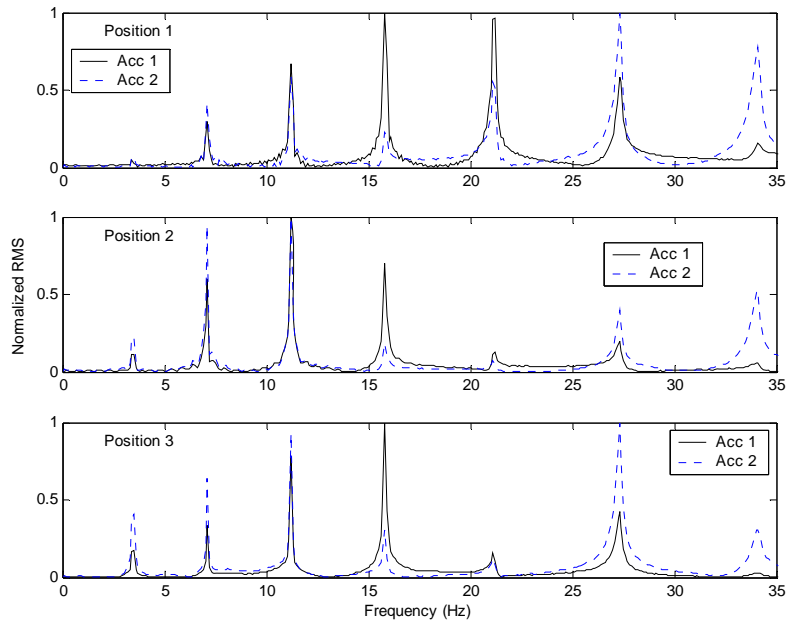
**Figure G.16 Normalized Root Mean Square (RMS) of NF 1**



**Figure G.17 Normalized Root Mean Square (RMS) of NF 2**



**Figure G.18 Normalized Root Mean Square (RMS) of NF 3**



**Figure G.19 Normalized Root Mean Square (RMS) of NF 4**

## Appendix H: Summarized Test Schedule for Cable Specimens

### H.1 CABLE 01

*Table H.1 Summarized Test Schedule for Cable 01*

Date	Cycle	Configuration		SoundPrint™ Report	Remark
		Force (kip)	Displacement (in)		
		Initial measurement			
9/01/05	0	0.8±0.5at0.6Hz			Test started
9/06/05		Measurement 1			
9/12/05	559,166	0.8±0.5at 1.25 Hz			
9/15/05	879,999	0.8±0.5 at 1.5Hz			
9/16/05		Measurement 2			
9/27/05		Measurement 3			
				10/03/05 1:42 am	Wire break(1)
10/03/05		Measurement 4			
				10/04/05 6:10 pm	Wire break(2)
10/05/05		Measurement 5			
10/14/05		LVDT Replacement (from force-control to displacement-control)/ Relocation of the Actuator			
10/17/05	3,401,982		1.5±1.25at 1.5 Hz		Restart
10/17/05		Measurement 6			
				10/24/05 6:50 pm	Wire break(3)
10/24/05		Measurement 6			
				10/25/051:22 am	Wire break(4)
				10/25/056:43 pm	Wire break(5&6)
				10/26/056:30 pm	Wire break(7)
				10/26/059:56 pm	Wire break(8)
10/27/05		Measurement 7			
				10/27/05 2:46 pm	Wire break(9)
				10/27/05 4/36 pm	Wire break(10)
				10/27/05 8:28 pm	Wire break(11)
				10/28/05 1:09 am	Wire break(12)
				10/28/05 3:35 pm	Wire break(13)
				11/1/05 3:15 am	Wire break(14)
11/01/05	5,044,194	Test terminated due to failure of specimen			

## H.2 CABLE 02

*Table H.2 Summarized Test Schedule for Cable 02*

Date	Cycle	Configuration (in)	SoundPrint™ Report	Remark
		Initial measurement 0		
2/21/06	0	1.52±1.25 at 1.5Hz		Test started
2/24/06		Measurement 1		
2/24/06	338,828	1.58±1.25 at 1.5 Hz		Reconfiguration
2/28/06	N/A	Measurement 2		
			3/02/06 12:53 pm	Wire break (1)
3/03/06		Measurement 3		
3/03/06	1,239,369	1.55 ± 1.25 at 1.5 Hz		Reconfiguration
			3/03/06 5:32 pm	Wire break (2)
3/06/06		Measurement 4		
3/06/06	1,627,765	1.42± 1.25 at 1.5 Hz		Reconfiguration
3/15/06		Measurement 5		
3/15/06	2,909,696	1.40± 1.25 at 1.5 Hz		Reconfiguration
3/21/06		Measurement 6		
3/21/06	3,567,128	1.54± 1.25 at 1.5 Hz		Reconfiguration
			3/22/06 10:28 am	Wire break (3)
			3/23/06 8:22 am	Wire break (4)
			3/23/06 6:27 pm	Wire break (5)
3/24/06		Measurement 7		
3/24/06	3,924,975	1.81± 1.25 at 1.5 Hz		Reconfiguration
3/27/06	N/A	Measurement 8		
3/27/06	4,323,719	1.96± 1.25 at 1.5 Hz		Reconfiguration
			3/28/06 5:32 pm	Wire break (6)
3/30/06	4,603,980	Final Measurement 9		
3/30/06		1.96± 1.25 at 1.5 Hz		Reconfiguration
4/01/06	4,899,220	Test terminated		

### H.3 CABLE 03

*Table H.3 Summarized Test Schedule for Cable03*

Date	Cycle	Configuration (in)	SoundPrint™ Report	Remarks
		Initial measurement 0		
4/25/06	0	1.5±1.4in at 1.25Hz		Test started
		Measurement 1-1~1-10		
4/25/06	12,000	1.5±1.4in at 1.5Hz		
4/26/06	134,543	Measurement 2		
4/28/06	364,735	Measurement 3		
			4/28/06 7:21 pm	Wire break(1)
			4/29/06 6:40am	Wire break(2)
			4/29/06 7:41 pm	Wire break(3)
			4/29/06 7:52 pm	Wire break(4)
5/01/06	748,655	Measurement 4		
			5/2/06 6:49 am	Wire break(5)
			5/2/06 6:59 pm	Wire break(6)
5/04/06	1,027,314	Measurement 5		
			5/8/06 6:23 am	Wire break(7)
			5/8/06 6:38 pm	Wire break(8)
5/09/06	1,651,467	Test terminated		
		Final measurement 6		

## Appendix I: Concrete Block Design

The concrete block was designed to support prestressing force of the tendon specimens. The computation details are given as below:

Prestressing:

$$12 \times 0.2185 \times 0.6 \times 270 = 425 \text{ kip (Tendon 01)}$$

$$9 \times 0.2185 \times 0.86 \times 270 = 425 \text{ kip (Tendon 02)}$$

Clearance distance from the center to edge of the surface for VSL anchor type E:

$$14.25/2 + \text{cover (1.5 in.)} \approx 9 \text{ in.}$$

where,  $f_y = 60 \text{ ksi}$ ,  $f_c = 4000 \text{ psi}$

Concrete block dimension was chosen as  $18 \times 18 \times 24 \text{ in.}$

1) Bursting Force:

$$T = 0.25 \times P \left(1 - \frac{h_b}{h}\right) = 0.25 \times 425 \times \left(1 - \frac{10}{18}\right) = 47.2 \text{ kip}$$

The required number of #4 stirrups to keep the stress in reinforcement below  $0.5 f_y$  is

$$\frac{47.2}{(2 \times 0.2) \times (0.5 \times 60)} = 3.9 \quad \text{Use 5- #4 @ 4 in}$$

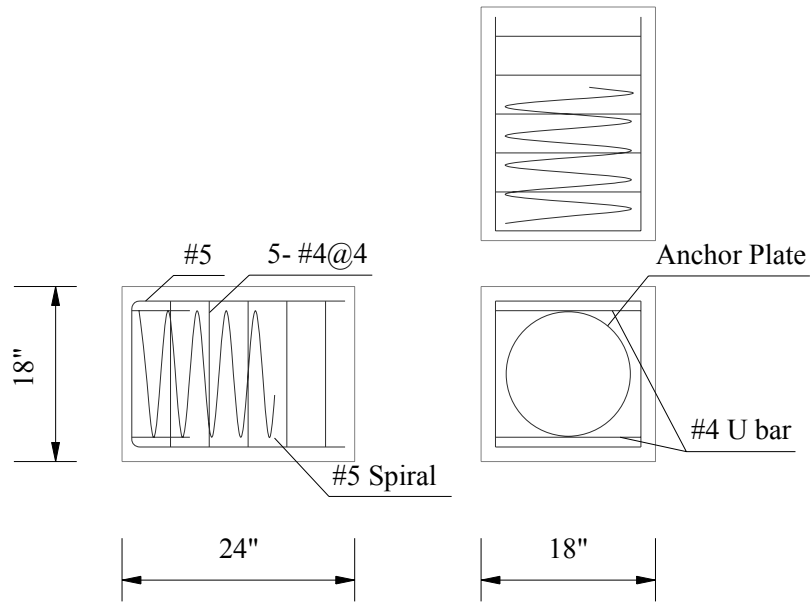
2) Spalling Force:

$$0.02 \times P = 0.02 \times 425 = 8.5 \text{ kip}$$

$$\frac{8.5}{0.2 \times (0.5 \times 30)} = 1.4 \quad \text{Use 2-# 4 U bars at the face of the block.}$$

The reinforcement of the concrete block is summarized in Figure I.1.





**Figure I.1 Reinforcement Arrangement for Concrete Block**

Bearing stress was considered by using #5 spiral provided by the VSL. The compressive test for cylinder proved the concrete satisfied the design assumption (Table I.1).

**Table I.1 Compressive Test Results (ksi)**

Sample	1	2	3	Average
7 days	3.67	3.50	3.44	3.55
28 days	4.70	4.54	4.66	4.64

## Appendix J: Summarized Schedule for Tendon 01

*Table J.1: Summarized Schedule for Tendon 01*

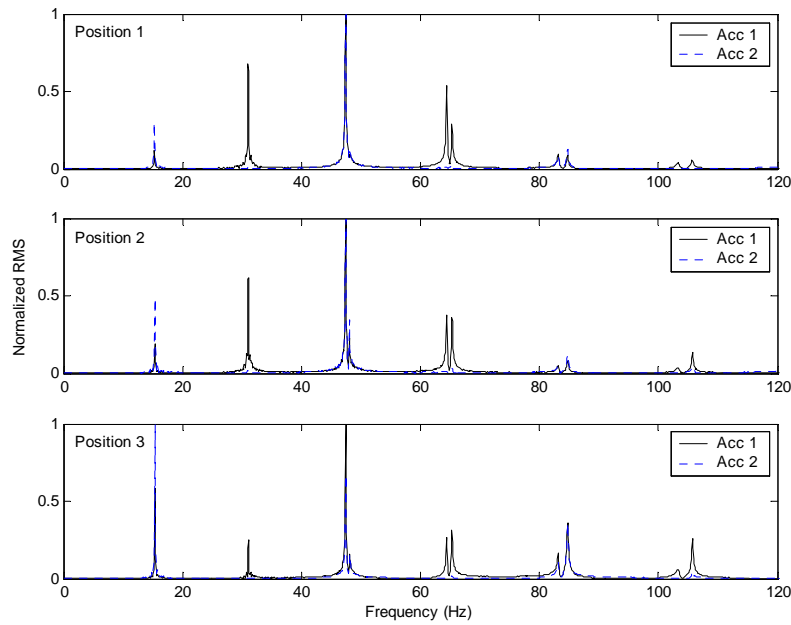
Date	Cycle	Configuration	Wire Break Report	Remarks
1/04/06		Initial measurement 0		
1/04/06	0	0±0.5" at 2.0Hz		Test started
1/05/06	155,358	Measurement 1		
			1/8/06 11:13 PM	SoundPrint report (1)
			1/9/06 7:31 AM	SoundPrint report (2)
1/09/06	809,410	Measurement 2		
			1/10/06 12:49 AM	SoundPrint report (3)
			1/10/06 7:46 AM	SoundPrint report (4)
			1/10/06 8:26 AM	SoundPrint report (5)
			1/10/06 10:00 AM	SoundPrint report (6) Broken during Test
1/10/06	957,348	Measurement 3		
			1/10/06 8:09 PM	SoundPrint report (7)
			1/10/06 8:43 PM	SoundPrint report (8)
1/10/06	1,030,133	Temporary stop		
			1/11/06 10:35 AM	SoundPrint report (9) Broken during test
1/11/06	1,030,714	Measurement 4		
1/11/06	1,047,695	0±0.3" at 2.0Hz		Reconfiguration
1/12/06		Temporary stop		
1/13/06	1,248,230	0.22±0.2" at 2.0Hz		Restart
			1/13/06 10:59 AM	SoundPrint report (10)
			1/14/06 7:00 AM	SoundPrint report (11)
1/15/06		Measurement 5		
1/15/06	1,593,858	0.22±0.2" at 3.5Hz		Reconfiguration
			1/16/06 3:36 AM	SoundPrint report (12)
1/16/06	1,846,850	Measurement 6		
1/16/06		0.22±0.2" at 4.0Hz		Reconfiguration
1/17/06		0.30±0.28" at 3.5 Hz		Reconfiguration
1/18/06		0.40±0.38" at 2.5Hz		Reconfiguration
1/19/06	2,623,439	0.50±0.48" at 2.5 Hz		Reconfiguration
1/19/06		Measurement 7		

1/19/06	2,660,152	0.6±0.58" at 2.0 Hz		Reconfiguration
1/19/06	2,726,011	0.65±0.58" at 2.0Hz		Reconfiguration
1/20/06	2,814,775	0.75±0.6" at 2.5 Hz		Reconfiguration
1/20/06	2,814,504	Measurement 8		
			1/20/06 12:19AM	SoundPrint report (13)
1/20/06	2,861,425	0.8±0.6" at 2.5 Hz		Reconfiguration
			1/20/06 4:47 PM	SoundPrint report (14)
1/21/06		Measurement 9		
1/21/06	3,026,868	0.9±0.6" at 2.0Hz		Reconfiguration
1/22/06		Measurement 10		
1/22/06	3,201,894	0.9±0.65" at 2.0Hz		Reconfiguration
1/23/06	3,369,590	1.1±0.65" at 2.0 Hz		Reconfiguration
			1/23/06 11:57 AM	SoundPrint report (15)
1/23/06	3,400,336	1.2±0.6" at 2.0 Hz		Reconfiguration
1/23/06	3,416,880	1.3±0.6" at 2.0 Hz		Reconfiguration
			1/23/06 8:06 PM	SoundPrint report (16)
			1/24/06 2:29 AM	SoundPrint report (17)
1/24/06		Measurement 11		
1/24/06	3,532,401	1.4±0.6" at 2.0 Hz		Reconfiguration
			1/24/06 4:23 PM	SoundPrint report (18)
			1/25/06 1:04 AM	SoundPrint report (19)
			1/25/06 9:49 AM	SoundPrint report (20)
1/25/06	3,715,920	Measurement 12		
1/25/06	3,773,862	1.5±0.6" at 2.0Hz		Reconfiguration
1/25/06	3,797,690	1.6±0.6" at 2.0 Hz		Reconfiguration
			1/26/06 10:28 AM	SoundPrint report (21)
1/26/06	3,904,211	Test terminated		
		Final measurement 13		

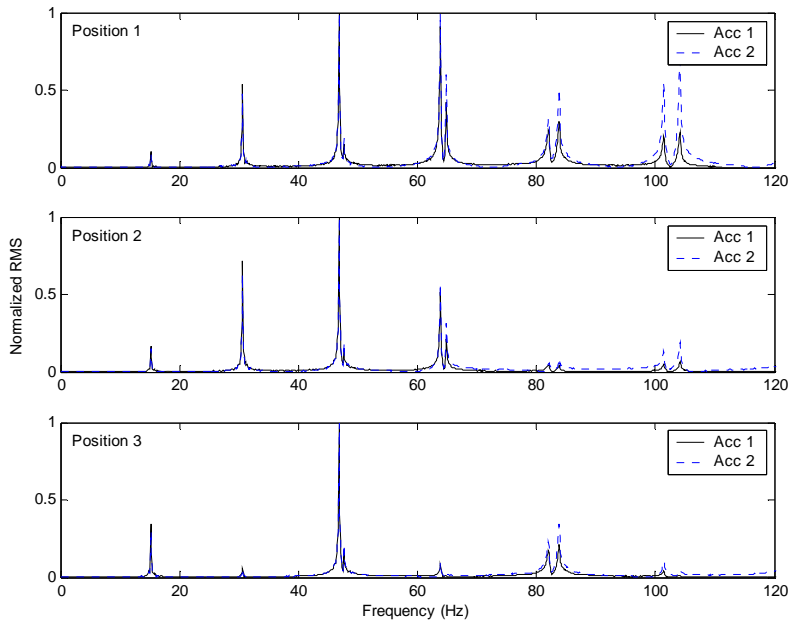
## Appendix K: Natural Frequencies of Tendon Specimens

The times series acquired from the frequency measurement are converted into frequency domain by Fast Fourier Transformation. The test results are displayed in Figure K.1 through Figure K.14 for Tendon 01 and Figure K.15 though Figure K.39 for Tendon 02, respectively.

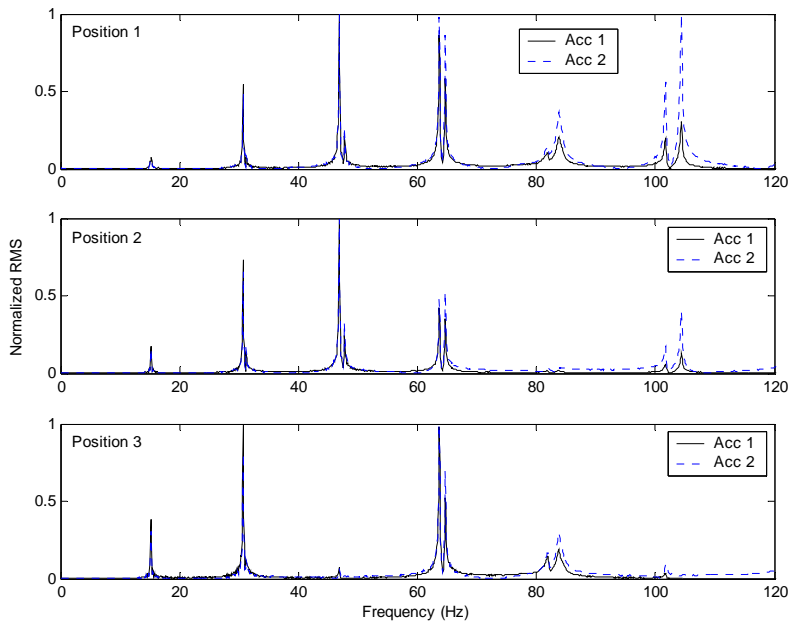
### K.1 TENDON 01



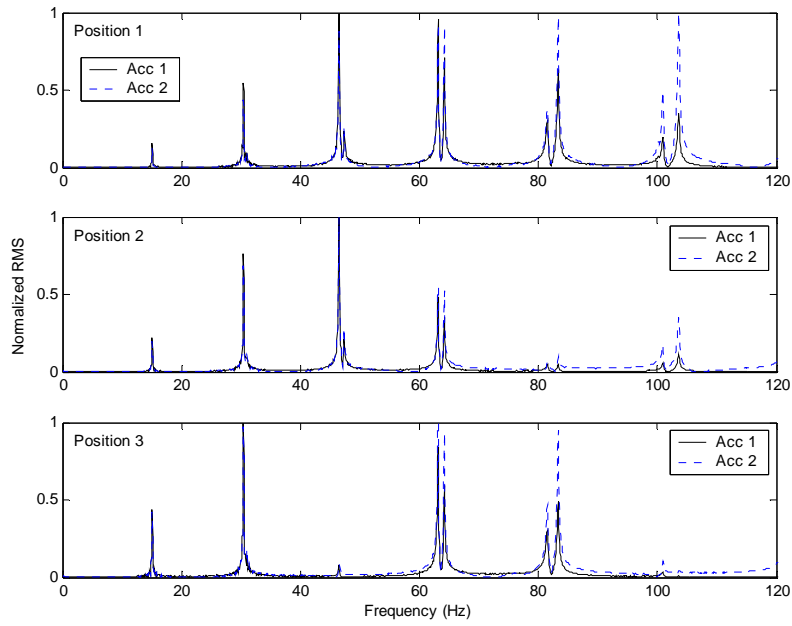
*Figure K.1 Normalized Root Mean Square (RMS) of NF 0*



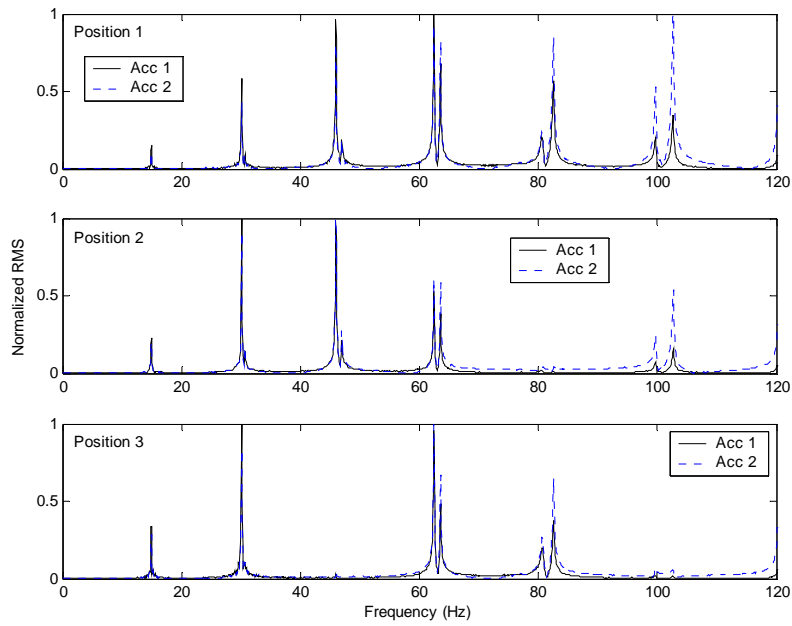
**Figure K.2 Normalized Root Mean Square (RMS) of NF 1**



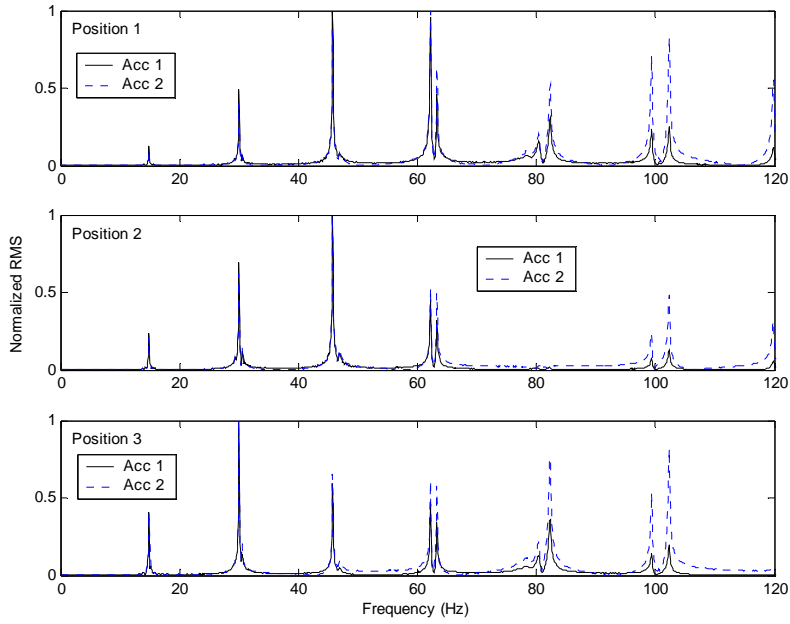
**Figure K.3 Normalized Root Mean Square (RMS) of NF 2**



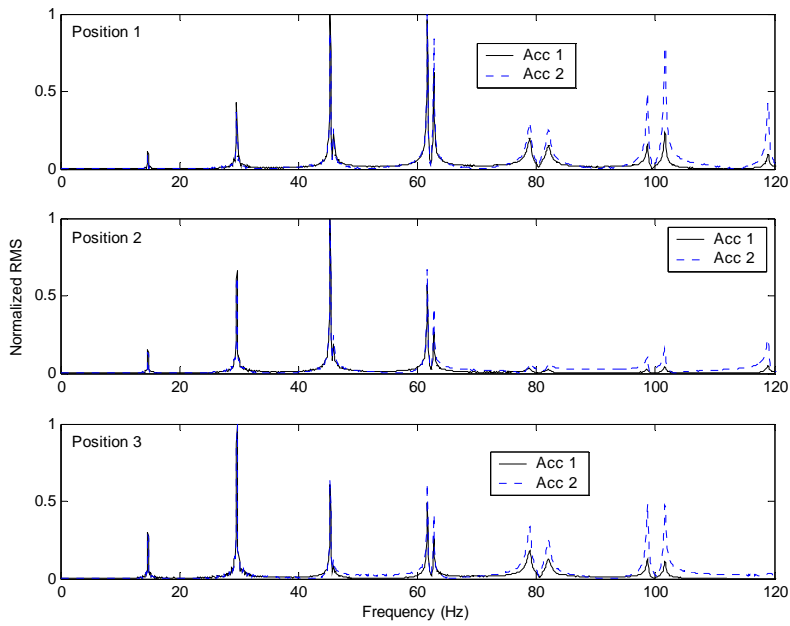
**Figure K.4 Normalized Root Mean Square (RMS) of NF 3**



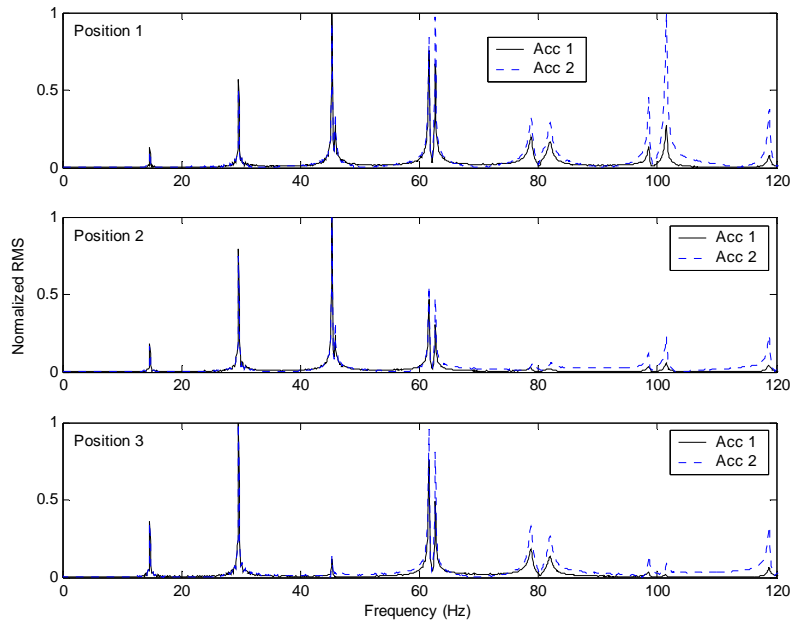
**Figure K.5 Normalized Root Mean Square (RMS) of NF 4**



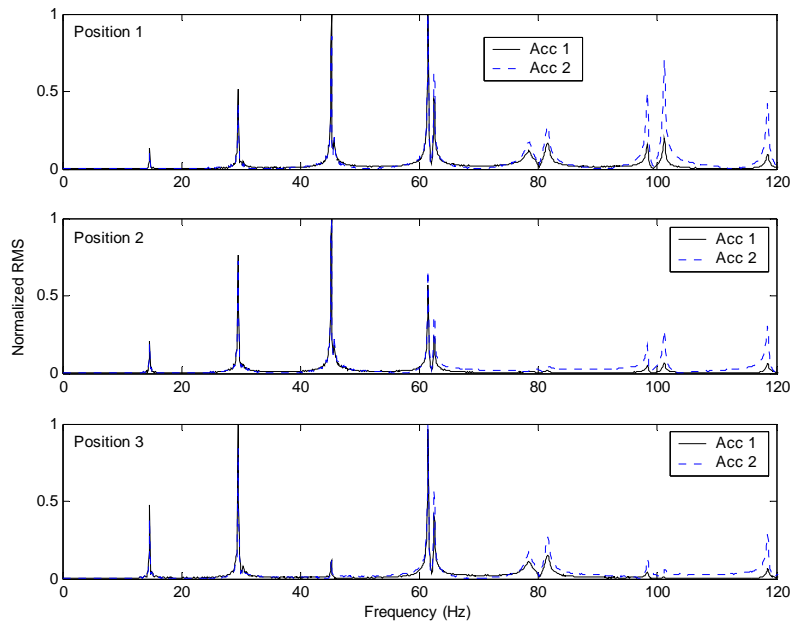
**Figure K.6 Normalized Root Mean Square (RMS) of NF 5**



**Figure K.7 Normalized Root Mean Square (RMS) of NF 6**

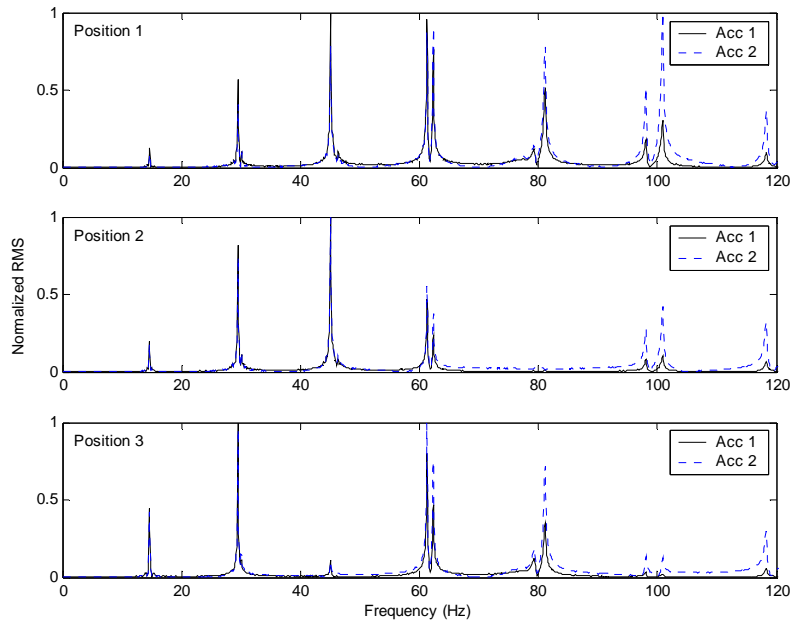


**Figure K.8 Normalized Root Mean Square (RMS) of NF 7**

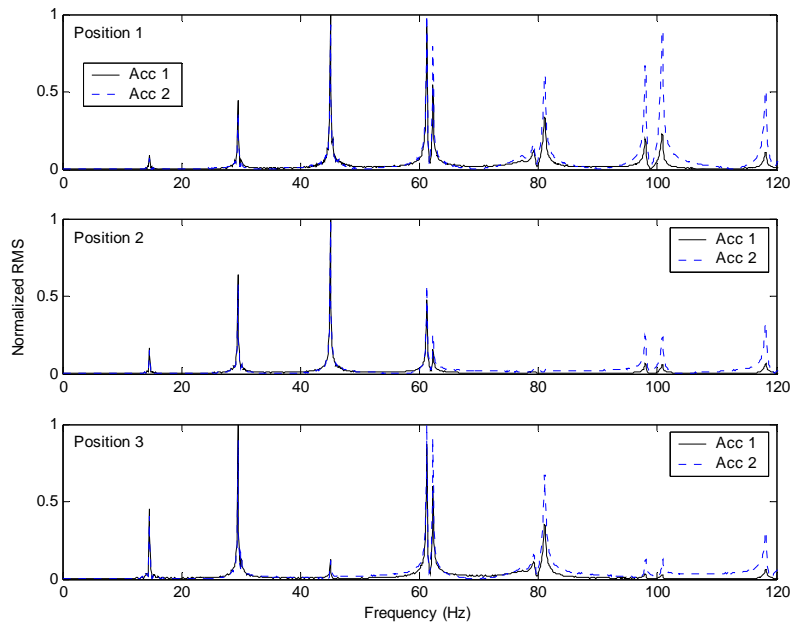


**Figure K.9 Normalized Root Mean Square (RMS) of NF 8**

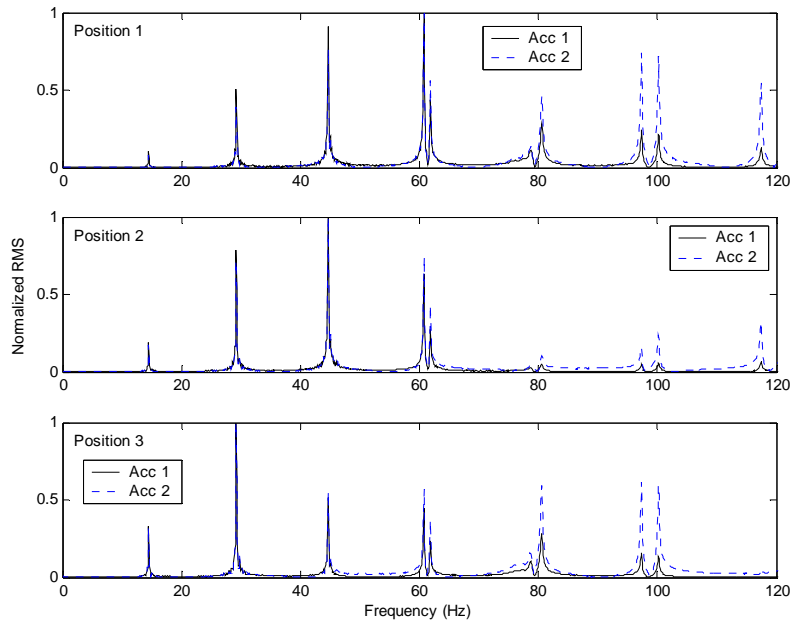




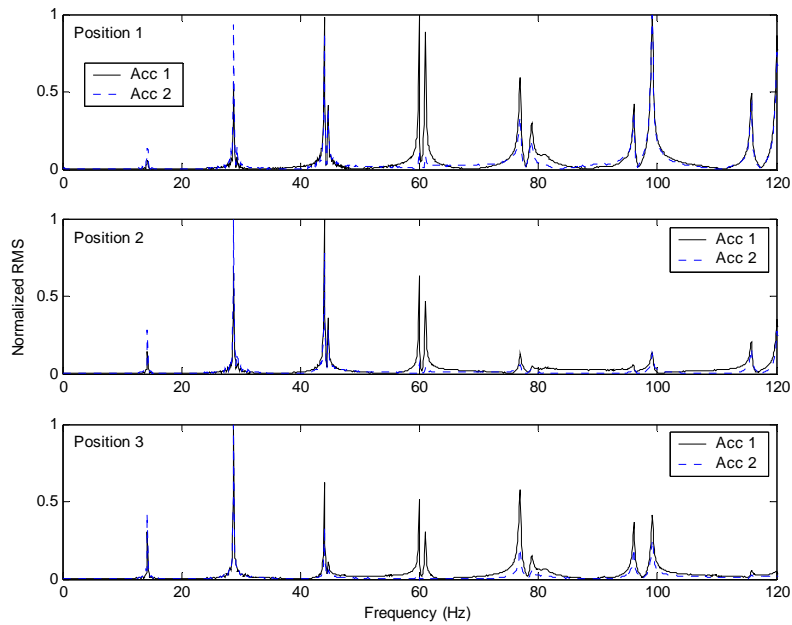
**Figure K.10 Normalized Root Mean Square (RMS) of NF 9**



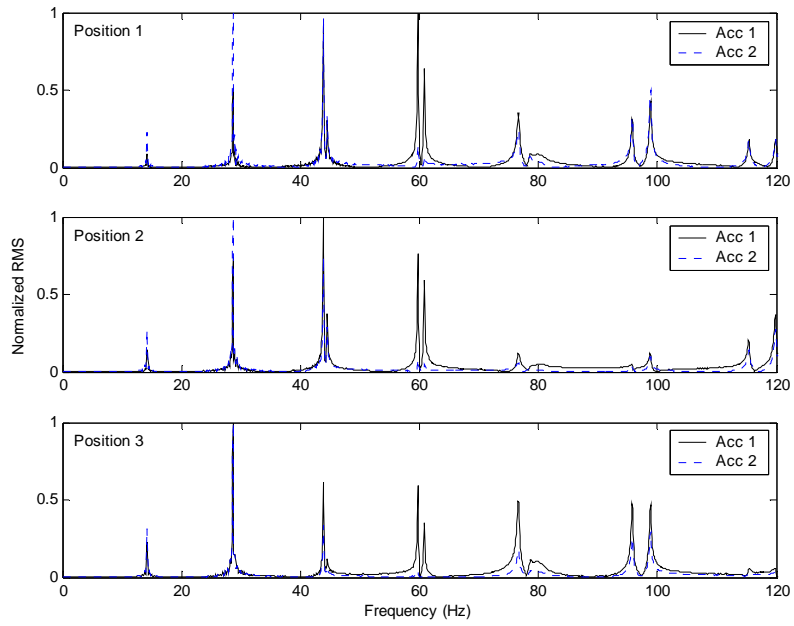
**Figure K.11 Normalized Root Mean Square (RMS) of NF 10**



**Figure K.12 Normalized Root Mean Square (RMS) of NF 11**

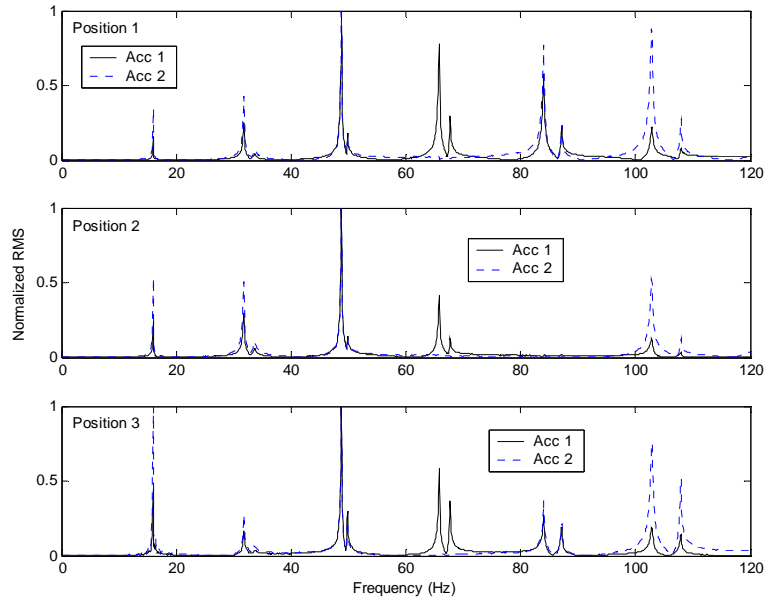


**Figure K.13 Normalized Root Mean Square (RMS) of NF 12**

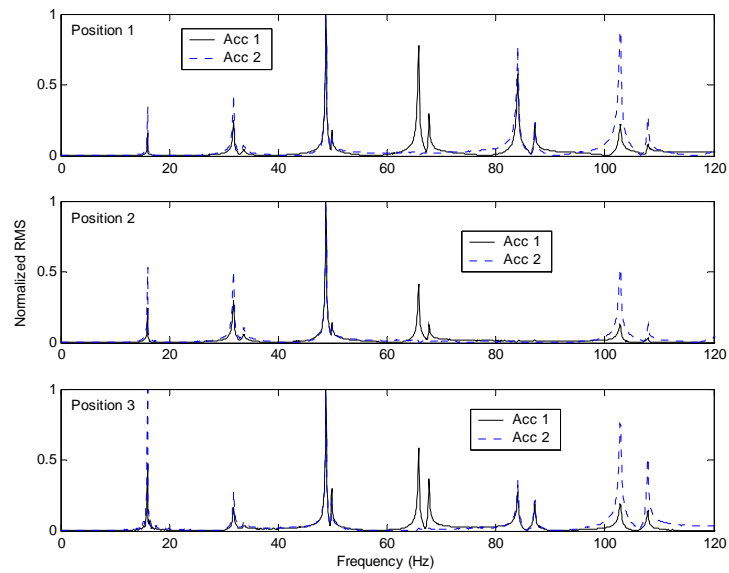


**Figure K.14 Normalized Root Mean Square (RMS) of NF 13**

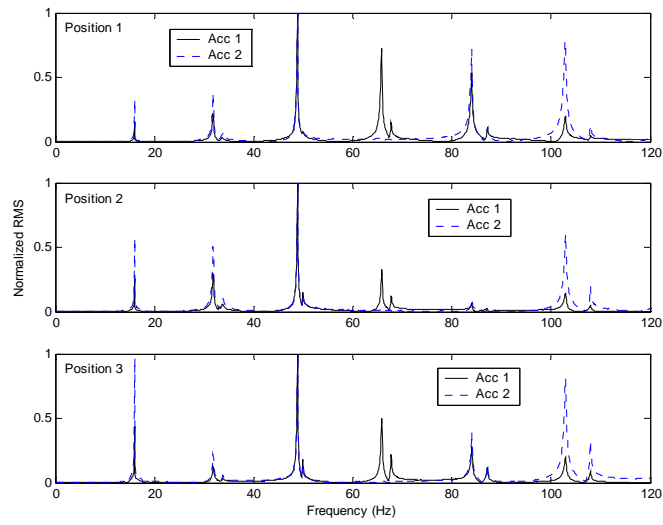
## K.2 TENDON 02



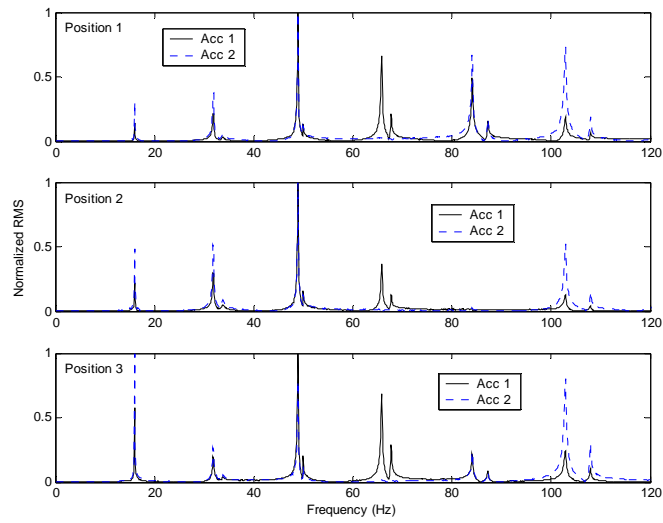
**Figure K.15 Normalized Root Mean Square (RMS) of NF 0-0**



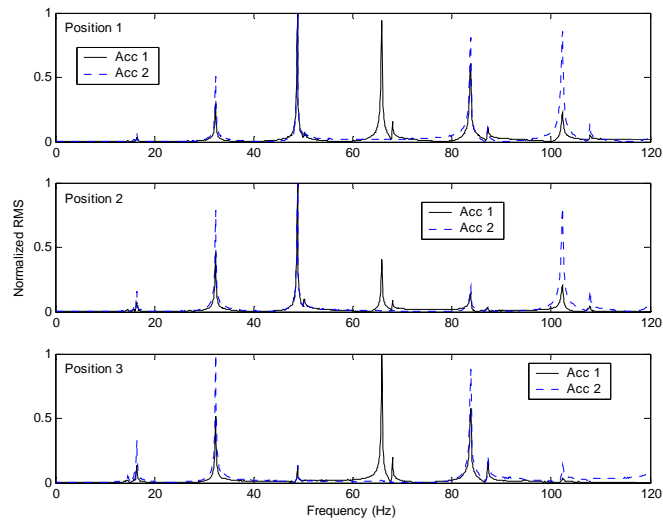
**Figure K.16 Normalized Root Mean Square (RMS) of NF 0-1**



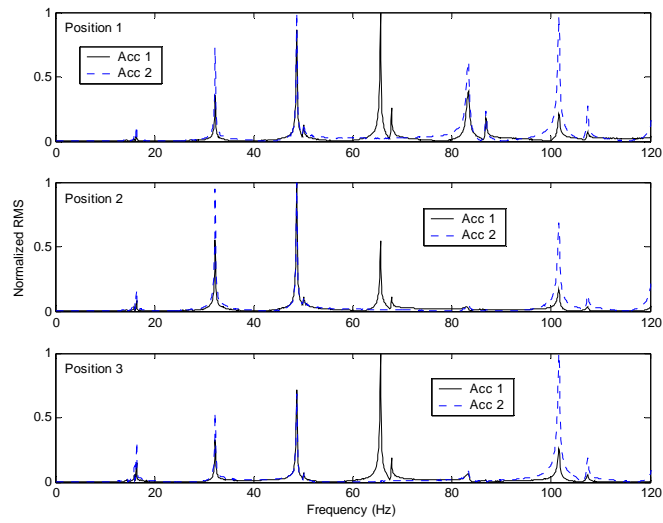
**Figure K.17 Normalized Root Mean Square (RMS) of NF 0-3**



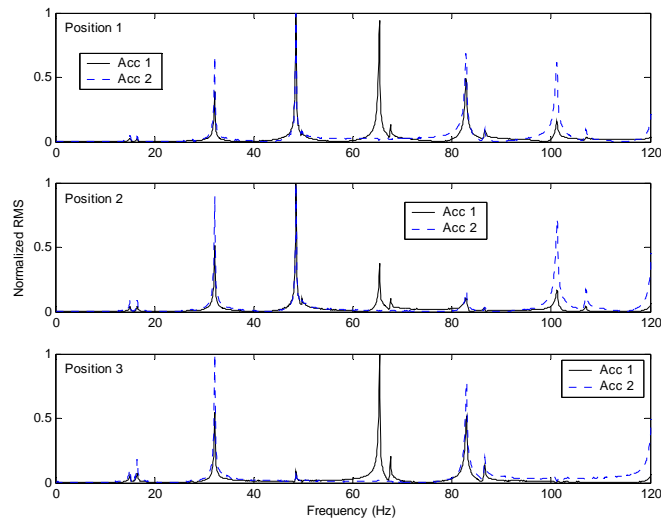
**Figure K.18 Normalized Root Mean Square (RMS) of NF 0-2**



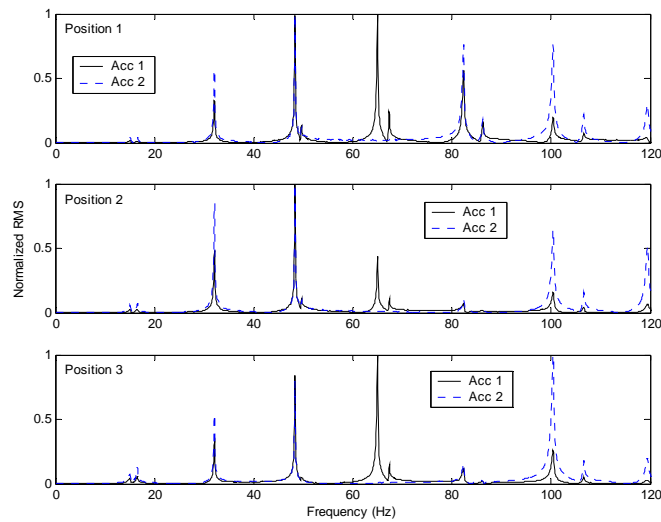
**Figure K.19 Normalized Root Mean Square (RMS) of NF 1**



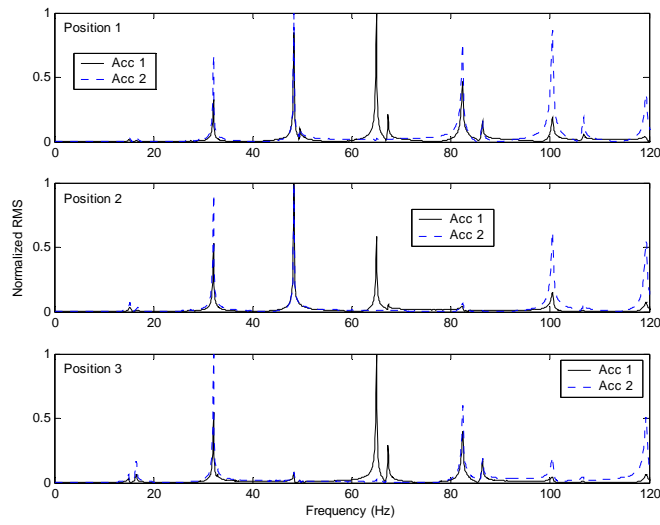
**Figure K.20 Normalized Root Mean Square (RMS) of NF 2**



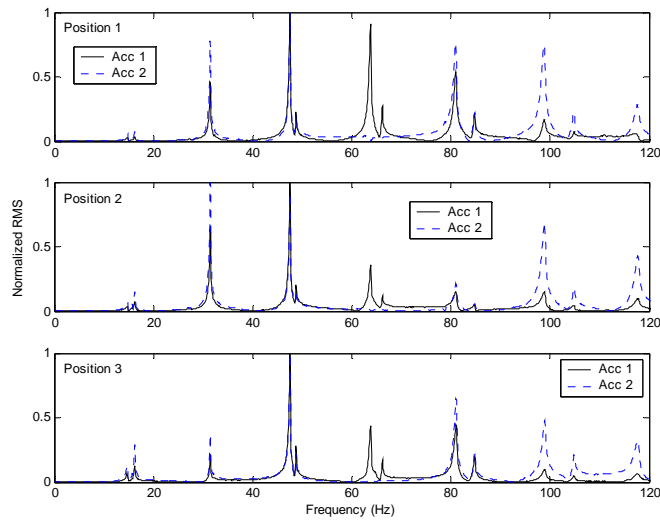
**Figure K.21 Normalized Root Mean Square (RMS) of NF 3**



**Figure K.22 Normalized Root Mean Square (RMS) of NF 4**

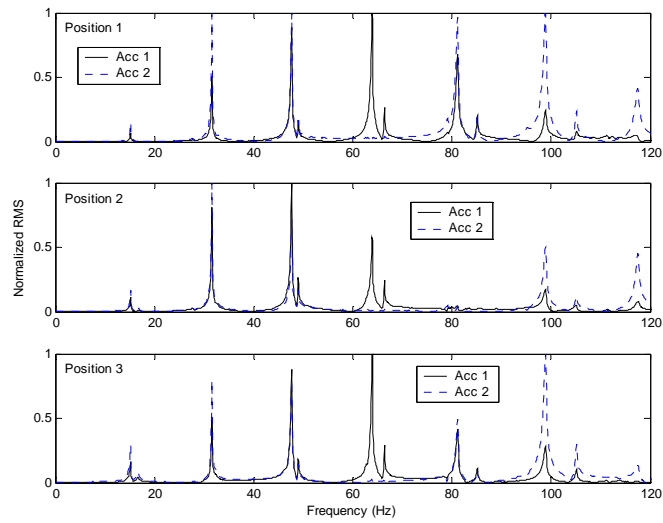


**Figure K.23 Normalized Root Mean Square (RMS) of NF 5**

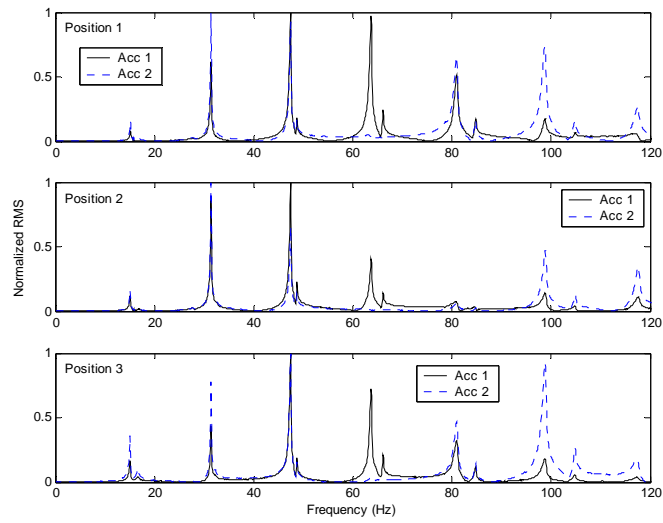


**Figure K.24 Normalized Root Mean Square (RMS) of NF 6**

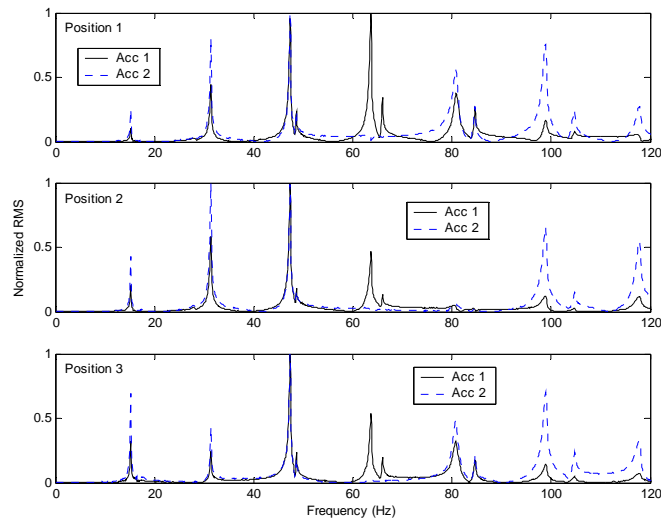




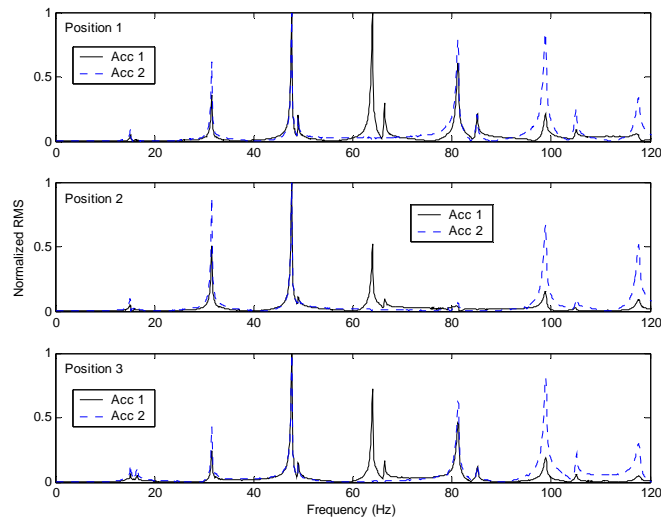
**Figure K.25 Normalized Root Mean Square (RMS) of NF 7**



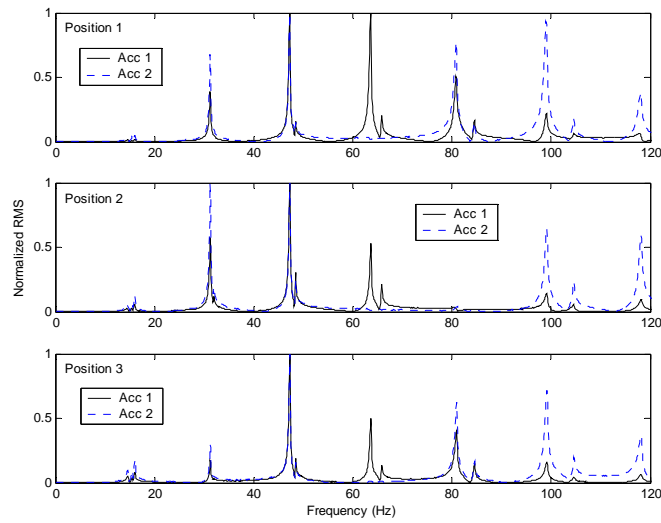
**Figure K.26 Normalized Root Mean Square (RMS) of NF 8**



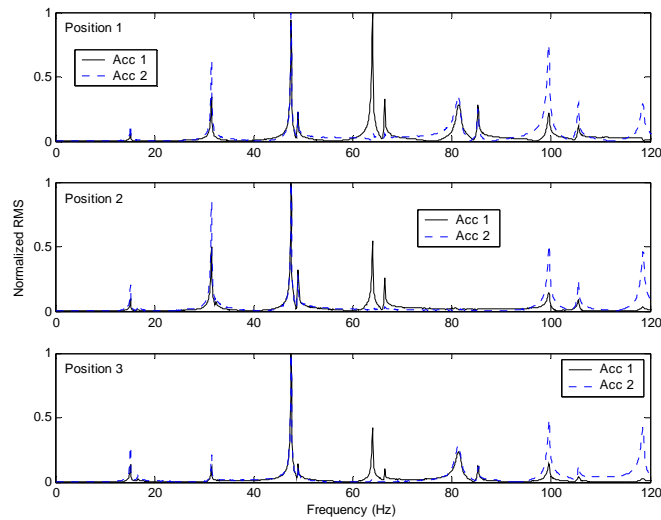
**Figure K.27 Normalized Root Mean Square (RMS) of NF 9**



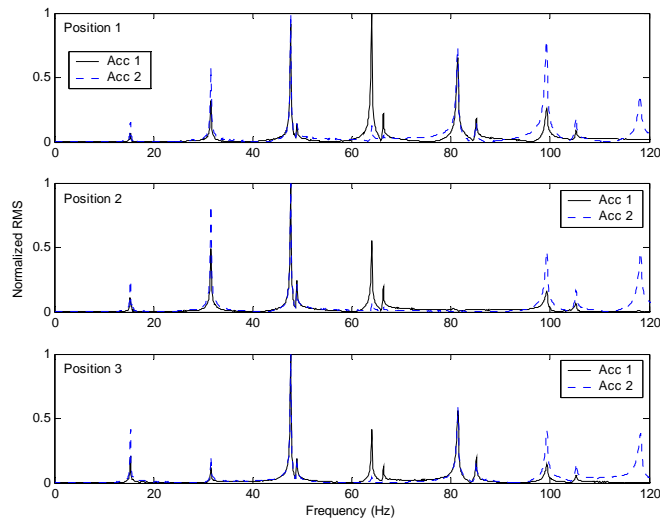
**Figure K.28 Normalized Root Mean Square (RMS) of NF 10**



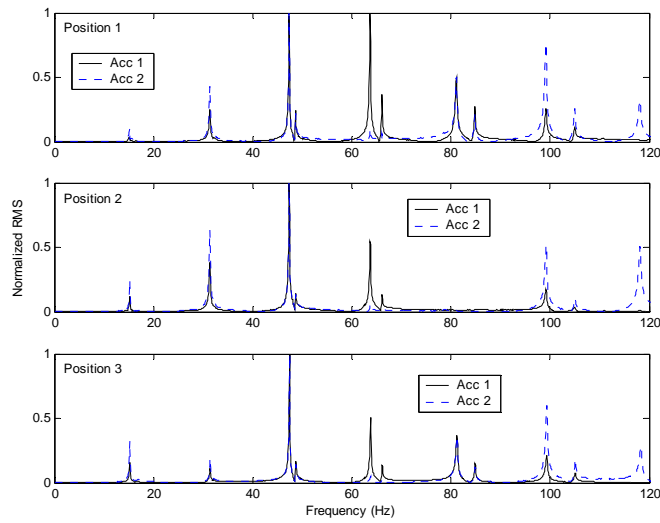
**Figure K.29 Normalized Root Mean Square (RMS) of NF 11**



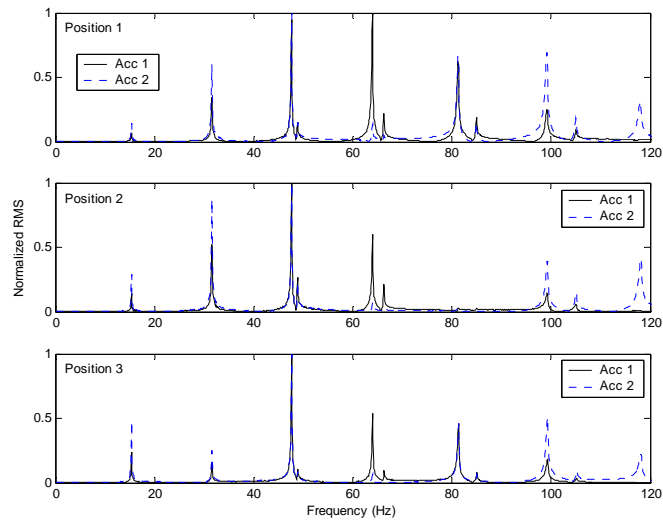
**Figure K.30 Normalized Root Mean Square (RMS) of NF 12**



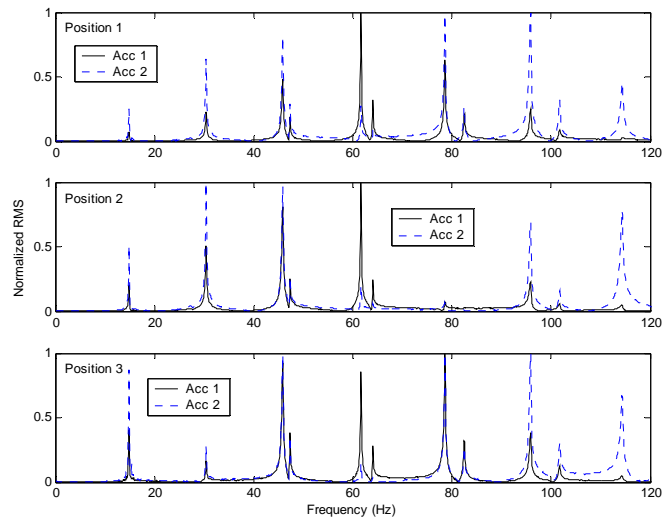
**Figure K.31 Normalized Root Mean Square (RMS) of NF 13**



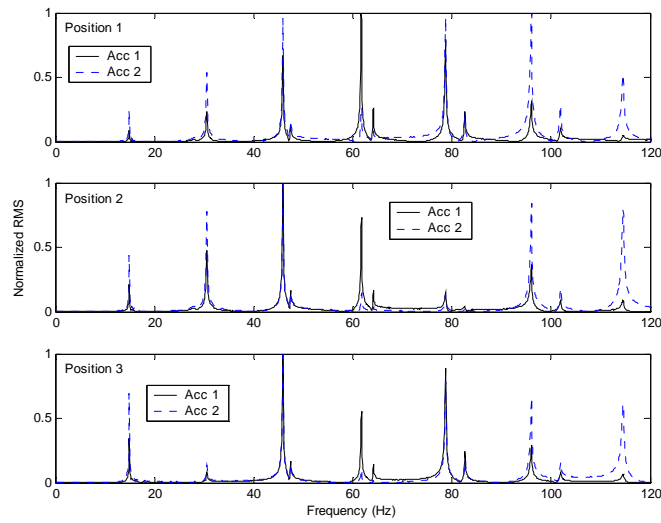
**Figure K.32 Normalized Root Mean Square (RMS) of NF 14**



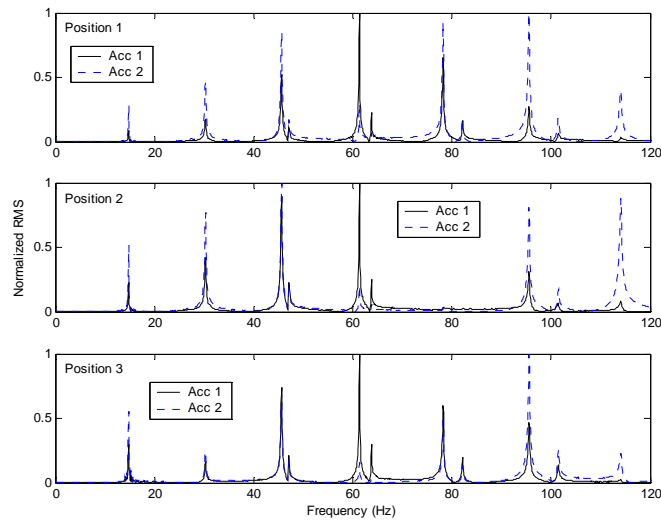
**Figure K.33 Normalized Root Mean Square (RMS) of NF 15**



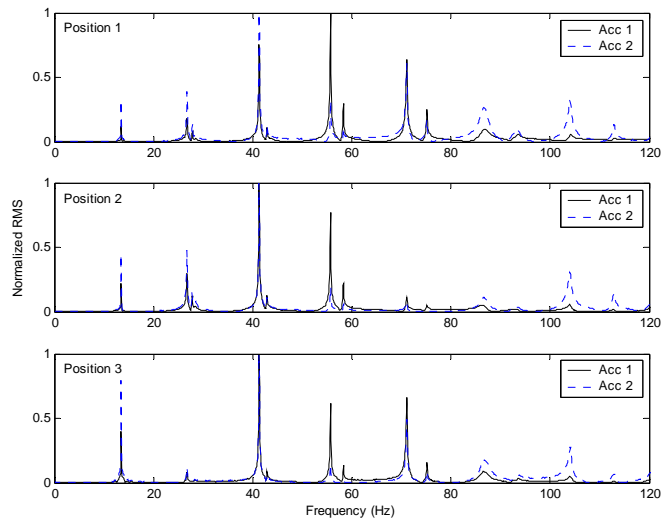
**Figure K.34 Normalized Root Mean Square (RMS) of NF 16**



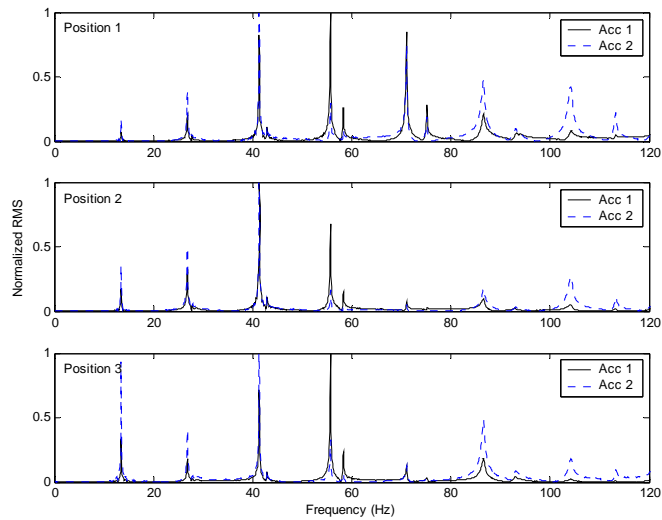
**Figure K.35 Normalized Root Mean Square (RMS) of NF 17**



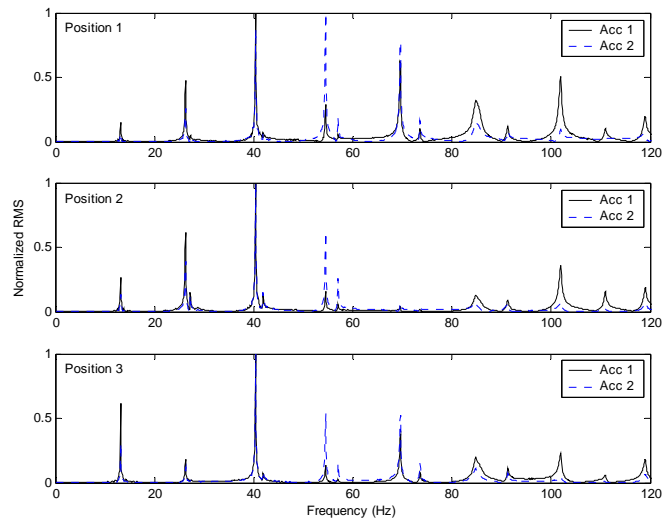
**Figure K.36 Normalized Root Mean Square (RMS) of NF 18**



**Figure K.37 Normalized Root Mean Square (RMS) of NF 19**



**Figure K.38 Normalized Root Mean Square (RMS) of NF 20**



***Figure K.39 Normalized Root Mean Square (RMS) of NF 21***

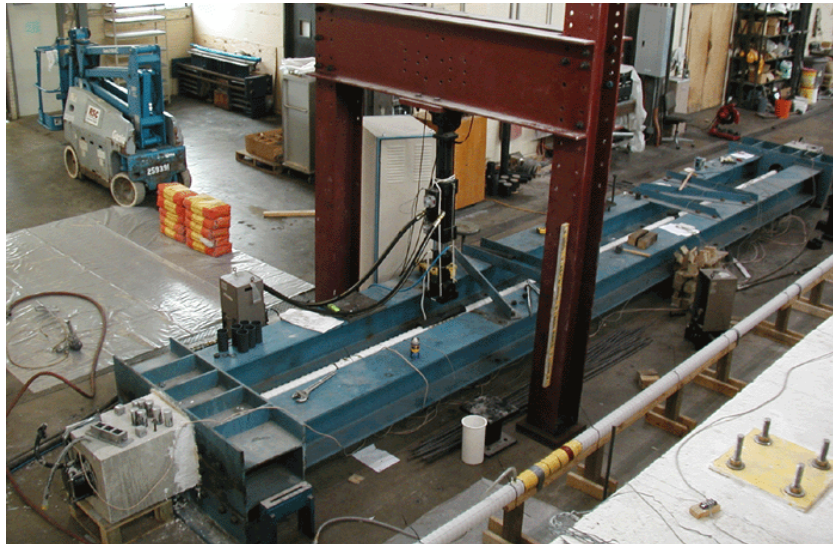


## Appendix L: Corrosion Propagation in Tendon 01

Aggressive corrosion was identified from the anchor heads of Tendon 01 when the test was terminated. The surface of the anchor head was originally designed to be covered with grout. However, the space in the anchor cap was not filled with grout and more than half of surface of the anchor head was exposed to the air. This observation was considered to be important in three points:

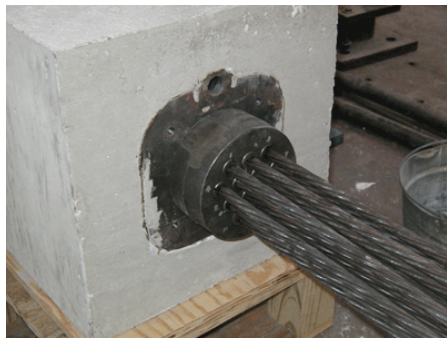
- Considerable corrosion developed in the short period
- Qualified post-tensioning hardware and materials were used for the construction
- The specimen was only located in the indoor laboratory environment

Tendon 01 was 36-ft long and comprised twelve 0.6-in. strands (Figure L.1). The post-tensioning components, VSL ECI 6-12 were used for the construction. This model included anchor heads, strands wedges, HDPE pipe, etc. The post-tensioning ducts were filled with a prepacked grout, Sika 300PT after stressing strands. The grouting was conducted on Nov. 11, 2005 and the corrosion was found on Jan. 26, 2006; a total of 76 days.

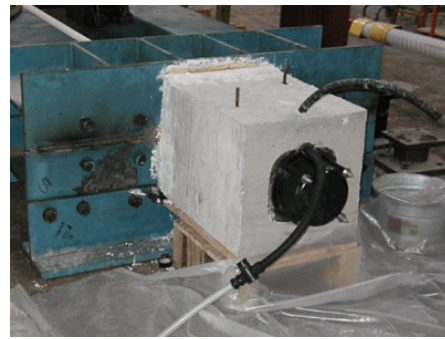


*Figure L.1 Overview of Tendon 01*

When each grout cap was opened, transparent water flowed from the grout cap and unfavorable odor was felt. The surface of the anchor head in south end was covered with grout about half but nearly none of grout existed in the anchor head in north end (Figure L.2c and d). The corrosion products were colored light-brown initially but tainted to dark-brown after exposing to the air. No corrosion was observed from the surface of the anchor heads covered with grout.



(a) After stressing



(b) Inlet and vent for grouting



(c) Anchor head (north)



(d) Anchor head (south)

***Figure L.2 Anchor Head Status***

No grout void was identified along the length of the specimen (Figure L.3), which indicated that grout did not flow over the anchor heads during the grouting. The existence of the transparent water in the anchor cap proved that the material separation between grout paste and water occurred; the grout bleeding. However, considering that condition of grout was intact along the length, the grout bleeding was unlikely to result from grout

material. Further disassembling of the specimen concluded that corrosion developed only at the exposed surface of the anchor heads and the anchor plates (Figure L.4).



(a) Middle section



(b) Concrete block



(c) Anchor plate



(d) Anchor head

***Figure L.3 Grouting Condition at Various Locations***

The grout bleeding generally occurs soon after the grouting procedure before the grout is hardened. In Tendon 01, the grout appeared to not penetrate into the holes in the anchor heads and rather separate into paste and water. The grout was pumped from the south end to north end. The grout inlet was located at the face of the anchor plate and two grout outlets were located on top of each concrete block (Figure L.5). The pumping was terminated after considerable grout flowed from the outlets.

The observations made during the autopsy suggest that the pressure of the pump was not sufficient to flow grout over the anchor head. The grout covered more the surface of the anchor head in south end where the electric pump was located than north end; thus, higher pressure was expected in south end than north end.





(a) Bearing plate



(b) Anchor head (north)



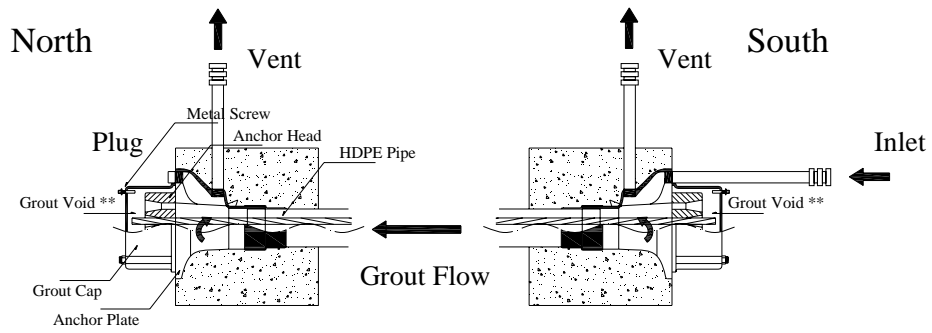
(c) Strands and wedges (south)



(d) Strands and wedges (north)

***Figure L.4 Corrosion Extent on Anchor Head and Plate***

The pressure resistance against applied pressure could increase by the trapped air in the anchor cap. The constructed anchor cap had the metal screw fitted a hole at top (Figure L.6a). This small hole appeared to intend to provide the air path to lower the pressure inside of the anchor cap during the grouting and then sealed using the metal screw later. However, the function of the screw was not understood during the grouting procedure; thus, the screw was initially installed to close the hole. As a result, it was likely that the difference in pressure prohibited for grout to flow into the anchor cap. The function of the metal screw was not explained in the drawings provided by the manufacturer.

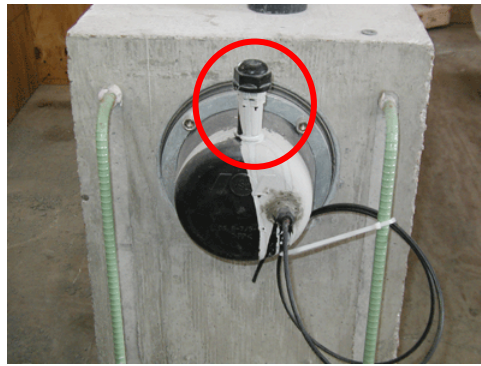


**Figure L.5 Grout Flow of Tendon 02**

The modified type of the anchor cap was recognized from the another project in the Ferguson Structural Engineering Laboratory (Figure L.6b). The cylinder was positioned on top of the anchor cap to provide air path and a small cap was designed to function as the metal screw in Tendon 01.



(a) Metal screw



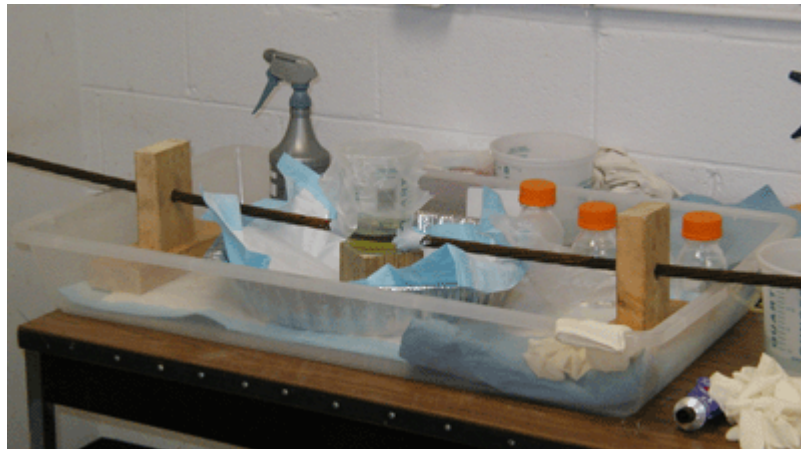
(b) Alternative grout cap

**Figure L.6 Alternative Grout Cap**

## **Appendix M: Acid Induced Corrosion on Strand without Prestressing**

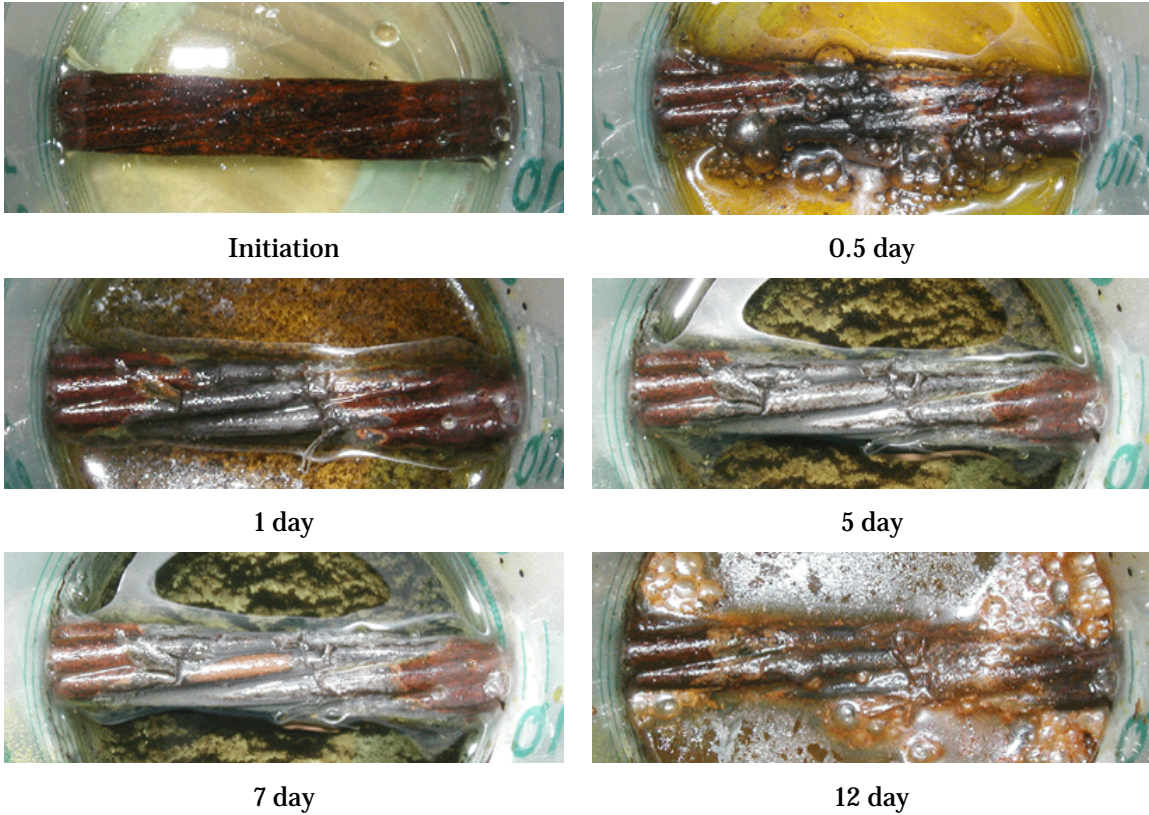
The preliminary acid immersion test was conducted before the acid immersion of Tendon 02. A 6-ft long 0.6-in. diameter strand exposed to a sodium chloride solution for 2 months was submerged locally in a 15% of hydrochloric acid solution for 12 days.

The strand was held by two wood supports from the end and pushed through the two holes of a plastic vessel (Figure M.1). After the holes were sealed using a sealant, the vessel was filled with the acid solution. The opening of the vessel was closed to prevent the evaporation of the solution. The strand status was visually observed.



*Figure M.1 Acid Immersion Test*

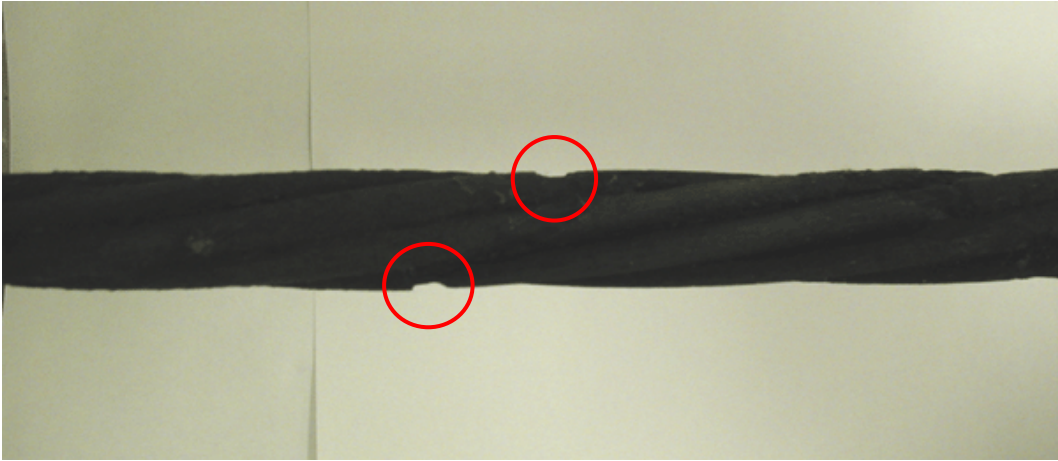
When the acid solution contacted metal, vigorous chemical reaction occurred. The corrosion products were removed first and bubbles covered the surface of the strand. After a one day of immersion, considerable particles precipitated in bottom and an amount of particles increased as the immersion period increased. At 12 days of immersion, the acid solution discolored in brown and the bubbles were observed again. The test was terminated due to limitation in visual observation. A series of observations are displayed in Figure M.2.



***Figure M.2 Preliminary Strand Immersion in Hydrochloric Acid Solution***

After the test was terminated, two significant pitting was identified (Figure M.3); but neither of pitting was located within the exposed region to the solution. These pittings positioned about 1 to 1.5-in. from exposed surface. The acid solution likely flowed through inter wire space.





*Figure M.3 Pitting after 12 days of Immersion*



## Appendix N: Estimation of Cross-Sectional Properties

The computed sectional properties for the idealized sections of the cable specimens and tendon specimens are presented in this section.

The computation of sectional properties based on given constants such as the elastic modulus of strands and grout, area of strand etc. The given constants are presented in Table N.1.

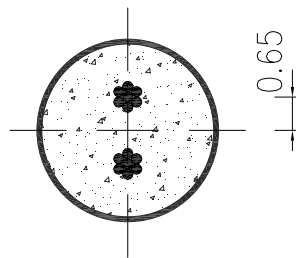
*Table N.1 Constants for Computation*

<p><b>Strand:</b>  <math>E = 29,400 \text{ ksi}</math>  <math>\text{Area} = 0.2208 \text{ in}^2</math>  <math>\text{Diameter} = 0.6 \text{ in.}</math>  <math>\text{Unit weight} = 0.74 \text{ lb/ft}</math>  <math>\text{Diameter of wire} = 0.2 \text{ in.}</math></p>	<p><b>Grout:</b>  <math>E = 3,500 \text{ ksi}</math>  <math>\text{Wet density} = 125 \text{ lb/ft}^3</math>  <math>n = E_{\text{strand}}/E_{\text{grout}} = 8.42</math></p> <p><b>HDPE:</b>  <math>\text{density} = 60 \text{ lb/ft}^3</math></p>
--	---

### N.1 CABLE SPECIMEN

The section of the cable specimen consisted of two 0.6-in. strands. Idealized section is presented in Table N.2 and the computation of mass quantity and the moment of inertia is given Table N.3 and Table N.4, respectively.

*Table N.2 Sectional Dimension of Cable Specimen*



(a) Idealized section

**Duct:**

**Inner diameter: 3.35 in.**

**Outer diameter: 3.54 in.**

(b) Dimension

**Table N.3 Computation of Mass Quantity of Cable Specimen**

Strand:

$$W_s = 0.74 \times 2 = 1.48 \text{ lb/ft}$$

Grout:

$$A_g = (1/4 \times \pi \times 3.35^2 - 2 \times 0.2208) \times 1.05 = 8.80 \text{ in}^2 \text{ (5\% for ribs)} = 0.061 \text{ ft}^2$$

$$W_g = 125 \times 0.061 = 7.64 \text{ lb/ft}$$

Duct:

$$A_d = 1/4 \times \pi \times (3.54^2 - 3.35^2) = 1.01 \text{ in}^2 = 0.007 \text{ ft}^2$$

$$W_d = 60 \times 0.007 = 0.42 \text{ lb/ft}$$

Total:

$$\sum W = W_s + W_g + W_d = 1.48 + 7.64 + 0.42 = 9.54 \text{ lb/ft}$$

**Table N.4 Computation of Moment of Inertia of Cable Specimen**

Strand:

$$I_{\text{ind}} \text{ (single strand)} = 7 \times 1/64 \times \pi \times 0.2^4 + 0.2208 / 7 \times (2 \times 0.2^2 + 4 \times (0.2/2)^2) = 0.00435 \text{ in}^4$$

$$I_s = 2 \times 0.00435 + 0.2208 \times (2 \times 0.65^2) = 0.195 \text{ in}^4$$

Grout:

$$I_g = 1/64 \times \pi \times 3.35^4 - 0.195 = 5.989 \text{ in}^4$$

$$I_g/n = 5.989/8.40 = 0.71 \text{ in}^4$$

Total:

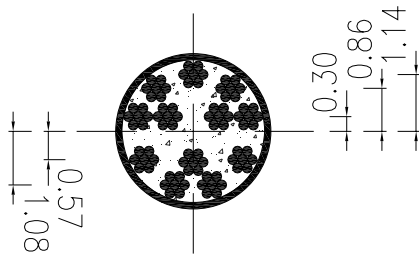
$$\sum I = I_s + I_g/n = 0.195 + 0.71 = 0.908 \text{ in}^4 = 0.000044 \text{ ft}^4$$

$$EI = 29,400 \times 0.000044 = 185.4 \text{ kip-ft}^2$$

## N.2 TENDON 01

Tendon 01 consisted of twelve 0.6-in strands stressed to 60% of GUTS. Idealized section is presented in Table N.5 and the computation of mass quantity and the moment of inertia is given Table N.6 and Table N.7, respectively.

**Table N.5 Sectional Dimension of Tendon 01**



Duct:

Inner diameter: 2.875 in.

Outer diameter: 3.125 in.

(a) Idealized section

(b) Dimension

**Table N.6 Computation of Mass Quantity of Tendon 01**

Strand
$W_s = 0.74 \times 12 = 8.88 \text{ lb/ft}$
Grout
$A_g = (1/4 \times \pi \times 2.875^2 - 12 \times 0.2208) \times 1.05 = 4.06 \text{ in}^2 = 0.028 \text{ ft}^2$ (5% for ribs)
$W_g = 125 \times 0.028 = 3.50 \text{ lb/ft}$
Duct
$A_d = 1/4 \times \pi \times (3.125^2 - 2.875^2) = 1.18 \text{ in}^2 = 0.008 \text{ ft}^2$
$W_d = 60 \times 0.008 = 0.49 \text{ lb/ft}$
Total
$\Sigma W = W_s + W_g + W_d = 8.88 + 3.50 + 0.49 = 12.87 \text{ lb/ft}$

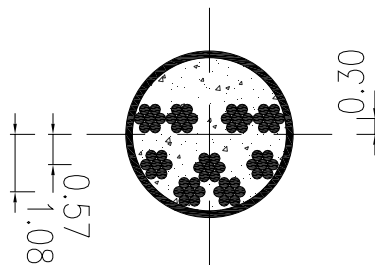
**Table N.7 Computation of Moment of Inertia of Tendon 01**

Computation of centroid:
Strand
$\sum A_s \cdot d_s =$
$1 \times 1.14 \times 0.2208 + 2 \times 0.86 \times 0.2208 + 4 \times 0.3 \times 0.2208 - 3 \times 0.57 \times 0.2208 - 2 \times 1.08 \times 0.2208 = 0.042$
Centroid
$\sum A_s \cdot d_s (n-1) / \{A_s (n-1) + A_g\} =$
$0.042 \times (8.40 - 1) / \{0.2208 \times 12 \times (8.40 - 1) + 1/4 \times \pi \times 2.875^2\} = 0.012 \text{ in.}$
Computation of moment of inertia:
Strand
$I_{ind} = 0.00435 \text{ in}^4$
$\sum I_s = 12 \times 0.00435 + 0.2208 \times (4 \times 0.3^2 + 2 \times 0.86^2 + 1 \times 1.14^2 + 3 \times 0.57^2 + 2 \times 1.08^2) = 1.475 \text{ in}^4$
Grout
$I_g = 1/64 \times \pi \times 2.875^4 - 1.475 = 1.880 \text{ in}^4$
Total
$\sum I_{trans} = I_s + I_g/n = 1.475 + 1.880/8.40 = 1.699 \text{ in}^4 \approx 0.000082 \text{ ft}^4$
$EI = 346.8 \text{ kip-ft}^2$

### N.3 TENDON 02

Tendon 02 consisted nine 0.6-in. strands stressed to 80% of GUTS. Idealized section is presented in Table N.8 and the computation of mass quantity and the moment of inertia is given Table N.9 and Table N.10, respectively.

**Table N.8 Sectional Dimension of Tendon 02**



(a) Idealized section

Duct:

Inner diameter: 2.875 in.

Outer diameter: 3.125 in.

(b) Dimension

**Table N.9 Computation of Mass Quantity of Tendon 02**

Strand
$W_s = 0.74 \times 9 = 6.66 \text{ lb/ft}$
Grout
$A_g = (1/4 \times \pi \times 2.875^2 - 9 \times 0.2208) \times 1.05 = 5.71 \text{ in}^2 = 0.040 \text{ ft}^2$ (5% for ribs)
$W_g = 125 \times 0.040 = 4.96 \text{ lb/ft}$
Duct
$A_d = 1/4 \times \pi \times (3.125^2 - 2.875^2) = 1.18 \text{ in}^2 = 0.008 \text{ ft}^2$
$W_d = 60 \times 0.008 = 0.49 \text{ lb/ft}$
Total
$\Sigma W = W_s + W_g + W_d = 6.66 + 4.96 + 0.49 = 12.11 \text{ lb/ft}$

**Table N.10 Computation of Moment of Inertia of Tendon 02**

Computation of centroid:

Strand

$$\sum A_s \cdot d_s =$$

$$4 \times 0.3 \times 0.2208 + 3 \times -0.57 \times 0.2208 + 2 \times -1.08 \times 0.2208 = -0.59$$

Centroid

$$\sum A_s \cdot d_s (n-1) / \{A_s (n-1) + A_g\} =$$

$$-0.583 \times (8.40 - 1) / (0.2208 \times 9 \times (8.40 - 1) + 1/4 \times \pi \times 2.875^2) = -0.21 \text{ in.}$$

Computation of moment of inertia:

Strand

$$I_{\text{ind}} = 0.00435 \text{ in}^4$$

$$\sum I_s =$$

$$9 \times 0.00435 + 0.2208 \times (4 \times (0.3 + 0.21)^2 + 3 \times (-0.57 + 0.21)^2 + 2 \times (-1.08 + 0.21)^2) = 0.690 \text{ in}^4$$

Grout

$$I_g = 1/64 \times \pi \times 2.875^4 + 1/4 \times \pi \times 2.875 \times 0.21^2 - 0.69 = 2.938 \text{ in}^4$$

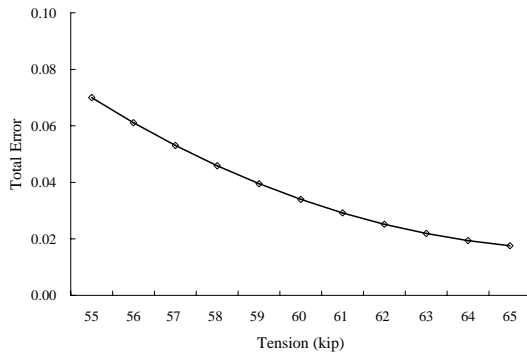
Total

$$\sum I_{\text{trans}} = I_s + I_g/n = 0.69 + 2.938/8.40 = 1.040 \text{ in}^4 \approx 0.000050 \text{ ft}^4$$

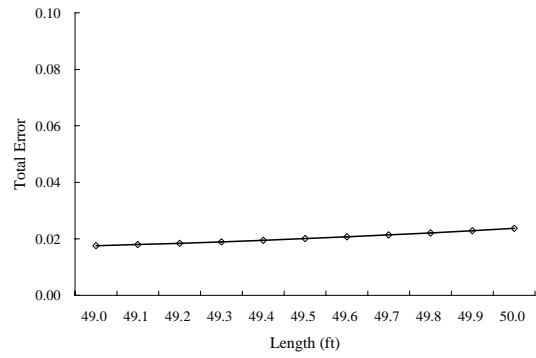
$$EI = 212.4 \text{ kip-ft}^2$$

# Appendix O: Sensitivity of Structural Parameters

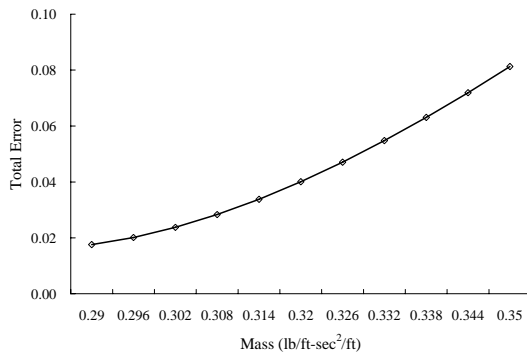
## O.1 CABLE 01



(a) Tension

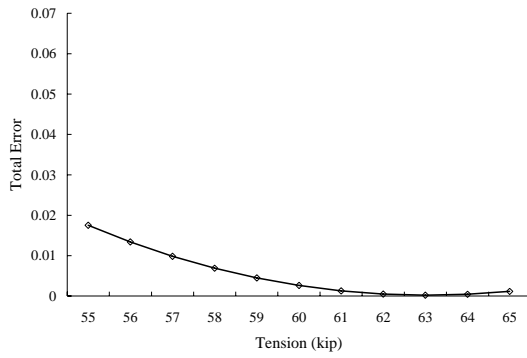


(b) Length

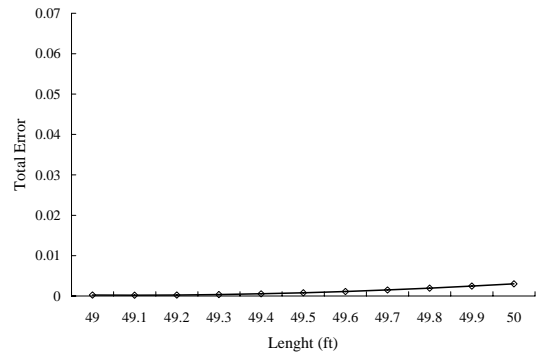


(c) Mass

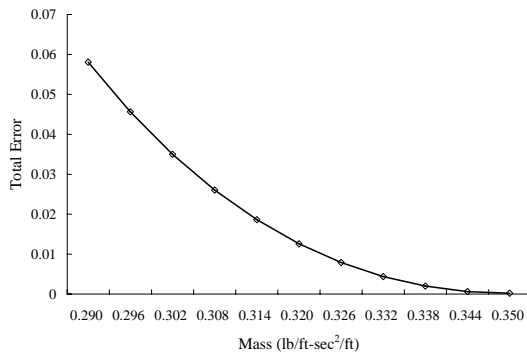
*Figure O.1 Sensitivity of Structural Parameters from Taut String Model*



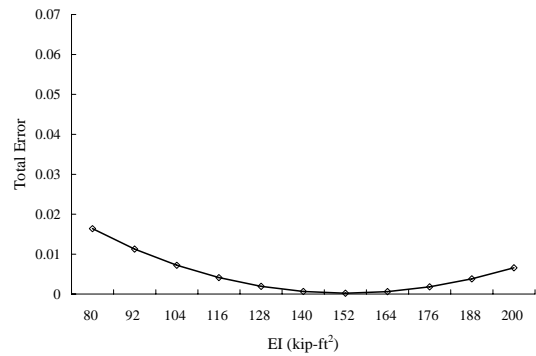
(a) Tension



(b) Length



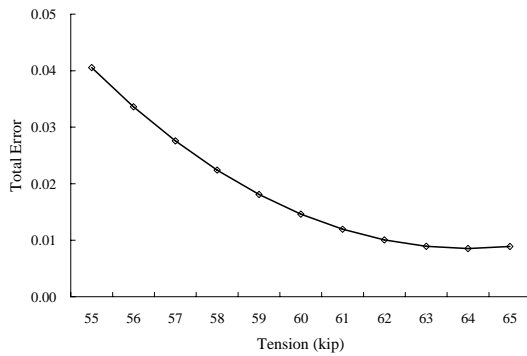
(c) Mass



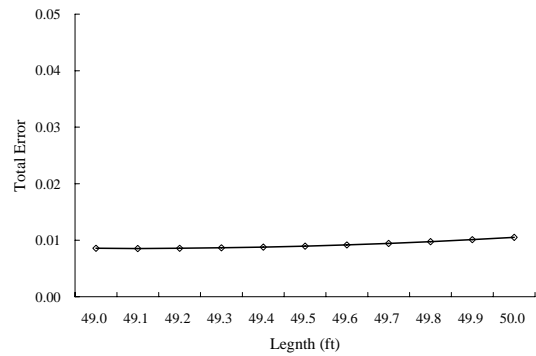
(d) EI

**Figure O.2 Sensitivity of Structural Parameters from Stiff String Model**

**O.2 CABLE 02**

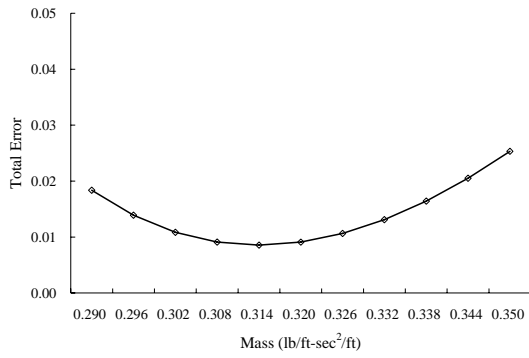


(a) Tension



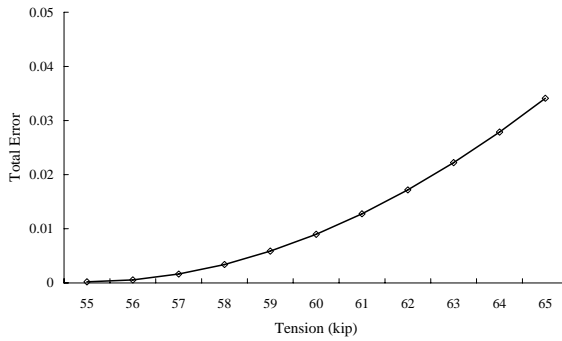
(b) Length



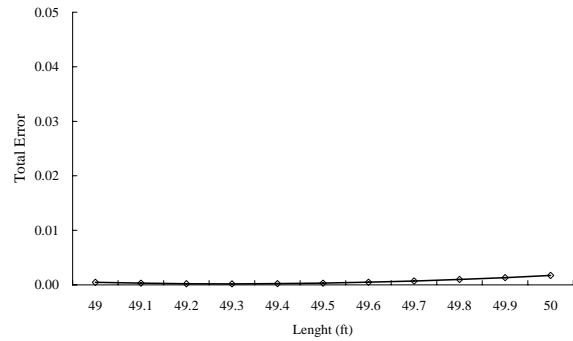


(c) Mass

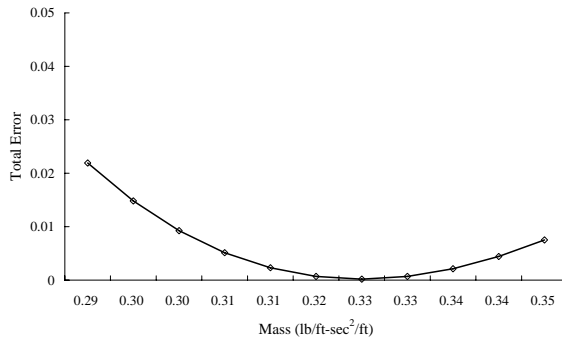
**Figure 0.3 Sensitivity of Structural Parameters from Taut String Model**



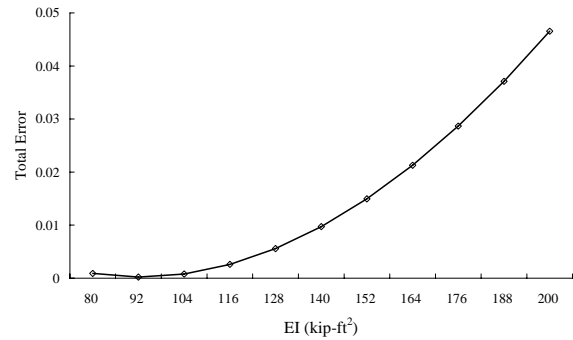
(a) Tension



(b) Length



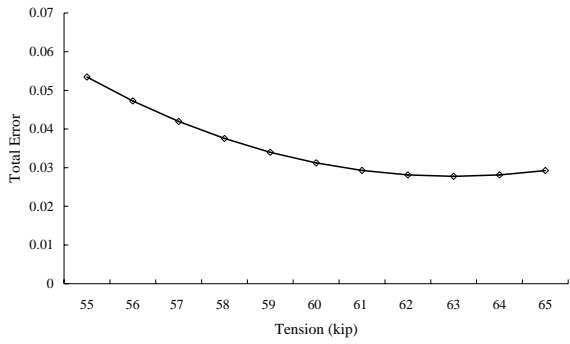
(c) Mass



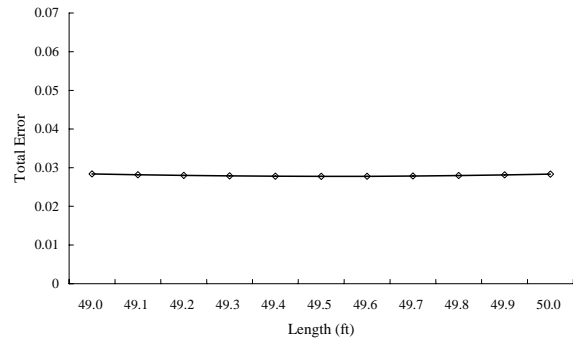
(d) EI

**Figure 0.4 Sensitivity of Structural Parameters from Stiff String Model**

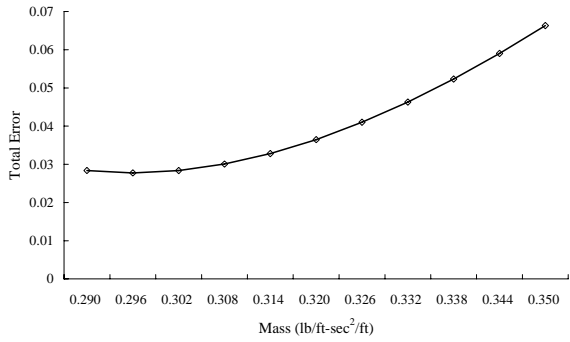
### 0.3 CABLE 03



(a) Tension

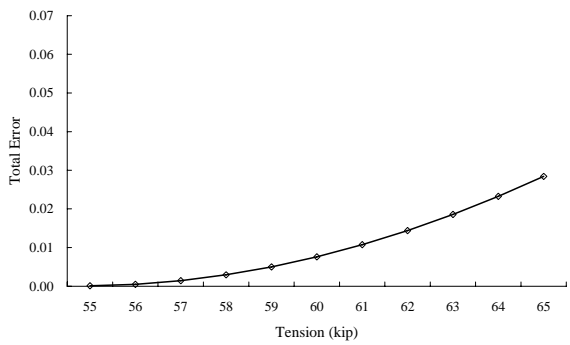


(b) Length

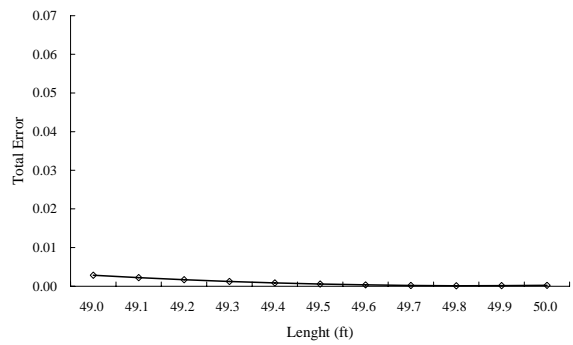


(c) Mass

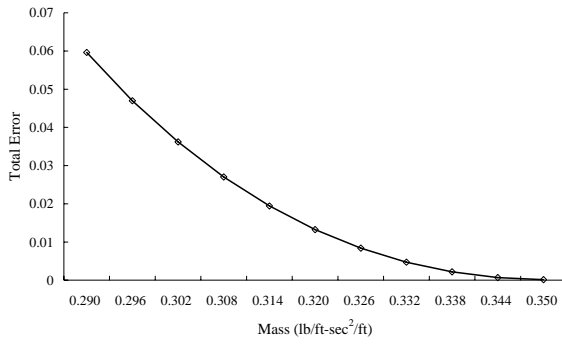
*Figure 0.5 Sensitivity of Structural Parameters from Taut String Model*



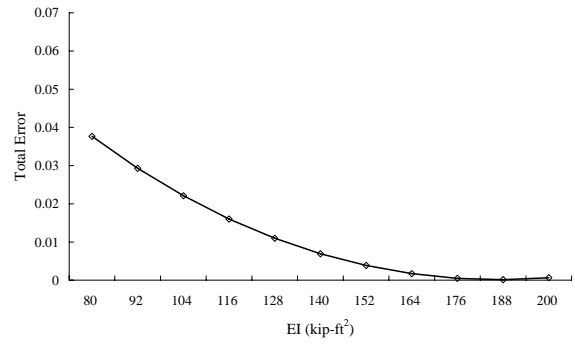
(a) Tension



(b) Length



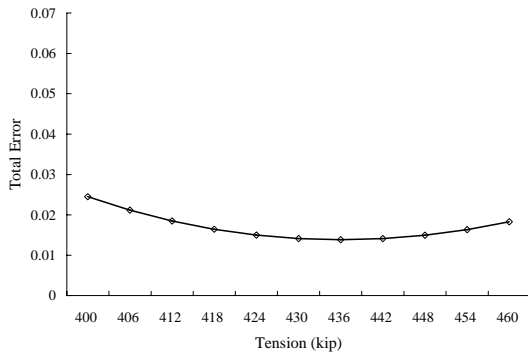
(c) Mass



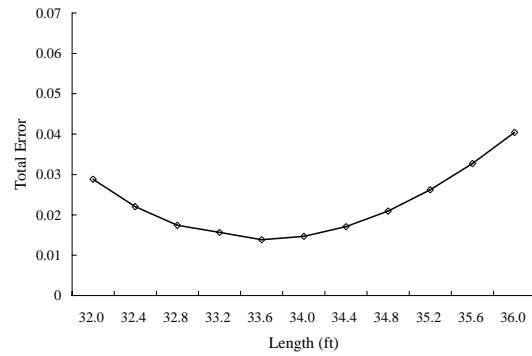
(d) EI

**Figure O.6 Sensitivity of Structural Parameters from Stiff String Model**

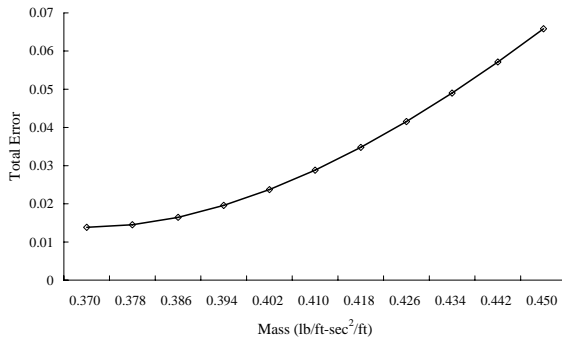
**O.4 TENDON 01**



(a) Tension

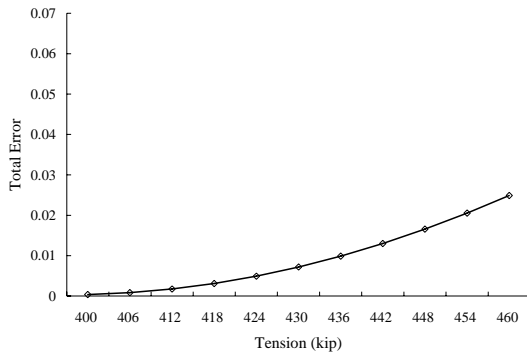


(b) Length

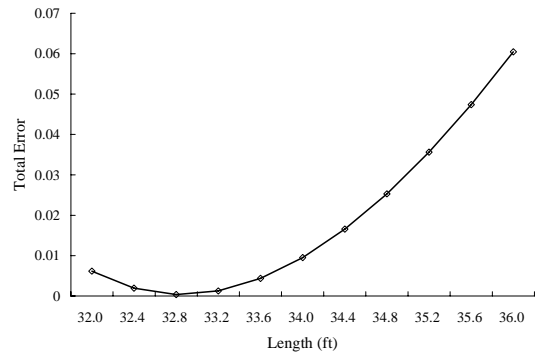


(c) Mass

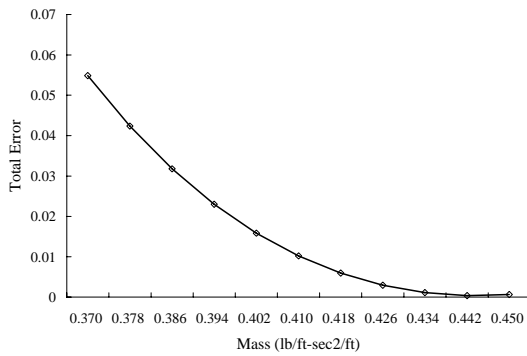
**Figure O.7 Sensitivity of Structural Parameters from Taut String Model**



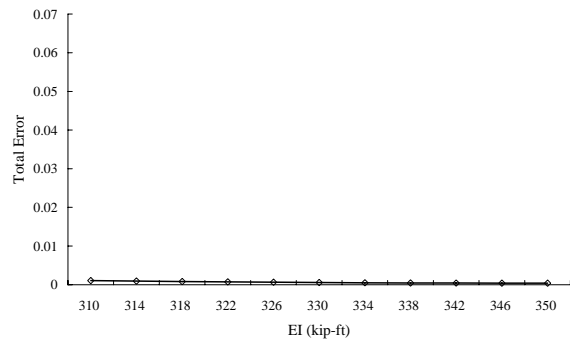
(a) Tension



(b) Length



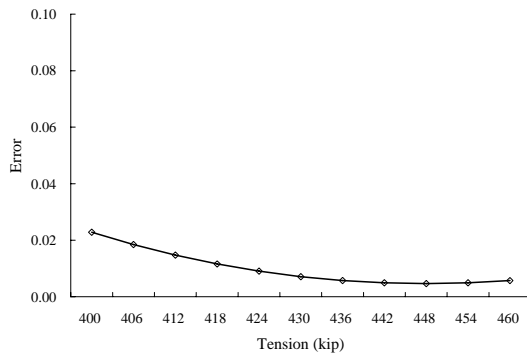
(c) Mass



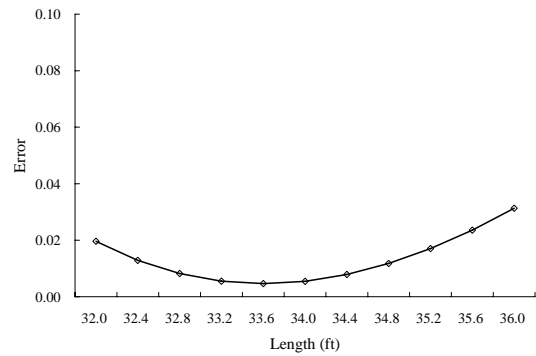
(d) EI

**Figure 0.8 Sensitivity of Structural Parameters from Stiff String Model**

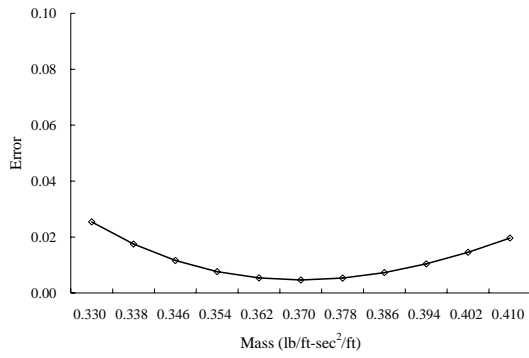
## 0.5 TENDON 02



(a) Tension

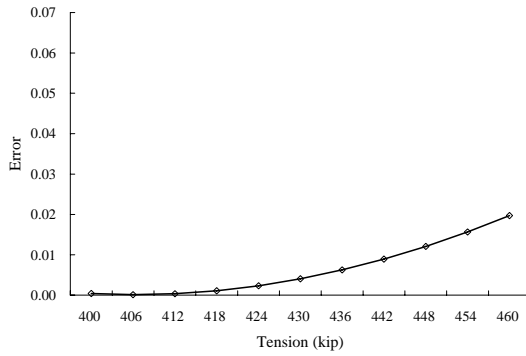


(b) Length

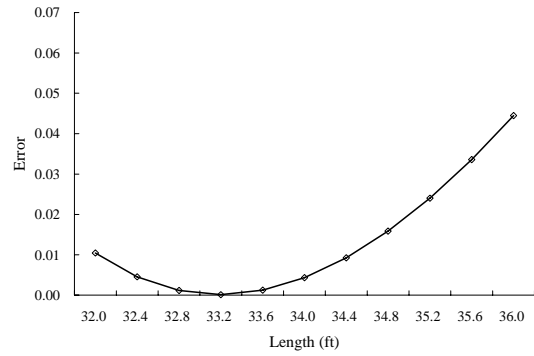


(c) Mass

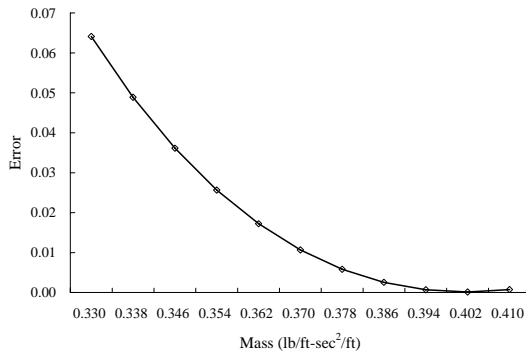
**Figure 0.9 Sensitivity of Structural Parameters from Taut String Model**



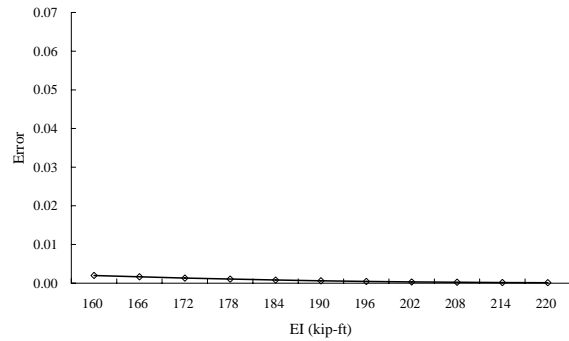
(a) Tension



(b) Length



(c) Mass



(d) EI

**Figure 0.10 Sensitivity of Structural Parameters from Stiff String Model**

## References

- ACI Committee 222, 2001, "Protection of Metals in Concrete against Corrosion," American Concrete Institute Manual of Concrete Practice, Committee Report ACI 222R-01, American concrete Institute, Michigan
- ACI Committee 228, 1998, "Nondestructive Test Methods for Evaluation of Concrete in Structures," Manual of Concrete Practice, Committee Report 228.2R, American Concrete Institute, Farmington Hills, Michigan.
- ACI Committee 228.2R-98, "Nondestructive Test Methods for Evaluation of Concrete in Structures," American Concrete Institute Manual of Concrete Practice, Committee Report 228.2R-98, American concrete Institute, Michigan
- ASTM, 2003, "Standard Practice for Preparing, Cleaning, and Evaluating Corrosion Test Specimens," ASTM G1-03, ASTM international, Pennsylvania
- ASTM, 2005, "Standard Specification for Steel Strand, Uncoated Seven-Wire for Prestressed Concrete," ASTM A 416/A 416M-05, ASTM international, Pennsylvania
- Bean, M. J., 2006, "Bending Fatigue Performance of Small-Scale Stay Cables," Master's thesis, the University of Texas at Austin, May
- Bergamini, A., Christen R., and Motavalli, M., 2003, "A simple approach to the automatic recognition of flaws in large diameter steel cables," International Symposium, Non-Destructive Testing in Civil Engineering 2003, Berlin Germany, September
- Ciolko, A. T., and Tabatabai, T., 1999, "Nondestructive Method for Condition Evaluation of Prestressing Steel Strands in Concrete Bridges, Final report phase I: Technology Review," NCHRP Project 10-53, Construction Technologies, Illinois, March
- Corven Engineering, Inc. 2001, "Mid-Bay Bridge Post-Tensioning Evaluation," Final Report, to Florida Department of Transportation District 3, Tallahassee, Florida, October
- DeHaven, T. A., 2003, "Grouting of Post-Tensioning Tendons: Overview of Recent Development," Structure magazine, October

- DMJM Harris, 2003, "Test and Assessment of NDT Methods for Post-Tensioning Systems in Segmental Balanced Cantilever Concrete Bridges," Central Structures Office, Florida Department of Transportation, Tallahassee, Florida, February
- Covern Engineering Inc., 2002, "New Directions for Florida Post-Tensioning Bridges," Florida Department of Transportation, Tallahassee, Florida, February
- fib, 1991, "Recommendations for Acceptance of Post-Tensioning Systems," Fédération Internationale de la Précontrainte, London, United Kingdom.
- fib, 2003, "Influence of Material and Processing on Stressing Corrosion Cracking of Prestressing Steel - Case Studies," Technical Report Bulletin 26, October
- fib, 2003, "Monitoring and Safety Evaluation of Existing Concrete Structures," Fédération Internationale de la Béton, Lausanne, Switzerland.
- Freyermuth, C. L., 2001, "Status of the Durability of Post-Tensioning Tendons in the United States," Durability of Post-Tensioning Tendons, fib-IABSE Technical Report Bulletin 15, November
- Heller, E. B., 2003, "Fatigue Response of Pretensioned Concrete Beams," Master's thesis, the University of Texas at Austin, August
- Jones, D., A., 1996, "Principles and Prevention of Corrosion," 2nd edition, Prentice Hall
- Jungwirth, D., 2001, "Problems, Solutions and Developments at Post-Tensioning Tendons from the German Point of View," Durability of Post-Tensioning Tendons, fib-IABSE Technical Report Bulletin 15, November
- Liu, W., Hunsperger, R. G., Chajes, M. J., Folliard, K. J., and Kunz E., 2002, "Corrosion Detection of Steel Cables using Time Domain Reflectometry," Journal of Materials in Civil Engineering, American Society of Civil Engineers, Vol. 14, No. 3, May-June
- Loudon, N., 2006, "Inspection, Monitoring, and Management of Post-Tensioned and Cable-Supported Bridges," Oral Presentation, Inspection, Monitoring & Management of Post-Tensioned & Cable-Supported Bridges: A Review of Past Performance and Current Practice, Transport Research Laboratory, Berkshire, England
- MacDougall, C., and Bartlett, F. M., 2002, "Test of Corroded Unbonded Seven-Wire Tendons with Broken Wires," American Concrete Institute Structural Journal, November-December

- Matt, P., 2001, "Non-destructive Evaluation and Monitoring of Post-Tensioned Tendons," Durability of Post-Tensioning Tendons, fib-IABSE Technical Report Bulletin 15, November
- Morse, P. M., 1948, "Vibration and Sound," 2nd edition, McGraw-Hill Book
- Mutsuyoshi, H., 2001, "Present Situation of Durability of Post-tensioned PC Bridges in Japan," Durability of Post-Tensioning Tendons, fib-IABSE Technical Report Bulletin 15, November
- Nakamura, S., 2004, "Mechanical Properties and Remaining Strength of Corroded Bridge Wires," Structural Engineering International, Journal of the International Association for Bridges and Structural Engineering, February
- Nürnberg U., 2001, "Corrosion Induced Failure Mechanisms," Durability of Post-Tensioning Tendons, fib-IABSE Technical Report Bulletin 15, November
- PCI, 1985, "Manual for Quality Control for Plants and Production of Precast and Prestressed Concrete Products," Precast/Prestressed Concrete Institute, Chicago, Illinois
- Poser, M., 2001, "Full-Scale Bending Fatigue Tests on Stay Cables," Master's thesis, the University of Texas at Austin, December
- Poston, R. W., Frank, K. H., and West, J. S., 2003, "Enduring Strength," Civil Engineering, American Society of Civil Engineers, September
- Powell, L. C., Breen, J. E., and Kreger, M. E., 1988, "State of the Art Externally Post-Tensioned Bridges with Deviators," Center for Transportation Research, Research Report 365-1, the University of Texas at Austin, June
- Ridd, J. E., 2004, "Fatigue Performances of Stay Cables," Master's thesis, the University of Texas at Austin, August
- Sagües, A. A., 2004, "Corrosion/ Durability Research," Oral Presentation, Florida Department of Transportation Research Projects, Tampa
- Sagües, A. A., and Kranc, S. C., 2000, "Initial Development of Methods for Assessing Condition of Post-Tensioned Tendons of Segmental Bridges," Final Report, the University of South Florida, May
- Sansalone, M. J., and Streett, W. B., 1997, "Impact-Echo: Nondestructive Evaluation of Concrete and Masonry," Bullbrier Press, Ithaca, New York
- Sason, S. A., 1992, "Evaluation of Degree of Rusting on Prestressed Concrete Strand," Journal of Prestressed Concrete Institute, May-June



- Scheel, H., and Hillemeier, B., 2003, "Location of Prestressing Steel Fractures in Highly Reinforced Concrete Members," International Symposium, Non-Destructive Testing in Civil Engineering 2003, Berlin Germany, September
- Virlogeux, M. P., 1990, "External Prestressing: from Construction History to Modern Technique and Technology", External Prestressing in Bridges, American Concrete Institute Special Publication 120
- Woodward, R., 2001, "Durability of Post-Tensioned Tendons on Road Bridges in the UK," Durability of Post-Tensioning Tendons, fib-IABSE Technical Report Bulletin 15, November

## Vita

Jun Ki Lee was born on September 14, 1975 in Dae-Gu in Republic of Korea and is the son of Myung Whan Lee and Chun Kyoung Kim. After completion of Se-Wha High School in Seoul, Jun Ki entered Korea University in Seoul, Republic of Korea where he was a civil engineering major. Jun Ki earned his Bachelor of Science degree from Korea University in spring of 1998 and entered the Department of Structural Engineering at Korea University in the same year. After Jun Ki received the Master of Science degree under the supervision of Professor Chul Soo Yoo in fall of 2000, he was employed for a year by Han-Seok Engineering and Consultant as a structural engineer. In fall of 2001, Jun Ki joined the Korea Railroad Research Institute as a research fellow for nearly a year. In the fall of 2002, he entered the Department of Structural Engineering at the University of Texas at Austin in the pursuit of a doctoral degree under the supervision of Dr. Sharon L. Wood. He earned his doctoral degree in May of 2007.

Permanent address: Sammaul Woobang APT 504-701, Dongan-Ku Galsan-Dong 1116, Anyang-City Kyoungki-Do 431-703 Korea(Republic of)

This dissertation was typed by the author.